वार्षिक प्रतिवेदन 2010-2011
Annual Report 2010-2011

भौतिक अनुसंधान प्रयोगशाला, अहमदाबाद
Physical Research Laboratory, Ahmedabad

पी.आर.एल. में सुविधाएं
Facilities at PRL

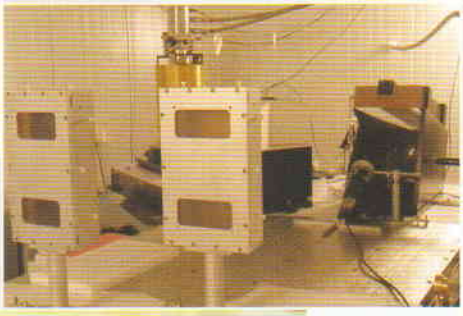

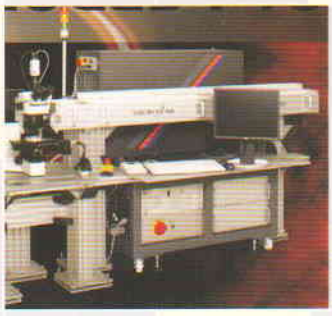

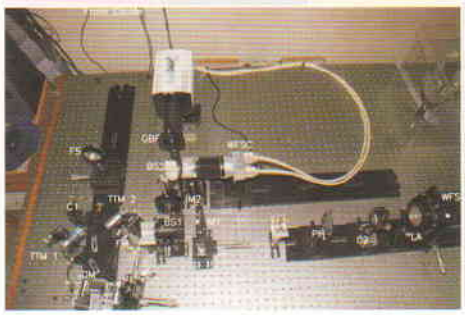

वार्षिक प्रतिवेदन

Annual Report

2010-2011

भौतिक अनुसंधान प्रयोगशाला, अहमदाबाद

Physical Research Laboratory, Ahmedabad

Front Cover: PRL Main Campus

Inside front cover: Facilities at PRL

Inside back cover: Events at PRL

Back cover: Spectra of a Sun type star and Th-Ar calibration spectra recorded simultanenously for radial velocity measurements (PARAS programme).

Compiled by:
Office of the Dean, PRL.

Published by:
Physical Research Laboratary, Ahmedabad.

Layout & Printed by:
Creative Printers Pvt. Ltd., Ahmedabad.

Council of Management

Chairman Professor U. R. Rao ISRO Headquarters, Government of India, Bangalore	Nominee, Government of India
Dr. K. Radhakrishnan Secretary, DOS and Chairman, ISRO, Government of India Department of Space, Bangalore	Nominee, Government of India
Dr. R.G. Nadadur Additional Secretary, Department of Space, Government of India, Bangalore	Nominee, Government of India
Shri Sanjay S. Lalbhai Ahmedabad Education Society Ahmedabad	Nominee, Ahmedabad Education Society
Shri Kartikeya V. Sarabhai Chidambaram, Usmanpura, Ahmedabad	Nominee, Karmakshetra Educational Foundation
The Principal Secretary, Department of Education (Higher & Technical Education) Government of Gujarat, Gandhinagar	Nominee, Government of Gujarat
Professor J. N. Goswami Director, Physical Research Laboratory, Ahmedabad	(Ex-Officio)
Member- Secretary Shri Y.M. Trivedi Registrar Physical Research Laboratory, Ahmedabad	(Ex-Officio)

Contents

Director's Foreword

Our collective endeavour to enhance and broaden the scope of scientific research at PRL has been moving in the right direction. The past year witnessed the creation of the "Computational Science Group" comprising of faculty members from across scientific divisions and novel ideas and proposals for exciting new research programmes to be taken up during the 12th five year plan. I am pleased to place on record that, major initiatives proposed under the current five year plan period have been executed as per schedule and, most of the new experimental facilities are now operational and yielding significant science results. Pre-shipment testing of the Multi-Application-Solar-Telescope (MAST) will take place soon and its anticipated installation at the Udaipur Solar Observatory site by the end of 2011 will provide a major boost to research in Solar Physics in the country. The success of the Chandrayaan-1 mission encouraged PRL scientists to propose several new experiments for the upcoming Indian planetary missions to Moon and Mars and two of PRL proposals have been selected for ISRO's Chandrayaan-2 mission. With the PLANEX programme gaining maturity, PRL is now reasonably equipped for design and development of payloads for planetary missions as well as interpretation of planetary remote sensing data.

Research at PRL during the year, resulted in an impressive number of publications in high impact factor journals. A brief outline of some of the selected studies is presented in the "Science Highlights" section and a more comprehensive narration of the research by the scientific divisions, that include Astronomy and Astrophysics, Solar Physics, Planetary Science and Exploration, Space and Atmospheric Sciences, Geosciences and Theoretical Physics, is provided in reports of the divisions. Studies under the DST sponsored national programme Isotope fingerprinting of water of India (IWIN), with PRL as the nodal centre and more than a dozen participating institutes across the country, made very good progress and have led to several new results.

The infrastructure at the Udaipur Solar observatory was upgraded to house MAST and the construction of the Space Instrumentation and Planetary data analysis facilities at the Thaltej campus that commenced a few months ago will be completed by early 2012. The Echelle spectrograph developed for the search of exo-planets was fully integrated with the Mt. Abu Telescope with excellent test results. Routine observations using this facility will commence during the post-monsoon observing season of 2011.

The strength of scientific and technical faculty is currently close to seventy five and efforts are on to induct new faculty members to initiate new programmes and to ensure continuity in selected areas in view of superannuation of a sizable number of faculty members within the next few years. PRL now has a healthy number of post-doctoral fellows, research scholars and project associates that exceeded our targeted mark of hundred by 2010. Research carried out during the year resulted in publication of about 160 papers in peer reviewed journals and 60 papers in Conference Pro-

ceedings. PRL faculty members wrote half a dozen invited reviews and edited two research publications and one popular science publication. A record number of sixteen research scholars completed their Ph.D. studies during the year.

Faculty and research scholars of PRL received honours and recognition for their work from both international and national academic forums. These include Full Membership of International Astronautical Academy, Fellowship of National Academy of Sciences, D.Sc. (Honoris Causa), J. C. Bose National fellowship, Member, American Chemical Society, National Ocean Science & Technology Award, National Geoscience Award, Young International Scientists Fellowship, NASA Group Achievement Award and Honorary Professorship within India and abroad. Several research scholars of PRL were selected for awards for their work at various national meets. Senior PRL faculty members received invitations to serve as Council/Board Member of Academic and Research Institutes, member of National and International Scientific/Working Groups, Guest Editor/Editorial Board Member of national and international journals during the year. PRL faculty members have also acted as convenors of half a dozen international workshop/meeting/conference. I am confident that the trend will continue in the coming years and PRL scientists will make even greater contribution both at the national and international scientific scene.

Several Conferences/Workshops/Schools have been held at PRL during the year. These include the International Workshop on "Advances in Planetary Atmospheres and Exploration", several workshops on Chandrayaan-1 data analysis, a two day brainstorming session on Mars Science and Exploration, and a Young Astronomers' meet. The colloquium and divisional seminar activities have been continued with vigour and apart from PRL faculty, a large number of scientists from within the country and abroad have presented their scientific work in this forum. Prof. Jurg Beer from Swiss Federal Institute of Aquatic Science and Technology delivered this years' K. R. Ramanathan memorial lecture.

The laboratory continues to expand its Human Resource Development activities. Nearly a hundred college and university students from both science and engineering streams carried out their training/projects at PRL as summer students or engineer trainees under close supervision of PRL scientists and engineers. PRL is regularly conducting the biennial Post-graduate Space Science Course of the UN Centre for Space Science & Technology Education in Asia and the Pacific and the 7th course in this series is currently underway. PRL continued to administer the PLANEX and RESPOND programmes of ISRO and presently over fifty research groups across the country in the areas of Planetary Science and Exploration and Space Sciences are being supported through these programmes. The Science day activities at PRL saw enthusiastic participation of more than a hundred schools from all over Gujarat and talented students were offered scholarship and other incentives based on their performances in the events conducted on that day. As a part of an initiative of the Indian National Science Academy, a monograph "Flavors of Research in Physics" containing a series of articles written by well known academicians from all over India and edited by a senior faculty member of PRL was brought out and distributed to a large number of students across the country. Progressive use of Hindi, particularly in the administrative areas has been enhanced and first steps for a bi-lingual website have been initiated with some of the general information of the laboratory provided both in Hindi and English. It is a matter of satisfaction that PRL received the First prize from the Town Official Language Committee, Ahmedabad, for excellent contribution towards implementation of official language policy during 2009-10.

The accomplishments of PRL during the year presented in this report have been possible due to the dedication and hard work of all my scientific, technical and administrative colleagues and other staff members of PRL and, it is with a deep sense of pride that I place on record, my deepest appreciation to all members of team PRL. However, we need to strive harder, particularly in view of the ambitious projects for the next plan that are currently under discussion and to justify the continued investment and faith reposed on us by the Dept. of Space. I express my gratitude to Chairman, PRL Council of Management and all other members of the Council for their sage advice, encouragement and continued support that facilitated smooth academic and administrative functioning of the laboratory.

J. N. Goswami

Director

Science Highlights

Astronomy and Astrophysics

- PARAS (PRL Advanced Radial-velocity All-sky Search) program achieved a major milestone with the in-house designed and developed high resolution optical Echelle spectrograph observing first light at Mt. Abu Observatory in April 2010. The stability of spectrograph was up to 2 ms^{-1} level for the Th-Ar calibration spectra. On sky stability of the system is about 8 ms^{-1} which is sufficient to detect Jupiter sized exoplanets.

- Infrared light curves and spectra from recent 2010 outburst of well-known recurrent Nova U Scorpii were recorded from Mt. Abu observatory and were used to derive physical parameters of the system. Detailed analysis of the spectral line profile indicates very high ejection velocities up to 10000 km/s, typically observed only in supernovae.

- Observations of blazers from Mt. Abu Observatory showed rapid intra-night variability. A new limit on the mass of the super massive black-hole in blazer PKS0716+71 was derived using these observations. A dedicated small telescope has been installed at Mt. Abu observatory for continuous optical observations of blazers.

- Study of the X-ray emission, the characteristics of the X-ray spectrum and flux variability of the active galactic nuclei (AGN) of low-surface-brightness (LSB) galaxy UGC 6614 demonstrated that, although LSB galaxies are poor in star formation, they may harbour AGNs with X-ray properties comparable to those seen in more luminous spiral galaxies.

- Timing and broad-band spectral properties of the Be transient high-mass X-ray binary pulsar GRO J1008-57 were investigated during its 2007 November-December outburst. The 93.737s pulsations were clearly detected in the light curves up to as high as 100 keV. The broad-band energy spectrum of the pulsar was reported.

- Analysis of long term observations of solar coronal rotation shows that solar corona rotates asymmetrically in the northern and the southern hemisphere.

- Observations of oppositely directed sudden impulses have revealed that energetic events on the rear side of the Sun can also propagate shock towards the earth and play a key role in occurrence of such events.

- A study of solar polar magnetic fields for the past three solar cycles has shown a steady decline in polar fields starting from 1995 to 2010 implying that the

build-up to the deepest solar minimum at the end of cycle 23 began over a decade ago.

- A modular multi-channel X-ray spectrometer based on Silicon Drift Detector (SDD) is under development for future space experiment that requires large sensitive area (few cm^2), low energy range (1 – 30 keV) and high energy resolution (< 200 eV @ 5.9 keV). Front-end electronics for the SDD detector meeting the performance requirement has been developed in-house.

- Study of energy dependent timing observations of thermal emission in M-class flares by the SOXS (Solar X-ray Spectrometer) experiment onboard GSAT-2 spacecraft has yielded the break-point energy separating thermal and non-thermal components between 14 and 21 keV.

Solar Physics

- The prototype adaptive optics system locked on to the sunspot in the active region NOAA 11072 on 25 May 2010 thereby demonstrating the successful performance of the complete system involving tip-tilt mirror for global tilt corrections and the deformable mirror for higher order corrections.

- Flare productivity in the solar active region NOAA 10486 was found to be associated with p-mode parameters, sub-photospheric flows and their temporal changes.

- Flare induced changes in penumbral flows seen in the solar active region NOAA 10930 led to an enhancement of global waves in the Sun.

- The acoustic power emitted by the spine structure of sunspot penumbral filaments was found to be consistently lower than the power emitted from intra-spine regions.

- Transient magnetic and Doppler velocity features were seen to be moving away from the flare site during the peak phase of an X class solar flare, and were spatially and temporally associated with the white-light flare ribbons and hard X-ray sources.

- A stereoscopic reconstruction technique was developed and used to obtain the heliographic coordinates of several features along the legs of two eruptive prominences observed by EUVI/STEREO spacecraft that allowed determination of the signs of the twisting motions in the two eruptions.

- Solar coronal loops were numerically modelled as non force-free structures with flow by applying the principle of a minimum energy relaxed state.

Planetary Sciences and PLANEX Program

- Crater Tycho is a unique dark haloed complex impact crater in the southern highlands, on the near side of Moon. High resolution images and reflectance data from Chandrayaan-1, Lunar Reconnaissance Orbiter and Kaguya have revealed volcanic vent, domes, pyroclastics, lava ponds and channels showing distinct cooling cracks and flow fronts on the central peak. Compositionally, the lava pond and channels have been found to be rich in high Ca–pyroxene while the host rock is anorthositic in nature, providing evidences of late stage volcanic activity on the central peak of Tycho crater.

- Study of lunar magnetic anomaly has been carried out using magnetometer data of Lunar Prospector. Contouring of magnetic strength shows high magnetic strength on lunar swirls. Space weathering study using data from Moon Mineralogical Mapper suggests that swirls represent immature material and contain a small admixuture of highland material along with mare material.

- Analysis of Chandrayaan-1 images of the Mare Imbrium region revealed a cluster of fresh and buried secondary craters exhibiting near circular mounds in the crater floor. Impact of ejected fragments produced at the time of formation of the Copernicus crater could be identified as their source. The presence of central mound can distinguish the secondary craters from the primary craters and help refining the chronology of lunar surface based on counting of small craters.

- Zircons with ages ranging from 3.2 to 3.5 billion years are present in metasedimentary rocks and orthogneisses from both the western and eastern Dharwar Cratons. In particular, the evolution of the southwest part of the eastern Dharwar craton involved a significant amount of older crust >3Ga. The geochronological data coupled with geological features and geodynamic setting suggest that the eastern and western Dharwar cratons formed part of a single terrain.

- Two payloads for the Chandrayaan-2 mission, X-ray Solar Monitor (XSM) for the orbiter and the Alpha Particle X-ray Spectrometer (APXS) for the rover are under development. We plan to cover the entire range of variations in intensity and spectra of the Solar X-

rays during large solar flares by using a new generation X-ray detector [Silicon Drift Detector (SDD)]. Sensitive and extremely low-noise front-end electronics needed for this detector have been successfully designed, developed and tested in-house. The data from XSM will provide real time measurement of the solar X-rays, an essential parameter for quantitative interpretation of lunar X-ray fluorescence spectra.

- SDD detector will also be used in the APXS payload in the Rover. It will consist of the APXS sensor head and APXS electronics. The sensor head will be mounted on a robotic arm of the ROVER for manipulation during measurement of lunar surface samples. APXS electronics will have interface with the rover subsystems. Evaluation of performance and suitability of the SDD modules from two sources [KETEK and AMPTEK] have been completed. We have achieved the required energy resolution (~150 eV @ 5.9 keV) with a low energy threshold of <1keV.

Space and Atmospheric Sciences

- Over urban areas natural aerosols dominate the aerosol mass concentration, while anthropogenic aerosols contribute to the optical properties and radiative effects. Inspite of the dominance of natural aerosol, the aerosol radiative forcing is dependent more on optical depth and single scattering albedo than on aerosol mass. There exists no linear relation between mass, optical depth and radiative effect of different aerosol species.

- The emission of alkenes over northern Indian Ocean is influenced by the monsoon circulation with high emission in summer and low in winter monsoon.

- Chemical transport model simulations of seasonal variation of carbon monoxide (produced mainly by anthropogenic activities) over India revealed that the model estimates are higher compared to the satellite observations. This emphasizes the need to develop high resolution emission inventory of trace gases.

- Observation made from Gadanki reveal transport of significant air mass from low to high latitudes before and during the sudden stratospheric warming event and explains the excess heat requirement for the sustenance of the event.

- Based on sodium airglow observations from low latitude stations in conjunction with satellite measurements, it is shown that the dominant periods associated with mesospheric gravity waves are less on nights when neutral instabilities occur within sodium airglow layer than on the nights when the instabilities occurred above the sodium airglow layer or do not occur within the emission layer.

- Investigation on the effect of magnetic fields in the Martian ionosphere over low latitude revealed that ion and electron densities are reduced by factor of three above 200 km due to transport of photoelectrons in presence of vertical magnetic fields.

Geo-Sciences

- The evolution of $^{87}Sr/^{86}Sr$ ratio of the Ganga water during the past hundred thousand years has been reconstructed by analysing $^{87}Sr/^{86}Sr$ in carbonate nodules collected from different depths of two sediment cores raised in the Ganga Plain near Kanpur. The nodules in general, display significantly lower $^{87}Sr/^{86}Sr$ ratio compared to contemporary Ganga river water at Kanpur. The recent increase in this ratio in the Ganga water could be a result of enhanced weathering of the Lesser Himalaya containing lithologies with higher $^{87}Sr/^{86}Sr$ ratio which could result from anthropogenic activities over the mountains and/ or due to climatic variability.

- Eruptive history of India's only volcano, Barren Island, was reconstructed by determining the timing of deposition of ash layers in a marine sediment core collected from 32 km southeast of the volcano. These ash layers were uniquely correlated to erupted materials on the volcano with the help of Sr-Nd isotopic ratio fingerprinting and dated using C^{14} method. The results reveal that the volcano had seven major ash eruptions at about 70, 69, 61, 24, 19, 15, and 10 ka. Between 24 ka and 10 ka, the volcano had large ash eruptions spaced at 4,500 year intervals. Our analysis also suggest that the caldera of Barren Island volcano is younger than 10 ka.

- Application of stable isotopes is extended further by simulating nitrogen loss process in the Arabian Sea. With the help of a new data set, spatiotemporal variation in the oxygen isotopic composition and salinity ($\delta^{18}O$-S) relation of the northern Indian Ocean is studied. The results are consistent with positive P-E (excess of precipitation over evaporation) over the Bay of Bengal and negative P-E over the eastern Arabian Sea. A significant spatiotemporal variability is also observed in the Bay; the temporal variability is difficult to discern in the Arabian Sea. Both the slope and intercept of the ($\delta^{18}O$-S) relation appear to be

sensitive to rainfall; the slope (intercept) is higher (lower) during years of stronger monsoon. The observed variability implies that caution needs to be exercised in paleosalinity estimations, especially from the Bay of Bengal, based on $\delta^{18}O$ of marine organisms.

- Water soluble inorganic phosphorous (PO_4^{3-}) measured in ambient aerosols, collected from marine atmospheric boundary layer (MABL) of Bay of Bengal during the late NE- monsoon (January-April), has provided the first field evidence for the role of chemical processing of mineral dust in supply of bioavailable phosphorus to the surface waters. However, anthropogenic fraction of water soluble phosphorous accounts for ~70-80% of the total inorganic phosphorous over Bay of Bengal, an evidence derived based on significant linear relation of NH_4^+ with PO_4^{3-}; suggesting ammonium phosphate fertilizer to be their common source.

- Concentrations of elemental carbon and organic carbon (EC and OC), polycyclic aromatic hydrocarbons (PAHs) and their isomer ratios in ambient aerosols from a sampling site, in north-eastern Himalaya reveals a characteristic PAHs/EC ratio of 3.0 mg g^{-1}, suggesting emissions from agricultural-waste burning as a dominant source of carbonaceous aerosols during January-March period. The isomers of PAHs with 4- and 6-rings appear to retain their source-signature even in the aged air-parcel, unlike 3- and 5- ring compounds. These results have implications in assessing the chemical reactivity of PAHs during long-range transport.

Theoretical Physics

- Ensembles with random two-body interactions for fermions systems with parity symmetry and bosonsystems with spin symmetry have been introduced. Analytical and numerical results for a variety of spectral properties of these ensembles have been derived which have applications to parity ratios in nuclei and spinor BEC, respectively. The work on random matrix theory and spectral distributions by PRL group has resulted in book and a review article during the year.

- Relativistic many-body methods are employed to obtain accurate values of isotope shift and variation of fine structure constant sensitivity parameters for many transitions in Na and Mg^+. It has also been shown how information about nuclear anapole moment can be obtained from the measurements of parity violating light-shifts in Ba^+ and Ra^+. A generalized relativistic coupled-cluster method is developed and employed to estimate the uncertainty due to black body radiation shift for the Al^+ atomic clock frequency standard measurement.

- Recent investigations of the foundations of statistical mechanics show problems with the orthodox ergodic approach. These were analyzed in detail and plausible resolution of the problem following the ideas of Khinchin and Landau was given.

- The dynamics of excitation energy transfer in photosynthesis was studied using non-Markovian quantum master equations. This explained the long coherence observed in 2D photon echo experiments.

- A study of the intensity correlation properties of optical vortices passing through a rotating ground-glass (RGG) plate has been done and the results are compared with those of the TEM_{00} mode of a He–Ne laser beam passed through the same RGG. The intensity correlation curves for optical vortices decrease much faster in the RGG than the corresponding curve for a TEM_{00} mode of the He–Ne laser. The rate of decay of the correlation increases with the increase of order of the vortices. The experimental results are supported by exact analytical results.

- Experimental as well as theoretical study of the spatial coherence function and the Wigner distribution function for one-dimensional projections of optical vortices of different orders was carried out. The information entropy derived from the spatial coherence functions has been used to quantify the information content of the vortices and compared with those obtained for the Gaussian beam. The experimental results verify earlier theoretical findings obtained at PRL.

- It has been shown that by using suitable diffractive optical elements, several copies of optical vortices could be created with the same topological charge. Theoretical calculations carried out are in excellent agreement with these experimental findings.

- The density profiles of the quantum degenerate Bose-Fermi mixture of ^{174}Yb-^{173}Yb, experimentally observed recently, is examined in the mean field regime. It is shown that in this mixture there is a possibility of tuning the Bose-Bose and Bose-Fermi interactions simultaneously using two well separated optical Feshbach resonances, and it is a good candidate to explore phase separation in Bose-Fermi mixtures.

- An iterative scheme for coupled-cluster calculations without truncating the dressed properties operator is developed and demonstrated. For validation, magnetic dipole hyperfine constants of alkaline Earth ions are calculated with relativistic coupled-cluster and role of electron correlation examined. Based on a detailed analysis of the higher order terms, an optimal form of the dressed operator is defined, which will significantly improve future calculations.

- The possibility of the determination at future experimental facilities of the three major unknowns in neutrino physics – mass hierarchy, the third mixing angle and CP violation was studied. The judicious use of a novel "bi-magical" baseline of 2540 km. for neutrino oscillation experiments was shown to permit the determination of all these simultaneously.

- A forward-backward asymmetry in top-pair production at the proton-antiproton accelerator Tevatron at Fermilab, has been reconfirmed with more accumulated data. It was shown that the cross section and the total asymmetry can be simultaneously explained with the contributions of light colour-sextet spin zero particles appearing in a particular non-supersymmetric SO(10) grand unification model with masses in the range of 300 GeV-2TeV. These are consistent with the requirements of grand unification and bounds on the proton lifetime.

- A study is made of how the measurement of top polarization at the Tevatron can be used to characterize and discriminate among different new physics models suggested to explain the anomalous top forward-backward asymmetry. Top polarization is found to have the advantage of catching the essence of the parity-violating effect characteristic of the different models. Other observables constructed from these asymmetries are also shown to be useful in discriminating between the models, even after taking into account statistical errors.

- The idea of asymmetric dark matter, viz., that the observed dark matter is an asymmetry between dark matter and anti-dark matter, generated through the same mechanism that explains why there is more matter compared to antimatter in the universe has been proposed. In simple extensions of the standard model this allows the prediction of the amount of dark matter in terms of the baryon asymmetry of the universe and the mass of the weakly interacting dark matter candidate. The allowed range of the mass of the dark matter candidate is testable at LHC.

- It was shown that if the Wino, the supersymmetric partner of the W boson, has mass of 4 TeV, it can serve as dark matter and explain the positron and antiproton fluxes observed by PAMELA. It can also give a thermal relic abundance of dark matter consistent with WMAP observations owing to the role played by a non-perturbative phenomenon called the Sommerfeld effect in the calculation of the relic density and the dark matter annihilation in galaxies.

- Effect of magnetic field on chiral symmetry breaking in a 3-flavor Nambu Jona Lasinio (NJL) model at finite temperature and densities was studied using an explicit structure of ground state in terms of quark and antiquark condensates. While at zero chemical potential and finite temperature, magnetic field enhances the condensates, at zero temperature, the critical chemical potential decreases with increasing magnetic field.

- The kinetics of chiral transitions in quark matter was studied in a two flavor Nambu-Jona-Lasinio model. A study of the dynamics by considering a phenomenological model (Ginzburg-Landau free-energy functional) showed that the morphology of the ordering system is characterized by the scaling of the order-parameter correlation function.

- A study was carried out of the non-ideal effects arising due to viscosity (both bulk and shear), equation of state and cavitation on thermal dilepton production from quark-gluon plasma at RHIC energies. It was found that ignoring the cavitations can lead to a wrong estimation of dilepton spectra. The shear viscosity (bulk viscosity) was shown to enhance (suppress) the thermal dilepton spectra.

Awards and Honours

Faculty Members

U. R. Rao

1. ISCA General President Gold Medal Award.

2. D. Sc, Honoris Causa, Dr. D. Y. Patil Vidyapeeth, Pune, 2010.

J. N. Goswami

3. Full Member, International Astronautical Academy, 2010.

4. D. Sc, Honoris Causa, Dibrugarh University, 2010.

S. Krishnaswami

5. Ocean Science and Technology Award, Ministry of Earth Sciences, Government of India, 2010.

A. K. Singhvi

6. Member, the International Science Program Committee and the Indian Representative to the International Ocean Drilling Program by the Ministry of Earth Sciences.

7. P.R. Pisharoty Memorial lecture of the Indian Society of Remote Sensing, Ahmedabad Chapter.

8. Member of Editorial Board, International Journal of Earth Environment, Chinese academy of Sciences.

9. Member of Editorial Board, Indian J. Geosciences.

A. S. Joshipura

10. J. C. Bose National Fellow, Department of Science and Technology, New Delhi, 2010.

V. K. B. Kota

11. Adjunct Professor of Physics for 2010-2015, Laurentian University, Sudbury, Canada.

R. Ramesh

12. Member, the American Chemical Society.

13. Member, Governing Council of the Birbal Sahni Institute of Paleobotany, Lucknow.

M. M. Sarin

14. Member, UN/GESAMP (United Nation Group of Experts on Scientific Aspects of Marine Environmental Protection).

15. Member, GESAMP WG 39: "Global trends in pollution of coastal ecosystems".

16. Member, GESAMP WG 38: "Atmospheric input of chemicals to ocean".

17. Adjunct Professor, University of Delaware, USA.

18. Member, Scientific Advisory Committee (SAC), Environmental Monitoring & Research Centre (EMRC), India Meteorological Department, New Delhi.

Utpal Sarkar

19. The Clark Way Harrison visiting professorship, Washington University in St. Louis, USA, 2011.

R. E. Amritkar

20. Fellow, National Academy of Sciences, Allahabad.

S. V. S. Murty

21. Appointed as member of Mars Mission Study Team to prepare science definition and mission scenarios for Mars exploration by ISRO.

S. A. Haider

22. Convener "Science and Exploration of Mars and Venus", 7th Annual AOGS meeting, Hyderabad, India, July 5-9, 2010.

Shyam Lal

23. Member Research Council of National Physical Laboratory (NPL), New Delhi.

S. Ramachandran

24. NASA Group Achievement Award for outstanding accomplishments in the successful Arctic Research of the Composition of the Troposphere from Aircraft and Satellites (ARCTAS) Mission in Alaska and Canada. 2009.

D. Pallamraju

25. Convener, Atmospheric Coupling Processes in the Sun-Earth System, 7th annual Asia Oceania Geosciences Society (AOGS) Meeting, Hyderabad, July 05–09, 2010.

26. Secretary, for the Solar Terrestrial (ST) Section of the Asia Oceania Geosciences Society (AOGS) for the term 2010 – 2012.

27. Chairman, Session C11: Recent Advances in Equatorial, Low- and Mid-Latitude Mesosphere, Thermosphere and Ionosphere Studies, 38th COSPAR Scientific Assembly, Bremen, Germany, July 18-25, 2010.

28. Guest Editor, Journal of Atmospheric and Solar-Terrestrial Physics (JASTP) Special Issue: "Atmospheric Coupling Processes in the Sun-Earth System".

Raghavan Rangarajan

29. Member, Senate of the Indian Institute of Technology, Gandhinagar.

J. S. Ray

30. National Geosciences Award, Ministry of Mines, Government of India, 2009.

Nandita Srivastava

31. Co-Chair of poster session ST5/NH8. on " Space Weather and its effects on terrestrial and Geospace environments " in European Geophysical Union (EGU) General Assembly, Vienna, May 2-7, 2010.

Ravi Bhushan

32. Visiting Professor, Atmospheric and Ocean Research Institute, University of Tokyo, Tokyo, October-Novemer, 2010.

B. K. Sahoo

33. "Young International Scientists Fellowship award", Chinese Academy of Sciences, 2010.

34. "Professor S. N. Ghosh Award" for Young Scientists in Atomic & Molecular Physics for the year by the Indian Association of Atomic and Molecular Physics.

Young Scientists

L. K. Dewangan et al.

35. Best poster award, "Infrared photometric study of the massive star forming region S235 using Spitzer-IRAC

and Mt. Abu JHK observations", Stars and Galaxy section, 29th Meeting of Astronomical Society of India, Raipur, February 23-25, 2011.

A. Bhattacharya et al.

36. Best Paper Award for the paper titled "Development and evaluation of a light sensing module for planetary exploration" by A. Bhattacharya, K. Durga Prasad and S.V.S. Murty, at SAMTI – 2011 at BARC, Mumbai , February 2-4, 2011.

Ram Ajor Maurya

37. Best contribution award by a young scientist in the First Asia-Pacific Solar Physics Meeting/3rd Indo-China Workshop, IIA, Bangalore, March 21-24, 2011.

Administration

38. PRL received First Prize conferred by Town Official Language Committee (TOLIC), Ahmedabad for excellent contribution towards implementation of Official Language Policy during 2009-2010. A certificate of appreciation was also given to Shri R.S. Gupta, Hindi Officer-II & OSD.

Theses Submitted

1. **Rohan Eugene Louis**

   "Study of Small Scale Processes on the Sun using High Resolution Techniques", Mohanlal Sukhadia University, Udaipur, June 2010.

2. **Ashwini Kumar**

   "Chemical characteristics of mineral aerosols: Sources, transport and atmospheric transformations", Mohanlal Sukhadia University, Udaipur, July 2010.

3. **Kirpa Ram**

   "Carbonaceous species in atmospheric aerosols: Sources and temporal variability", Mohanlal Sukhadia University, Udaipur, July 2010.

4. **L. K. Dewangan**

   "Multi-Wavelength Investigations on Galactic Star Forming Regions", Gujarat University, Ahmedabad, July 2010.

5. **Ram Ajor Maurya**

   "A Study of Oscillations in Solar Active Regions", Mohanlal Sukhadia University, Udaipur, August 2010.

6. **Shuchita Srivastava**

   "Study of Trace Gases and Related Meteorological Parameters in Lower Atmosphere" Mohanlal Sukhadia University, Udaipur, August 2010.

7. **Sumita Kedia**

   "Regional and Seasonal differences in aerosol radiative forcing over India and adjoining oceanic regions", Mohanlal Sukhadia University, Udaipur, August 2010.

8. **Waliur Rahaman**

   "Chemical and Isotopic studies of Estuaries and the Ganga Basin sediments", Mohanlal Sukhadia University, Udaipur, August 2010.

9. **Naveen Gandhi**

   "Carbon fixation in the hydrosphere: quantification for the Indian region using ^{13}C and ^{15}N isotopes", Mohanlal Sukhadia University, Udaipur, September 2010.

10. **Sumanta Sarkhel**

    "Upper Atmospheric Investigations using Radio and Optical Techniques", Mohanlal Sukhadia University, Udaipur, October 2010.

11. **Bhavik Kodrani**

"Studies of models of fermion masses and mixing", submitted to Mohanlal Sukhadia University, Udaipur, January 2011.

12. **Brajesh Kumar Mani**

"Studies on the consequences of discrete symmetry violations in atoms", submitted to Mohanlal Sukhadia University, Udaipur, January 2011.

13. **G.R. Tripathy**

"Isotope Geochemistry of Black Shales and Recent 0.Marine sediments", Mohanlal Sukhadia University, Udaipur, January 2011.

14. **Arvind Singh**

"Characterization of carbon and nitrogen uptake by marine biota in the Indian Ocean", Mohanlal Sukhadia University, Udaipur, February 2011.

15. **Sudhanwa Patra**

"Beyond the standard model and its cosmological consequences", submitted to Gujarat University, Ahmedabad, February 2011.

16. **A. H. Laskar**

"Stable and radioactive carbon in Indian soils: implications to soil carbon dynamics", Mohanlal Sukhadia University, Udaipur, March 2011.

Human Resource Development

Visitors/Colloquia/Public Lectures

Dr. Dibyendu Nandi

Ramanujan National Fellow, Indian Institute of Science Education and Research, Kolkata

Physics of Space Weather and Climate

Prof. Jean-Claude Vial

The Institut d'Astrophysique Spatiale, Orsay, France

A Space Institute for Astrophysics Research: Science, Instrumentation and Results

Prof. Biswarup Mukhopadhyaya

Harish-Chandra Research Institute, Allahabad, India

Hunting after roots: The Large Hadron Collider and New Physics

Prof. K.N. Joshipura

Department of Physics, Sardar Patel University, Vallabh Vidyanagar

Interactions and scattering of electrons with atomic molecular systems-Theoretical aspects

Prof. L. S. Shashidhara

Indian Institute of Science Education and Research (IISER), Pune

Behavioral Adaptations and Evolution

Prof. Christopher Measures

Department of Oceanography, University of Hawaii at Manoa, Honolulu, USA.

Trace elements and isotopes in the ocean; how they get there and why they are important to understanding global climate

Prof. Wing Huen Ip

Institutes of Astronomy and Space Science National Central University, Taiwan

From Venus, Earth and Mars to Habitable Exoplanets

Prof. Bharat Ratra

Kansas State University, USA.

The "Standard" Model of Cosmology

Prof. Girish S. Agarwal

Oklahoma State University, USA

Electromagnetically Induced Transparency and Nonlinear Optics in Mechanical Effects of Light

Prof. T.P. Prabhu

Indian Institute of Astrophysics, Bangalore.

Science from High Altitudes

Prof. R.K. Varma

Former Director and Emeritus Scientist, Physical Research Laboratory

A Novel Interferometric Mass Spectroscopy Concept

Prof. R. Sridharan

CSIR Emeritus Scientist, Physical Research Laboratory

Chac(s)ing the moon

Dr. Dileep Kumar

National Institute of Oceanography (NIO), Goa

Why is the North Indian Ocean so interesting biogeochemically?

Prof. V. Rajamani

Jawaharlal Nehru University, New Delhi

Geological Commons

Prof. Abhijit Sen

Institute for Plasma Research, Gandhinagar

Collective Dynamics of Strongly Coupled Dusty Plasmas

Dr. K. S. Krishna

National Institute of Oceanography (NIO), Goa.

Formation of a nascent plate boundary in the central Indian Ocean - a possible response to the uplift of the Tibetan Plateau

Prof. Jean-Pierre St-Maurice

Tier 1 Canada Research Chair in Environment Sciences, University of Saskatchewan, Saskatoon, Canada

A peek at some of the physical processes at work in the aurora borealis

The Fascinating and mysterious aurora borealis

Prof. N. Mukunda

Indian Academy of Sciences, Bangalore.

The Relation between Mathematics and Physics

Prof. S. Dattagupta

Indian Institute of Science Education and Research, Kolkata

Two Hundred (….and More Years of Diffusion)

Prof. Amitava Raychaudhuri

Harish Chandra Research Institute, Allahabad

A Passage to India: Exploring neutrinos from the far corners of the earth at INO

Prof. Ashok Sahni

Centre of Advanced Study in Geology, Lucknow University, Lucknow

The Physics of Biomaterials

Prof. Emmanuel A. Paschos

University of Dortmund, Germany

Some Highlights in Neutrino Physics

Prof. Steven Tomsovic

Washington State University, Pullman, USA

Quantum Chaos: Origins and Developments

Prof. Ashok Das

University of Rochester, Rochester, New York, USA

A quantum mechanical description for pseudo-Hermitian Hamiltonians

Prof. Ramakrishna V. Hosur

Department of Chemical Sciences, TIFR, Mumbai & UM-DAECentre for Excellence in Basic Sciences Mumbai University campus, Kalina, Mumbai

Moving Frontiers of NMR

Prof. V. M. Kenkre

University of New Mexico, USA

Abrupt Transitions in Bio/Eco Systems—Interplay of Nonlinearity and Inhomogeneity

Shri S. K. Shivakumar

ISRO Satellite Centre (ISAC), Bangalore

Indian Deep Space Network (IDSN)

Dr. David W. Fahey

National Oceanic and Atmospheric Administration (NOAA), Chemical Sciences Division Boulder, CO USA.

What is important to know about ozone depletion and the Montreal Protocol: A 2010 Update

Dr. M. S. Sheshshayee

University of Agricultural Sciences (UAS), Bangalore.

Can we make plants to produce more? How much of Physics should we know?

Prof. Vijay Prasad Dimri

National Geophysical Research Institute (CSIR), Hyderabad.

Impact of Climate Change and Carbon Dioxide Sequestration in Suitable Geological Formations

Dr. P. K. Manoharan

National Centre for Radio Astrophysics, Tata Institute of Fundamental Research, Ooty.

Evolution of Solar Wind in the Inner Heliosphere

Prof. Kazuo Shiokawa

Solar Terrestrial Environment Laboratory (STEL), Nagoya University, Japan

Ground optical observations of auroral physical processes at sub-auroral and middle latitudes

Prof. V. Ramaswamy

US National Oceanic and Atmospheric Administration, Geophysical Fluid Dynamics Laboratory, Princeton University, Princeton, USA

The Earth's Changing Climate System: Past to Future

Prof. K. R. Ramanathan memorial lecture

Prof. Jurg Beer

Eawag, Swiss Federal Institute of Aquatic Science and Technology, Switzerland.

Solar variability and climate change

Conferences /Symposia /Workshops

Astronomy and Astrophysics

1. Young Astronomers' Meet (YAM) held at Physical Research Laboratory and jointly sponsored by DST and Physical Research Laboratory, PRL, Ahmedabad 03-05 September, 2010.

Planetary Sciences and PLANEX Program

2. Workshop on "Data Analysis of Chandrayaan-1 Imaging payloads HySI and TMC" : jointly organized by PLANEX - Physical Research Laboratory and Space Application Centre, PRL, Ahmedabad, 28-30 November, 2010 .

3. Workshop on "Data Analysis of Chandrayaan-1 Imaging payload MiniSAR" organized at Space Application Center, 27 December, 2010.

4. 11th PLANEX Workshop on "Exploration of Mars and Moon", Physical Research Laboratory, Ahmedabad, 3-7 January, 2011.

5. Brainstorming session on "Mars Science and Exploration", Physical Research Laboratory, Ahmedabad, 24-25 March, 2011.

Geo-Sciences

6. "OS08: Trace Elements and Isotopes in Oceans", organized at in AOGS2010, Hyderabad, 5-9 July, 2010.

7. "4th Coordination Meeting of all partner institutions of the IWIN National Programme" organized at National Institute of Oceanography, Goa, 11-12 January, 2010.

8. "5th Coordination Meeting of all partner institutions of the IWIN National Programme" organized at Anna University, Chennai, 27-28 January, 2011.

Space and Atmospheric Sciences

9. International workshop on "Advances in Planetary Atmospheres and Exploration" organised by Physical Research Laboratory, PRL, Ahmedabad, 12-13 July, 2010.

Invited Talks

Astronomy and Astrophysics

K. S. Baliyan

1. "Optical variability in AGNs as a tool to constrain emission models", RAC-NCRA, Ooty, 20 December, 2010.

2. "Optical variability study of Blazarsfrom MIRO: Some recent results", Theme meeting on VHE Gamma-ray Astronomy at GOALS, Mt. Abu, 28-30 March, 2011.

Sachindra Naik

3. "Broad-band spectroscopy of X-ray binary pulsars", International conference on "Wide-band X-ray Astronomy: Frontiers in Timing and Spectroscopy", IUCAA, Pune, 13-16 January, 2010.

Hari Om Vats

4. "The Complex Rotation of the Sun and its Atmosphere", AOGS 7th Annual Meeting Hyderabad, 5-9 July 2010.

5. "Characteristics of Sun and Interplanetary Magnetic Field", Workshop on advances in Planetary Atmospheres and exploration, PRL, 13 July, 2010.

6. "Solar Rotation", 25th Annual IAPT convention and symposium of Atronomy, Astrophysics and Space Science, Saurastra University, Rajkot, 22 October, 2010.

K. Singal

7. "'Absolute' Motion of the Earth - A Journey Through Space!", YAM 2010, PRL, 3 September, 2010.

Rajmal Jain

8. "The Dynamic Sun", National Level Seminar on 'Solar Activity & Cosmic Ray Modulation', Satna, Madhya Pradesh, 09-10 October 2010.

Solar Physics

Ashok Ambastha

9. Two invited talks on "Solar Flares", DST-SERC School "Space Weather", IIG, Navi Mumbai, Panvel, Mumbai, 7-8 April, 2010.

Bhuwan Joshi

10. "Sun and Solar Activity", Regional Science Congress, Navodaya Vidyalaya Samiti, Rajsamand, Rajasthan, 15-20 November, 2010.

11. Popular talk on the topic "The dynamic Sun" in the 42nd Rajasthan State Science and Development fair 2009-2010 organized by SCERT and sponsored by NCERT held in Pali, Rajasthan, 10-14 July, 2010.

Rohan Eugene Louis

12. "Supersonic Downflows at the Umbra–Penumbra Boundary of Sunspots", Hinode 4:Unsolved Problems and Recent Insights, Palermo, Italy, 11 October, 2010.

13. "Achieving High Spatial Resolution using Adaptive Optics at the Udaipur Solar Observatory", Indian Institute of Astrophysics, Bangalore, 28 October, 2010.

Ram Ajor Maurya

14. "Variation in High-Degree p-mode Parameters with Flare Activity", in First Asia-Pacific Solar Physics Meeting 2011/3rd Indo-China Workshop on Solar Physics, Indian Institute of Astrophysics, Banglore, India, 22 March, 2011.

15. "Long Term Variations in p-modes and Sub-photospheric Flows of Super Active Regions", 29th Meeting of Astronomical Society of India, Pt. Ravishankar Shukla University, Raipur, India, 24 February, 2011.

16. "Kinetic and Magnetic Helicities in Solar Active Regions", GONG/SOHO meeting, Aix en Provence, France , 28 June, 2010.

Planetary Sciences and PLANEX Program

J. N. Goswami

17. "The new face of the Moon" Invited Lecture, Indian Institute of Geomagnetism, Mumbai, 7 April, 2010.

18. "The new moon: Results from Chandrayaan-1", Keynote Speech, International Symposium on Planetary Exploration , Chiba Institute of Technology, Japan, 20 May, 2010.

19. "Ian Axford and Planetary Exploration" Invited talk at Sir Ian Axford Commemoration Symposium, AOGS 2010; Hyderabad, 8 July, 2010.

20. "Chandrayaan-1 and Beyond", Colloquium at the Indian Institute of Science Education and Research, Kolkata, 1 September, 2010.

21. "Planetary Exploration" Invited Talk at the Indian Institute of Science & Technology, Trivandrum, 22 September, 2010.

22. "Chandrayaan-1 and water on Moon", Highlight Lecture, 61st International Astronautical Congress", Prague, 30 September, 2010.

23. "Water in the solar system: The case for the moon", Evening Talk, 29th meeting of Astronomical Society of India, Raipur, 24 February, 2011.

S.V.S. Murty

24. Three talks "Comparative Planetology" ; "Future lunar missions: Science objectives" and "Mars: Recent discoveries and new questions" at the 11th PLANEX Workshop on "Exploration of Mars and Moon", Physical Research Laboratory, Ahmedabad, 3-7 January, 2011.

25. "Mission to Mars: ISRO Plans", at AOGS-2010, Hyderabad, 5-9 July, 2010.

26. "Indian Mars mission: Science Goals", at the International Workshop on 'Advances in Planetary Atmospheres and Exploration', PRL, Ahmedabad, 12-13 July, 2010.

27. "Meteorites and the early solar system" at the Workshop on 'Foundations of Space Science and Technology', at Kalpana Chawla Center for Space and Nano Science, Kolkata, 17 May, 2010.

28. Two invited talks on "Chandrayaan-1: Mission and some important results" and "Future ISRO Missions to Moon and Mars" at IIRS, Dehradun, 9-10 December, 2010.

S.V. Vadawale

29. "India's first mission to The Moon - Chandrayaan-1". COSMO – 2010 Workshop, IIT Gandhinagar, April, 2010.

30. "Space Instrumentation at PRL-X-ray experiments" IIST-USRA Workshop, IIST Valiamala Campus, Thiruvananthapuram, September, 2010.

K. Durga Prasad

31. "Wireless Sensor Networks for Planetary Exploration", 11th PLANEX Workshop on

"Exploration of Mars and Moon", Physical Research Laboratory, Ahmedabad, 3-7 January, 2011.

32. "In-situ studies of Mars with Phoenix and Mars Science Laboratory", Brainstorming session on Mars Science and Exploration, Physical Research Laboratory, Ahmedabad, 24-25 March, 2011.

K. K. Marhas

33. "Stardust in Laboratory" Workshop on laboratory astrophysics: Applications to cosmic dust , M. G. science Institute, Ahmedabad, 12-13 November, 2010.

34. "Solar System Bodies" PLANEX workshop, Physical Research Laboratory, Ahmedabad, 3-7 January, 2011.

Vinai K. Rai

35. "Understanding Mars through study of SNC meteorites" in Brainstorming Session on Mars Science and Exploration, Physical Research Laboratory, Ahmedabad, 24-25 March, 2011.

M. Shanmugam

36. "Alpha Particle X-ray Spectrometer (APXS) for Chandrayaan-2 Rover", 11th PLANEX workshop on "Exploration of Mars and Moon", PRL, Ahmedabad, 3-7 January, 2011.

Neeraj Srivastava

37. "Space Weathering", Workshop on Data Analysis of Chandrayaan- 1 Imaging Payloads: HySI and TMC, PRL and SAC, 28-30 November, 2010.

D. Banerjee

38. "Gamma ray spectrometer for Mars orbiter", AOGS Hyderabad, July, 2010.

39. "Estimation of dose-rates for Mariana hydrothermal sites and comparisons with laboratory measurements", 27th Workshop on ESR Applied Methodology, JAMSTEC, Yokohama, March, 2011.

40. "The effect of solar activity and compositional variations on the X-ray fluorescence signals from moon", 27th Workshop on ESR Applied Methodology, JAMSTEC, Yokohama, March, 2011.

J. Pabari

41. "Wireless Technologies and Application to Lunar Surface Science", STTP on 'Latest Wireless Technologies and Mobile Application Development' GEC, Bhavnagar, 17 January, 2011.

Y.B. Acharya

42. "Bharat Chandramaa ki aur" National Science workshop on Dharati Se Amber Tak, jointly organized by Sharda Vidya Mandir, Ahmedabad, INSA (Guj.) & PRL, 23 December, 2010.

43. "Space Instrumentation", Planex Workshop on Exploration of Mars and Moon, Physical Research Laboratory, Ahmedabad, 3-7 January, 2011.

44. "Gamma ray Spectrometer for a Mars Orbiter mission", Brain storming session on Mars Science and Exploration, Physical Research Laboratory, Ahmedabad, 24-25 March, 2011.

Space and Atmospheric Sciences

Y.B. Acharya

45. "Detection of Lightning in planetary atmospheres, International workshop on Advances in planetary atmosphere and exploration", 12-13 July, 2010.

B Bapat

46. "Spectroscopy of Unstable Molecular Ions " at UGC Sponsored National Conference on "Recent Trends in Theoretical and Experimental Physics", Vallabh Vidyanagar , 18-19 February, 2011.

D. Chakrabarty

47. "Investigations on the effects of interplanetary electric field and substorm on the low latitude ionosphere-thermosphere system", AOGS, Hyderabad, 5-9 July, 2010.

48. "On the coupling issues of low latitude ionosphere-thermosphere system during space weather events", Space Climate Symposium 4: Goa, India, 16-21 January, 2011.

Harish Chandra

49. "Mesospheric turbulence in the low latitude region studied using coordinated MST radar and rocket-

borne in-situ measurements", Advances in Atmospheric remote sensing, weather prediction & climate change, S V University, Tirupati, 10-11 March, 2011.

50. Invited talk in Hindi on "Ionospheric radio: developments in the 20th century, NARL, Gadanki, 16 March, 2011.

Lokesh Sahu

51. "Inter-comparison of BC measurements", Third Observatory Meeting of Project Atmospheric Brown Cloud (ABC) of United Nations Environment Programme (UNEP)", Asian Institute of Technology (AIT), Bangkok, Thailand, 22-23 October, 2010.

D. Pallamraju

52. "Optical techniques and observations" (2 lectures), the SERC School on Space Physics , IIG, Mumbai, April, 2010.

53. "Ionosphere – Thermosphere Interactions at High-Latitudes During Varying Geomagnetic Conditions", 7th annual Asia Oceania Geosciences Society (AOGS) Meeting, Hyderabad, 05-09 July, 2010.

54. "Wave Dynamics of Dayglow Emissions over Low-Latitudes", Recent Advances in Equatorial, Low- and Mid-Latitude Mesosphere, Thermosphere and Ionosphere Studies, 38th COSPAR Scientific Assembly, Bremen, Germany, 18 - 25 July, 2010.

55. "Optical signatures of Space Weather disturbances", National Workshop on Atmospheric and Space Sciences, S. K. Mitra Center for Research in Space Environment, Institute of Radio Physics and Electronics, Calcutta University, Kolkata, 23-24 November, 2010.

56. "Space weather effects in the Geospace", Seminar on Current Trends in Physics, Organizers: Indian National Science Academy Gujarat/Rajasthan Chapter and Physical Research Laboratory, 05 December, 2010.

57. "A brief overview of the CAWSES-India Programme", International Space Weather Initiative – India meeting, Indian Institute of Astrophysics, Bangalore, 25 March, 2011.

S. Ramachandran

58. "Black carbon aerosols: Radiative forcing and climate impact", 7th Annual Meeting of Asia Oceania Geosciences Society, Hyderabad, 5-9 July, 2010.

59. "Volcanic aerosols and Earth's climate", National workshop on Advances in Science of Climate Change and Indian Monsoon, Indian Institute of Tropical Meteorology, Pune, 31 August- 1 September, 2010.

60. "Ozone", International Ozone Day, Gujarat Science City, Ahmedabad, 16 September, 2010.

61. "Radiative forcing of aerosol species over urban region", International workshop on Impact of Asian megacity development on local to global climate change, Beijing, China, 10-12 October, 2010.

62. "Aerosol-climate: Challenges in measurements and modeling", NICES Action Plan Meeting, National Atmospheric Research Laboratory, Gadanki, 9 December, 2010.

63. "Global warming and air pollution", Teacher's workshop on Climate Change Science, Indian Centre for Climate and Societal Impacts Research, Ahmedabad, 29 January, 2011

64. Volcanic aerosols and Earth's climate, National workshop on Tropical Stratosphere-Troposphere: Implications on Indian Monsoon and Climate, Indian Institute of Tropical Meteorology, Pune, 31 January -1 February, 2011.

65. "Global warming and air pollution", Science Utsav 2011, Gujarat Science City, Ahmedabad, 1 March, 2011.

66. "Global warming, ozone and aerosols", One-day seminar on Astronomy, Astrophysics, Planetary and Space Sciences, Sardar Patel University, Vallabh Vidya Nagar, Anand, 2 March, 2011.

R. Sekar

67. "Recent coordinated observations and theoretical investigation on plasma irregularities from equatorial region", AOGS, Hyderabad, 5-9 July, 2010.

Shyam Lal

68. "Ozone and Trace Gases: Recent Results and Future Plans" in Indo US Workshop, CRRI, Delhi, 10-11 February, 2011.

69. "Transport Effects on the Distribution of Ozone in the Troposphere over the Marine Regions Surrounding India", SPARC Workshop, IITM, Pune, 31 January -1 February, 2011.

70. "Some Aspects of Missing Atmospheric Chemistry in India 3rd Review Meeting of ATCTM ISRO GBP IICT", Hyderabad, 24-25 January, 2011.

71. "Atmospheric Trace Gases and Aerosols: Their Role in a Atmospheric Chemistry and Radiation Budget", NPL, Delhi, 19 November, 2010.

72. "Physics of Climate Change" INSA meeting at PRL, Ahmedabad, 29 July, 2010.

K. P. Subramanian

73. "Production of complex molecules in interstellar ice: Study of molecular genesis" IUCAA sponsored workshop on 'Laboratory Astrophysics: Applications to Cosmic Dust', M G Science College, Ahmedabad, 12-13 November, 2010.

Varun Sheel

74. "Modeling the Changing Composition of the Atmosphere", NICES Meeting, NARL, Gadanki, 09 December, 2010.

75. "Atmospheric Chemistry: observational techniques & modeling and implications on global climate", seventh course on Satellite Meteorology & Global Climate, Space Application Centre, Ahmedabad, 29 December, 2010 - 3 January, 2011.

Geo-Sciences

M. G. Yadava

76. "Isotopic signatures of precipitation events and their climatic implications", National Seminar on Climate Change and its impact on water resources, at University Centre for Earth and Space Sciences University of Hyderabad, 8-9 November, 2010.

77. "Monsoon in the Indo-Gangetic belt during the last 10000 years: oxygen isotope evidence from spleothems",the XXXIV Indian Social Science Congress, at Gauhati University, Guwahati, 28 December, 2010.

78. "Residence time of Carbon in Indian Soils Inferred from Radiocarbon", National Seminar on Forest resources: Diversity, Utilization and Conservation, at University of Agriculture Sciences, Bengaluru, March, 2011.

Navin Juyal

79. "Climatic implication of Quaternary glaciations in Himalaya, Center for Glaciology", WIHG, Dehra Dun, 7 September, 2010.

80. "Late Quaternary climate variability in Himalayan Orogen: present status and future perspective", National Seminar on Late Quaternary geology of the Himalayan orogen and the foreland basins, at Department of Geology Lucknow University, Lucknow, 16 - 17 February, 2011.

R. Bhushan

81. "GEOTRACES – Indian Ocean Perspective" Workshop on "Advances in Science of Climate Change and Indian Monsoon" held at Indian Institute of Tropical Meteorology, Pune, during 31 August-01 September, 2010.

M. M. Sarin

82. "Atmospheric Science Challenging Issues"; DST-INSPIRE Camp, MS University - Vadodara, 30 June, 2010.

83. "Widespread chloride depletion in sea-salt aerosols over Bay of Bengal: Implication to climate forcing"; AOGS-2010, Hyderabad, 5 July, 2010.

84. "Atmospheric deposition of N, P and Fe to the northern Indian Ocean"; AOGS-2010, Hyderabad, 6 July, 2010.

85. "Climate forcing by anthropogenic aerosols"; Nat'l Meeting on "Science of Climate Change"; IITM-Pune, 31 August, 2010.

86. "Atmospheric Chemistry: Environment and Climate Change Issues"; DST-INSPIRE Camp, Kachchh University-Bhuj, 24 September, 2010.

87. "Toxic trace metals and Cl-depletion in marine aerosols over Tropical Bay of Bengal: Impact of continental outflow"; 5th Int'l DMS(P) Symposium, NIO-Goa, 20 October, 2010.

88. "Atmospheric Nano-particles: Potential Role in Chemistry-Climate Interaction"; Foundation-Day-IITM (Pune), 17 November, 2010.

89. "Atmospheric Chemistry and Environmental Change Issues"; DST-INSPIRE Camp, SVNIT-Surat, 21 December, 2010.

90. "Atmospheric Anthropogenic Carbon: Environmental Change Issues"; Indian Science Congress- SRM University, Chennai, 5 January, 2011.

91. "Atmospheric CO_2 and Nano-particles"; DST-INSPIRE Camp, MS University-Vadodara, 20 January, 2011.

92. "Is Ocean Fertilization Creditable – Sustainable Development, Issues & Concern"; NVPC-Vallabh Vidyanagar, 22 January, 2011.

R. Ramesh

93. "Applications of stable isotopes in oceanography" NAARRI International Conference on Isotope Technologies and applications- New Horizons, Dept. of Atomic Energy, Govt. of India, Mumbai,13-15 December, 2010.

94. "Climate Change and Ocean Productivity" Keynote address at the International Conference on Census of Marine Living Resources, Kochi, 2-3 December, 2010.

95. "Reconstructed long term solar activity from cosmogenic nuclides and its relation with proxy climatic records", AOGS Conference, Hyderabad, 5-9 July, 2010.

96. "Stable isotopes and salinity variation in the southern Indian Ocean", Conference on the Science and the Geopolitics of the Arctic and the Antarctic, New Delhi, 14-15 January, 2011.

97. "Paleomonsoon and solar activity" Space Climate Symposium IV, Goa, 16-21 January, 2011.

A. K. Singhvi

98. Keynote Inaugural address on the "Societal Dimensions of Geosciences", National Seminar on Basin of India, their resources and management, Chidambaram, 17-18 February, 2011.

99. "Societal dimensions of Geosciences",Wadia Institute of Himalayan Geology, Institute Colloquium,17 March, 2011.

100. "Luminescence and electron spin resonance dating and dosimetry: new -materials, -protocols, and – possibilities" the International Solid State Dosimetry Congress, Sydney, 19-24 August, 2010.

101. "Luminescence Dating of Fluvial Archives: New Methodological Aspects", International Fluvial Archives group meeting in Portugal, 4-12 September, 2010.

102. "Luminescence dating in Paleoseismology and Neotectonics: An overview":International seminar on seismology, Institute of Seismological Research, 24-26 January, 2011

103. "Luminescence and Electron Spin Resonance Studies at Ahmedabad", Leibnitz Pact International Seminar, Geowissenschaften Institute, Hannover, Germany, 26-28 October, 2010.

S. K. Singh

104. "Erosion and weathering in the Ganga-Brahmaputra System: Contribution to geochemical and sedimentary budgets of the Bay of Bengal and the Arabian Sea" in Indo-French Workshop on "Deep Earth processes- interactions between solid, fluid earth and environment" at Mahabalipuram (Chennai), India, 1-5 February, 2011.

105. "Isotope Studies in Groundwater" in refresher training course on Application of Geophysical techniques in groundwater exploration and management at Rajiv Gandhi National Ground Water Training and Research Institute, Raipur, 2-13 August, 2010.

Theoretical Physics

R. P. Singh

106. "Dynamic light scattering of optical vortices", XXXV OSI Symposium- International Conference on Contemporary Trends in Optics and Optoelectronics, at IIST Thiruvananthapuram, India, 17-19 January, 2011.

107. "Photon correlation spectroscopy: Gaussian beam vs. optical vortices", International Conference on Quantum Optics and Quantum Computing (ICQOQC-11), Department of Physics and Material Science & Engineering, Jaypee Institute of Information Technology, Noida , India, 24-26 March, 2011.

B.K. Sahoo

108. "Status of the theory for atomic parity violation", International workshop on "Violations of Discrete Symmetries in Atoms and Nuclei", European Centre for Theoretical Studies in Nuclear Physics and Related Areas (ECT*), Trento, Italy, 15-19 November, 2010.

109. "Correlation studies in the estimation of isotope shifts and fine structure constant variation parameters", XVIIIth National conference on Atomic and Molecular physics held as "2nd DAE-BRNS Symposium on Atomic, Molecular and Optical Physics (SAMOP-2011)", Karnataka University, Dharwad, 22- 25 February, 2011.

V. K. B. Kota

110. "Two-body random matrix ensembles for quantum many-body chaos", Workshop on "Quantum Chaos and Quantum Information", IIT Madras, Chennai, 18-25 July, 2010.

111. "Spectral distribution theory for nuclear structure: Past and future", Symposium on "Neutrino Physics and Nuclear Physics", SINP, Kolkata, 27 August, 2010.

112. "Chaos in nuclei and random matrix theory", Interaction meeting on "Theoretical Nuclear Physics", IIT, Roorkee, 3-5 September, 2010.

Manan Vyas

113. "Two-body random matrix ensembles: Monte-Carlo results", National conference on "Computational Techniques in Physics", M.S. University of Baroda, Vadodara, 1-2 February, 2011.

P. C. Srivastava

114. "Large scale shell model study of fp-shell nuclei" Symposium on "Cutting-edge Physics of Unstable Nuclei", Aizu-Wakamatsu, Japan, 10-14 November, 2010.

H. M. Mishra

115. "Kinetics of chiral phase transitions in quark matter", Conference on Quantum Chromodynamics and Beyond, International center for Theoretical Physics (ICTP), Trieste, Italy,

116. "Domain growth in Chiral phase transition", Conference on "Extreme QCD", Bad Honnef, Germany, June, 2010.

117. "Domain growth and ordering kinetics in dense quark matter", International Conference on "Critical Point and Onset of Deconfinement 2010" (CPOD2010), the Joint Institute for Nuclear Research (JINR), Dubna, Russia, 23-28 August, 2010.

Raghavan Rangarajan

118. "Non-Gaussian fluctuations of the inflaton and constancy of correlations of zeta outside the horizon", PFNG 2010 (Primordial Features and Non-Gaussianities), HRI, Allahabad, 14-18 December, 2010.

J. Banerji

119. "Generation of Schrödinger cats and sub-Planck structures in quantum states of light", XXXV OSI Symposium- International Conference on Contemporary Trends in Optics and Optoelectronics, IIST Thiruvananthapuram, 17-19 January, 2011.

120. "Formation of Schrödinger cats and kittens in a Kerr medium: a simple, unified and analytical recipe", International Conference on Quantum Optics and Quantum Computing (ICQOQC-11), Department of Physics and material Science & Engineering, Jaypee Institute of Information Technology, Noida, 24-26 March, 2011.

Navinder Singh

121. "The dynamical and statistical foundations of statistical mechanics" , 2nd Stellenbosch Workshop on Statistical Physics- "Equilibration and Equilibrium", National Institute for Theoretical Physics, Wallenberg Research Centre, Stellenbosch, South Africa, 7-18 March, 2011.

S. D. Rindani

122. "Top and Higgs physics at the LHC", course of lectures at the XXV SERC School on Theoretical High Energy Physics, Chandigarh, April, 2010.

123. "Physics potential of a future e^+e^- collider", Workshop on Synergy between High Energy and High Luminosity, TIFR Mumbai,10-12 January, 2011.

A. S. Joshipura

124. "Mass models & CP violation", Plenary talk at the 12th Int.Workshop on Neutrino Factories, Supermbeams and Betabeams, Mumbai, 20-25 October, 2010.

125. "Pathways to Grand unification",Invited lecture in Frontiers in High Energy Physics, Lecture Series in celebration of 75th Birthday of Prof. G. Rajasekaran, Inst. Of. Mathematical Sciences, Chennai, February, 2011.

126. "Neutrinos: Theoretical status", Plenary talk at DAE-BRNS High Energy Physics Symposium, Jaipur, 13-18 December, 2010.

D. Angom

127. "Dynamics of vortex dipoles in binary condensates", National Conference Nonlinear Systems and Dynamics, Bharathidasan University, Tiruchirapalli, 27-30 January, 2011.

128. "Atomic many-body theories" (seven lectures), DST-SERC School on atomic and molecular physics hosted by BITS, Pilani, 10-28 January, 2011.

129. "Position swapping and pinching in Bose-Fermi mixtures", Conference on Research Frontiers in Ultra Cold Atomic and Molecular Gases, International Conference organized by ICTP at Goa,10-14 January, 2011.

130. "HPC in PRL: from climate models to particle physics", International Conference on Meta Computing, NIO, Goa, 15-18 December, 2010.

131. "Computational aspects: numerical solutions of GP equation", National Workshop on Computational Methods for Nonlinear Dynamics, Bharathidasan University, Thiruchirapalli, 22-24 September, 2010.

132. "Dynamics of condensates with external purturbations", National Conference on Computational Methods for Nonlinear Dynamics, Bharathidasan University, Thiruchirapalli, 25 September, 2010.

133. "HPC in precision atomic calculations", Workshop on high performance computing, IUAC, Delhi, 27-28 April, 2010.

Partha Konar

134. "Mass measurements at the LHC with missing particle", "Discussion meeting on Physics at early run of the LHC", Association for the Cultivation of Science, Kolkata, 22 - 23 March, 2011.

135. "Mass reconstruction at the LHC","Dark Matter in the LHC Era", SINP, Kolkata, 4 - 8 January, 2011.

136. "Beyond Standard Model Physics", Plenary talk at "XIX DAE-BRNS High Energy Physics Symposium", Jaipur, 13 - 18 December, 2010.

Srubabati Goswami

137. "2540 km: Bimagic baseline for Neutrino Oscillation Parameters", Working Group Talk, NuFACT-2010, TIFR, October, 2010.

138. "Renormalization Group Effects and Large 1-3 Mixing", Working Group Talk, PASCOS 2010, Valencia, Spain, July, 2010.

139. "Probing the Neutrino Mass Matrix", Invited Talk in the meeting to celebrate 25th year of THEP SERC School, Indian Instiute of Technology, Mumbai, May, 2010.

Subhendra Mohanty

140. "Sommerfeld effect in Dark Matter Signals", at the International Workshop on "Dark Matter in the LHC Era: Direct and Indirect Searches", SINP, Kolkata, 4-8 January, 2011.

141. "Dark Matter", at the 29th meeting of the Astronomical Society of India, Pt. Ravishankar Shukla University, Raipur, 23-25 February, 2011.

Ketan M. Patel

142. "Fermion Masses in Supersymmetric SO(10)", talk at the XXV SERC School on Theoretical High Energy Physics, Chandigardh, 2-22 April, 2010 .

143. "Quasi-degenerate Neutrinos in SO(10)" talk at the 12th Int. Workshop on Neutrino Factories, Supermbeams and Betabeams, Mumbai, 20-25 October, 2010 .

144. "Fermion Masses and Mixing in Non-supersymmetric SO(10)" talk at the XIX DAE BRNS High Energy

Physics Symposium, Jaipur, 13-18 December, 2010

145. "An Origin of Quark-Lepton Complementarity in SO(10) Model with Flavor Symmetry" talk at the XIX DAE BRNS High Energy Physics Symposium, Jaipur 13-18 December, 2010.

146. "Neutrino Masses and Mixing in Non-supersymmetric SO(10)" talk at the NuHoRIzons-IV, Int. Conference on Neutrinos in Particle and Astroparticle Physics, Allahabad, 23-25 February, 2011.

Lectures at Universities / Institutions

Astronomy and Astrophysics

Hari Om Vats

1. "Interactive science education" (Hindi), Sarasvati High School Telnar (Gujarat), 24 April, 2010.

2. "Observations: The pathway to learn" (Hindi), Teacher's training workshop on Astronomy, Kevadia colony, district Narmada, 28 June, 2010.

3. "Solar coronal rotation by different observations", Space Physics Seminar, University of California, Los Angeles USA, 27 August, 2010.

4. "Estimation of solar coronal rotation by flux modulation", University of California, Berkeley, 7 September, 2010.

5. "The complex nature of solar coronal rotation", Colloquium at NCAR, High Altitude Observatory Boulder, 8 September, 2010.

6. "Multi-Wavelength Measurements of Coronal Rotation", Colloquium at National Solar Observatory, Tucson, 15 September, 2010.

7. "Coronal rotation from Radio and X-ray images of the Sun", Lockheed Martin SAL Palo Alto, 23 September 2010.

8. "IMF and solar rotation", Wilson Solar Observatory, Stanford University, 4 October, 2010.

9. "Differential Solar Rotation", National Seminar on "Solar activity and cosmic ray modulation" G A PG College, Satna, 10 October, 2010.

10. "The Sun and solar phenomena", Bhavan's College Ahmedabad, 5 December 2010.

11. "Solar coronal rotation", Radio Astronomy Centre, Ootacamund, 20 December, 2010.

12. "Differential rotation of the solar corona", Colloquium at National Centre for Radio Astrophysics, Pune, 07 February, 2011.

13. "Measurements of solar rotation from the near Earth observations of the interplanetary magnetic field (IMF)", National Conference on Recent Trends in Theoretical and Experimental Physics (NCRTTEP-2011) VP & RTP science college Vallabh Vidyanagar, 19 February, 2011.

14. "Asymmetry in the solar coronal rotation" (Hindi), Technical seminar in Hindi on PRL scientific and technical programs in the international perspective, PRL Ahmedabad, 18 March, 2011.

A. K. Singal

15. "A principle of partial coherence in a synchrotron source", colloquium in NCRA, TIFR, Pune, 22 October, 2010.

16. "Coherence inherent in an incoherent synchrotron radio source", RRI, Bangalore, 1 March, 2011.

17. "A principle of partial coherence in a synchrotron source", PRL colloquium 17 March, 2011.

Rajmal Jain

18. "X-ray emission from Solar Flares", colloquium at Mullard Space Science Laboratory (MSSL), UK, 20 September, 2010.

S. Ganesh

19. "Workshop on Laborator Astrophysics:Applications to Cosmic Dust", M. G. Science Institute, Ahmedabad, 12-13 November, 2010.

U. C. Joshi

20. "Workshop on Laboratory Astrophysics: Applications to Cosmic Dust", M. G. Science Institute, Ahmedabad, 12-13 November, 2010.

Solar Physics

Ashok Ambastha

21. A popular lecture on "Udaipur Solar Observatory – Past, Present and future", Vidya Bhavan Senior Secondary School, Udaipur, 22 October, 2010.

22. A popular lecture on "The Life of a Star", Vivekananda Kendra Vidhyalaya, Gulabpura, Bhilwara, 25 October, 2010.

23. A Radio talk/interview on "Facts and Myths of Solar Eclipses - Partial eclipse of 4th Jan 2011", Lake City 101 FM, 4 January, 2011.

24. PRL Colloquium on "Solar Oscillations on Global and Local Scales: Probing the Sun's Interior and the Sub-Surface Weather", 29 December, 2010.

Nandita Srivastava

25. "Coronal mass ejections (ii) Space Weather Prediction: Solar Perspective (iii) Use of statistical models for predicting geo-effective events", (three lectures), SERC School on Space Weather, IIG Mumbai, 7-27 April, 2010.

26. "Automated Detection of Filaments and Their Disappearance Using Full-Disc H-alpha Images", Solar-Terrestrial Centre of Excellence, Royal Observatory of Belgium, Brussels, 28 April, 2010.

27. "Solar Activity, Terrestrial Influences and Space Weather", M.Tech course, UN school, Ahmedabad, 4, August, 2010.

Brajesh Kumar

28. "Evidence of correlation between flare induced local and global oscillations in the Sun" at Service d' Astrophysique, CEA-Saclay, France, 5 July, 2010.

Bhuwan Joshi

29. "Evolution of X-ray sources and magnetic reconnection in solar eruptive flares", 38th COSPAR scientific assembly, Bremen, Germany,18-25 July, 2010.

Ram Ajor Maurya

30. A seminar on "Seismic Study of Solar Active Regions using Ring Diagrams", Indian Institute of Astrophysics, India, 25 November, 2010.

31. Popular Lecture on "Probing the Interior of the Sun using Sound Waves", at Vivekanand Kendra Vidyalaya, Hurda, Rajastha, India, 25 October, 2010.

32. A talk on "Active Region Seismology Using Ring Diagram Analysis" at MPS, Lindau, Germany on 8 July, 2010.

33. A talk on "Active Region Seismology Using Ring Diagram Analysis" at Institut d'Astrophysiqu Spatiale, Orsay, France, 5 July, 2010.

Vema Reddy

34. A Seminar on "Solar magnetic Field Extrapolations", in SERC School "Astronomy & Astrophysics", NCRA-TIFR, Pune, 2 July, 2010.

Planetary Sciences and PLANEX Program

S.V.S. Murty

35. "PLANEX & Planetary Exploration Program of ISRO", in the Physics Department Calicut University, Kerala, 19 March, 2011.

36. "Exploration of Solar System" NGENIUM-2011, Nirma University, Ahmedabad, 29 March, 2011.

Vinai Kumar Rai

37. Four lecture Planetary Science Courses given to M.Sc. Geology final year students at Banaras Hindu University, Varanas, 30-31 October, 2010.

Space and Atmospheric Sciences

B. Bapat

38. "Molecular Fragmentation Studies at Indus-1", BHU, Varanasi, October, 2010.

39. "Recoil Ion Momentum Spectroscopy", BHU, Varanasi, October, 2010.

40. "Spectroscopy of Unstable Molecular Ions", IISER Mohali, March, 2011.

S. P. Gupta

41. Equatorial Geophysical Research Laboratory (IIG),Tirunelveli, 22-24 February, 2011.

    i. Balloon measurements of stratospheric conductivity from Hyderabad: Long term changes.

    ii. Nature of E region irregularities at magnetic quator and six degree north of magnetic equator: rocket borne results.

    iii. Meteor induced irregularities over low latitude, rocket and MST radar borne results.

Harish Chandra

42. Course on Space Sciences: 65 lectures to 8th CSSTEAP at PRL, August-October, 2010.

43. 13 lectures on ionosphere and radio techniques at Gujarat University, September-November, 2010.

44. 15 lectures on ionosphere at Dibrugarh University, 22 February-2 March, 2011.

45. "Space weather", SV University, Tirupati, 17 March, 2011.

R. Sekar

46. Series of lectures were given on "Ionospheric irregularities" in SERC school on space weather conducted at Indian Institute of Geomagnetism, 7-27 April, 2010.

47. "Importance of narrow band and narrow field of view photometry in the investigation of ionosphere-thermosphere system", Saurashtra University, Rajkot on 29 October, 2010.

H. S. S. Sinha

48. "In situ techniques on space platforms and basic space technology", (46 Lectures), 8th Course in Space and Atmospheric Sciences of CSSTEAP organized by PRL, Ahmedabad, August-September, 2010.

K . P. Subramanian

49. "A New Dimension to Being Dimensionless", Calicut Uni., May, 2010.

Varun Sheel

50. "Elements of Climate: Earth System & Atmosphere; Atmospheric Chemistry; Greenhouse Gases", as part of the M.Sc. course on Climate Change Impacts Management, Gujarat University and Centre for Environment and Education, Ahmedabad, January, 2010.

D. Pallamraju

51. "Space Weather effects in the Sun-Earth environment". An introductory seminar on

Astronomy, Astrophysics and Planetary Space Sciences, Sardar Patel University, Vallabh Vidyanagar, 02 March, 2010.

52. "Signatures of Space Weather disturbances in the upper atmosphere", Solar Dynamical Processes as drivers of Space Weather, Indian Institute of Astrophysics, Bangalore, 25 March, 2011.

S. Ramachandran

53. "Global warming and air pollution", Rotary Club, Ahmedabad, 3 August, 2010.

Geo-Sciences

S. Krishnaswami

54. "Natural Radionuclides in Aqueous Systems: Tracing and Timing Biogeochemical processes and Particle Dynamics", IIT, Kharagpur, March, 2011.

R. Ramesh

55. "Climate Change- Satellite Perspective", IMSA workshop on satellite Meteorology: 50 year Journey, Space applications centre, Ahmedabad, 29 October, 2010.

56. "Applications of Stable Isotopes in Paleoclimatology" SERC school on Global Warming and Climate Change at IITM, Pune, 06 December, 2010.

57. "Reconstructions of paleomonsoon" National Workshop on Advances in Science of Climate Change and Indian Monsoon, IITM, Pune, 01 September, 2010.

58. "How much of the recent climate change can be attributed to the sun?", National Centre for Antarctic and Ocean Research, Goa, Hyderabad, 17 May, 2010.

59. "Advanced course on Statistics" 15 lectures at the National Centre for Antarctic and Ocean Research, Goa, 13-17 September, 2010.

60. "Paleoclimatology" Four lectures at the CSSTEAP, SAC, Ahmedabad, 3-6 January, 2011.

61. "Oceanography as an exciting branch of science" INSPIRE programme of DST, M.S. University of Baroda, Vadodara, 30 June, 2010.

62. "Research Methodology" four lectures at the University of Hyderabad, Hyderabad, 3-6 January, 2011.

63. "Tree rings and climate: new results" TIFR National Centre for Biological Sciences, Bangalore, 2 July, 2010.

64. "New production in the Indian Ocean", National Institute of Oceanography Regional Centre, Kochi, 5 May, 2010.

65. "How are Isotopes useful in detecting climate change?" Refresher Course in Environmental Science, Goa University, Goa, 19 December, 2010.

M. G. Yadava

66. "Monsoon reconstruction using spleothems" at the Teacher's workshop on Climate Change Science, at Indian Centre for Climate and Societal Impacts Research (ICCSIR), Ahmedabad, January, 2011.

R. Bhushan

67. "Radiocarbon Measurements in the Arabian Sea and the Bay of Bengal : Implications to Ocean Circulation and Air-Sea CO_2 Exchange Rates" in the Department of Marine Inorganic Chemistry, Atmospheric and Ocean Research Institute (AORI), University of Tokyo, Tokyo, 21 October, 2010.

68. "Trace Elements in the Sea: GEOTRACES Indian Perspective" at Institute for Chemical Research, Kyoto University, Kyoto, Japan, 09 November, 2010.

69. "Paleoclimatic records from the Bay of Bengal sediments" in the Department of Marine Inorganic Chemistry, Atmospheric and Ocean Research Institute (AORI), University of Tokyo, Tokyo, 23 November, 2010.

R. D. Deshpande

70. "Isotope Fingerprinting of Indian Hydrological Cycle", Institute of Environmental Physics (IUP), University of Heidelberg, Germany, 25 November, 2010.

71. "Water Resources of India: Challenges and Solutions", Sanskar Dham, Ahmedabad, 12 September, 2010.

72. "Water Resources of India: Threat, Challenges and Solutions", Sharda Mandir, Ahmedabad, 23 December, 2010.

73. "Chemistry of Water: Challenges and Solutions", National Science Day Theme Lecture, PRL, Ahmedabad 26 February, 2011.

Theoretical Physics

A. C. Das

74. "Introduction to Solar Physics, Magnetospheric Physics and Space Weather", (50 Lectures), Seventh post-graduate course in Space and Atmospheric Sciences of CSSTEAP, PRL, Ahmedabad, August, 2010 - February, 2011.

75. "Solar-Terrestrial Relation and Space Weather" (10 Lectures), part of a course on Advanced P.G diploma in Geo-informatics and Satellite Communication, Gujarat University, 2-24 December, 2010.

76. "The Sun and its Interaction with Earth's Magnetosphere" (20 Lectures), Centre of Atmospheric Studies, Physics Department, Dibrugarh University, Assam, 3-17 March, 2011.

H. Mishra

77. "Lectures on Quantum Field Theory", Six lectures given at Academic staff College, Sambalpur University, December, 2010.

Raghavan Rangarajan

78. "Reheating of the Universe, Gravitinos and Leptogenesis", Institute for the Early Universe, Ehwa Womens University, Seoul, S. Korea, 24 September, 2010.

79. "Cosmology - The Story of our Universe", 8-hour course given at the Indian Institute of Technology, Gandhinagar, August - September, 2010.

80. "Exploring the Fundamental Particles in the Universe", Christ College, Rajkot, 20 July, 2010.

81. "A Career as a Physicist", Christ College, Rajkot, 20 July, 2010.

S. D. Rindani

82. "Polarization as a tool for learning new physics", Theoretical Physics Colloquium at TIFR, Mumbai, 25 May, 2010.

83. "Probing new physics at an e^+e^- collider with polarized beams", seminar at the Helsinki Institute of Physics, Helsinki, 21 September, 2010.

84. "Probing new physics at an e^+e^- collider with polarized beams", seminar at the Centre for High Energy Physics, Indian Institute of Science, Bangalore, 23 December, 2010.

D. Angom

85. "Ground state structure and dynamical instabilities in mixtures of quantum gases", Indian Institute of Science Education and Research, Pune, 25 March, 2011.

86. "Coupled-cluster calculations in atomic systems", Indian Institute of Science Education and Research, Pune, 25 March, 2011.

Utpal Sarkar

87. "Neutrino Condensate Dark Energy", Physics Department, Washington University in St. Louis, USA, 24 February, 2011.

Partha Konar

88. "The Invisible side of Universe", Public talk for Dark Matter Awareness Week at Gujarat Science City, 03 December, 2010.

Srubabati Goswami

89. "Probing the Neutrino Mass Matrix", Max Planck Institute, Heidelberg, July, 2010.

90. "Probing the Neutrino Mass Matrix" Indian Association for the Cultivation of Sciences, June, 2010.

R. P. Singh

91. "Optical vortices: An introduction", Department of Physics, IIT Guwahati, India, 19 May, 2010.

SCIENCE

Astronomy and Astrophysics

The Astronomy and Astrophysics Division is engaged in research covering a wide spectrum of topics such as explosive events like novae, massive star formation regions, variability of distant active galactic nuclei, galactic X-ray binary systems, solar X-rays etc. The division is also actively involved in developing new instruments both for the optical/infrared observations from Mt. Abu Observatory as well as satellite based experiments for X-ray astronomy. A sophisticated Echelle spectrograph PRL Advanced Radial velocity All-sky Search (PARAS) for detection of exo-planets has been recently commissioned at Mt. Abu Observatory. A small 20 inch telescope has been setup at the observatory for continuous study of AGN variability as well as for study of exoplanet transits and other transient events like GRB afterglows. A new study of deep imaging of high Z radio galaxies at 150 MHz using GMRT has been initiated in collaboration with NCRA.

Recurrent Nova U Scorpii

Cataclysmic variables with multiple nova outbursts in a human lifetime are known as recurrent novae (RNe). These outbursts are the product of thermonuclear runaway in the accreted material on the surface of the white dwarf (WD). The outburst mechanism is identical to that of classical novae, but the presence of a high-mass WD (mass $\geq$1.3 $M_{\odot}$) and a high accretion rate cause the short recurrence timescale. RNe, of which only 10 are known in our galaxy, are special because they are strong progenitor candidates of a class of objects which are vitally important cosmologically viz. Type Ia supernovae.

The well-known RN U Scorpii underwent its most recent eruption in 2010 which was studied in an extensive global effort across all wavelengths. The present eruption was preceded by at least six previous outbursts between 1863 and 1999. We obtained the IR light curve and recorded several spectra, starting as early as 0.59 days after outburst which is unprecedented in the IR, to derive physical parameters of the system and record the IR evolution of the nova. A peculiarity of the spectra is the presence of very broad wings in several spectral lines, with tails extending up to 10,000 km/s along the line of sight. It is unexpected to have a nova with ejection velocities equal to those usually thought to be exclusive to supernovae.

(D.P.K. Banerjee, N.M. Ashok and R.K. Das)

Nova like outburst of Synbiotic Mira Variable V407 Cyg

Symbiotic novae are eruptive variable stars that exhibit nova like outbursts. The symbiotic variable V407 Cygni consists of a white dwarf (WD) accreting material from an oxygen rich cool Mira variable pulsating with a 745 day period. Though V407 Cyg had shown brightening in 1936 and 1990, the nature of these outbursts was not clear. The 2010 outburst discovered on March 10.8 UT by Nishiyama and Kabashima was spectacular with V407 Cyg

reaching a brightness of V = 7.6 magnitude Realizing the peculiarity and importance of this outburst, we extensively studied infrared and optical wavelengths. This outburst was also studied at other wavelengths like gamma rays and radio by other international groups.

The IR spectra taken from 1.2m telescope at Mt. Abu show prominent hydrogen recombination lines from the Paschen and Brackett series. In addition He I and O I lines are also present. These observations clearly show that the 2010 outburst is caused by a thermonuclear runaway similar to the nova outburst. Interestingly in the earlier phases of the outburst the emission line profiles are dominated by a strong narrow component superposed on a weak broader component. The broad component with a large starting velocity of around 1800 km/s slowed down as the ejected material from the nova outburst swept the existing material from the stellar wind from the Mira companion.

The 2010 outburst of V407 Cyg is similar to the 2006 outburst of recurrent nova RS Oph that was studied by our group. The observed features are very similar to a fast He/N nova erupting on a massive white dwarf in a dense surrounding medium resulting from stellar wind of the cool Mira companion.

This work was done in collaboration with U.Munari at INAF Astronomical Observatory of Padova, Italy.

(Vishal H Joshi, N.M.Ashok and D.P.K.Banerjee)

PRL Echelle Spectrograph (PARAS) at Mt. Abu Observatory

We have started at PRL an exoplanet program using the technique of precision Doppler radial-velocity measurements. We have designed and built an optical fiber fed high-resolution Echelle spectrograph. The project has been acronym as PARAS, which stands for PRL Advanced Radial-velocity All-sky Search for detection/confirmation and characterization of exoplanets.

The heart of the PARAS project is an optical fiber-fed high resolution cross-dispersed Echelle Spectrograph. It is capable of a single-shot spectral coverage of 3700Å to 8600Å at R ~ 63,000 and is under very stable conditions of temperature (0.04°C at 23°C). It can be also under pressure control of 0.1mbar, which is achieved by enclosing the entire spectrograph in a low-pressure vacuum chamber. It is attached to the Mt. Abu 1.2m telescope using two 50micron core optical fibers (one for the star and another for simultaneous Th-Ar spectral calibration).

After the spectrograph saw the first star-light in April 2010, we began our engineering verifications of various parameters namely the efficiency and the stability of the spectrograph. Figure 1 shows spectra of a 7th magnitude star along with the simultaneous reference technique.

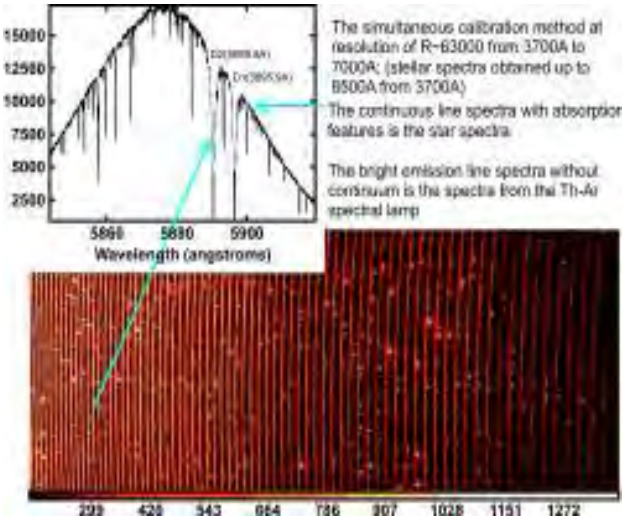

Figure 1: Spectra of a 7th magnitude star along with calibration lines (emission lines) from the Thorium-Argon spectral lamp. The inset shows the sodium D1, D2 lines extracted from one particular order from the star spectra. On an average each spectral order covers about 75Å of spectra.

From the slit position to the detector at blaze peak on every Echelle order spectrograph is about 30% efficient which is one of the most efficient among competitive spectrographs around the world. If we include the fiber optics throughput and FRD, and the telescope efficiency, the total efficiency is about ~15% with ~1.5 arcsec seeing or better and under photometric sky conditions. Thus, we can obtain S/N of about 45 on a 9th magnitude star in ~15 minutes of exposure under even poor seeing say 2 arcsec. The RV survey limit is therefore up to 9th magnitude stars under poor sky conditions, and up to 10th magnitude under good sky and photometric conditions.

We measure the stability of the spectrograph using the simultaneous reference technique with the Thorium-argon spectral lamp (Figure 1). Since the spectrograph is inside a stable environment of ± 0.05^{o}C at say 27^{o}C and also if required under pressure control, we have observed absolute drift of not more than 30m/s in terms of radial velocity (RV) during the night of observations and by referencing with respect to the Thorium-Argon fiber simultaneously, this absolute drift have been taken care of down to a level of 2m/s and this defines the intrinsic stability of the spectrograph under temp. control of ± 0.05^{o}C. However, under the temperature control of ± 0.1^{o}C the intrinsic stability is worsens to about 4m/s to 5m/s. Thus the spectrograph is very sensitive to temperature control, and so we maintain it as close as possible to ± 0.05^{o}C at 27^{o}C (Figure 2).

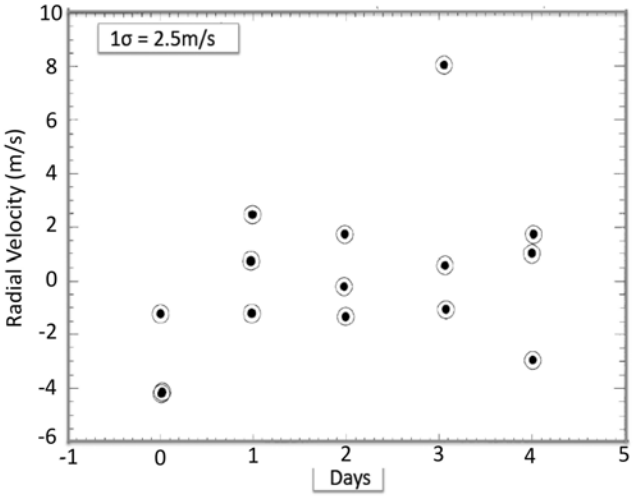

Figure 2: Radial Velocity precision measured on the sky over a period of 5 to 6 days of time-line under temperature control alone. The stability was measured observing a very stable Radial-Velocity standard star.

Currently on the sky PARAS can have Radial-Velocity precision of about 2 to 3m/s at best on stars brighter than 7th magnitude with S/N ~100 or higher and 5 to10m/s on fainter stars up to 10th magnitude for signal to noise ratio of 30 or higher. We have achieved such stability under temperature control alone and over a time-line of 5 to 6 days. In the near future we will be having the spectrograph under pressure control also along with temperature control and then we expect to achieve similar stability over a longer period of time up to several months or a year time. Thus such long term stability will give us ability to detect Neptunes on bright stars and Jupiters and Saturns on fainter targets.

(Abhijit Chakraborty)

Infrared photometric study of the massive star forming region S235 using Spitzer-IRAC and JHK observations

S235 complex is known to be a site of triggered star formation due to the expansion of HII regions. We present the Spitzer-IRAC images and IRAC ratio maps of the S235 star forming complex. In addition, we present the Mt. Abu near-infrared images of the two HII regions in the complex, called S235A & S235B. The IRA photometry reveals on-going star formation, with 86 Class 0/I and 144 Class II Young Stelar Objects (YSOs) in the entire S235 complex. We have identified a new young protostar "e2s3" in the region passing through its accretion phase. The IRAC ratio map of Ch2/Ch4 reveals that the source "e2s3" may be associated with shock-excited molecular hydrogen emission outflow. The Spectral Energy Distribution (SED) modeling of this new source indicates that it is a very young massive star that is not yet able to drive an HII region. A few young stellar objects (YSOs), possibly in an arc-like formation, are identified towards the south of S235A in the S235A-B region, which may be an evidence for magnetically super-critical collapse. One of the sources in the arc-like formation, namely S235AB-MIR, seems to be a young, massive star that is still accreting matter. The IRAC ratio map of Ch2/Ch4 traces clearly the Brackett alpha emission associated with the HII region of S235A within the horse-shoe envelope. Outside the horse-shoe structure, the ratio map indicates shock-excited molecular hydrogen emission.

(L. K. Dewangan, B. G. Anandarao)

Angular Diameters of Miras and Semi-regular variables from Lunar Occultations in the near Infrared

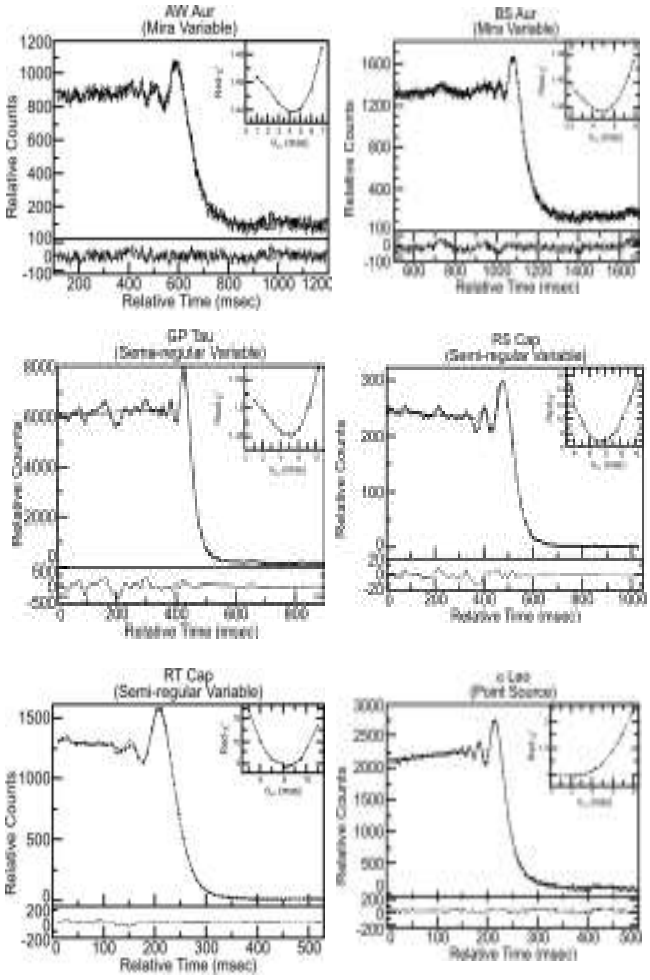

Figure 3: Infrared Lunar Occultation light curves of two Miras and three semi-regular variables along with that of a calibration point source are shown. All five sources are well resolved. Inset in each light curve depicts the error curve the minima of which are used to derive the angular size. The limit of resolution as given by the point source error curve is about 2.5 milliarcseconds (mas). Residuals (Data - model) are given at the bottom of each light curve.

Asymptotic Giant Branch (AGB) stars which include Miras and semi-regular variables are highly evolved cool stars in the final stages of stellar evolution before turning into Planetary nebulae. They are characterized by high mass loss rates and relatively low surface temperatures and very extended atmospheres. A common feature of AGB stars is the variability of their radiative output mainly due to pulsation of their atmospheres. High angular resolution measurements of these stars leading to angular diameters provide an important means of understanding their atmospheric extension and pulsation properties. Using the lunar occultation technique in the broad K band at 2.2 microns at the I.2m telescope at Mt. Abu we report the observations of two Miras (AW Aur and BS Aur), three semi-regular variables (SRb) (GP Tau, RS Cap and RT Cap). The observations were taken with either the single channel InSb photometer or in the fast subarray mode of NICMOS IR camera. Detailed modeling of the occultation light curves (Figure 3) has resulted in the determination of the following uniform disk (UD) K band angular diameters in units of milli arcseconds(mas) : 4.33 ± 0.46 mas (AW Aur); 5.00 ± 0.70 mas (BS Aur); 4.85 ± 0.50 mas (GP Tau); 7.70 ± 0.50 mas (RS Cap) and 8.14 ± 0.50 mas (RT Cap). For the two Miras and GP Tau these are the first reported angular sizes while for RS Cap and RT Cap our values are in good agreement with earlier reported angular diameters in the K band.

(Tapas Baug and T. Chandrasekhar)

Study of variability in Blazars

Blazars, a subclass of active galactic nuclei (AGNs) which are seen at a small angle to the relativistic jet emanating from close to black hole, make interesting set of objects to study AGN emission mechanisms and jet structure. Since the central engine is too compact to be spatially resolved, variability in total intensity and polarized flux is used as a tool to probe its structure and properties. With this aim, we monitored a sample of blazars in optical and near-IR using optical CCD (1296x1152 pixels) and polarimeter (PRLPOL) mounted on the 1.2m telescope at Mt. Abu Infrared Observatory. Since blazars time scales - vary ranging from years to minutes, apart from long term monitoring, fast sampling is required to detect micro variations with time scales of few tens of minutes. The shortest timescale of variation provides upper limits on the size of the emission region. Some interesting results from blazar monitoring are; rapid variations in the flux of PKS0716+71, intra- and inter-night photopolarimetric variations in Wcom etc. CGRaBS J0211+1051, a source which flared in gamma-rays during Jan 2011, was simultaneously observed in optical polarization (1.2m telescope) and optical flux (50 cm ATVS), was found to have high degree of polarization (upto 21%) with increased brightness. These were first detailed observations of this source categorizing it as low energy peaked blazar (LBL).

(K S Baliyan, S Chandra, S Ganesh, U C Joshi)

Rapid optical variations in PKS0716+71: estimating mass of the black-hole

Rapid optical variability was noticed in the blazar S5 0716+71 during 2010 March 08-10 & 19-20 in the CCD observations made from the Mt. Abu Infrared Observatory. The light curves are constructed for the duration longer than 3-hours each night, with very high temporal resolution (~45 seconds in R-band). During 2010 March 08 the source smoothly decayed by about 0.15 mag in 2.88 hours, apart from a fast flicker lasting about 30 mins. S5 0716+71 brightened up during March 09 and 10 showing high activity while it was relatively faint (> 14 mag in R) albeit variable during March 19-20. March 9 & 10 light curves show rapid flickerings in the intensity modulating the intra-night (~3 hours) variation (Figure 4). The present observations suggest that the blazar S5 0716+71 showed night-to-night and intra-night variability at various time scales with 100% duty cycle for variation along with micro variability at significant levels.

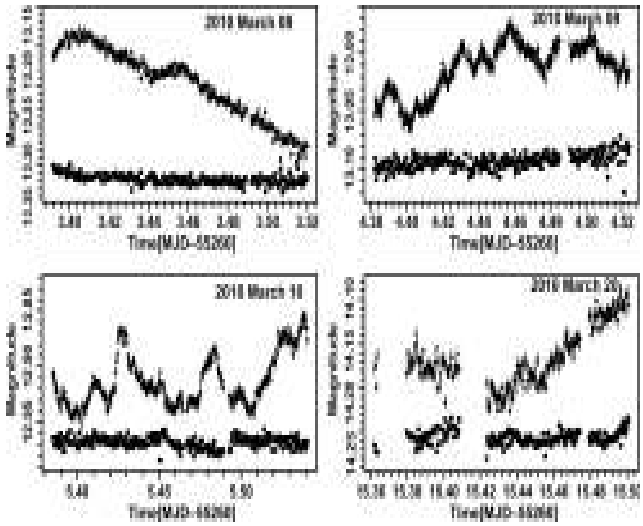

Figure 4: Intra-night variability in the R-band light-curves of the blazar PKS0716+71 during March 08 to 20, 2010. Rapid variation with time scales of few tens of minutes are superposed on the slowly varying component.

On night-to-night basis, the source exhibits mild bluer when brighter nature favouring intrinsic mechanisms for variation vis-a-vis geometric ones. Rapid variability can be produced when a relativistic shock wave or a blob propagates down the jet with turbulent plasma. Based on our shortest intra-night variation time scale of 1.24 hrs, the upper limit on the size of the emission region is about 10^{15} cm taking it

as a bound on the Schwarzschild radius of the black hole, mass of the central object is estimated as $1.1 \times 10^9 M_\odot$.

(S Chandra, K S Baliyan, S Ganesh, U C Joshi)

Intra-night variations in the optical polarization of Wcom

Wcom is the first intermediate energy peaked blazar (IBL) to be detected as emitter of high energy gamma-rays. It is seen that optical polarization and high energy emission are correlated indicating their co-spatial emission. In an attempt to test such a scenario, we made polarization measurements, resolving white light curves down to timescales of few minutes. The observations were made during April 14-16, 2010. The source shows high polarisation, ranging from 5% to12% during this period. On April 14, a gradual increase in linear polarization by about 2% in 1.5 Hrs, followed by a sharp decrease of 4% within half an hour are noticed. Several events of similar nature are displayed during three days of monitoring. In addition to degree of polarisation, position angle also shows intra-night variation by more 2σ level. On April 14 and 16, Wcom gets fainter by 0.5 and 0.3 magnitude, respectively. Mild inter-night variations in all the quantities are also seen. The evolution of the degree of linear polarization can be expressed in terms of two components, one consisting of flickers with timescales of several tens of minutes, superposed on the other component varying on the timescales of several hours. The change in the polarization could either be due to the shock moving down the inhomogeneous jet having variable magnetic field or the synchrotron flaring in the accretion disk. In the light of short time scale variations, former scenario is inferred. These are probably the best temporally sampled polarization data ever obtained for this object.

(S Chandra, K S Baliyan, S Ganesh, U C Joshi)

Automated Telescope for Variability Study (ATVS)

First installed on January 21/22, 2010 in the existing small dome behind main 1.2m telescope building at the Mt. Abu Observatory, Gurushikhar, the 50cm CDK-20 telescope now sits on a newly constructed larger diameter pier. It was necessitated as the older 12'' diameter pier had unacceptable vibrations even under mildly windy (10km/hour) conditions. The work on the automation of the dome, shutters and their integration with the movement of the telescope is going on satisfactorily. To make the observations fully automated, a pipeline is also being developed side by side. Presently, observations in the manual mode are being made along with testing of various operations. The telescope is equipped with a computer controlled filter wheel (with standard UBVRI filters) and Andor EMCCD camera (1024x1024 pixels), mounted at the focal plane as an imaging instrument. Attached light curve (Figure 5) shows R-band monitoring of the source CGRaBS J0211+1051. These observations were made simultaneously with V-band observations on the 1.2m main telescope.

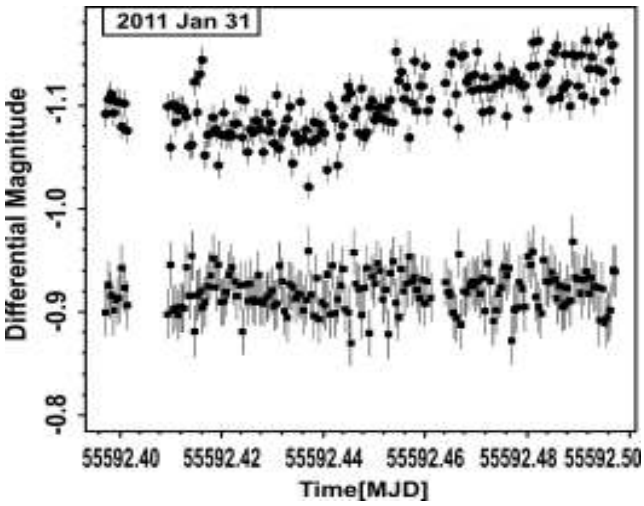

Figure 5: Intra-night light curve for CGRaBS J0211+1051 on Jan 31, 2011. The source varies by ~0.08mag in about 2.5 Hrs. The observations were taken with EMCCD mounted on the 50cm telescope (ATVS) keeping exposure time 45 seconds in R band.

(S Ganesh, K S Baliyan, S Chandra, S N Mathur)

The Sidereal rotation period from interplanetary magnetic field observed near Earth:

The Advanced Composition Explorer (ACE) orbits the L1 liberation point which is a point of Earth-Sun gravitational equilibrium about 1.5 million km from Earth and 148.5 million km from the Sun. The correlation analysis with X, Y and Z components of the IMF was carried out and reveal evidence of solar rotational modulation. The rotation periods were estimated. These estimates during 1998-2009 were found to have temporal variability (Figure 6).

The comparison indicates that these differ quite significantly from similar estimates from the disk integrated radio flux at 2.8 GHz. Whereas, these have better comparison with the equatorial values of sidereal rotation period obtained using 17 GHz and X-ray. The temporally overlapping data is shown by different colours in this Figure.

This work is being done in collaboration with Satish Chandra of Kanpur and Mehul Mehta of VP Science College Vidyanagar.

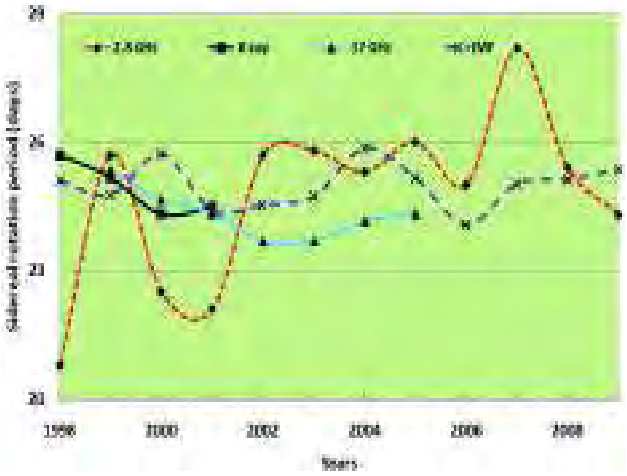

Figure 6: Temporal variation of sidereal rotation period estimated from the analysis of IMF data observed by ACE satellite at L1 point. These are compared with X-ray and radio estimates.

(Hari Om Vats)

North-south asymmetry in coronal rotation:

The study of differential rotation and its temporal and spatial variation in the solar atmosphere is an important task of solar physics. Various solar observations have been used for such investigations. The solar images at 17 GHz by the Nobeyama Radio Heliograph and in X-rays by the soft X-ray telescope (SXT) on board the Yohkoh satellite have been of particular interest for the estimation of solar coronal rotation using the flux modulation approach. These studies established that the solar corona rotates differentially. The radio images estimate an equatorial rotation period lower than those estimated by the X-ray images. The latitude profiles of the coronal rotation have temporal variability and space–time plots of sidereal rotation period clearly reveal north–south (NS) asymmetry. An example of this is shown in the Figure 7 which is obtained from the analysis of radio images. This shows that the rotation period is higher in the northern hemisphere and that in southern hemisphere.

The asymmetry appears to change its sign in odd and even activity cycles of the Sun. Changes in the northern and southern hemispheres can be interpreted as oscillations with a 22-yr period. The present study supports this finding of NS asymmetry in the solar coronal rotation that (1) in odd solar cycles (e.g. 23 yr) the southern hemisphere rotates faster than the northern hemisphere and (2) in even solar cycles (e.g. 22 yr) the northern hemisphere rotates faster than the southern hemisphere. It can be concluded that the NS asymmetry in the solar corona and chromosphere is in phase. The rotational asymmetry probably leads to the manifestation of NS asymmetry in many solar features observed by various methods and is certainly, in a complex manner, related to the solar dynamo.

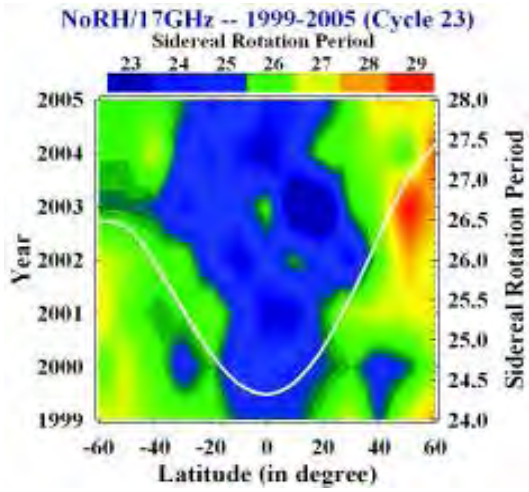

Figure 7: Space-time plots of sidereal rotation period estimated using 17 GHz radio images of the Sun during 1999-2005, average latitude profile of sidereal rotation is shown by white continuous curve.

This work is being done in collaboration with K N Iyer of Saurashtra University, Rajkot and Satish Chandra of PPN College Kanpur, UP.

(Hari Om Vats)

Periodicities in the coronal rotation and sunspot numbers:

The present study is an attempt to investigate the long term variations in coronal rotation by analyzing the time series of the solar radio emission data at 2.8 GHz frequency for the period 1947 - 2009. Here, daily adjusted radio flux (known as Penticton flux) data are used. The autocorrelation analysis shows that the rotation period varies between 19.0 to 29.5 sidereal days (mean sidereal rotation period is 24.3 days). This variation in the coronal rotation period shows evidence of two components in the variation; (1) 22-years component which may be related to the solar magnetic field reversal cycle or Hale's cycle, and (3) a component which is irregular in nature, but dominates over the other components. The cross correlation analysis between the annual average sunspots number and the coronal rotation period also shows evidence of its correlation with the 22-years Hale's cycle. The 22-years component is found to be almost in phase with the corresponding periodicities in the variation of the sunspots number.

This work is being done in collaboration with Satish Chandra of PPN College Kanpur, UP.

(Hari Om Vats)

An X-ray bright nucleus in the low-surface-brightness galaxy UGC 6614

Most of the X-ray bright active galactic nuclei (AGN) are either bulge-dominated early-type galaxies or disk galaxies that have recently undergone minor mergers or bar instabilities. The later processes are accompanied by vigorous star formation and gas infall towards the nucleus. Hence the host galaxies are optically bright and their nuclei often show strong AGN activity. Late-type spiral galaxies are, however, not as bright as early-type galaxies. They are generally poor in star formation and if AGN activity is present, it is usually weak. The nuclear activity of such late-type systems is not as well studied or understood as those found in bright galaxies. We carried out a study of the X-ray spectrum of an extreme-type of late-type spiral galaxy, a low surface brightness (LSB) galaxy. These galaxies are poorly evolved, halo-dominated systems and have diffuse, optically dim disks. AGN have been detected in their nuclei at optical wavelengths, at radio frequencies and in X-ray emission. AGNs in LSB galaxies are usually associated with bulge-dominated LSB galaxies.

Our research was aimed at the study of the X-ray emission from the nuclear region of the LSB galaxy UGC 6614. Very little is known about the central objects in LSB galaxies, especially their X-ray properties and X-ray spectra. In this project we have used XMM-Newton data to study the characteristics of the X-ray spectrum and the X-ray flux variability of the active galactic nucleus (AGN) in the LSB galaxy UGC 6614. The nucleus of UGC 6614 is very bright in X-ray emission with an absorption-corrected 0.2-10.0 keV luminosity of $\sim 1.1 \times 10^{42}$ erg s^{-1}. The X-ray spectrum is found to be power-law type with a moderate column density. A short time-scale of intensity variation and large X-ray flux are indicative of the presence of a black hole at the centre of this galaxy. Using the method of excess variance, we have determined the black hole mass to be $\sim 0.12 \times 10^6 M_{\odot}$. The X-ray spectral properties are similar to that of the Seyfert I-type AGNs. Our study thus demonstrates that although LSB galaxies are poor in star formation, they may harbour AGNs with X-ray properties comparable to that seen in more luminous spiral galaxies.

This work was done in collaborations with M. Das, C. Jain and B. Paul of RRI, Bangalore.

(Sachindra Naik)

Detection of GRB 090618 with the RT-2 Experiment on Board the Coronas-Photon Satellite

Gamma-ray bursts (GRBs) are very fascinating cosmic objects in the universe. Since their discovery in 1973, GRBs opened up a new domain of astrophysical research due to the rich observational characteristics of the afterglows in a vast range of electromagnetic spectrum from Υ-rays to radio wavelengths. There is general consensus in the literature that the diverse observational characteristics are due to the interaction of relativistic matter with the surrounding medium. The nature and energy source for this relativistic matter, particularly in the context of the long GRBs, could be in the nature of the bulk motion of ions, cannon balls emitted from a compact object newly formed in a supernova explosion, or particles accelerated by magnetized winds. The prompt gamma-ray emission has several characteristic correlations like the peak energy Ep against the isotropic luminosity Eiso, spectral lag against the peak luminosity etc. These relations are used even in predicting the redshift of long duration GRBs, although with a large uncertainty (close to a factor of two). A detailed understanding of the prompt emission is necessary to put these correlations in a firm footing so that GRBs can be used as cosmological candles and also to have a clear understanding of the central engine and the basic jet/cannon-ball emission mechanism.

We tried to understand the properties of a particular GRB by analysing the prompt gamma-ray emission from GRB 090618 using the RT-2 Experiment on board the Coronas-Photon satellite. GRB 090618 shows multiple peaks, and a detailed study of the temporal structure as a function of energy is carried out. As the gamma-ray burst (GRB) was incident at an angle of 77° to the detector axis, we have generated appropriate response functions of the detectors to derive the spectrum of this GRB. We have augmented these results using the publicly available data from the Swift Burst Alert Telescope detector and show that a combined spectral analysis can measure the spectral parameters quite accurately. We also attempt a spectral and timing analysis of individual peaks and find evidence for a systematic change in the pulse emission characteristics for the successive pulses. In particular, the peak energy of the spectrum, Ep, is found to monotonically decrease with time, for the successive pulses of this GRB.

This work was done in collaborations with A. R. Rao and his group at TIFR, Mumbai and S. K. Chakrabarti and his group at ICSP, Kolkata.

(Sachindra Naik)

Suzaku Observation of the Transient X-ray Pulsar GRO J1008-57

High Mass X-ray Binary (HMXB) systems are strong X-ray emitters via the accretion of matter from the OB companion. The majority of the HMXBs are known to be

Be/X-ray binaries. The mass donor in the Be binary systems is generally a B star that is still on the main sequence and lying well inside the Roche surface. In these Be binary systems, the compact object (a neutron star) is typically in a wide orbit with moderate eccentricity with orbital period in the range of 16-400 days. The neutron star in these Be systems spends most of the time far away from the circumstellar disc surrounding the Be companion. Mass transfer from the Be companion to the neutron star takes place through the circumstellar disc. Strong X-ray outbursts are normally seen when the neutron star (pulsar) passes through the circumstellar disc or during the periastron passage. Here in the project, we carried out our study on one of the transient Be/X-ray binary pulsar GRO J1008-57. The pulsar GRO J1008"57 was discovered on 1993 July 14 by the BATSE experiment on board the *Compton Gamma Ray Observatory* (*CGRO). Based on the detection of recurring outbursts in the pulsar with a periodicity of 260 days,* the mass of the binary companion was estimated to be in the range of 3–8 $M_{\odot}$) indicating the system as a HMXB.

We investigated the timing and broad-band spectral properties of the Be transient high-mass X-ray binary pulsar GRO J1008-57 using a Suzaku observation in the declining phase of its 2007 November–December outburst. Pulsations with a period of 93.737 s were clearly detected in the light curves of the pulsar up to as high as 100 keV. The pulse profile was found to be strongly energy dependent, a double-peaked profile at soft X-ray energy bands (<8 keV) and a single-peaked smooth profile at hard X-rays. The broad-band energy spectrum of the pulsar, reported for first instance in this project for this source, is well described with three different continuum models, namely (i) a high energy cut-off power law, (ii) a Negative and Positive power law with Exponential (NPEX) cut-off and (iii) a partial covering power law with high energy cut-off. In spite of large value of absorption column density in the direction of the pulsar, a blackbody component of temperature ~0.17 keV for the soft excess was required for the first two continuum models. A narrow iron K_{α} emission line was detected in the pulsar spectrum. The iron emission line is generally interpreted as due to the fluorescent line from the cold matter in the surrounding region of the neutron star. The partial covering model, however, is found to explain the phase-averaged and phase-resolved spectra well. The dip-like feature in the pulse profile can be explained by the presence of an additional absorption component with high column density and covering fraction at the same pulse phase.

This work was done in collaborations with B. Paul (RRI, Bangalore) and C. Kachhara (Kohima Science College, Kohima, Nagaland).

(Sachindra Naik and S. V. Vadawale)

Unique observations of Geomagnetic SI^{+}- SI^{-} pair and Solar wind Fluctuations

Observations of a Geomagnetic SI^{+}- SI^{-} pair have shown the relation between the interplanetary structures and their worldwide magnetic response, first observed through Indian magnetic observatories. The event has also clearly shown a close correspondence of the solar wind density with the changes in geomagnetic field component, ΔX at ground stations. However, no correlation with solar wind velocity or magnetic field makes this event rather unique. In addition, it has been found that rear side solar events can propagate shock towards the earth and play a key role in occurrence of such events.

Oppositely directed sudden impulses (SI) in the geomagnetic fields at ground stations, called as SI^{+}-SI^{-} pairs, are caused due to the simultaneous forward and reverse shock arrival at the earth's magnetosphere by changing the H-component of magnetic field of the earth. Such a SI^{+}- SI^{-} pair was identified at three Indian geomagnetic

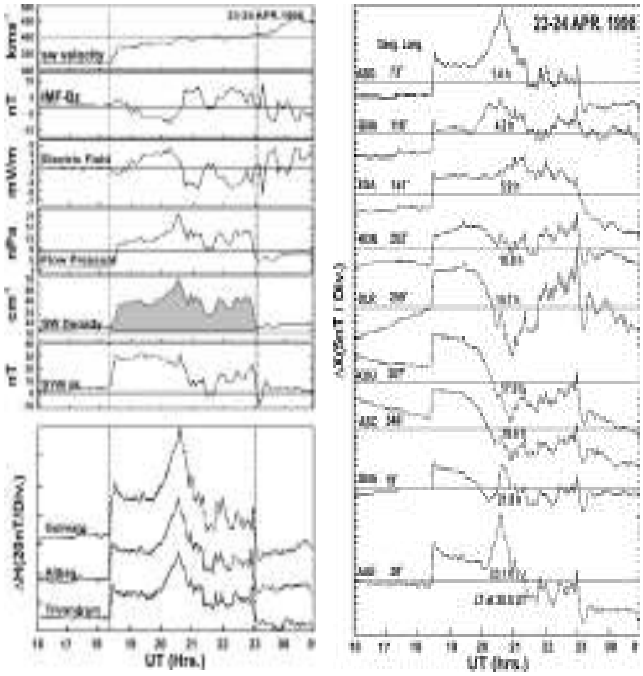

Figure 8: (right panel) The first six panels starting from top show the variations as a function of time in UT on 23-24 April 1998 of the solar wind velocity, BZ, the electric field, the solar wind pressure, the solar wind density (shaded grey) and the sym/H field respectively. Observations of the H field at Indian stations Gulmarg, Alibag and Trivandrum are shown in the bottom panel. (left panel) Variation of the horizontal component of thegeomagnetic field projected onto the x-direction at 11 low-latitude stations around the world on 23-24 April 1998. The vertical dashed line is marked at 20.5 UT, and shown alongside it, for each curve, is the corresponding local time at each station. Also indicated on the left of each curve is the geographic longitude of the station.

observatories on 23-24 April 1998. Figure 8 (bottom panel) shows the tracings of H magnetograms at Gulmarg, Alibag and Trivandrum between 1835 UT and 2300 UT. A sudden positive impulse in H was recorded at all Indian stations at 1835 UT followed by a sudden negative impulse at 2300 UT. Figure 8 (starting from top and going down) shows the corresponding variations of the solar wind velocity, Bz, the interplanetary electric field, the solar wind flow pressure, the solar wind density and the symmetrical H field index respectively. The vertically oriented parallel dashed lines demarcate the time interval between the SI^+ impulse and the SI^- impulse. It is to be noted that the symmetric variation of H (SYM/H) at all middle latitude stations around the world, too had remarkably similar variations as the H at Indian stations. This therefore implies that the SI pair was a global event. To further check the effect of solar wind parameters during the interval between two SI impulses, the variation of northward geomagnetic field, ΔX at different low latitude stations around the world are shown in Figure 8.

When we searched for the source locations of this event, two solar sources were identified as the cause of this SI^+ – SI^- event. One was a rear side, fast partial halo CME and the second was an optically occulted GOES M1.4 class flares just behind the south west limb. The flare and the rear side CME would thus provide the forward and reverse shocks to cause the SI^+ and SI^- pair.

(Rastogi R.G., P. Janardhan, A.C. Das, and Susanta K. Bisoi)

Deep 150 MHz GMRT Observation: Searching for High Red-shift Radio Galaxies

High red-shift radio galaxies (HzRGs) have emerged as a unique probe to cosmic evolution containing important information on the physics and the properties of the early Universe. It had been well established that radio sources with steep radio spectra are more distant than sources with normal spectra. This correlation between spectral index, "α" and red-shift, "z" has been exploited for the last three decades which yielded about 45 radio galaxies at $z > 3$ till date. The median flux density of all these known HzRGs is 1.3 Jy at 150 MHz which is around two orders of magnitude well above the detection limit of the GMRT at 150 MHz. The GMRT 150 MHz has high angular resolution of 20'' and better sensitivity about 1 mJy, suggesting a large number of HzRGs, two orders of magnitude less luminous than all known objects, can be detected with GMRT. To this effect, we have carried out deep 150 MHz observations of three of the four DEEP2 (Deep Extragalactic Evolutionary Probe 2) fields, which has optical spectra of 50,000 objects.

Preliminary results from our observing program to search for HzRGs to about 10 to 100 times fainter than the known populations till today are reported: One of the deep DEEP2 fields centered on 2330+0000 was analyzed and the final image obtained has an rms noise about 1 mJy/beam with a resolution of 20''. The 150 MHz source catalog of this field contains nearly 400 radio sources to 20% peak primary beam response with flux density limit of about 6 mJy while the median flux density is 100 mJy. The spectral index was estimated by comparison of 150 MHz flux density with that of NVSS and FIRST at 1.4 GHz.

A total of 368 sources from GMRT 150 MHz catalog have counterparts found in the FIRST and/or NVSS catalogues. Figure 9a shows the spectral index distribution of sources and Figure 9b shows the spectral index distribution of sources as a function of 150 MHz flux density. Above a cutoff of $\alpha = 1$, there are about 100 steep spectrum sources. These constituted the ultra-steep spectrum (USS) sample as a necessary initiation to search HzRGs.

Close inspection of all these steep spectrum sources showed structures like double radio sources, one-side jets, FRI and FRII. Most of them are unlikely to be at high red-shift. However, one radio source, unresolved at 150 MHz but (FRII morphology), using FRI and FRII break luminosities, expected to be at $z = 2$.

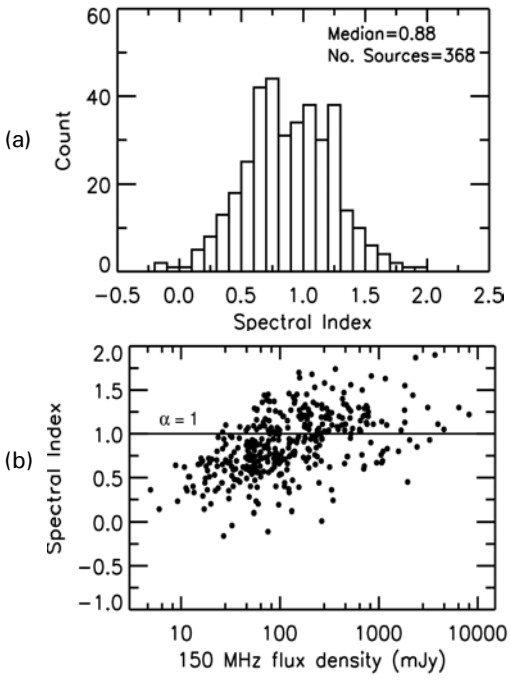

Figure 9: Histogram of spectral index of sources (a) and spectral index distribution of sources as a function flux density at 150 MHz band of the GMRT (b).

The FIRST position of these sources will be used to search SDSS and DEEP2 optical catalogs to eliminate nearby radio sources. The unidentified radio sources will be the potential candidates for HzRGs.

This work has been carried out in collaboration with Ishwara-Chandra and Sandeep K. Sirothia from NCRA-TIFR, Pune.

(P. Janardhan and Susanta K. Bisoi)

Recent (2008) outburst study of V1647 Orionis

V1647 Orionis is a young variable star located in the vicinity of the NGC2068 Star-forming region in the northern part of the Orion B Giant molecular cloud. It went into an outburst towards the end of November / December 2003 and rose in brightness by about 3 mag in the near-infrared JHK bands. It reached the peak brightness by 120 days and remained there until October 2005. It started moving towards its quiescent phase during 2006. Most interestingly, however, it underwent another strong outburst during August 2008. Initially it was speculated that V1647 Ori belonged to a class of young variable stars designated as "FUor" after the class progenitor, FU Orionis. The relatively short outburst period (approximately 26 months) observed in V1647 Ori suggest it to be an Exor type eruption. Exor events (after the progenitor Ex Lupi) are recurrent with outburst durations lasting for few weeks to years. Recent Mt. Abu observations showed slight fluctuations in the near-infrared magnitudes. Spectra taken on a few occasions showed variability in the Brackett-series lines and CO bands. This may be possibly due to the variation in the mass accretion-rate through the circumstellar disk. The observed change in the extinction during the outburst and quiescent phase are due to the varying accretion disk luminosity that induce changes in the inner disk structure.

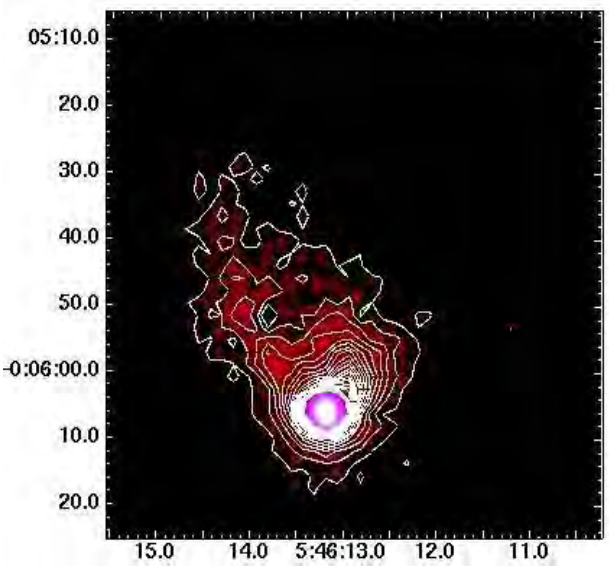

Figure 10: JHK Colour composite image of V1647 Orionis observed on 26 October 2010 using NICS

(V.Venkata Raman & B.G.Anandarao)

An ab initio derivation of electromagnetic fields of a charge with an arbitrary motion

Electromagnetic fields of an accelerated charge are derived from the first principles using Coulomb's law and the relativistic transformations. The electric and magnetic fields are derived first for an instantaneous rest frame of the accelerated charge, without making explicit use of Gauss's law, an approach different from that available in the literature. The derivation explicitly shows the genesis of various terms in the field expressions, when expressed with respect to the time retarded position of the charge. A straightforward transformation from the instantaneous rest frame using relativistic Doppler factors yields expressions of the electromagnetic fields for the charge moving with an arbitrary velocity. The field expressions are derived without using Linard-Wiechert potentials, thereby avoiding evaluation of any spatial or temporal derivatives of these potentials at the retarded time.

(Ashok K. Singal)

Gyro-orbit size, brightness temperature limit and implausibility of coherent emission by bunching in synchrotron radio sources

We show that an upper limit on the maximum brightness temperature for a self-absorbed incoherent synchrotron radio source is obtained from the size of its gyro-orbits, which in turn must lie well within the confines of the total source extent. For radio variables, the intra-day variability implies brightness temperatures $\sim 10^{18\text{-}19}$ K in the co-moving rest frame of the source. This, if interpreted purely due to an incoherent synchrotron emission, would imply gyro radii $\gtrsim 10^{28}$ cm, the size of the universe, while from the causality arguments the inferred maximum size of the ource in such a case is $\lesssim 10^{15}$ cm. Such high brightness temperatures are sometimes modelled in the literature as some coherent emission process where bunches of non-thermal particles are somehow formed that radiate in phase. We show that bunches would disperse over dimensions larger than a wavelength in time much shorter than the gyro orbital period. Therefore a coherent emission by bunches cannot be a plausible explanation of the high brightness temperatures seen in variable extragalactic radio sources.

(Ashok K. Singal)

"Absolute" motion of the earth in the universe:

The velocity of earth was determined with respect to a reference frame in which the distribution of matter in the universe appears isotropic. For this the distribution of distant radio sources was used to define such a reference frame. In particular any departures from isotropy were looked for in the angular distribution of radio sources in sky as a result of earth's motion. The results gave a direction of the velocity of earth in agreement with those determined from the Cosmic Microwave Background Radiation (CMBR) measurements by COBE and WMAP satellites.

This work was done in collaboration with Shubham Agarwal and Shashank Naphade of IIT Gandhinagar.

(Ashok K. Singal)

Design and Development of Silicon Drift Detector based X-ray Spectrometer for future space missions

The large sensitive area (few cm^2) and low energy (<1 to 30 KeV) X-ray spectrometer has many space science applications like remote X-ray fluorescence of planetary surface for elemental (Mg, Al, Si, Ti, Ca and Fe) mapping, complimentary X-ray monitor in X-ray polarimeter for polarisation measurement of astronomical objects (crab, black hole etc.), Soft x-ray spectroscopic imaging of Sun corona etc. To realise such spectrometer for future space mission, the state of the art Silicon drift detector (SDD) based development is carried out. SDD has virtue of very good energy resolution (<180 eV @ 5.9 KeV, -35^0C) associated with high count rate (500K).

A modular multi-channel X-ray spectrometer is under development based on large active area (92 mm^2) Silicon Drift Detector (SDD). The block-schematic (Figure 11) shows the design concept. The detector package is vacuum sealed with inbuilt Thermo-Electric-Cooler (TEC) and Field-Effect-Transistor (FET). TEC cools detector element with $\Delta T = 55^0$C when 4W power is applied. Integrated FET provide the first stage very low noise charge amplification. The Charge-Sensitive-Pre-Amplifier (CSPA) has been designed using continuous anode "Reset" technique to avoid charge saturation and elimination of feedback thermal noise. The five pole shaping amplifier (SA) is designed with 1 μsec peaking time to achieve 100K system count rate. The single pixel analog front end channel consists of CSPA, SA, Peak detector and Trigger logic. The gain and offset of each pixel channel can be tuned and triggered-channel address can be recorded. Such three pixel channels module is being developed having 276 mm^2 active area. The multiple modules can be further cascaded to realise required larger area X-ray spectrometer / monitor / imager.

State of the art commercially available multi-channel analyzer is being used to acquire single channel data. Characterization data has been acquired and analysis result is reported in spectrum diagram Figure 12. Field Programmable Gate Array (FPGA) based multi-channel readout system is under development. Readout system consists of 8- Channel analog multiplexer, 12-bit parallel ADC, Fast trigger and Reset logic, System controller, Telemetry and Tele-command logic. A microcontroller based ground check-out system has been developed to simulate satellite bus interface to test readout electronics in lab.

TEC integrated with SDD consumes 4W power to cool detector with max. $\Delta T = 55^0$C. The heat generated by this

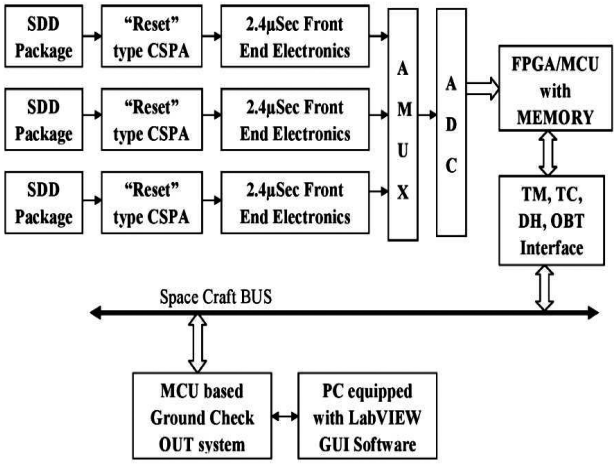

Figure 11: Block schematic of multi-channel X-ray Spectrometer

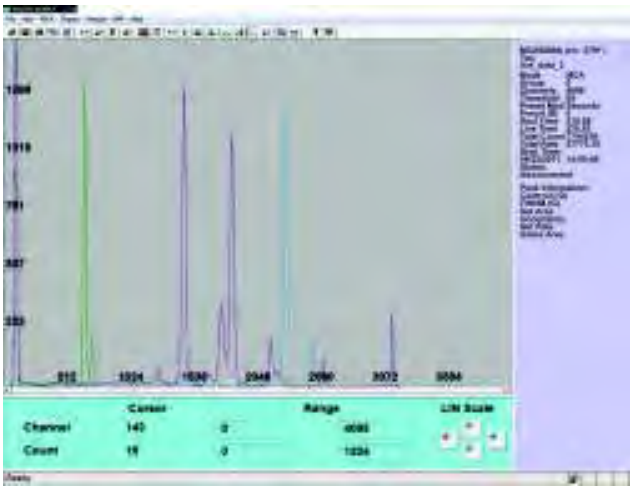

Figure 12: Single SDD irradiated with Fe^{55} (green), Am^{241} (magenta) and Cd^{109} (sky-blue) radiation sources and combined spectrum is shown. At ambient temperature of 22^0C, <210 eV resolution @ 5.9 KeV is achieved. Noise threshold is <900 eV. Better resolution can be achieved with $<20^0$C ambient temperature.

power dissipation can efficiently drain out only by bulky heat-sink. Hence it is very challenging to design compact three-channel module. In view of very limited power, mass and volume budget of space payload, mechanical design becomes more complex and challenging. Every pixel channel electronics need to be isolated from EMI and cross-talk noise, this also add-up challenges to mechanical and electronics design. To realise very large soft X-ray sensitive area (Tenths of cm^2) using SDD, many space missions have used monolithic SDD array, passive cooling and readout ASIC. Access to such technology ease above listed challenges a great extent for space payload. Science objectives for such detectors include high resolution X-ray spectroscopy for Solar physics as well as for studies of Galactic X-ray binaries.

(Amish B. Shah, Satish L. Kayasth, Dhara Patel)

Probing the Role of Magnetic-Field Variations in NOAA AR 8038 in Producing Solar Flare and CME on 12 May 1997:

We carry out a detailed multi-wavelength investigation of a Coronal Mass Ejection (CME) and associated flare observed on 12 May 1997 in the NOAA Active Region 8038. This region was quiet and decaying, and produced only very small flare activity during its disk passage from 07-16 May 1997. However, on 12 May 1997 it produced a CME and associated medium-size 1B/C1.3 flare. Detailed analyses of Há filtergrams and MDI/SOHO magnetograms reveal continuous but discrete surge activity, and emergence and cancellation of flux in this active region. The movie of these magnetograms reveals two important results that the major opposite polarities of pre-existing region as well as in the emerging flux region were approaching towards each other and moving magnetic features (MMF) were ejecting out from the major north polarity at a quasi-periodicity of about 10 hours during 10—13 May 1997. These activities are appearing to be caused by the magnetic reconnection in the lower atmosphere driven by photospheric convergence motions, which were evident in magnetograms. The quantitative measurements of magnetic field variations such as magnetic flux, gradient, and sunspot rotation revealed that in this active region, free energy was slowly being stored in the corona. The slow low-layer magnetic reconnection may be responsible for the storage of magnetic free energy in the corona and the formation of a sigmoidal core field or a flux rope leading to the eventual eruption (Figure 13- top panel). The occurrence of EUV brightenings in the sigmoidal core field prior to the rise of a flux rope suggests that the eruption was triggered by the inner tether-cutting reconnection, but not the external breakout reconnection. We observe an impulsive acceleration from fast separation of the Há ribbons (Figure 13 – bottom left panel) for the first 150 seconds suggests the CME accelerated in the inner corona, which is also in consistent with the temporal profile of the reconnection electric field (Figure 13– bottom right panel). Based on observations and analysis we propose a qualitative model, and we conclude that the mass ejections, filament eruption, CME, and subsequent flare were connected with one another and should be regarded within the framework of a solar eruption.

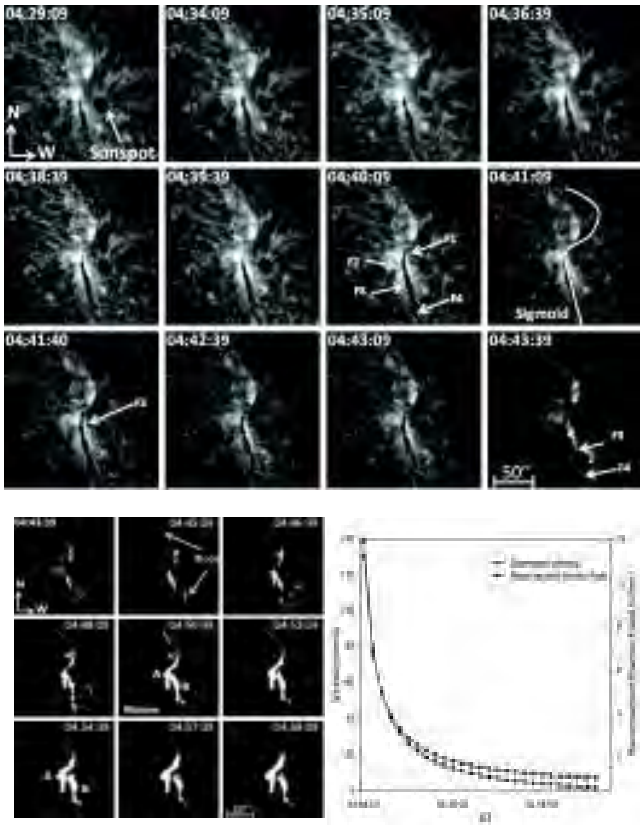

Figure 13: Top Panel - The sequence of H_α filtergrams showing filament activity on 12 May 1997 prior to CME-flare eruption. The F1 part of the filament shows frequent activity, while F2 and other parts disrupted before the flare and CME around 04:43 UT. The filament also shows reverse shaped sigmoidal structure. Bottom Left Panel - The sequence of Há filtergrams images showing the flare ribbons separation during the flare activity on 12 May 1997. Bottom Right Panel - The deceleration of flare ribbons and the reconnection electric field variation over the flare duration.

This work was done in collaboration with Babita Chandel at Dept. of Physics, Manav Bharti University, H. P., Lokesh Bharti at M. P. S., Lindau, Germany, Y. Hanaoka at NAOJ, Tokyo, Japan and A. L. Kiplinger at Centre for Integrated Plasma Studies, University of Colorado, USA

(Rajmal Jain and Arun Kumar Awasthi)

Multi-Wavelength Diagnostics of the Precursor Phase in Solar Flares

X-ray emission in Solar flares can be categorized in three phase viz. precursor, impulsive and gradual phase. The impulsive and gradual phases are very well studied however the origin of the precursor phase emission is still not well understood owing to high resolution observations. Therefore we plan to study the underlying physical processes of energy release in precursor phase in 20 flare events observed between year 2003 and 2004. We employ the X-ray spectrum observed by the Si and CZT detectors onboard "Solar X-ray Spectrometer (SOXS)" mission and X-ray and EUV (171 and 195 Å) images from the RHESSI and TRACE missions respectively. We define the precursor phase in <30 keV energy band before the onset of the impulsive phase in solar flares. We estimate the flare plasma parameters viz. temperature (T), emission measure (EM) and relative abundance (A) of Fe to Fe/Ni line features by processing the X-ray observations with the help of SolarSoft written in IDL. We estimate T, EM and A in precursor phase between 7-20 MK, 0.01-0.08 $\times$ 1049 cm^{-3} and 0.1-0.5 respectively. Further, we undertake the analysis of EUV observations from TRACE mission in order to understand the relationship between energy release site of precursor and main phase flare emission. We process the EUV images obtained in 171 Å and 195 Å in order to visualize the changes at the time of preflare and main flare emission. We obtain following findings: (1) conduction heating in the precursor phase of the flare for all events under investigation, (2) isothermal plasma behavior in pre-flare phase in 17 flare events while multi-thermal behavior in 3 events, and (3) the precursor phase emission is originated from low-altitude coronal loops, however, in co-spatial with the main phase energy release site (Figure 14).

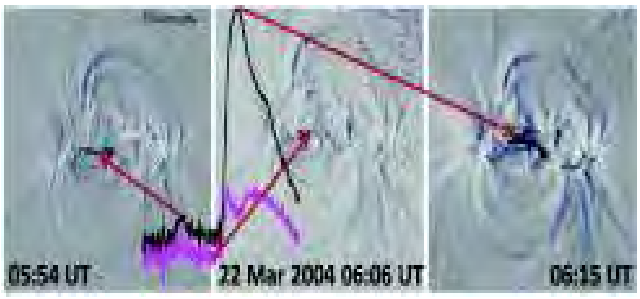

Figure 14: Time series of difference images in 171 Å in TRACE observation for the flare event of 22 March 2004. Left panel: Difference image of 05:54 and 05:50 UT, the peak time of precursor phase emission. Middle panel: Difference image of 06:06 UT and 05:50 UT, the quiet time between precursor phase and main phase energy release. Right panel: Difference image 06:15 UT and 05:50 UT, corresponding to main flare peak time. Light curve of X-ray emission in two different energy bands 4-15 (black) and 15-25 keV (pink) respectively for flare event of 22 March 2004 is over-plotted.

(Arun Kumar Awasthi and Rajmal Jain)

Relationship between high energy processes in solar flares/ CMEs and geomagnetic storms

We are probing the possible role of high energy processes such as X-ray/ gamma ray and solar energetic particles (SEPS) emission taking place during flares and CMEs in producing geomagnetic activity. The fundamental idea is to improve the understanding on the mechanisms of the high energy processes in relation to the magnitude of the particle acceleration during initial process of the energetic phenomena. The high energy processes are triggered as a result of conversion of free magnetic energy in the corona in the stressed configuration of the active regions, which incidentally is also responsible for various particle acceleration processes in the inner heliosphere. On the other hand, CMEs carrying the magnetic field with them and undergoing various shock accelerations are also part of high energy processes. In this investigation we are studying X-ray emission characteristics associated with flares/CMEs that have generated geomagnetic storms. Simultaneously, we also extend our study to Solar Energetic Particles (SEPs) found associated with CMEs propagating towards earth.

We employ the existing data from YOHKOH, SOXS, RHESSI, for X-ray emission, and GOES, ACE and WIND for energetic particles: electrons, protons and ions of various energies. The photospheric magnetic fluxes of the active regions have been derived from MDI/SOHO.

Our preliminary study of the relationship between the velocity of CMEs and plasma temperature of the associated X-ray solar flares suggests that the velocity of CMEs increases with flare plasma temperature ($R=0.82$) as may be noted in Figure 15 (left panel). On the other hand we find the strong relationship between velocity of CME and hardness of the hard X-ray spectrum (Figure 15 – right panel). Based on these results we propose that initiation and kinematics of CMEs perhaps depend upon the dominant process of conversion of the magnetic field energy of the active region to heating/ accelerating the coronal plasma in the reconnected loops. Results show that flare and associated CME are two components of one energy release system, perhaps, magnetic field free energy.

This work was done in collaboration with Nipa J. Bhatt at C. U. Shah Science College, Ahmedabad, India; Malini Aggarwal at Solar and Space Weather Research Group, Korea Astronomy and Space Institute, Korea; Subhash

Kaushik at Jivaji University, Gwalior, M. P., India; Parvaiz Khan and A. K. Gwal at Dept. of Physics, Barkatullah University, Bhopal, M. P., India.

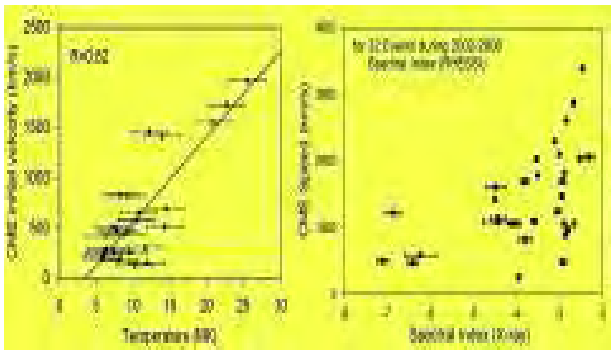

Figure 15: Correlation of CME speed with flare temperature as well as with spectral index of hard X-ray emission.

(Rajmal Jain, Sharad C. Tripathi, Arun K. Awasthi)

New Facility

Liquid Nitrogen Plant at Gurushikar

During the year a small liquid nitrogen plant (Kelvin International) with a capacity of delivering 30 liters/day of cryogen was acquired and installed at Mt. Abu Observatory at Gurushikar. The plant also has a storage capacity of 120 litres. The LN_2 has been in continuous operation for the last six months and is catering fully to the increased demand for LN_2 in the observatory which has two Infrared Camera dewars (NICMOS and NICS) to be kept cold for the entire observing season. Figure 16 shows the LN_2 plant in operation at Mt. Abu Observatory. So far the plant has produced over 4000 litres of Liquid Nitrogen.

(S.N. Mathur, T. Chandrasekhar, N.M. Ashok and R.R. Shah)

Figure 16: A small Liquid Nitrogen plant recently installed at Mt Abu Observatory at Gurushikar.

SCIENCE

Solar Physics

At Udaipur Solar Observatory (USO), the research and development activities revolve around the central theme of solar activity, eruptive processes and high resolution solar observations. Tools of helioseismology are being used to probe the sub-surface structures and flows of solar active regions, and dig into the origin of eruptions that are observed in the outer solar atmosphere. Solar magnetic fields are measured and analysed to monitor storage of magnetic energy and to decipher the candidate processes that trigger energetic solar transients, such as, flares and coronal mass ejections (CMEs). Chromospheric and coronal phenomena, observed from various ground-based and space-borne instruments, are being studied with particular emphasis on space-weather phenomena driven by solar events. These studies are being carried out for developing the ability to forecast the magnitude of geomagnetic storms and their time of arrival. Combination of archived data, mathematical modelling and construction of sophisticated instruments are being employed to achieve the desired scientific goals.

On the Association of Flares and p-Modes Energy in Solar Active Regions (ARs)

To further establish our earlier results on the p-mode energy amplification by the X17 flare of October 28, 2003 in NOAA 10486, we have carried out a statistical analysis of 74 flare productive Active Regions (ARs) of solar cycle 23. We have computed the p-mode energy in the ARs using ring-diagram analysis of Dopplergrams and flare energy from GOES X-ray fluxes. Figure 17 shows the relationship between the computed mode- and flare-energies of 74 ARs. It is evident that p-mode- and flare-energy are associated. However, it is to note that we have computed the mode energy for the ARs of our sample using data-cubes corresponding to the periods of their maximum flaring. Also, the net results included the effects of absorption by sunspots and amplification by flares. In ARs

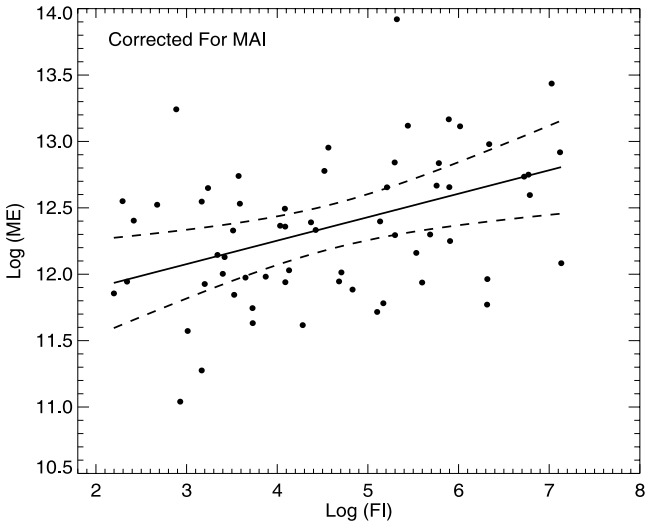

Figure 17: Association of p-mode energy (ME) and flare index (FI). The straight line fit using a linear regression model is shown by solid lines while the dashed lines represent 95% confidence levels.

having large sunspots with strong magnetic fields, i.e., large magnetic index but lower flare index, the effect due to mode absorption would dominate. On the other hand, if the flare energy is larger than the energy absorbed by sunspots, then the mode amplification effect due to flares would dominate. Accordingly, when we corrected the mode energy for magnetic index of the ARs, we found that the association of flare and p-mode amplification for ARs became stronger. These results support the p-mode excitation by flares at the local spatial scales of ARs.

(R.A. Maurya and A. Ambastha)

Evolution of p-Mode Parameters in NOAA 10486 during the disk transit of 25 October-1 November 2003

In order to examine properties of ARs, we have compared the p-mode characteristics and sub-photospheric flows of the extremely flare-productive super active region NOAA 10486 with dormant and quiet regions observed during the period 25 October-1 November 2003. Using the ring diagram technique, we obtained the flows, as shown in Figure 18, where vectors correspond to horizontal flows and background color represents the frequency shift ($\Delta\nu$) in p-modes averaged over n = 0 to n = 5 for 27 October 2003. Positive (negative) frequency shifts are shown in red (blue) colors. It is evident that there are large, positive frequency shifts present at the locations of ARs such as 10484, 10486 and 10488. We have found that the frequency shifts evolved with the ARs. For instance, NOAA 10486 was initially associated with small positive $\Delta\nu$ value on 25 October 2003, which increased thereafter to attain a maximum on 29 October 2003. Afterwards, it decreased in magnitude. We note that the maximum $\Delta\nu$ values

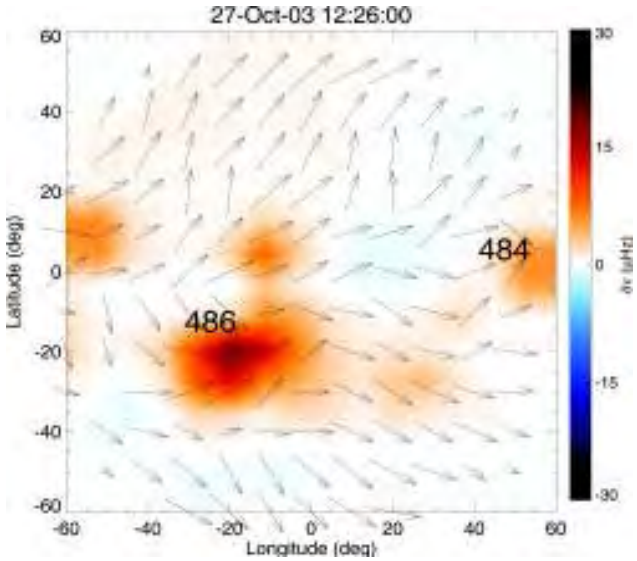

Figure 18: Background half tone image of frequency shift in ±60 degree longitude and latitude overlaid with horizontal flow vectors.

occurred around the period 28-29 October 2003 when NOAA 10486 produced two major flares, i.e, X17/4B and X10/2B events. These results provide further evidence that energetic transients and flare productivity of NOAA 10486 were associated with p-mode parameters, sub-photospheric flows and their temporal changes

(R.A. Maurya and A. Ambastha)

Deep Focus Time-Distance Helioseismology of Solar Active Regions

Time-distance (TD) technique is one of the main tools of local helioseismology to provide the internal characteristics of solar active regions. In a simple TD technique, acoustic signals are cross correlated at two different locations of the AR separated by a certain distance. The cross-correlations are further used to derive the travel-time and other parameters of the AR. We have developed a more robust method, called "deep focus time-distance geometry" for computing the cross-correlations for depth of interest in an AR. A theoretical geometry for the deep focus method is illustrated in Figure 19. For a desired depth (d), we compute the temporal cross-correlations between two

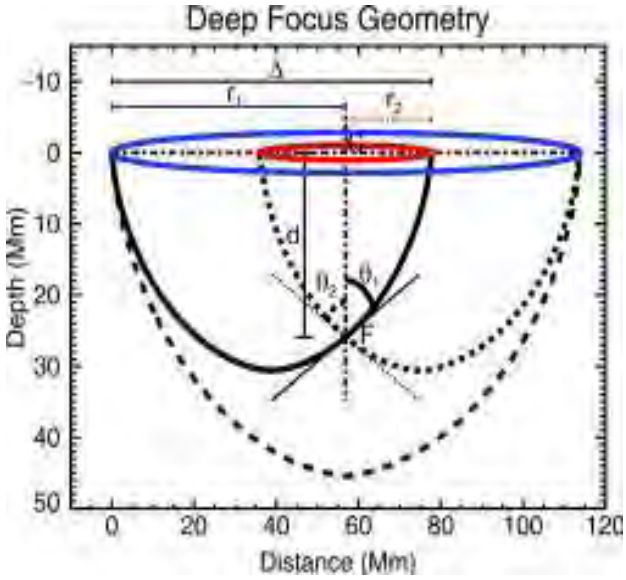

Figure 19: Deep focus time-distance geometry for acoustic frequency 3.5 mHz and harmonic degree 200.

opposite points of the two annuli with radii r1 and r2. From our theoretical model, we construct two annuli (r1 and r2) for given acoustic wave such that rays starting from one annulus (r1) reach to other annulus (r2) after focusing at desired depth point (F). Since all such waves will have same focus depth, they will give good signal to noise ratio for the in-homogeneity at the focus point F. From our model, we can also construct two annuli such that the rays traveling in opposite directions will meet at

90 degree at the focus depth d which is more sensitive to flows at F. The travel-time map using this method can be used to find the sub-surface information of AR.

This work was done in collaboration with S.P. Rajaguru of IIA, Bangalore, India.

(R.A. Maurya and A. Ambastha)

Analysis of flare induced changes in penumbral flows and evidence for correlated enhancement of global waves in the Sun

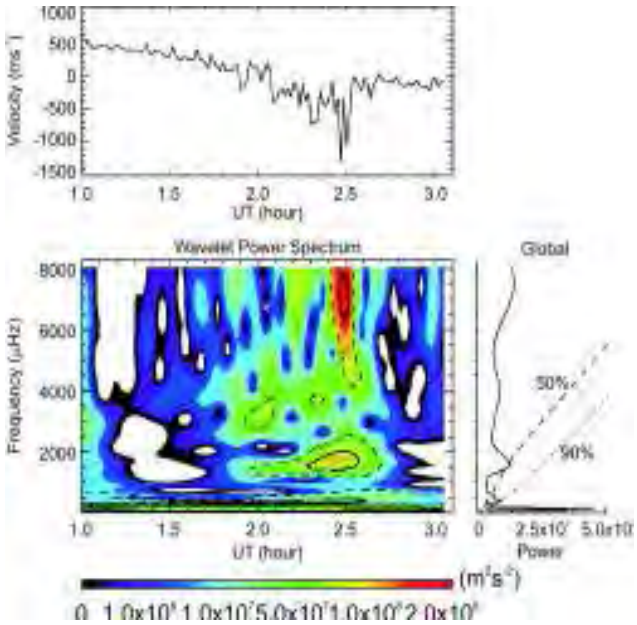

Figure 20 (a): The upper panel shows the temporal evolution of velocity flows in the centroids of the flare affected penumbral region as seen in the GONG Dopplergrams during 01:00-03:04 UT spanning the flare event of 13 December 2006. The lower panels show the Wavelet Power Spectrum (WPS) and the Global-wavelet Power Spectrum (GWPS) computed from this time series. In the WPS, the solid lines correspond to regions with 90% confidence level whereas the dashed lines are for 50% confidence level and the hatched region indicates the cone of influence. In the GWPS, the dashed line is for 50% significance level and the dotted line is for 90% significance level.

During the minimum phase of the solar activity cycle 23, a major flare occurred on 13 December 2006 in the active region NOAA 10930. This flare event has remained interesting for solar researchers for studies related to particle acceleration during the flare process and the reconfiguration of magnetic fields as well as fine scale features in the active region. The energy released during the flares is also known to induce velocity oscillations in the Sun. We have analyzed the line-of-sight velocity patterns in this active region during the flare using the Dopplergrams obtained by Global Oscillation Network Group (GONG) Telescope. We have also analyzed the disk-integrated velocity observations of the Sun obtained by Global Oscillation at Low Frequency (GOLF) instrument onboard SOHO (Solar and Heliospheric Observatory) spacecraft during this flare to study any possible correlation between the flare related changes seen in the local and global velocity oscillations in the Sun. We have applied wavelet transform to the time series of the localized velocity flows as well as the global velocity oscillations in the Sun spanning the flare event. We observe peculiar evolution of velocity flows in some localized portions of the penumbra of this active region during the flare. The Wavelet Power Spectrum of these velocity flows reveals that there is major enhancement of velocity oscillations in the high-frequency regime ($5 < \nu < 8$ mHz), while there is feeble enhancement in the p-mode oscillations ($2 < \nu < 5$ mHz) in the aforementioned location (Figure 20 (a)). We also observe enhancement in the high-frequency global velocity oscillations in the Sun after the flare (Figure 20 (b)). It appears that during the flare process there might be a common origin for the excitation of local and global high-frequency oscillations in the Sun.

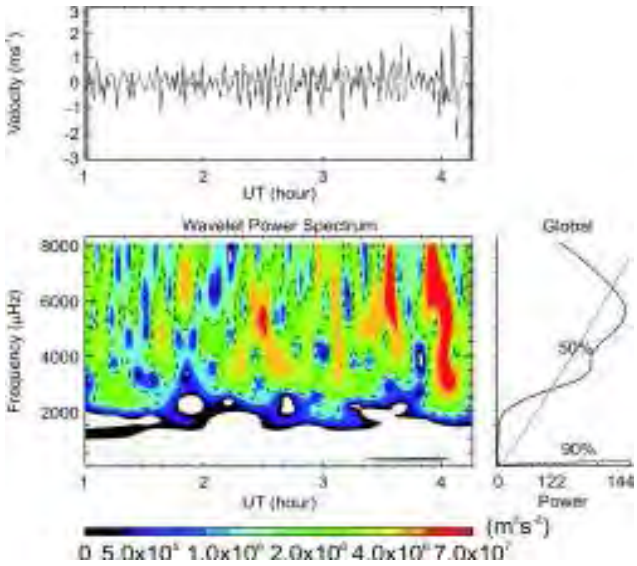

Figure 20 (b): The upper panel shows the temporal evolution of disk-integrated velocity observations of the Sun obtained by SOHO/GOLF instrument during 01:00-04:15 UT spanning the flare event of 13 December 2006. The lower panels show the Wavelet Power Spectrum (WPS) and the Global-wavelet Power Spectrum (GWPS) computed from this time series. In the WPS, the dashed lines correspond to regions with 50% confidence level whereas in the GWPS, the dotted line is for 50% significance level.

This work has been done in collaboration with Savita Mathur of High Altitude Observatory, Boulder, USA, and R. A. Garcia of Laboratoire AIM, CEA/DSM-CNRS, Universite Paris, IRFU/SAp, Centre de Saclay, Gif-sur-Yvette, France.

(Brajesh Kumar, P. Venkatakrishnan, and Sanjiv Kumar Tiwari)

Acoustic Power Absorption and its Relation with Vector Magnetic Field of a Sunspot

The distribution of acoustic power over sunspots shows an enhanced absorption near the umbra–penumbra boundary. Earlier studies revealed that the region of enhanced absorption coincides with the region of strongest transverse potential field. In this work we i) utilize the high-resolution vector magnetograms derived using Hinode SOT/SP observations and study the relationship between the vector magnetic field and power absorption and ii) study the variation of power absorption in sunspot penumbrae due to the presence of spine-like radial structures. It is found that i) both potential and observed transverse fields peak at a similar radial distance from the center of the sunspot, and ii) the magnitude of the transverse field, derived from Hinode SOT/SP observations, is much larger than the potential transverse field derived from SOHO/MDI longitudinal field observations. In the penumbra, the radial structures called spines (intra-spines) have stronger (weaker) field strength and are more vertical (horizontal). The absorption of acoustic power in the spine and intra-spine shows different behaviour with the absorption being larger in the spine as compared to the intra-spine.

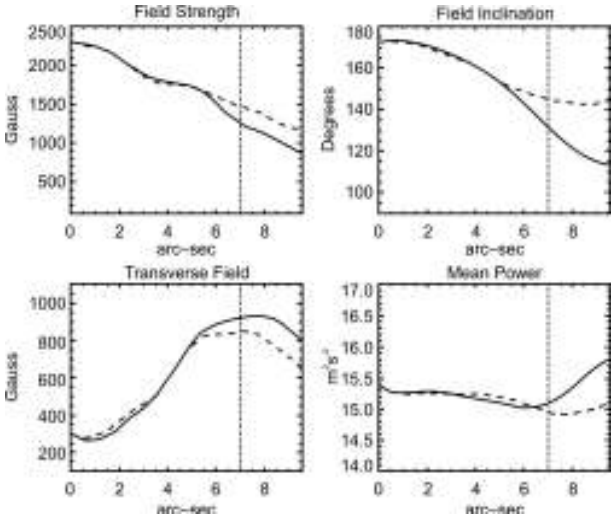

Figure 21: The profiles of the magnetic parameters and acoustic power absorption along the intra-spine (solid) and spine (dashed). The vertical dashed line represents the umbra-penumbra boundary.

(S. Gosain, S.K. Mathew, and P. Venkatakrishnan)

Transient Features driven by the X2.2/White-Light Flare of 2011 Feb 15 in NOAA 11158

The first X-class (X2.2) flare of the solar cycle 24 in NOAA 11158 occurred on 15 February 2011. It was observed by the Helioseismic and Magnetic Imager (HMI) on board Solar Dynamics Observatory (SDO) which provided unprecedented high resolution magnetic and Doppler images without the degrading effects of Earth's atmosphere. From the movies made from these images, we have detected transient magnetic and Doppler velocity features moving away from the flare site during the peak phase of the flare. We had earlier reported similar features associated with the X17 flare in the super-active region NOAA 10486 of solar cycle 23. (Figure 22) shows a mosaic of AR NOAA 11158 images at different heights in the solar atmosphere, where the locations of observed transients are marked. The temporal evolution of these transients is shown in Figure 23. It is evident from (Figure 22) that the transient appeared near the cool umbral/penumbral site of the AR. These transients are found to be spatially and temporally associated with the white-light flare (WLF) ribbons and hard X-ray (HXR) sources. From (Figure 23) it is evident that the transient features were distributed along the narrow lanes marked as curves L1 and L2. Also, we found them to be better associated with WL flare ribbons as compared to the HXR sources. The center of the HXR source moved toward the right as time progressed while the transient features remained located along the curves L1 and L2. Detailed examination of these transients with the flare is being pursued further.

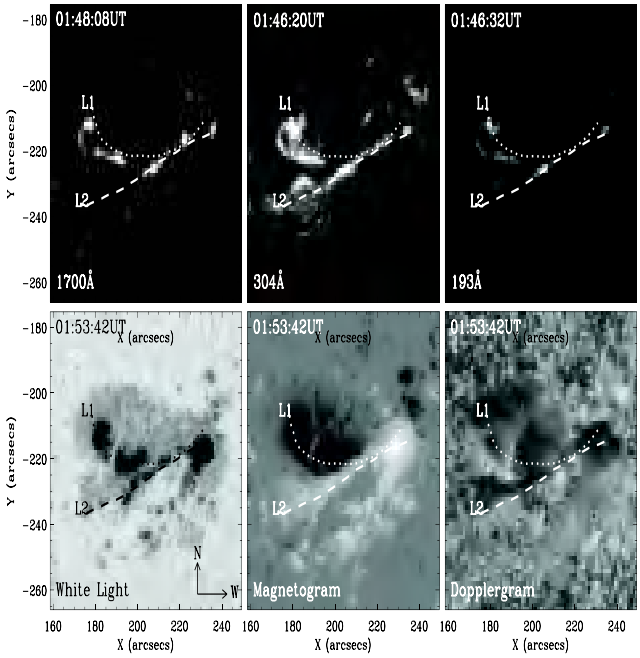

Figure 22: Mozaic of the AR NOAA 11158 during the X2.2 flare of 2011 February 15. Top (from left),: SDO-Atmospheric Imaging Assembly (AIA) images at wavelengths 1700 Å (continuum from the photosphere and temperature minimum), 304 Å (He II from the chromosphere and transition region) and 193Å (Fe viii, xx, xxiii from the corona and hot flare plasma). Bottom (from left):SDO- HMI intensitygram, magnetogram and dopplergram images. Green curves marked by L1 and L2 represent the locations of the magnetic and Doppler velocity transients.

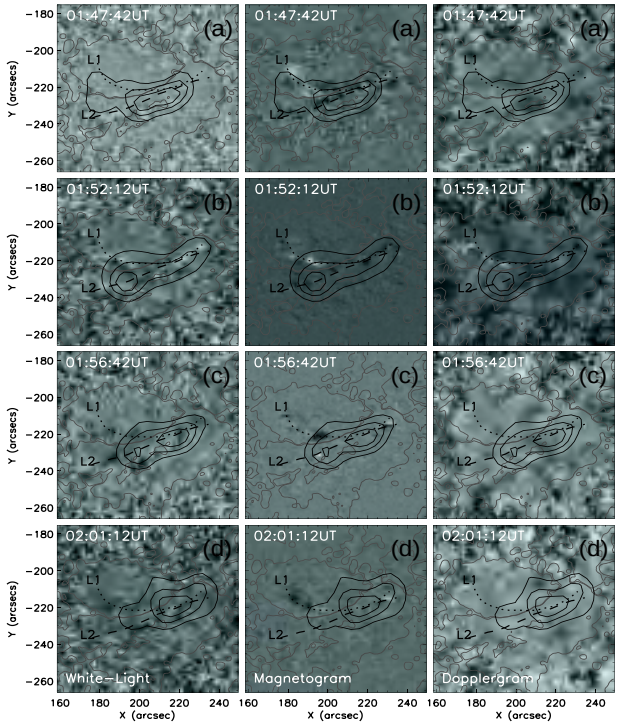

Figure 23: Difference images (I_i - I_{i-1}) of SDO-HMI white-light intensity, magnetogram and Dopplergrams (from left to the right column) with time (from top to bottomrows). Curves L1 and L2 mark the locations of transients features. Red (Blue) contours shows the magnetic flux with +50 (-50)G levels while black contours represent the RHESSI HXR levels at 40, 60 and 80% of the maximum flux in the energy band 12-25 keV.

(Ram Ajor Maurya, Vema Reddy and Ashok Ambastha)

Filament eruption leading to two ribbon M1.0 flare and CME

To understand the driving and triggering mechanisms of Flare/CME, we studied AR NOAA 11093 that appeared on August 7, 2010. We employed analysis of observational data in multi-wavelengths obtained mainly from recently launched spaced based mission Solar Dynamic Observatory (SDO) with supplemented data from various other space and ground based observatories. We inferred an upward rising motion of an inverse S-shaped filament lying along the polarity inversion line (PIL) originating at the main sunspot. This motion appears to have triggered filament eruption subsequent to the reconnection. As a result overlying field lines expanded, exploded as CME and material ejection occurred along the flux rope as observed in STEREO/EUVI-A. We calculated the CME velocity as 574 ± 23 kmps. We also evaluated the energetics of the flare by measuring velocities of flare ribbon separation along different directions, and calculated reconnection rates and flare energy, (Figure 24). We found velocities in the range 12-16kms^{-1} and reconnection rates with 1-3 Vcm^{-1}. The flare ribbons separated out with significantly lower velocities as compared to that reported previously for some other flares, but the reconnection rates were similar in magnitude and agreed with standard flare model. We also examined the photospheric magnetic flux changes as the active region evolved. Flux emergence and cancellation regions were found in and around the filament at the onset time of flare/CME of the orders of 10^{20} Mx. We suggest that observed emergence/cancellation of magnetic fluxes near the filament caused the flux rope to rise, resulting in the tethers to cut, and reconnection to take place; in agreement with the tether cutting model.

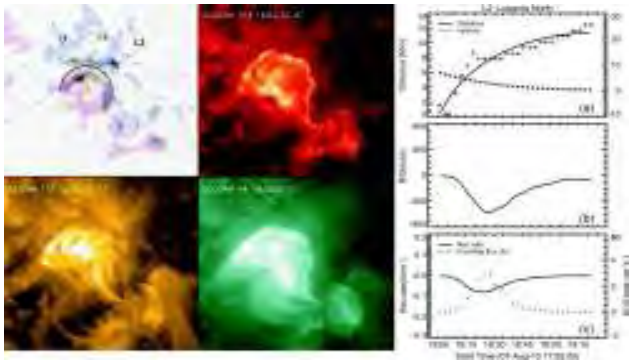

Figure 24: Various physical parameters calculated along the line L2 in northern direction. (a)"+" represents the measured distances of ribbons from PIL with time, and the solid lines through them represent the Boltzmann sigmoid fits. Corresponding velocities are shown by dotted lines. (b) LOS magnetic field at the points of ribbon measurements, and (c) the reconnection rate (solid) and Poynting flux(dotted). It clearly shows connectivity of ribbons with field lines in SDO/AIA 304, 171, and 94 Å as they correspond to different atmospheric layers.

(Vema Reddy, Ramajor Maurya, and Ashok Ambastha)

Evolution of twist-shear and dip-shear during X-class flare of 13 December 2006: Hinode observations

The non-potentiality (NP) of the solar magnetic fields is measured traditionally in terms of magnetic shear angle i.e., the angle between observed and potential field azimuth. Here, we introduce another measure of shear that has not been studied earlier in solar active regions, i.e., the one that is associated with the inclination angle of the magnetic field. This form of shear, which we call as the "dip-shear", can be calculated by taking the difference between the observed and potential field inclination. We study the evolution of dip-shear as well as the conventional twist-shear in a sunspot using high-resolution vector magnetograms from Hinode space mission. We monitor these shears in a penumbral region located close to flare site during 12 and 13 December 2006. It is found that: (i) the penumbral area close to the flaring site shows high

value of twist-shear and dip-shear as compared to other parts of penumbra, (ii) after the flare the value of dip-shear drops in this region while the twist-shear in this region tends to increase after the flare, (iii) the dip-shear and twist-shear are correlated such that pixels with large twist-shear also tend to exhibit large dip-shear, and (iv) the correlation between the twist-shear and dip-shear is tighter after the flare. The present study suggests that monitoring twist-shear during the flare alone is not sufficient but we need to monitor it together with dip-shear.

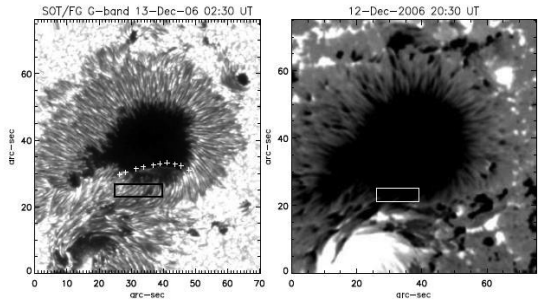

Figure 25: The left panel shows the G-band filtergram of the sunspot in NOAA AR 10930 during 12 December 2006 02:30 UT, with the location of the flare ribbon marked by '+'symbols. The flare ribbons sweep across the rectangular box during 02:20 to 02:26 UT. The right panel shows the map of the longitudinal field component for this sunspot. The black (white) rectangle in left (right) panel marks the region where we monitor the evolution of twist-shear and dip-shear.

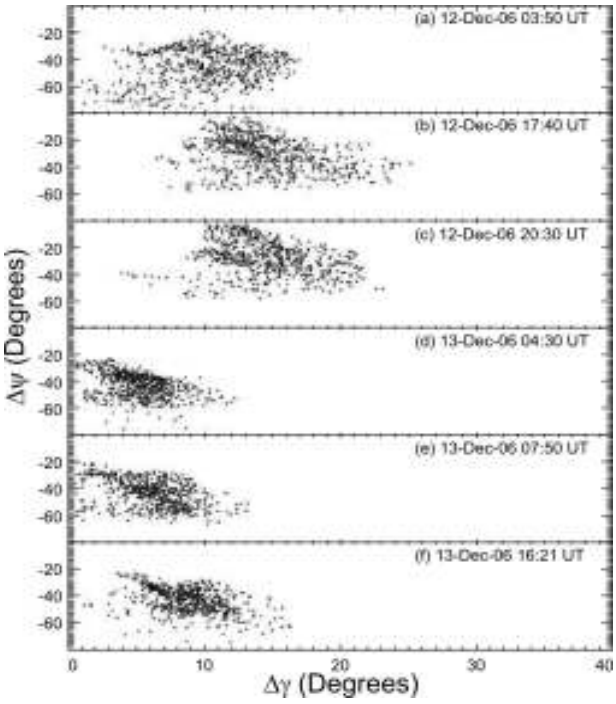

Figure 26: The panels (from top to bottom) show the evolution of twist-shear and dip-shear inside the region marked by rectangle in Figure 25.

(S. Gosain and P. Venkatakrishnan)

Pre-flare activity and role of magnetic reconnection during the evolutionary stages of a solar eruptive flare.

In order to understand the triggering mechanism of solar eruptions, it is essential to examine the pre-flare phase and investigate if there is a causal relation between the activities in the precursor and flare main phase. For this purpose, we have carried out a comprehensive multi-wavelength analysis of a well observed while-light flare of GOES class M3.2 from active region NOAA 10486 on November 1, 2003 which shows considerable pre-flare activities. The study utilizes the excellent set of high resolution observations from three space missions, viz., RHESSI, TRACE, and SOHO. The flare exhibits significant pre-flare processes for ~9 minutes before the onset of impulsive phase. The initial pre-flare activities are inferred from TRACE images at EUV/UV wavelengths as the brightening in the bipolar core region close to the filament and changes in the configuration of short, low-lying loops. This initiation phase is followed by the X-ray precursor phase, which is manifested in RHESSI measurements below ~30 keV. During this phase, the X-ray emission is dominantly thermal with the plasma temperature ~27 MK already at the very start (Figure 27). The examination of high temporal resolution SOHO/MDI magnetograms of the flaring region reveals the rise of an emerging flux region (EFR) of positive polarity with the start of precursor phase which evolved throughout the flare main phase. The very first signature of eruption was observed at this time as the bright arc-like structure. The sequence of activities during the pre-flare phase is suggestive of an "internal slow reconnection" and consistent with the tether-cutting process triggered by the flux emergence.

Plasma temperature attains a maximum (~30 MK) in the early impulsive phase during which EUV flaring region undergoes large structural changes. The impulsive phase is characterized by two HXR bursts at a separation of ~3 minutes with X-ray emission originating from two foot-point sources and a loop-top source. During this phase, the flare spectrum is composed of a thermal component of temperature ~22-30 MK, and a non-thermal component with photon spectral index γ = 3.6-6 (Figure 27). The present study indicates a causal relation between the activities in the preflare and main flare. The study further suggests that the reconnection during the pre-eruption phase could be very different from the post-eruption coronal econnection which is the fundamental part of the standard flare model.

This work has been done in the collaboration with Astrid Veronig (University of Graz, Austria; S. -C. Bong, and K. –S. Cho (KASI, Daejeon, South Korea); S. K. Tiwari (Max Plank Institute of Solar System Research, Germany; J. Lee (NJIT, USA).

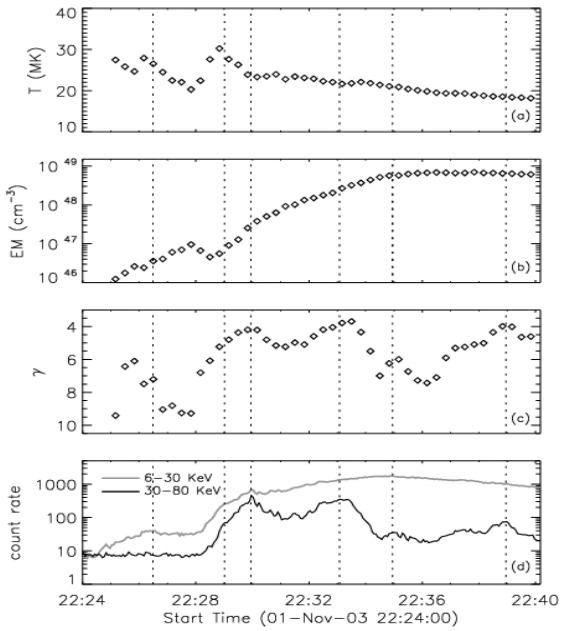

Figure 27: Temporal evolution of various spectroscopic quantities derived from RHESSI X-ray spectral fits of consecutive 20 s integration time. From top to bottom: plasma temperature (T), emission measure (EM), photon spectral index (γ), and RHESSI X-ray light curves in 6-30 and 30-80 keV energy bands. We note that the plasma temperature is very high ($\sim$27 MK) at the beginning of X-ray precursor phase. Vertical lines denote various stages of flare evolution as seen in the X-ray light curve.

(Bhuwan Joshi)

Kinematics of Two Eruptive Prominences from EUVI/ STEREO

We have analysed two helically-twisting northern hemisphere polar crown prominences observed on 2010 April 13 and 2010 August 1, using 304 Å images from EUVI instrument on board the twin STEREO spacecraft. The stereoscopic reconstruction technique developed by us was used to obtain the heliographic coordinates of several features along the prominence legs, as shown in Figure 28. In both the prominences, features 1 to 5 belong to one leg, while features 6 to 9 belong to the other prominence leg. From the changes in latitudes and longitudes of the features, we find that the spine of 2010 April 13 twisted in clockwise direction, while that of 2010 August 1 twisted in the anticlockwise direction. The prominences showed two phases consisting of the slow rise and the fast-eruptive phase. Additionally, during the fast-eruptive phase, the latitudes of both the prominences decreased, indicating non-radial equatorward propagation.

The two aspects of eruptive prominences, namely, helical twist and non-radial propagation have been studied separately. However, for the first time we have shown using stereoscopic reconstruction applied to EUVI images, that the two motions produce different acceleration in the two prominence legs. For the 2010 April 13 prominence, the leg in which the motions acted in the same direction experienced an acceleration of 11ms^{-2}, as against 5ms^{-2} in the leg in which the motions acted in opposite directions. The corresponding values of acceleration for the 2010 August 1 prominence are 20ms^{-2} and 10ms^{-2}. This study offers a new perspective on the effect the motions of a prominence has on its acceleration, and shows that the two prominence legs need not experience the same acceleration.

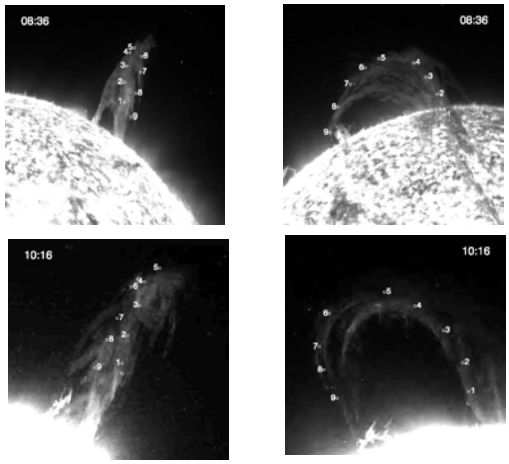

Figure 28: EUVI 304 Å images of the 2010 April prominence from STEREO B (left) and A (right). Features 1 to 9 are marked along the prominence spine. Helical twist in the spine could be seen in the images from STEREO B.

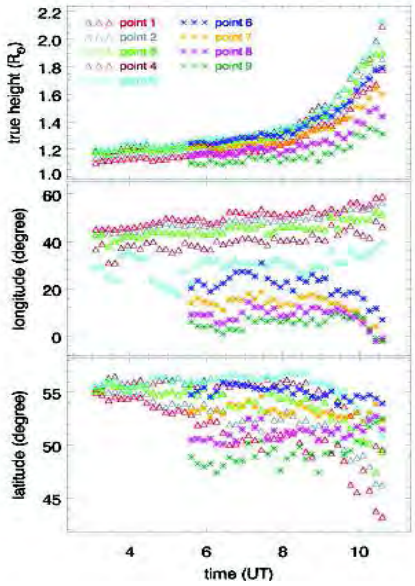

Figure 29: Heliographic coordinates of features along the spine of prominence on 2010 April 13. Features 1 to 5 belong to one prominence leg, while features 6 to 9 belong to the other prominence leg.

(Anand D. Joshi and Nandita Srivastava)

Acceleration of CMEs and the Associated Prominences

We have analysed six cases of coronal mass ejections (CMEs), on 2007 November 16, 2007 December 31, 2008 April 9, 2009 December 16, 2010 April 13 and 2010 August 1, and the prominence eruptions associated with the three CMEs on 2008 April 9, 2010 April 13 and 2010 August 1, using data from the SECCHI suite of instruments on board the STEREO spacecraft. Stereoscopic reconstruction technique was used to obtain the true coordinates of a feature in the leading edge of the CMEs, and in the associated prominence for the selected events. Acceleration of all the features selected and tracked was determined by fitting a high-order polynomial function to the height versus time data. The CME on 2007 December 31 was associated with a C8 flare, however it still showed acceleration as high as 1500ms^{-2}, which is very unusual. This challenges the current belief that the CME acceleration is directly dependent on the X-ray class of the associated flares. Three of the CMEs which were associated with flares showed a bimodal acceleration profile, i.e., after the main peak of acceleration, a second 'residual' peak appears at a higher height. This is consistent with the findings reported by Chen & Krall (2003, J.Geophys.Res. 108, 1410). Interestingly, the CMEs associated with eruptive prominences do not show the residual acceleration phase. Another important finding from our study shows, that of the three prominence-associated CMEs, the ones on 2008 April 9 and 2010 April 13 showed an increasing trend in the acceleration up to a height of almost 4$R_{\odot}$ from the Sun centre, while the corresponding CMEs did not show this behaviour, suggesting that the forces acting on CME and the associated prominence cannot be regarded to be the same.

(Anand D. Joshi and Nandita Srivastava)

Spontaneous current sheet formation: Numerical study

The spontaneous formation of current sheets (CSs), or equivalently magnetic tangential discontinuities, is a fundamental research problem in ideal agneto-hydrodynamics (MHD) characterized by an infinite electrical conductivity. As a consequence of this infinite electrical conductivity, the magnetofluid can be partitioned into contgiuous magnetic sub-volumes, each entrapping its own magnetic field. Two such magnetic sub-volumes then may push into each other by squirting out the interstitial magnetofluid. The magnetic field being entrapped into each magnetic sub-volume, diffusion of field lines from one interacting sub-volume to the other is prohibited. Under such circumstances then, the magnetic field becomes discontinuous across the surface of interaction. From Ampere's law then the current density corresponding to this discontinuous magnetic field is confined entirely at the surface of discontinuity and forms a CS. This phenomenon of CS formation and its subsequent decay because of small scale dynamics is believed to be play a major role in heating the solar corona to its million degree temperature. The objective of our work in this area of research is to understand the dynamics of CS formation through numerical simulations. For the purpose, a three dimensional time dependent viscous magnetohydrodynamic (MHD) code has been developed. The novel feature of this code is in its representation of magnetic field in terms of magnetic flux surfaces enabling a direct visualization of the dynamics of CS formation. Figure 30 represents a pair of such intersecting flux surfaces with axes along the z (red-colored) and x (blue-colored) directions, as an initial condition for a pilot numerical experiment. The lines of intersections of the two flux surfaces are the magnetic field lines depicted in Figure 31. For the given pair of flux surfaces, all field lines are closed, non-circular and reverses sign in between two black colored loops. As this system is evolved from a static initial state, the Lorentz force pushes the plasma and converts magnetic energy to kinetic energy, the latter being dissipated by viscosity. Figure 32 shows the time evolution of a new set of flux surfaces constructed from the red-colored flux surfaces depicted in Figure 30. The negative space in Figure 32 contains the field reversal layer across which the magnetic field reverses its sign. The dynamics of CS formation can easily be visualized from Figure 32 where the time sequence shows that a CS is formed as the Lorentz force pushes the magnetofluid on each side of the field reversal layer towards each other by squirting out the interstitial fluid.

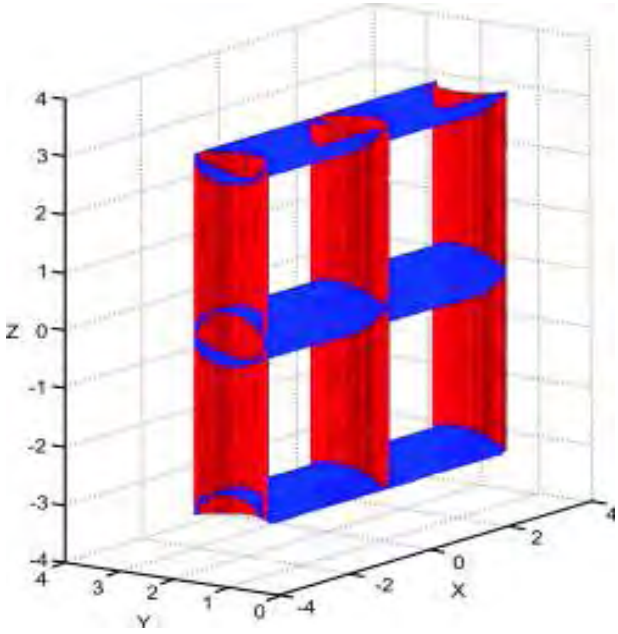

Figure 30: A pair of intersecting flux surfaces at t = 0 with axes along the z (red-colored) and x (blue-colored) directions.

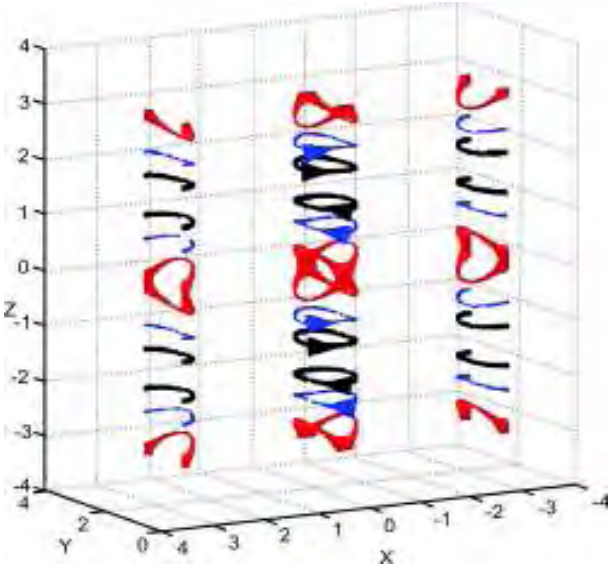

Figure 31: Magnetic field lines on a red-colored flux surface with axis in the z direction.

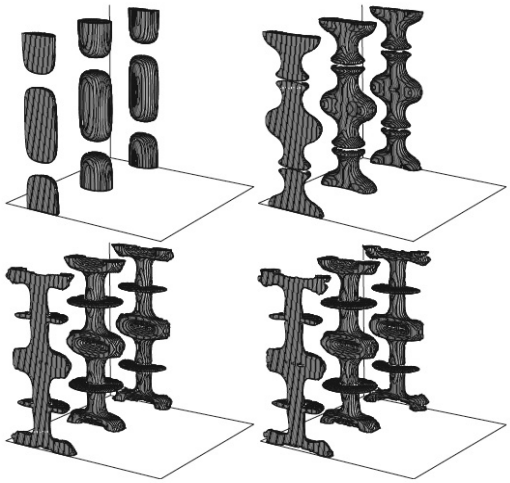

Figure 32: Time evolution of a new set of flux surfaces constructed from the red-colored flux surfaces. The negative space of this new set of flux surfaces contains the magnetic field reversal layer across which the magnetic field reverses its sign.

This work was done in collaboration with B. C. Low and Piotr K. Smolarkiewicz of the National Center for Atmospheric Research, Boulder, USA.

(Ramit Bhattacharyya)

Solar coronal loops as non force-free, flow containing minimum energy relaxed states

In this work solar coronal loops are proposed as flow containing, minimum energy relaxed states characterized by a non zero Lorentz force (non force-free) as opposed to the more conventional force-free states. The work is motivated by the observation that it is only the mid-corona, sandwiched between the upper and the lower corona, which is tenuous enough to be approximated as force-free i.e., the Lorentz force is zero. However in the lower and the upper corona, the magnetic field deviates from its force-free configuration with a Lorentz force comparable in magnitude to the plasma pressure. It is also known from stability analysis that for an ideal magnetofluid, the cylindrical and toroidal magnetic structures are unstable at the Alven time scale. This time scale being of the order of seconds for the coronal parameters, the life time of the coronal magnetic loops ranging from few seconds to days cannot be explained by the conventional MHD stability analysis. This "long-lived" property then may indicate the possibility of a magnetofluid relaxation process in the corona with the magnetic loops as the terminal or relaxed states of a spontaneously occurring natural process. In this work, this relaxed state is obtained by minimizing the total ordered energy (magnetic + kinetic) of the magnetofluid while having global generalized helicity invariant.

The resulting Euler-Lagrange (EL) equations are of general nature compared to the conventional linear fore-free state and sustain self-consistent plasma flow. The linear force-free state is a subset of the above EL equations for a plasma flow parallel to the magnetic field. The (EL) equations are solved by the superposition of two Chandrasekhar-Kendall eigenfunctions (CK) each of which represents a linear force-free field. Further, to solve the EL equations we have adopted a Cartesian geometry with $z>0$ half-space representing the corona whereas the $z=0$ surface represents the photosphere. The corresponding magnetic field lines are depicted in Figure 33, where α and Υ represents the deviation from the force-free state and twist of the field lines respectively. The Figure 34 depicts the projection of two sets of field lines with the same α but opposite γ (i.e., opposite twist) on the xy plane. Such forward and backward sigmoid structures are observed on the photosphere. The non force-free magnetic fields depicted in Figure 33 can be compared with the corresponding force-free field lines with the same twist plotted in Figure 34 and the potential field lines characterized with zero volume current density shown in Figure 35. Two points are of worth mentioning. The potential fields are found to be non-twisted. This is expected, since the twist in a magnetic field line is essentially induced by a current flowing along the field line whereas the potential field does not sustain any current at all. Also the loop height of the non force-free field lines are greater than that of the force-free field which is in general agreement with the understanding that the magnetic fields in the higher corona are non force-free.

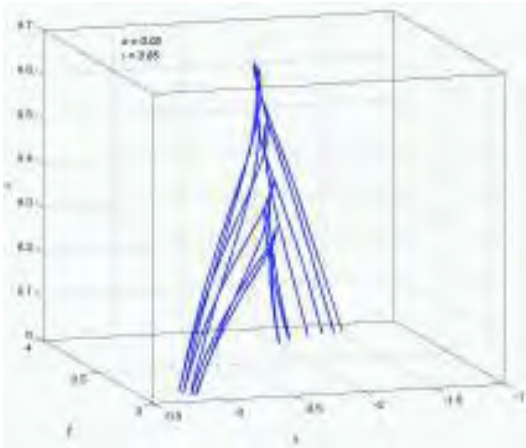

Figure 33: Three dimensional non force-free, twisted magnetic field lines. The parameters á and ã represents the deviation from the corresponding force-free field lines and the twist of the field lines respectively

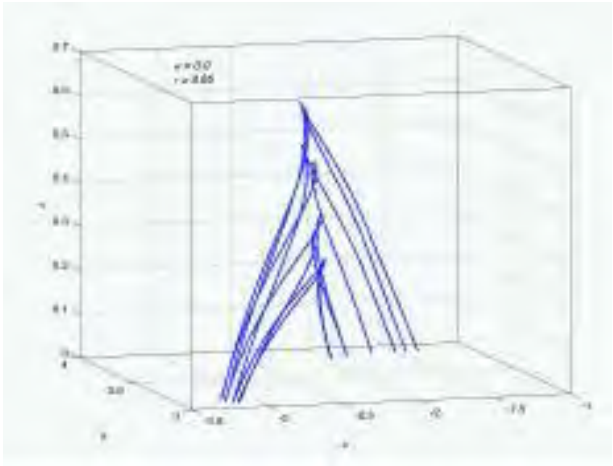

Figure 34: Projections of the twisted three dimensional magnetic field on the xy plane. The forward and the backward sigmoid shapes are for the positive and negative twists of same magnitude respectively.

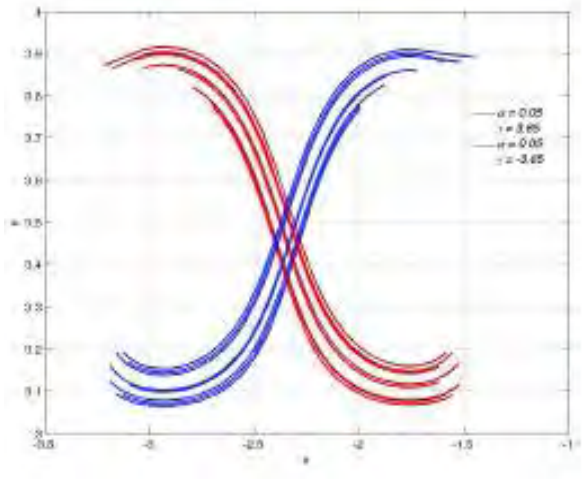

Figure 35: Force-free magnetic field lines with the same twist as shown in the Figure 33.

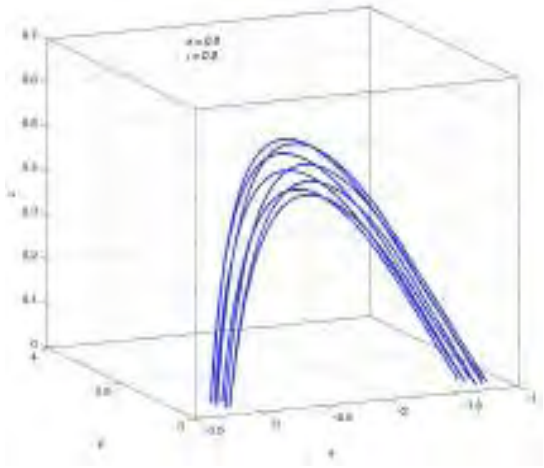

Figure 36: Potential field lines showing zero twist.

(Ramit Bhattacharyya and Dinesh Kumar)

Demonstration of Adaptive Optics

The Udaipur Solar Observatory was developing a prototype adaptive optics system that is capable of on-line correction of image distortions produced by the turbulence in the earth's atmosphere. This system was able to demonstrate locking on to a sunspot image (NOAA 11072) on 25 May 2010 under closed loop condition, operating at a speed of 1000 frames per second. This is the first ever demonstration in the country, of adaptive optics capability on real-time images at such high speeds. This achievement will be very useful for other applications also. Figure 37 shows a comparison of images with and without adaptive optics correction.

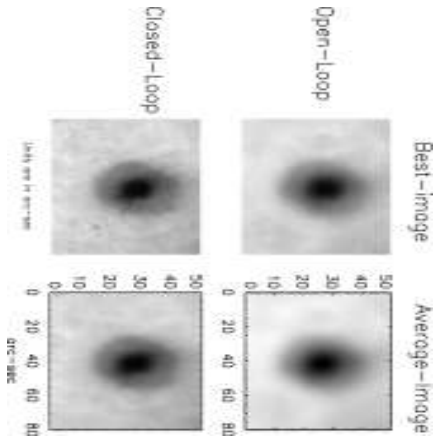

Figure 37: The top row shows the image of a sunspot without locking the system. The best image of the series is on the left while the average image integrated over the entire sequence is shown on the right. The bottom row shows the corresponding images after applying on-line real-time correction.

(Adaptive Optics Team of Udaipur Solar Observatory)

SCIENCE

Planetary Sciences and Planex Program

The activities in the Planetary Sciences Division and the PLANEX program during the year are centered around investigations on meteorites to understand early solar system processes, analysis of remote sensing data from lunar missions to understand surface features and surface processes on Moon and development of laboratory prototypes of instruments for planetary exploration. Standardisation and development of operational protocols for the three newly acquired analytical tools, NanoSIMS (Nano Secondary Ion Mass Spectrometer), MC-ICP-MS and MC-NGMS has also been accomplished. In this report, we provide a glimpse of these activities under three heads, Planetary Science, remote sensing data analysis from lunar missions and Planetary Exploration.

Identification and mineral and chemical characterisation of the micro phases is a tedious but most important aspect, before detailed isotopic measurements by NanoSIMS. Similarly, development of chemical separation procedures and/or measurement protocols for a given system of isotopes is a prerequisite for MC-ICP-MS and MC-NGMS instruments. Major efforts have been spent during the year in addressing these issues. Also, dating of hydrothermal sites has been initiated, using electron spin resonance (ESR) and optically simulated luminescence (OSL) techniques.

Imaging of Cold Bokkeveld in search of presolar silicates:

Astronomical observations indicate silicates as the main dust (most abundant of the presolar grains) around most of the stars. Since silicates are not resistant to acids, they dissolve during conventional chemical separation process (formation of H_2SiF_6). Along with this, the fact that presolar silicates make up only a tiny fraction makes it an impossible task to decipher presolar silicate grain from the rest of the silicate meteorite material. Small size (average size ~ 200-300 nm) of presolar silicates acts as additional hinderance making their in situ detection by conventional ion probe difficult. In situ search of presolar silicate grains was possible only with the advent of NanoSIMS (Nano Secondary Ion Mass Spectrometer) exploiting its high spatial resolution (50 nm) capability.

Isotopic study of presolar grains leads to understanding of nucleosynthesis taking place in individual parent stellar source. Apart from this, abundance of presolar grains in primitive meteorite gives a clue to the survival of these grains into the early solar system. Cold Bokkeveld meteorite was chosen for presolar silicate search on the basis of its noble gas isotopic composition and carbon content (bulk samples) indicating it is rich in presolar grains. Total matrix area of ~11,300 sq. micron has been rastered for ^{16}O, ^{17}O and ^{18}O, ^{28}Si and $^{27}Al^{16}O$ with nanoSIMS Cs^+ beam of ~100 nm to check for oxygen isotopic anomalies. Interactive data language (IDL) program is being modified in order to reduce the images to check for the presence of presolar grains, if any, in the analysed images. Preliminary examination of images shows absence of any presolar silicate grain indicating inferred lower limit for the abundance of presolar silicate grains from this work as ~0.14 ppm.

(K. K. Marhas)

Characterisation of CAI for further isotopic studies

Calcium Aluminum Inclusions (CAIs) will be analyzed for ^{26}Al, ^{10}Be and ^{7}Be in order to identify the source of short lived nuclides in early solar system. Proper mineral phases, suitable for the study of these isotope systems have to be identified through careful scrutiny of several CAIs. CAIs, the first formed solids from the solar nebula are high temperature mineral condensates found in the primitive chondritic meteorites composed mainly of oxides and silicates of calcium, aluminum, magnesium, and titanium. CAIs range in shape from irregular, highly porous aggregates of tiny crystals, to nearly spherical, densely crystalline objects. CAIs are broadly classified based on their structure and size as coarse and fine grained. Coarse grained are further sub-classified based on their composition and mineralogy as Type A, Type B (B1/B2) and Type C.

The very largest CAIs are up to 2–3 cm in size, but these occur in only one chondrite type (CV3); most CAIs are <1 mm in maximum size. A total of 65 ion probe sample mounts (epoxy thick sections) were prepared from various meteorites from CV3 group, identifying CAI via naked eye. Electron probe was used to the final identification and classification of primitive CAIs which was based on their mineral composition scheme proposed by earlier workers. We have classified 17 type B CAIs (melilite $\sim$5- 20%, anorthite $\sim$20 - 45%), 2 type A (melilite rich) and 2 fine grained spinel rich CAIs from these sections. Type B CAIs are further classified, 7 are type B1 having well formed Wark-Lowering rim and melilite rich mantle, rest are type B2. In case of type A both are compact type A (A1) having melilite content $\sim$50-60% and anorthite content $\sim$10%.

(Y. Kadlag and K. K. Marhas)

Quasi Simultaneous Arrival: Topography, Matrix effects and/or instrument transmission effect

In NanoSIMS, production of multiple secondary ions is possible from impact of a single primary ion. Almost simultaneous arrival of these secondary ions (called quasi-simultaneous arrival or QSA) at the first dynode of the electron multiplier is detected as a single event due to the electronically fixed dead time of the electron multiplier. Thus, counts recorded by electron multiplier for the major isotope is lower than actual/true number, leading to erroneous ratios. This affect is clearly observed in case of elements with high ionistaion efficiencies (for e.g. C, N, Si, O, S). Knowing secondary to primary ion ratio (k) and measured isotopic ratio, the true isotopic ratio can be calculated (based on Poisson statistics) as:

$$R_{meas} = R_{true} * (1 + \beta * k)$$

The "β" value varies from the theoretical value of 0.5 in nanoSIMS mainly due to variation in transmission, which is combined effect of (1) topography of the sample (grains), (2) matrix variation and (3) instrument transmission. Different nanoSIMS settings have been used to calculate the individual contribution of these three paramaters and to delineate the most prominent parameter dealing with QSA effect. Different matrices with same settings for similar isotopic analyses have been used to calculate QSA led by matrix variation. Effects of topography have been observed on individual grains with constant matrix and constant transmission. Finally instrument transmission can be calculated by using different setting of instrument apertures and slits on individual grains. Value obtained for SiC standard to be set as correction factor for QSA on the sample for Si, C and N varies from 0.6 to 0.7, 1.2-1.4 and 0.6-0.7 respectively.

(Y. Kadlag and K. K. Marhas)

New chemical extraction procedure for sulfur isotopic study from different mineral phases by MC-ICPMS

Sulfur is very useful element because of two reasons: i) it is redox sensitive and present in multiple valance states in nature and ii) it undergoes mass independent fractionation during UV photolysis. Therefore it has been used as tracer for various geochemical and cosmo-chemical processes. In general the sulfur isotopic composition of terrestrial or extraterrestrial samples has been measured by Stable Isotope Ratio Mass Spectrometer either as SO_2 or SF_6 as analyte gas. The measurement of S isotopic composition using SO_2 is easier but has memory problem because SO_2 is very corrosive and sticky gas whereas measurements using SF_6 involve complex chemical processes. Recently High Resolution-MC-ICPMS has been used to analyze sulfur isotopes with comparable precision but they are performed only on bulk sulfur. Here at PRL we developed a new column purification and chemical extraction procedure to analyze the S isotopes from various sulfur minerals such as soluble sulphate (Gypsum), barite and pyrite phases which is suitable for MC-ICPMS study.

Sulfur isotopes in MC-ICPMS have been measured on high resolution mode to resolve isobaric interference due to $^{32,33,34}O_2^+$, ^{32}SH, $^{64,68}Zn^{++}$ etc. Since all the molecular interferences are on the heavier side of the peak, sulfur isotopes are measured on low mass shoulder which is purely due to sulfur isotope. Since the width of shoulder is very small, exact positioning of mass is very important parameter for precise and accurate measurements. We performed measurements within $\pm$0.003 amu from the visual center of shoulder in steps of 0.001 amu and found out the proper position for analysis. In Figure 38, measurements of zero enriched samples (i.e., both sample

and standard are same) from different analytical sessions are given. It can be seen that the measurements are very precise.

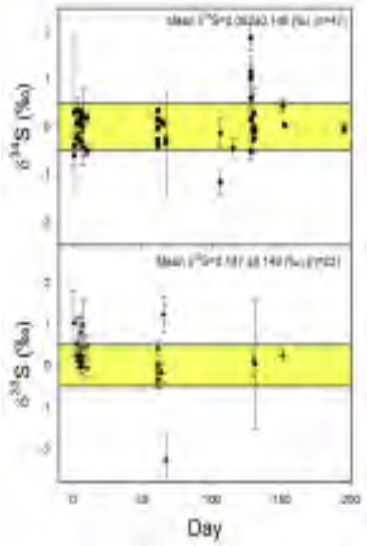

Figure 38: Sulfur isotopic analysis MC-ICPMS at PRL. measurements are performed in high resolution (some of the $\delta^{34}S$ data are from Medium resolution analysis as well), 20 cycles, using sample standard bracketing and performed in different analytical session during last six months.

(Prajkta Mane and Vinai K Rai)

Laser heating for analysis of noble gases in individual grains

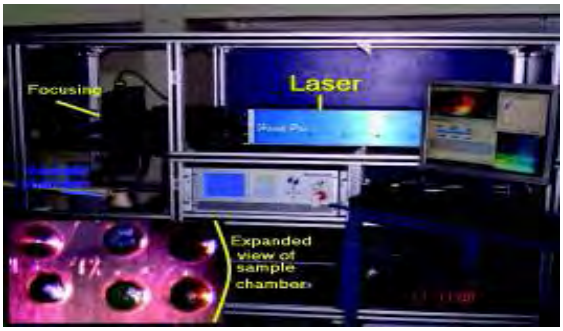

Figure 39: Laser Heating System (LHS) for the multi collector noble gas mass spectrometer, to enable very low blank gas extraction from single grains of few hundred μg. Various parts of LHS have been labelled.

We have recently procured an Nd-YaG laser as a heating tool for gas extraction from single grains. The laser heating system (LHS) has been integrated to the NOBLES, multi collector noble gas mass spectrometer and the necessary sub systems fabricated and put in place (see Figure 39). LHS enables the extraction of noble gases from sub milligram samples (individual grains) with minimal blank contribution. Typical blank levels achieved when maximum laser power is fired on the empty Cu holder for ^{22}Ne, ^{36}Ar, ^{84}Kr and ^{132}Xe are (in units of 10^{-14}ccSTP) 150, 7, 0.5 and 0.4 respectively. In addition to video recording of the heating process, the present system is equipped with a pyrometer to precisely record the temperature continuously. This later provision allows the determination of cooling rates precisely.

(R.R. Mahajan, S.V.S. Murty, N. K. Agrawal and Ranjit Kumar)

Chemical composition of individual chondrules

We are investigating cosmogenic noble gases (^{3}He, ^{21}Ne and ^{38}Ar) in individual chondrules from primitive chondrites, in search of precompaction irradiation signatures in them. Determination of production rates of the cosmogenic isotopes for individual chondrules is required for this. These production rates are chemical composition dependant. Considering the sample availability to be in the milligram range, it is a challenging task to determine the composition. We have developed techniques for analyzing the major, minor and trace elements in sub-milligram amounts of chondrules by ICP-MS. Two types of comparisions have been made to validate the results. Several aliquots of Allende standard, in milligram amounts have been run and the results compared with literature for accuracy and reproducibility. Also, where possible, a polished section of the same chondrule that has been analysed by ICP-MS has been studied by EPMA and the composition of the major elements cross compared. We focus here on the platinum group elements (PGE) in individual chondrules. The differences among the PGE abundances among the Dhajala chondrules (Figure 40) represent both the relative abundance of metal, as well as its cosmochemical evolution.

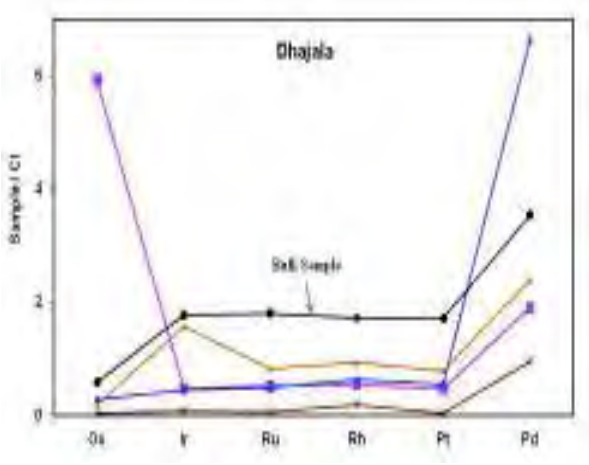

Figure 40: PGE abundances in the bulk sample and individual chondrules of Dhajala meteorite have been plotted. PGEs have been arranged in the increasing order of volatility (Pd most volatile).

(N. K. Agrawal and S.V.S. Murty)

Antiquity of the Eastern Dharwar Craton

Ion microprobe lead isotope (^{207}Pb-^{206}Pb) dating of zircons in samples of metasediments as well as ortho- and para-gneisses from both the western and the eastern parts of Dharwar craton yielded ages ranging from 3.2 to 3.5 billion years for detrital zircons present in metasedimantory rocks and also similar ages for the orthogneisses from both parts. Imprint of younger events have been discerned in the ages of overgrowths on older zircon cores in samples collected throughout the craton. The ages of the metasediments and gneisses show that the evolution of the southwest part of the eastern Dharwar craton involved a significant amount of older crust >3Ga. Our data suggest that crust formation in both the western and eastern parts of the Dharwar craton took place over similar time interval starting around 3.5 Ga and continuing until 2.5 Ga. The geochronological data coupled with geological features and geodynamic setting of the Dharwar craton tend to suggest that the eastern Dharwar craton and western Dharwar craton formed part of a single terrane.

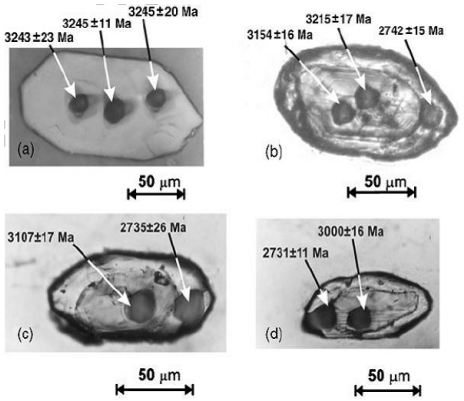

Figure 41. Reflected light photomicrograph of a homogeneous zircon (fig. a) that yielded concordant ages for multiple analyses. Transmitted light photomicrographs (b-d) of heterogeneous zircons showing distinct core-overgrowth morphology; ages obtained for the core and the younger overgrowth are also ahown in each case.

This work is done in collaboration with R. Srinivasan, Geomysore Services Pvt Ltd

(B. Maibam and J. N. Goswami)

Estimation of dose-rates for Mariana hydrothermal sites using gamma spectrometry and Al_2O_3:C dosimetry

The Mariana Trough is a present-day spreading backarc basin behind the Mariana Trench, where the Pacific Plate subducts under the Philippine Sea plate. The Mariana Trough is also characterized by active hydrothermal circulation with heat and chemical fluxes from the seafloor. Determination of the timescales of hydrothermal activity in the Southern Mariana trough has become important after the discovery of large hydrothermal plumes, with sudden changes in hydrothermal and volcanic activity in the sea floor. The long-term change of hydrothermal activities is also interesting in respect of ore formations. A systematic geochronological study of hydrothermal activities has not been possible due to the lack of methods which cover the age ranges of interest. In light of this, Electron Spin Resonance (ESR) dating of barites ($BaSO_4$) has been attempted in chimneys deposited from hydrothermal vents at the Archean site in the South Mariana spreading center and in the Okinawa Trough.

Estimation of ESR ages requires evaluation of onsite annual dose-rate estimation or laboratory measurements of radioactivity. Gamma spectroscopy of samples can be performed using scintillation or semiconductor detectors. We used a NaI(Tl) scintillation detector for measurements of gamma spectra at the Archean, Pika and Snail deep sea hydrothermal sites. At the Archean sites, dose-rate values were in the range 0.74 –1.87 mGy/a, whereas dose-rates of 0.23 and 0.92 mGy/a were observed at the Pika site. Measurements at the Snail site suggest dose-rate values of 0.21-2.03 mGy/a. The relative dose-rate values are nearly two orders of magnitude higher than background at the Archean sites, and at least an order of magnitude higher at the Pika site. Furthermore, a correlation was observed between rock type and relative dose-rate at all hydrothermally active sites.

Dose-rate measurements at the Pika site were performed using Al_2O_3:C dosimeters. Al_2O_3:C has a photon energy response similar to that of quartz and feldspar, and has an OSL sensitivity two orders of magnitude higher than TL sensitivity of LiF dosimeter. An Al_2O_3:C dosimeter package was placed for 29 days at the Pika site during the YK 10-10 cruise to Southern Mariana Trough, and was subsequently recovered during YK 10-11 cruise. The gamma dose-rate value estimated from Al_2O_3:C based OSL measurements are 0.84 at the above site, and is consistent with the dose-rate value of 0.92 mGy/a determined using NaI(Tl) gamma spectrometry.

This work is done in collaboration with S. Toyoda of Okayama University of Sciences, Japan.

(D. Banerjee)

Optical dating of quartz from hydrothermal sites in Middle and Southern Okinawa Trough

The Okinawa Trough is a 1200 km long, northeast-trending basin behind the Ryukyu Arc. Since it is a back-arc basin

in early spreading, modern submarine hydrothermal activity and mineralization have many characteristics which have aroused wide attention. The long-term change of hydrothermal activities is of interest in respect not only of ore formations but also of evolution of biological communities supported by the hydrothermal activities. Submarine hydrothermal fluids from the Okinawa Trough tend to be strongly influenced by interaction of the hydrothermal fluids with organic matter in the sediment resulting in high alkalinity and NH_4^+ concentrations of the fluids. The fluids also contain high concentrations of CO_2 of magmatic origin. A systematic geochronological study of hydrothermal activities has not been possible due to the lack of methods which cover the age ranges of interest. We have initiated a feasibility study using OSL (optically stimulated luminescence) to determine the age of quartz grains in two cores collected from Tarama Knoll, and the Izena Cauldron in the Middle and Southern Okinawa Trough. We extracted quartz from both core samples using standard chemical procedures, and subsequently used the SAR (single-aliquot regenerative-dose) method for estimating the OSL equivalent dose.

Preliminary results indicate an equivalent dose of ~6 Gy for the 1108-MB sample from the Tarama Knoll. For the core sample from Izena Cauldron, equivalent doses have been observed to have a bimodal distribution, and the average equivalent dose based on nine aliquots is ~40 Gy. Dose-rates were estimated from K, U and Th measurements using a low background pure germanium gamma ray detector, and preliminary ages of hydrothermal activities in the Middle and Southern Okinawa Trough have been estimated at the above two sites. The K, U, Th concentrations for the core sample from Izena Cauldron are 2.6%, 8.5 ppm and 10.2 ppm respectively. The total dose-rate is estimated to be ~3.5 mGy/a, and the OSL age of the hydrothermal activity is determined to be ~11.3 ka. The K, U, Th concentrations for the core sample 1108-MB from the Tarama Knoll are 2.0%, 2 ppm and 9.6 ppm respectively, implying an age of ~2.9 ka for hydrothermal activity at Tarama Knoll.

This work is done in collaboration with S. Toyoda of Okayama University of Sciences, Japan.

(D. Banerjee)

Component resolved optically stimulated luminescence investigations and age determination for a quartz sample from marine terrace sediments in Fukui region, central Japan

Optically stimulated luminescence measurements are usually performed using continuous-wave stimulation (CW-OSL) where the excitation power is kept constant during luminescence measurements. OSL measurements can also be carried out by linearly increasing the stimulation light intensity from zero to a maximum value. Thus, a measured LM-OSL spectrum shows peaks associated with traps having different photoionization cross-sections. We have analyzed the blue stimulated LM-OSL signal for coarse (75-150 micron) quartz extracts from a marine terrace sample in the Fukui region of Japan to isolate thermally stable and easy-to-bleach OSL components from the total LM-OSL signal. The sample is collected from marine sediments of the M2 terrace and is correlated with the Obaradai terrace. We have also investigated the dose-response, thermal stability and the effect of infrared stimulation on different components of the LM-OSL signal.

The LM-OSL curve was fitted with a sum of five components, and the photoionization cross-sections for the fast (F), medium (M), and slow components S1, S2 and S3 were estimated to be 5.8×10^{-18} cm^2, 1.6×10^{-18} cm^2, 2.8×10^{-19} cm^2, 5.2×10^{-20} cm^2, 2.7×10^{-21} cm^2 respectively. The associated lifetimes of the individual components are 1.5 s, 5.5 s, 30 s, 160 s and 3150 s respectively. Using the single aliquot regenerative-dose method for quartz, and a preheating treatment of 240°C for 10 s, we estimated the equivalent dose (De) in this sample to be 120 ± 27 Gy (n = 4). The background estimation was performed using the last 25 channels (5 seconds) for the CW-OSL signal. No background subtraction was used in estimation of LM-OSL signal components. The CW-OSL based average equivalent dose estimate for a 10 s, 280°C preheat is 183 ± 15 Gy for nine independent measurements. Furthermore, using a LM-OSL SAR procedure and a 280°C, 10s preheat treatment, we estimated the fast component in our LM-OSL signals, and determined the equivalent dose using the fast component to be 179 ± 21 Gy(n = 5). This value agrees with the CW-OSL estimate for equivalent dose. The Th, U and K concentrations were measured to be 9.73 ppm, 1.51 ppm and 2.05% respectively. Using a measured saturation water content of 49.5%, the dose-rate for this sample was estimated to be 1.95 ± 0.1 mGy/a. The age of the sample is thus determined to be ~94 ± 9 ka. The age of this terrace has been previously estimated to be 110-115 ka based on Sambe-Kisuki tephra. The OSL age of 94 ka agrees with the lower limit of the expected age to within 10%. This slight underestimation in age arises due to parameters associated with dose-rate estimation such as cosmic-ray dose, and errors associated with sensitivity correction procedure involved in the estimation of equivalent dose.

This work is done in collaboration with S. Toyoda of Okayama University of Sciences, Japan and M.Takada of Nara Women's University, Japan.

(D. Banerjee)

Remote Sensing data analysis from lunar missions:

Optical remote sensing data from payloads of Chandrayaan-1 (HySI, TMC, M3), Kaguya (MI-VIS) and LRO (NAC) missions have been analysed to understand specific surface features and evolutionary aspects through detailed morphological, chemical, mineralogical and physical parameters.

Secondary Craters on Moon

Analysis of Chandrayaan-1 Terrain Mapping Camera image of the Mare Imbrium region revealed a cluster of fresh and buried craters in the size range of 20-1300 m. A good fraction of the large (>150 m) fresh craters exhibits near circular mounds in the crater floor (Figure 42) and their size depends on the host crater size. Based on global lunar image and Chandrayaan-1 Hyper-Spectral Imager data, the origin of this cluster of secondary craters could be traced to impact of ejected fragments produced at the time of formation of the Copernicus crater. Our data provide further evidence for secondary crater formation by low velocity impact of a cloud of clustered fragments. The presence of central mound can distinguish the secondary craters from the primary craters and will be helpful in refining the chronology of lunar surface based on counting of small craters.

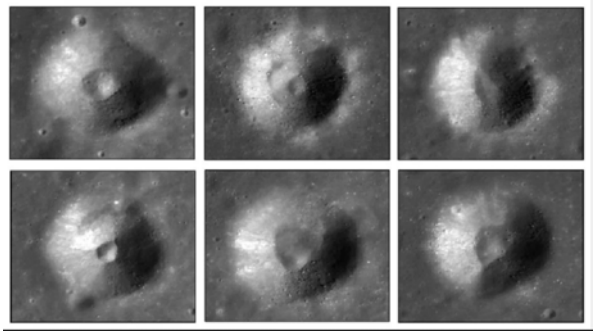

Figure 42. Secondary craters on moon hosting central mound displaying a wide range of morphologies.

This work is done in collaboration with P. Senthil Kumar (NGRI), A. Senthil Kumar and V. Keerthi (NRSC), B. Gopala Krishna and A. S. Kiran Kumar (SAC)

(J. N. Goswami)

Mg-Spinel lithology: A new rock type on the lunar farside

High resolution compositional data from Moon Mineralogy Mapper (M-cube) for the Moscoviense region of the lunar farside reveal several unusual rock types along the inner basin ring characterized by high concentration of orthopyroxene, olivine and Mg-rich spinel (OOS). They occur as small (a few km) outcrop and are widely separated within the highly feldspathic setting of the basin rim. The Mg-rich spinels, a new rock type, contains very little mafic minerals (<5% olivine and pyroxene). The OOS surfaces are old and are undisturbed since basin formation and are effectively invisible in image data and can only be identified spectroscopically due to their distinctive composition. They are embedded within the highly anorthisitic material from the lunar crust and could be near contemporaneous with crustal products from the cooling lunar magma ocean. The origin of these unusual lithologies may be linked to one or more magmatic intrusions into the lower crust and subsequent processes such as fractional crystallization and gravity settling leading to concentration of mafic components over localized km-sized areas.

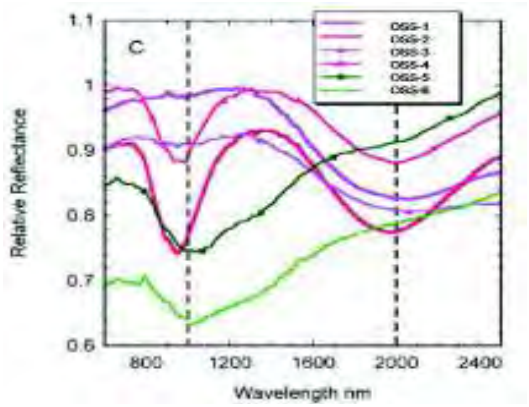

Figure 43. Relative reflectance spectra of OOS regions relative to a featureless local area of lunar soil having similar albedo. The spinel-rich lithologies are characterized by spectra (purple) with strong absorption near 2000 nm and featureless around 1000 nm, ortho-pyroxene spectra (red) have characteristic absorption at both wavelength regions, while the olivine spectra (in green) have a broad feature around 1000 nm and nearly featureless at 2000 nm.

This work is done In collaboration with Carle Pieters & M-cube team

(J. N. Goswami)

Volcanism on the Central Peak of Tycho Crater:

Crater Tycho (diameter ~102 km; 43.4^0 S, 11.1^{0}E, age: 108 Ma) is a unique dark haloed complex impact crater in the southern highlands, on the near side of Moon. High resolution reflectance datasets from Terrain Mapping Camera (TMC), Moon Mineralogy Mapper (M^3), Narrow Angle Camera (NAC) and Multi-band Imager (MI) onboard recent Moon missions such as Chandrayaan-1, Lunar Reconnaissance Orbiter and Kaguya have been used to study the morphology and composition of its central peak to understand its formation and subsequent modification. Volcanic vent, domes, pyroclastics, lava ponds and

channels showing distinct cooling cracks and flow fronts have been identified on the central peak (Figure 44 a,b). Compositionally, the lava pond and channels have been found to be rich in high Ca –pyroxene and the host rock is anorthositic in nature (Figure 44c,d). Thus, our investigation brings out clear evidences of late stage volcanic activity on the central peak of Tycho crater.

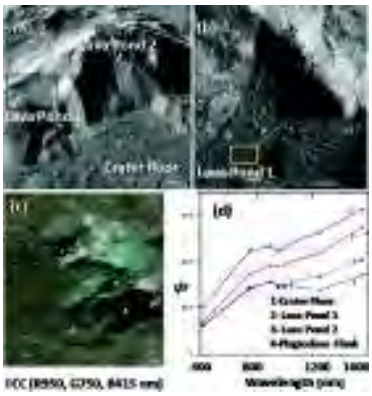

Figure 44: a) TMC derived 3D image of the central peak of Tycho Crater showing Lava ponds; b) LROC -NAC image of Lava pond 1 showing varied flow and pyroclastic relationships; c) False color representation of the central peak using SELENE MI data; d: MI derived spectral reflectance curves of the units marked in (c) showing abundance of High Ca pyroxene rich lithology over the central peak.

This work has been carried out in collaboration with Scientists from Space Applications Center, Ahmedabad.

(Neeraj Srivastava and J.N. Goswami)

Insight to KREEP volcanism on the Moon: Integrated analysis of M^3, DIVINER and LOLA data

KREEP is enriched in Potassium, Rare Earth Elements and Phosphorous with respect to other lunar rocks and is of volcanic origin. They are mostly confined to Procellarum KREEP Terrain (PKT) and are believed to have formed from solidification of the residual magma left after crystallization of ferromagnesium minerals as well as Ca-rich feldspars. Understanding the origin, evolution and distribution of KREEP rock is important in establishing link in the geological evolutionary history of the Moon. KREEP samples from the sample return missions have shown that they are enriched in volatiles and incompatible elements including Th and U. If KREEP is residual product of fractional crystallization of lunar global magma ocean then one may expect constituting minerals to be enhanced in their silica and more sodic/potash feldspar compared to lunar anorthosite or mare basalt. Extrusion of such magma will give rise to volcanic features that differ from basalts. It s observed that the boundary of the PKT has some unique domes with steeper slopes and higher elevation than domes observed on mare. It may be considered that these domes might have formed by other source than mare and understanding these domes may shed light into the volcanic history of moon.

The aim of the present work is to establish a relationship between KREEP volcanism and the distribution of silica enriched rocks on lunar surface by studying the domes found on the boundary of PKT with the help of remote sensing data sets. Initially, we have selected Gruithuisen domes (36.6° N, 40.5° W) on NE boundary of Oceanus Procellarum as a case study. The spectral characteristics

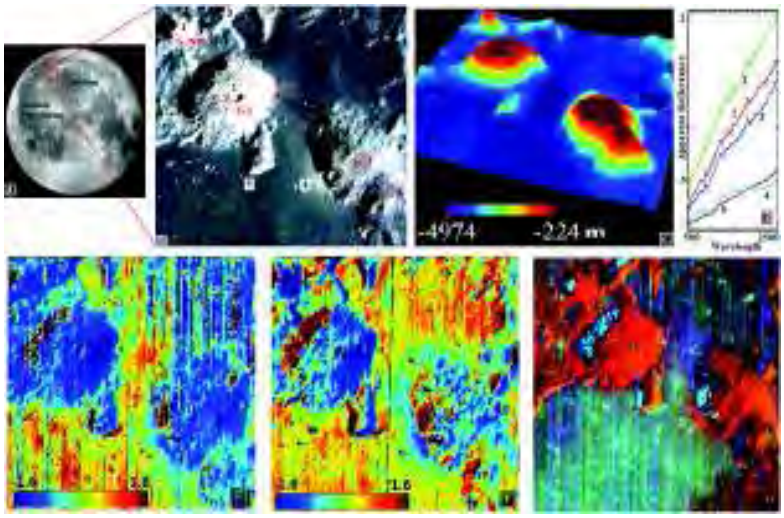

Figure 45. A) Location map of Grithuisen domes; B) M3 data showing three Gruithuisen domes, viz. G. γ, G. δ and G.NW.; C) 3D view showing topography of domes; D) Spectra of domes, highland material, fresh mare basalt and mature mare soil, location of spectra are given in Figure B.; E) Ti abundance image; F) Fe abundance image and G) FCC generated by assigning red color to R1580, green color to 1μm IBD and blue color to 2μm IBD.

of the domes are studied using Moon Mineralogy Mapper (M^3) and DIVINER data. The global mode M^3 radiance image (spectral range: 0.46 – 3.0 μm) was converted to apparent reflectance value. Method described by Lucey has been used for mapping abundance of Fe and Ti. The concentration of mafic mineral (pyroxene and olivine) is estimated by means integrated band depth (IBD) of 1 and 2 μm. The Diviner data for day and night time has been converted to emissivity and Christensen Frequency (CF) has been mapped. LOLA DEM (64 PPD) has been used for calculating the Morphometric parameters of these domes. The Gruithuisen constructs comprise of 3 domes, Gruithuisen γ, δ and NW (Figure 45A). The spectral studies using the M^3 show that the Gruithuisen constructs have different spectral characteristic compared to the highland and mare region. The M3 spectra of domes are in general featureless and have higher albedo. Domes are characterized by very low Fe and Ti content. The dome material show very low band depth in 1 and 2 μm IBD indicating a lower concentration of the mafic minerals in the area. Analysis of Diviner data shows that the pixels corresponding to Gruithuisen domes have lower CF value, which indicates felsic nature of dome material. The mineralogical, morphological characteristics of the Gruithuisen domes suggest a different origin compared to the surrounding area. The morphology resembles some of the volcanic domes on Earth and indicating a more viscous nature of eruption. We are currently working on the age of the domes using crater counting method. We will expand the study area so as to cover all the non-mare domes in the PKT region.

(K. N. Kusuma, Nita Sebastian and S.V.S. Murty)

Lunar Swirls: Connection with space weathering and magnetic anomaly

Lunar swirls are albedo anomalies associated with strong crustal magnetic fields. Generally lunar swirls have high albedo, low optical maturity and often exhibit dark lanes that interweave with brighter features. The present study aims to understand spectral properties of lunar swirls, and their implication to space weathering and magnetic anomaly. Study of lunar magnetic anomaly has been carried out by using magnetometer data of Lunar Prospector. Contouring of magnetic strength of the lunar swirls shows high magnetic strength on lunar swirls. These magnetic strength contours also show that few non swirl areas have high magnetic value. Space weathering trend can be studied by plotting 950/750 nm reflectance (low values of which are used strong ferrous band strength at ~1000 nm) vs. 750 nm reflectance. Results of space weathering study of Lunar swirls using Kaguya MI-VIS and Moon Mineralogical Mapper data shows that swirls exhibit a different trend than their background. The brighter portion of swirls shows a linear trend that is displaced to higher 750 nm values and slightly lower 950/750 ratios which is illustrated as trend 1 in Figure 46. The background material shows trend 2, in which higher maturity pixels of mare region are found in upper left while the immature pixels are found in the lower right of the plot (Figure 46a and 46b) and their corresponding location. Trend 2 is for the well developed soils (low albedo upper left) and small fresh crater in the area (high albedo lower right). Earlier investigations have found that when mare locations are contaminated with highland ejecta, their maturity trend was broadened and displaced in the same direction in 750 nm as seen in trend 1. Therefore from the space weathering trend it can be inferred that swirls contain immature material which may contain a small amount of highland material along with the mare material. Future study will cover the correlation among magnetic strength, space weathering and topographic relief.

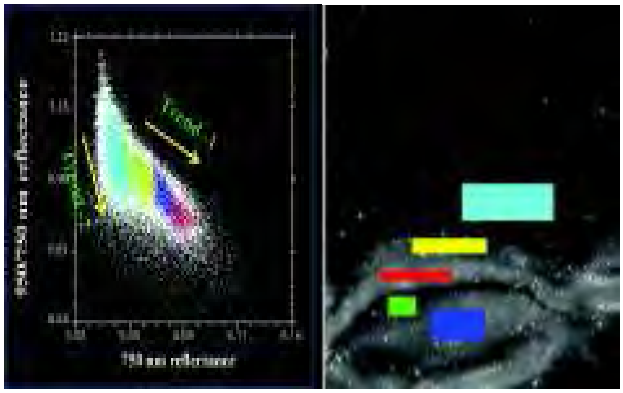

Figure 46: Approximate band strength (950/750 nm) vs. albedo 750 nm for the region in swirls for Reinner Gamma using M3 data.

(Diganta Kumar)

Mineral Mapping of Orientale Basin using Chandrayaan-1 M^3 data

The mare Orientale ("eastern sea") is one of the youngest multi-ring impact basins and most striking large scale lunar features located western limb on the Moon covering 930 km in diameter centred at 20°S 95°W. The morphological features and mineralogical diversity of Orientale basin have developed interest among geoscientist to further study this region. Material from this basin was not sampled by the Apollo program so the basin's precise age is not known. Unlike most other basins on the Moon, Orientale is relatively less flooded by mare basalts, exposing much of the basin structure to view. Hence, Orientale Basin is important to our overall understanding of the geology of large impact basins. The distribution of minerals in the lunar surface play vital role in studying the lunar origin and evolution. Hence, the present study concentrates to identify and estimate the mineral abundance in the Orientale

basin based on the absorption features and the linear spectral unmixing hyperspectral techniques. The Orientale data were acquired in M^3's reduced resolution mode at 40 nm spectral resolution and 140 m/pixel across the 40 km field of view. The RELAB spectral library of clinopyroxene, orthopyroxene, olivine and plagioclase has been used for this mapping. Based on these mineral spectra, the spectral mixtures of 8 rock end members have been created from plagioclase, clinopyroxne & orthopyroxene and 4 rock end members formed from plagioclase, pyroxene and olivine with different ratios. Linear Spectral Unmixing is to determine the relative abundance of materials that are representing in hyperspectral images based on the materials 'spectral characteristics'. The reflectance at each pixel of the image is assumed to be a linear combination of the reflectance of endmembers present within the pixel. The preliminary results show that, this area is mostly dominated by plagioclase and clinopyroxene minerals and gabbroic anorthosite and anorthositic gabbro rock types which are bearing plagioclase and clinopyroxene. The Lucey's algorithm used to derive the FeO and TiO_2 estimation has confirmed the low-medium TiO_2 basalts. The results are validated through previous reviews and Apollo returned samples mineralogy. The Hapke radiative transfer model to estimate the composition is ongoing and expecting additional results from this analysis.

(S. Arivazhagan)

Payload Development activities

Two payloads are under preparation for the Chandrayaan-2 mission, scheduled for launch in 2013. One of the payloads, X-ray Solar Monitor (XSM) is for the orbiter and the second one, Alpha Particle X-ray Spectrometer (APXS) is for the rover. In addition to these time bound programs, we are also developing a Gamma Ray Spectrometer for the future orbiter missions, an Auger Electron Spectrometer for in situ surface analysis and developing the new technology of Wireless Sensor Networks for the in situ exploration of planetary surfaces in future missions. A brief progress report on these activities is detailed here.

Radiation Environment in Earth-Moon space

The Radiation Monitor (RADOM) on board Chandrayaan-1 monitored the local radiation environment in near earth and in lunar space. It started observations about two hours after launch of Chandrayaan-1 and continued till the end of mission. Signature and intensity of proton and electrons in the earth's radiation belt as well as of galactic cosmic rays and solar energetic particles en-route to moon were measured. The maximum value of measured dose in the electron and proton radiation belts were ~40,000 mGy/h and ~130,000 mGy/h, respectively. These values are consistent with doses measured on board International Space Station. En-route to moon the particle flux (~3 particles cm^{-2} s^{-1}) and corresponding dose (~12 mGy) were rather small. The total accumulated dose during transfer from Earth to Moon was found t be ~1.3 Gy. The dose value at 200 km orbit was slightly higher than that at 100 km lunar orbit. A mild suppression in radiation dose, caused by shielding of the moon during orbit around moon, could also be detected.

This work is done in collaboration with T. P. Dachev and B. T. Tomov (Bulgarain Academy of Sciences) and V. Girish (ISAC)

(S. V. Vadawale and J. N. Goswami)

Solar X-ray Monitor (XSM) onboard Chandrayaan-2

The aim of the instrument is to obtain high resolution solar X-ray spectra in the energy range 1-20 keV. This payload is a part of the remote X-ray fluorescence spectroscopy experiment; the second part – lunar X-ray spectrometer (known as CLASS) is being built by ISAC, Bangalore. The data from XSM will provide real time measurement of the solar X-rays, which is essential for quantitative interpretation of lunar X-ray fluorescence spectra as x-ray fluorescence from lunar surface depends mainly on the incident solar flux.

It is well known that the intensity and spectra of the Solar X-rays are extremely variable. The X-ray intensity changes by four to five orders of magnitude within few minutes during large solar flares. Thus it is a great challenge to cover the entire range by a single detector, which we aim to achieve in our design of the XSM payload by using a new generation X-ray detector known as Silicon Drift Detector (SDD). This type of detector requires very sensitive and extremely low-noise front-end electronics which has been successfully designed and tested in-house.

XSM will have two packages namely XSM sensor package and XSM electronics package. XSM sensor package will be mounted on a satellite deck such that the detector is pointed towards sun. This package will house the SDD detector and its associated analog front-end electronics – namely charge sensitive pre-amplifier and shaping amplifier. The shaping amplifier is designed to accommodate extremely high count-rate (up to ~200,000 counts per second) expected during large solar flares. The complete detector chain is being optimized for the best energy resolution. The SDD requires operating temperature of 35°C which is achieved by means of internal TEC which maintains the required detector temperature by means of a TEC controller

designed and built in-house. The XSM electronics package will have FPGA based data acquisition and storage along with the interface with Data Handling (DH) subsystem of Chandrayaan-2 spacecraft. The FPGA based data acquisition and storage system will use RTSX32SU/72SU space qualified FPGA with 8k x 16 bit Dual Port RAM (DPRAM), 12 bit parallel ADC and other associated interface electronics. The package will also house telemetry; tele-command as well as power subsystem required for XSM operation and will be mounted inside the space craft. Overall electronic, mechanical and thermal design of the XSM payload is in the advance stages of being finalized. Laboratory model of the XSM payload based on the current design is under fabrication.

(M. Shanmugam, S. Goyal, S. V. Vadawale, Y. B. Acharya, Ejaj Ahmad, Bhumi Shah and Arpit Patel)

Alpha Particle X-ray Spectrometer (APXS) on-board Chandrayaan-2 rover

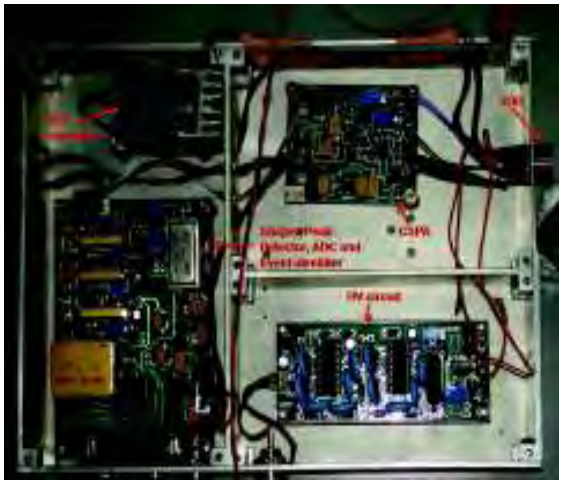

Figure 47. Breadboard model of the APXS detector package, wherein the SDD detector and the other processing subsystems have been marked.

Alpha Particle X-ray Spectrometer (APXS) instrument has been selected for Chandrayaan-2 rover to carry out in situ chemical analysis of lunar surface samples. The developmental status of APXS, during the past year is presented here. Briefly, APXS involves the measurement of characteristic X-rays emitted from the sample due to α particle induced X-ray emission (PIXE) and X-ray florescence (XRF) processes. We use ^{244}Cm as source of both Alpha particles and X-rays with energies of 5.8 MeV and 14.1 keV, 18 keV respectively. PIXE is dominant for low Z elements while XRF is more prominent for high Z elements, allowing the determination of elements from Na to Br, spanning the energy range of 0.9 to 16 keV. The activity of each alpha source is $\sim 5 \pm 25\%$ mCi and the total activity of the six alpha sources is about 30 mCi. Each source is of 8mm circular disc and $<$1mm thickness, with 6 mm active spot at the center. These sources are coated on Si substrate and sealed with 3 micron thick light tight titanium (Ti) foil. Silicon Drift Detector (SDD) with ~ 20 mm^2 active area will be used as X-ray detector. This detector module contains in-built peltier cooler and heat sink to maintain the detector at $\leq$ -30^{o}C by providing required power and dissipating the heat by means of additional heat dissipation mechanism. The flight model of the APXS payload will have two packages namely APXS sensor head and APXS electronics. APXS sensor head will be mounted on a robotic arm which will bring the sensor head close to the lunar surface, during the measurement on command. Once the acquisition is done, sensor head will be kept in rest position. APXS electronics will have interface with rover subsystems and will be housed in Warm Electronics Box (WEB) which is situated on the rover base.

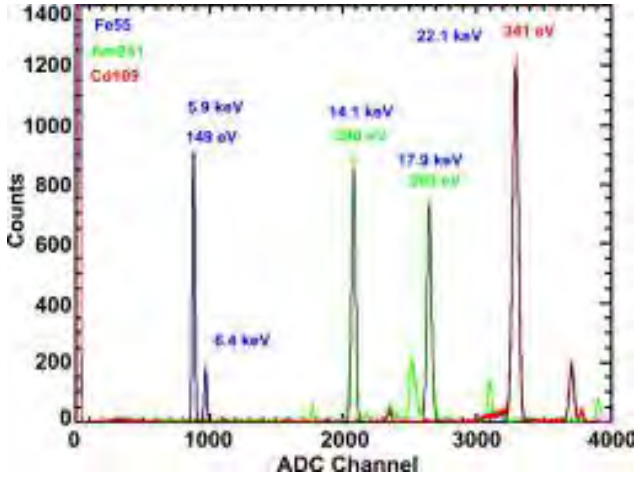

Figure 48. The X-ray spectra taken with standard sources (^{55}Fe, ^{241}Am and ^{109}Cd) with the breadboard model is shown. The energies and the corresponding FWHM are marked for some peaks.

Presently we have developed bread-board level subsystems for the APXS. The sub-systems developed for the APXS instrumentation are CSPA, Shaper-Peak detector-ADC, HV bias and Peltier controller. CSPA, Shaper and Peak detector circuits have been developed using hybrid modules as these devices are readily available in qualified form with optimal power and packaging requirements. The CSPA has been designed with "Reset" type and shaper with shaping time constant of 2μs. The ADC used in the design has 12 bit resolution. SDD requires HV bias of about -130V at RX (Outer ring), -20V at R1 (Inner ring) and -60V at RB (Back contact). These voltage levels have been generated using voltage multipliers as the total load current is ~ 20 μA. Peltier controller has been designed with PWM technique and it allows the required current through the peltier to get desirable ΔT. It has been tested with stability of $<$1^{o}C,

achieved within two minutes time from power on. The breadboard model of the APXS subsystems is shown in Figure 48. A sample spectra obtained from the bread-board model of the APXS electronics using three x-ray sources (^{55}Fe, ^{241}Am and ^{109}Cd) is shown in Figure 48. During the spectral acquisition, the detector temperature was maintained at -30°C. The energy resolution achieved with these settings is about 150 eV @ 5.9 keV with a low energy threshold of < 1keV. Presently we are evaluating the performance and suitability of the SDD modules from KETEK, GmbH (20 mm^2 detector area) and AMPTEK, USA (25 mm^2 detector area). We are also working towards realizing the engineering model of the payload and subsequently qualification and flight models for CH-2 rover.

(M. Shanmugam, Y.B. Acharya, S.V.S. Murty, S.K. Goyal, Bhumi Shah and Ejaj Ahmed)

Development of Gamma Ray Spectrometer (GRS) for Laboratory Testing

Using the laboratory Gamma ray spectrometer we can measure the natural radioactive isotopes of K, Th, U, as well as the reactor produced and/or cosmic ray produced activities from several elements (ex. Mg, Ti, Ca, Al, Fe, Si etc.). We chose a 3x3 inch $LaBr_3$:Ce coupled with a PMT and preamplifier with voltage divider, as the gamma detector. The advantage of this detector is that it does not require any cooling.

We have designed and tested a number of subsystems for the GRS. With the initial development work using the shaping and High voltage module we could get resolution of 2.6% at 1274 keV. We have modified the shaping and HV modules and improved the resolution to 2.4% at 1274 keV (Figure 49). We are working for achieving still better resolution, by further improving the sub-systems like shaping amplifier, discrimilator module, peak detector module etc. The earlier version of shaping amplifier was tested with single time shaping mode. A new board has been designed with multiple timing modes. The timing can be selected either by software or by hardware mode. The testing is in progress. Using this circuit the resolution and the linearity of the energy scale will be tested. In the new HV module we have replaced the locally made transformer with a commercially available transformer with some filter circuit to reduce the noise. The discriminator module is designed and fabricated in general purpose board and tested. This board will be used with the Peak detector module. Development of the peak detector module is in progress. The control signal required for the Peak detector module has been generated by microcontroller and tested. The testing of 10-bit internal ADC is done using a potentiometer.

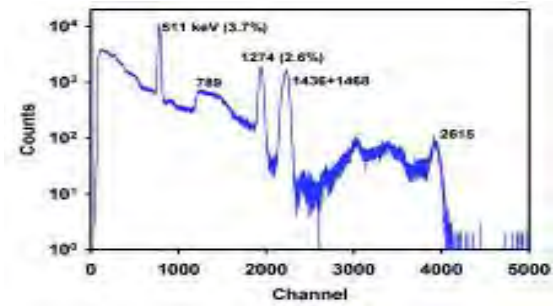

Figure 49: The spectra obtained from standard sources for the $LaBr_3$:Ce detector and homemade electronics modules is shown. Peak energies (in keV) and their corresponding resolutions (%) are marked.

(Dipak Kumar Panda, Shiv Kumar Goyal, Y.B. Acharya and D. Banerjee)

Development of an Auger Electron Spectrometer for a Planetary Mission

The project aims to develop a compact electron spectrometer for measuring the Auger electron spectrum of a solid target bombarded by photons or charged particles. The final goal is to use such a device on a planetary mission for identification of the elemental composition (especially low Z elements) of the terrain along the rover traverse, using Auger electrons as signatures. The analyser chosen for this task is a cylindrical retarding potential analyser (CRPA), based on the design of Enloe.

A CRPA was designed by us and was fabricated in the PRL workshop. It uses a channel electon multiplier as a detector. Initally, the analyser was tested for its resolving power by direct incidence of an electron beam from a gun. This test gave a resolving power of 2 eV at 2.0 keV incident energy. Later, the CRPA was used to observe the emitted electrons in various configurations and conditions, such as UV photoionisation of gaseous targets, and electron impact ionisation of solid and gaseous targets, with and without the application of an electric field to extract the electrons. By scanning the retarding voltage a pass curve (electron counts vs. retarding voltage) was generated. Multichannel scaling electronics and externally controlled, scannable high voltage modules used for the experiment were borrowed from old stock in the laboratory astrophysics group. Differentiation of the pass curve is expected to yield a normal spectrum. Difficulties, stemming mainly from random electrons and specular scattering of the incident beam, made it difficult to derive a spectrum in most cases, except the case of UV photoionisation of gases. Although some features/structures could be visually discerned in the pass spectrum, it was not easy to derive a spectrum from it. Since the experimental conditions were similar to the field conditions (i.e. in so far as the lack of control over

scattered electrons), it was felt that attention should be paid to deriving a spectrum by processing the data to eliminate the noise and scatter, rather than to working upon improving the experimental conditions. An algorithm was developed to smooth the pass curve while searching for deviation from a smooth pattern, based on a segmented least squares fitting of the function f(x) = 1/(x^{-a} + b) to the pass curve. Changes in the fitting parameter were exploited to identify structures. This approach has been applied to identifcation of Auger lines from a solid (ZnS and aluminium) as well as gaseous targets Ar, N_2 and CO_2, under electron impact. There are indications of Auger lines at the energies expected, but this needs further testing. Work is on to make the algorithm robust and to make it capable of determining line strengths and line widths. In the next phase blind samples will be tested for identification of Auger lines under electron impact. We also intend to test the CRPA on various targets using soft x-rays from the Indus-1 synchrotron.

(Bhas Bapat, Koushik Saha and Swaroop Banerjee)

Development of Charged Particle Detectors for SWEPS project

We are developing a "Charged Particle Monitor - Solar Wind and Energetic Particle Spectrometer" (SWEPS) to fly on any orbiter space mission to study the charged particle environment. The SWEPS experiment is originally aimed at studying processes within earth's magnetotail, lunar wake, and interplanetary environment, but in principle can monitor any planetary/interplanetary environment. We are developing solid-state semiconductor type charged particle detectors with high-resolution capabilities for this purpose.

Currently we aim to measure electrons, protons and heavier ions of solar origin in several energy ranges, viz. 0.3-720 keV, 0.8-100 MeV and 0.8-100 MeV, respectively using Si detectors. We propose ΔE type telescopic detector system of Si detectors for separation of electrons, protons and heavier ions. Detector package along with front-end, processing and common electronics for the whole experiment will be configured in one package. A single 12-bit ADC pulse-height-analyzer (PHA) is proposed to measure the spectra for all species. We have procured two units of each ΔE and E type Si detectors with active area 100 mm^2. Presently we are developing special charge sensitive pre-amplifier (CSPA) for each type detector to obtain the required pulse shape for the ions of our interest. We are also designing front-end and processing electronics for this system. The necessary hybrids and other electronics components have also been procured for the electronics development.

(Rajmal Jain, Jayesh Khunt, Arun K. Awasthi and V.D. Patel)

Wireless Sensor Network for Lunar and Planetary Exploration

This developmental activity has two components: development of nodes with sensors to detect one or a combination of geophysical/environmental parameters, and development of plausible and optimistic scenarios for deployment of nodes and the communication among the nodes and to the space craft. During the year, we have developed a WSN module and have integrated light and temperature sensors to it. We have also developed impedence spectroscopy for water detection to be a part of WSN. In addition, deployment scenarios and communication protocols have also been worked out.

Custom Design and development of Sensing Modules for Lunar WSN

Using WSN, Temperature and ambient light are two key parameters of interest and needs to be measured to a high degree of accuracy on a planetary surface. Since WSN itself is highly resource constrained, sensing module should be highly optimized and miniaturized, without compromising in performance. WSN compatible Sensor modules are being designed for measuring temperature and ambient light on a planetary surface.

Wide Range Temperature Sensing Module: A wide range temperature sensing module (-200°C to +200°C) using platinum RTD has been designed. Two miniaturized prototypes have been designed and evaluated. The dual channel prototype-2 has a footprint of just 2.5 cm X 3.5 cm which can be further reduced. The designed module is a low power single integrated design compatible with all RTDs. The design uses an innovative approach of employing just two amplifier blocks to provide gain, current and offset adjustments. Calibration and testing of the module have been done utilizing standard procedures. The performance of the module is evaluated by means of laboratory as well as field testing.

(K. Durga Prasad and S.V.S. Murty)

Ambient Light Sensing Module:

Prototypes of ambient light sensing modules have been designed and their performance is being evaluated. The two prototypes separately use an analog (TSL 257) and digital (TSL 2561) sensors for sensing ambient light. An USB interface is provided to enhance the compatibility and versatility of the module while wireless transmission is achieved by mean of a Zigbee Radio. The performance of

the modules has been evaluated by means of various experiments.

(A. Bhattacharya, K. Durga Prasad and S.V.S. Murty)

Wireless Impedance Sensor Node: Wireless sensor network may use various types of sensors to characterize lunar regolith. Permittivity of the soil can be measured by an impedance sensor. A Wireless Impedance Sensor Node (WISN) has been developed to study soil science. It works at 2.4 GHz in wireless mode and measures impedance of the sample under test. Permittivity and conductivity are derived using the impedance data. Testing of terrestrial soil and lunar soil simulant JSC-1A has been carried out in various phases. The results obtained by the sensor are verified by testing Milli-Q water, whose permittivity is known. The sensor is compact enough to prove its applicability for future planetary missions. In addition, the sensor may also be useful for other applications, based on impedance spectroscopy.

(Jayesh P. Pabari and Y. B. Acharya)

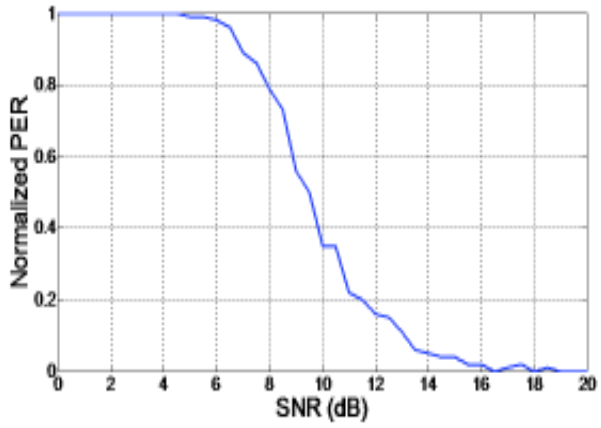

Figure 50: The signal to noise ratio (SNR) is shown against the normalised value of packet error rate (PER).

Lunar Multipath Environment:

Lunar regolith properties may be studied by a wireless sensor network on surface of the moon, by using appropriate types of sensors. These sensors can measure soil properties and communicate the result, as and when ready. However, communication scenario on lunar surface is quite different as compared to that on earth. There can be multipath effect during wireless communication on the moon. It is therefore, suggestive to study the lunar multipath environment and to predict the wireless link performance beforehand. Power Delay Profile (PDP) prediction method has been suggested to study lunar multipath environment. Using Digital Elevation Model (DEM) of the lunar site under consideration, Bit Error Rate (BER) and Packet Error Rate (PER) have been derived. BER and PER results convey the necessary Signal-to-Noise Ratio (SNR) for a given receiver. Also, maximum transmission data rate, without the use of an equalizer, is predicted based on lunar DEM. Exclusion of an equalizer simplifies the receiver design and consequently, reduces mass and size of the hardware, which are at premium in any space application. Figure 50 shows PER of a typical wireless link on lunar surface.

(Jayesh P. Pabari and Y. B. Acharya)

Deployment scenarios for lunar WSN- Simulation studies

Two different scenarios (orbiter and Lander/Rover based) can be employed for deploying a Wireless Sensor Network targeted for probing permanently shadowed regions of the Moon. Numerical Simulations have been carried out for both the scenarios to estimate the number of nodes required and their required communication range for covering the target crater. Some of the results obtained from the simulations are presented below.

Simulation for Orbital Deployment Scenario: Simulations have been carried out with various numbers of nodes with different communication ranges for three different permanently shadowed / anomalous lunar craters 1) Shackleton crater near lunar south pole (89.9° S, 0.0° E) with diameter of 20 km. 2) Rozhdestvensky Crater (84.3° N, 157° W) with a diameter of 9 km and 3) Byrgius Crater (21.3°S, 64.4° W) with a diameter of 6 km) that are expected to have greater probability of water/ice deposits. Simulations for orbital deployment have been done for four different scenarios for each of these craters, but results are presented in Figure 51 only for the Shackleton crater for two cases. The simulation results show that although effective coverage is achieved with nodes having range of 1 km, a range of 2 km between the nodes is to be preferred for complete coverage. Further, a total number of 25, 50 and 400 nodes would be required to cover Byrgius, Rozhdestvensky and Shackleton craters, respectively. A large area of coverage requires a comparably larger number of nodes than smaller areas, but with a non-linear relationship as the probability of all the nodes falling within the communication range becomes less when the coverage area is increased.

Simulation for Rover Deployment Scenario: The results show that coverage from the rim to the centre of the crater is achieved with a minimum of 25 nodes, each having 2 km range or 50 nodes, each having a range of 1 km. Taking

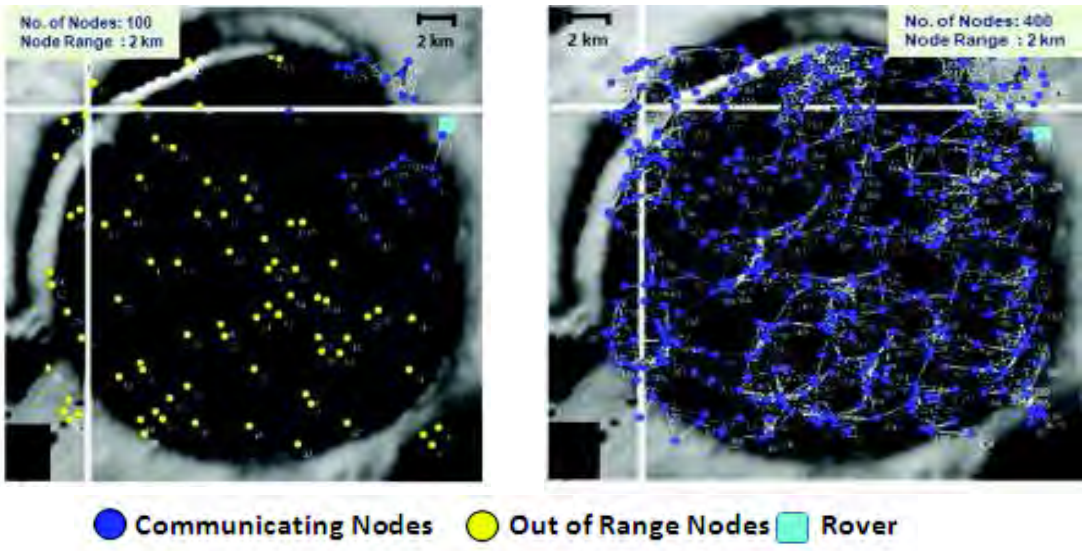

Figure 51: Simulation results are shown for the shackleton crater, for orbiter deployment scenario with communicating Rover.

redundancy into consideration, 50-100 Wireless Sensor Nodes will be required to be launched into the crater interior in the case of a Lander/Rover deployment scenario.

(K. Durga Prasad and S.V.S. Murty)

Performance Evaluation of Lunar environment chamber

A metal chamber has been built to simulate the pressure and temperature conditions of lunar surface. This chamber is intended for studying the physical properties of lunar surface and subsurface (using soil simulants) and also to validate the technology readiness of newly developed payloads planned for future lunar surface missions (Lander/ Rover). In order to evaluate the performance of the chamber, we have tried to simulate the surface environment of the Moon inside the chamber. The experiment is carried out to study the vacuum level, heating and cooling characteristics inside the chamber without and with soil sample. The experiment is setup as per a defined protocol. Experiment is carried out under both heating and cooling phases. During heating phase, the best vacuum that could be achieved with the sample was around 10^{-3} Torr whereas the same was around 10^{-6} Torr without the sample. This is due to the outgassing of adsorbed moisture and gases within the sample. It is possible to either pre-heat the soil in a vacuum oven or degass it for sufficient time inside the chamber, to achieve a better vacuum. The results showed that the base plate has achieved an equilibrium temperature of 400 K within 90 minutes of heating which is the daytime temperature of the lunar surface. The temperatures of the sample in the cup exhibited a gradient of nearly 60 K-70 K between the base plate and the sample which can be further improved by employing a better design.

During cooling phase, a vacuum of nearly 10^{-9} Torr is achieved in this case as the base plate starts acting as a cryo-pump at low temperatures. In this case the base plate attained an equilibrium temperature of 100 K which is near to the lunar night-time temperature in less than 90 minutes. At equilibrium, in both heating and cooling phases the temperature gradient between the external copper rod and the base plate was found to be nearly 20 K. Therefore, this demonstrates that the simulated lunar environment for both lunar day and night conditions can be achieved using this chamber which can be used for many applications. In order to demonstrate one such application, we have measured the thermal and electrical properties of the soil sample and studied their behaviour during both heating and cooling phases. A series of experiments to understand the properties and processes of lunar regolith are also planned using this chamber.

(S.V.S. Murty and K. Durga Prasad)

Space and Atmospheric Sciences Division

The research activities covered in Space and Atmospheric Sciences division pertain to the planetary atmospheres, solar terrestrial interactions, dynamical processes in middle atmosphere and the climatic impacts due to natural and/or man-made sources in the lower atmosphere. In addition, laboratory based simulation experiments relevant to near Earth environment have been pursued. Research investigations are carried out experimentally using the state-of-the-art instruments and substantiated with theoretical models. New laboratory experiments of mimicking astrophysical environment are being planned.

Size segregated chemical composition of aerosols using an aerosol time-of-flight mass spectrometer

An aerosol time-of-flight mass spectrometer which can provide size segregated aerosol chemical composition in the sub-micron and micron size range was procured, and installed in PRL during April 2010. The most important advantage of single particle aerosol measurement using aerosol time-of-flight technique is that it provides real-time information on the size and chemical composition of individual aerosol particles. These measurements can only provide the required crucial information on aerosol physical and chemical characteristics that are not available through any other methods. Single particle spectra of positive and negative ions of a 0.5 μm size aerosol particle measured in Ahmedabad on 3 May 2010 is shown in Figure 52.

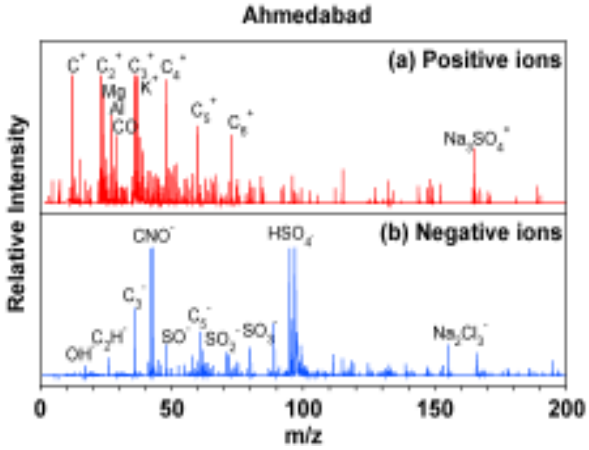

Figure 52: (a) Positive and (b) negative ion mass spectra of an aerosol particle of size 0.5 μm measured using an aerosol time-of-flight mass spectrometer (ATOFMS) in Ahmedabad on 3 May 2010. Peak identifications correspond to the most probable ions and compounds for the particular m/z ratio.

The positive ion spectra show the presence of carbon containing particles with magnesium, aluminium and potassium, and cluster of sulfate. The presence of peaks due to hydrocarbon clusters and potassium (m/z = 39 and 41) suggests this particle was produced by biomass burning. The negative ion mass spectra for the same particle confirm the presence of carbon containing particle with clusters of sulfate and chlorine (salt) (Figure 52). Preliminary analysis of the aerosol size spectra indicates that during

the pre-monsoon season the particles in the fine mode are dominated by organic carbon whereas the dust contributes 80% in the coarse mode. The winter season shows higher amount of elemental and organic carbon as compared to pre-monsoon season due to increase in biomass burning and decrease in boundary layer height.

(S. Ramachandran and T.A. Rajesh)

Aerosol radiative forcing from observations and models over an urban location

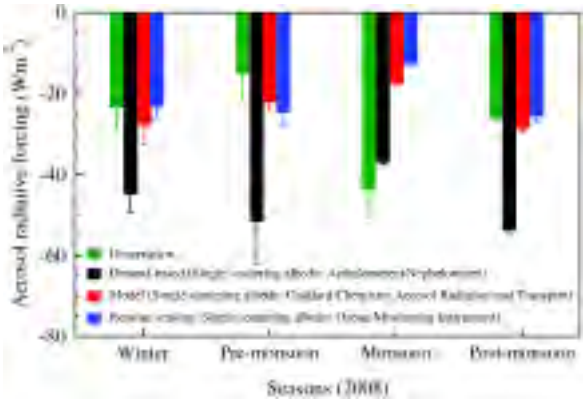

Figure 53: Seasonal mean aerosol radiative forcing at the surface derived from observation over Ahmedabad in comparison with aerosol radiative forcing estimated using single scattering albedo obtained from ground-based measurements (aethalometer + nephelometer), model (Goddard Chemistry Aerosol Radiation and Transport (GOCART)), and remote sensing (Ozone Monitoring Instrument (OMI)). Vertical bars correspond to $\pm 1\sigma$ variation from the mean.

Aerosol radiative forcing at the Earth's surface is estimated by simultaneous measurements of broad-band global fluxes and aerosol optical depths (AODs) over Ahmedabad an urban location in western India during 2008. AODs at 0.5 μm show large seasonal variability with higher values (0.52) during monsoon. Higher AOD during monsoon is mainly due to increase in relative humidity which overwhelms the effects of wet removal and addition of sea salt. Forcing efficiency for monsoon season is found to be lower as compared to other seasons. Surface aerosol radiative forcing is highest (-44 Wm^{-2}) during monsoon (Figure 53). Single scattering albedo (SSA) is higher in monsoon and the lowest in post-monsoon. SSA derived from ground-based measurements (aethalometer and nephelometer) is lower than columnar SSA estimated from Goddard Chemistry Aerosol Radiation Transport (GOCART) model, and derived from Ozone Monitoring Instrument (OMI) onboard Aura satellite. Model estimated surface forcing for ground-based SSA is about two times higher than the observed forcing for different seasons except for monsoon (Figure 53). However, model estimated forcing using columnar SSA agrees well with observations except in monsoon. The differences during monsoon are probably due to overestimation of SSA from GOCART and OMI. The study reveals that a small change in SSA can lead to significant change in aerosol radiative forcing.

(R. Srivastava, S. Ramachandran, T.A. Rajesh and S. Kedia)

Influence of aerosol mixing state on aerosol optical properties and radiative forcing

A simple and effective approach is proposed to determine the probable mixing state of aerosols over a location using measured aerosol optical properties. Single scattering albedo (SSA) for core (black carbon (BC)) - shell (sulfate) is lower than that of externally mixed aerosols and SSA does not change when the percentage of BC mass increases beyond 50%. Aerosol optical depth (AOD) is higher for external mixture, while SSA is higher for BC (core) and water soluble (shell) mixture in an urban environment. Aerosol radiative forcing at the surface calculated from measurements matches well with forcing estimated for probable mixing states determined for SSA derived from Ozone Monitoring Instrument (OMI) except in monsoon. During monsoon forcing of probable mixing state corresponding to ground-based (nephelometer and aethalometer) SSA follows observed forcing. Top of the atmosphere forcing is positive when SSA is lower while it is negative when SSA is higher. Forcing in atmosphere for probable mixing states derived for ground-based SSA is ~3 to 7 times higher when compared to those obtained for OMI SSA. Probable mixing states of aerosols and variable mass fractions of aerosol species (BC, dust, sea salt, water soluble and insoluble) involved in core-shell mixing vary as a function of season, and with SSA. The study reveals that knowledge on aerosol mixing state is important in assessing the impact of aerosols on regional and global climate.

(R. Srivastava and S.Ramachandran)

Natural vs. Anthropogenic aerosols: A new approach to characterize their radiative impact

A method to delineate the contribution of different aerosol species to aerosol radiative forcing using measurements over Ahmedabad and models is outlined. Mid-visible aerosol optical depth (AOD) does not show a strong seasonal variation, however, Ångström wavelength exponent (α) exhibits significant seasonal variation. α is higher during winter and post-monsoon when fine mode aerosols are dominant, and it is lower during pre-monsoon and monsoon when coarse mode aerosols are abundant. The contribution

of mineral dust to the total aerosol mass is >55% as Ahmedabad is located in a semi-arid region. Natural aerosols (mineral dust and sea salt) dominate the aerosol mass concentration (75%), while anthropogenic aerosols (water soluble aerosols and black carbon) dominate the aerosol optical depth (65%) and radiative effects (mainly black carbon, >50%). The study confirms that aerosol radiative forcing is dependent more on AOD and the chemical composition (SSA) than on the mass concentration of aerosols, and that there exists no linear relation between aerosol mass, optical depth and their radiative contribution.

(S. Ramachandran, R. Srivastava, S. Kedia and T.A. Rajesh)

Aerosol radiative effects over Indo-Gangetic plain: Implications and sensitivity

The seasonal variations in aerosol radiative effects over two environmentally distinct locations, Kanpur (urban site) and Gandhi College (rural location) in the Indo-Gangetic plain, a regional aerosol hot spot, are examined utilizing the measured optical and physical characteristics of aerosols. Shortwave aerosol radiative forcing at the top of the atmosphere (TOA) is < -10 Wm^{-2} over Kanpur and Gandhi College. Aerosol forcing at the surface is ≥ -30 Wm^{-2}. Atmospheric warming (ATM) is maximum during pre-monsoon (>30 Wm^{-2}). The net (shortwave + longwave) heating rate due to aerosols is >0.5 Kelvin/day (K/d) over Indo-Gangetic plain and peaks during pre-monsoon at ~0.9 K/d due to lower single scattering albedo (SSA). Results from the sensitivity study shows that TOA and ATM forcing undergo maximum change when SSA decreases; when solar insolation increases surface forcing shows the maximum variation which increases the atmospheric warming by 50%. The presence of curvature in the spectral distribution of AODs is found to reduce the aerosol radiative forcing significantly. The magnitude of longwave forcing and atmospheric cooling in an absolute sense is small and contributes about 20% or less to the net (shortwave + longwave) forcing. Atmospheric warming and surface cooling produced by aerosols over Kanpur and Gandhi College are an order of magnitude higher when compared to greenhouse gas forcing over the Indo-Asian region.

(S. Ramachandran and S. Kedia)

Impact of monsoon circulations on oceanic emissions of light alkenes over Bay of Bengal

Surface level measurements of ethene (C_2H_4) and propene (C_3H_6) were made in the marine boundary layer (MBL) of Bay of Bengal (BOB) during the summer and winter monsoon campaigns. The time series trends in the mixing ratios of alkenes were similar to that of wind speed, while no clear relations were observed with other meteorological parameters. The diurnal variations of ethene and propene concentrations show correlations with the intensity of solar flux as their daytime mixing ratios were ~45% higher than the nighttime measurements during summer. While winter measurements of alkenes do not depend on local time. The mixing ratios of alkenes were particularly elevated during the episodes of cyclones and convective activities in the summer season over BOB. The uptake rate of nutrients shows similar trend to those of mixing ratios of alkenes in summer, the measurements of phytoplankton indicate high primary production during the episodes of elevated alkenes over central BOB. The mixing ratios of alkenes showing minima in winter and maxima in summer are similar to the seasonal patterns reported for global oceans, however, their variability over BOB was less pronounced compared to the extra-tropical oceans. The mixing ratios of ethene/propene concentrations were comparable to a mean ratio of 2.3 pptv/pptv derived from the database for global oceans confirming the fresh oceanic emissions of alkenes over BOB. The emissions of alkenes were mainly controlled by the distribution of dissolved organic carbon in sea waters and action of wind speed in the presence of sunlight. This study is an important step to understand the processes controlling the emissions of alkenes from equatorial oceans and also to improve their global budget estimates.

(L. K. Sahu, S. Lal and S. Venkataramani)

Seasonality in the latitudinal distributions of NMHCs over Bay of Bengal

Surface level measurements of light non-methane hydrocarbons (NMHCs) were conducted during summer and winter monsoon campaigns over Bay of Bengal (BOB). The mixing ratios of major NMHCs during winter monsoon were significantly higher compared to the summer monsoon. During both the seasons, the distributions of NMHCs show clear north-south decreasing gradients over open oceanic region of BOB. During the summer (winter) monsoons, the latitudinal gradients of ethane, propane and acetylene were 29 (136) pptv deg^{-1}, 14 (46) pptv deg^{-1} and 14 (46) pptv deg^{-1}, respectively over open oceanic region of BOB. For measurements during summer monsoon, the latitudinal gradients in the mixing ratios of NMHCs were caused by the transport of pollutants from peninsular India to the northern BOB and flow of cleaner marine air over southern BOB. On the other hand, the gradients in the mixing ratios of NMHCs during winter monsoon are due to the dilution and photochemical loss towards the southern BOB. For the winter season, the estimates of photochemical age and

transport time over coastal and open ocean of BOB are give in (Figure 54). In both the seasons, no such clear latitudinal trends were observed along the east coast of India. The measurements along the coastal tracks were influenced by stagnant flow which also lacks clear north-south directionality. Alkenes show opposite seasonality to that of major NMHCs as the mixing ratios of both ethene and propene concentrations during summer monsoon were higher than the winter values. In addition, the distributions of alkenes also show significant heterogeneity, however, no clear latitudinal trends can be seen during both the seasons. The investigations of wind and ocean color parameters suggest substantial emissions of alkenes from surface sea waters which also support the seasonality of these species over BOB.

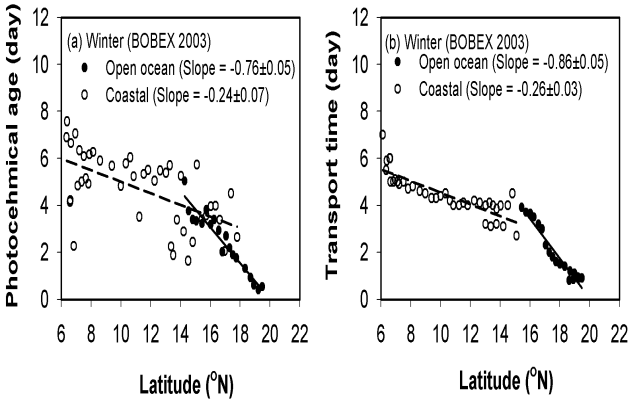

Figure 54: The latitudinal variations of (a) photochemical age of air mass estimated from the ratio of NMHCs and (b) transport time of air mass from the nearest continental point in the upwind region calculated using the trajectory data during the winter monsoon over Bay of Bengal.

(L. K. Sahu, S. Lal and S. Venkataramani)

Distributions of surface O_3 and its various precursors over the Bay of Bengal and the Arabian Sea during spring, 2006

Mixing ratios of ozone (O_3), carbon monoxide (CO), methane (CH_4) and few light NMHCs were measured on board the ocean research vessel Sagar Kanya over the Bay of Bengal and the Arabian Sea during spring 2006 as a part of an Integrated Campaign for Aerosol, gases and Radiation Budget (ICARB). Large differences are evident in the abundances of these trace gases over the Bay of Bengal (BoB) and Arabian Sea (AS) with higher mixing ratios of most of these gases over the northern part of Bay of Bengal (Figure 55). The seven days back-trajectories show the outflow of Indo-Gangetic Plain over this marine region. Effects of local marine air are observed over the southern parts of these regions. These species are found well correlated with each other over the BoB showing their common collocated sources over the Indian subcontinent. The latitudinal gradients of most of these species are found to be higher over northern part of this region compared to those observed during previous campaigns. Surprisingly and in contrast to the observations over BoB, the levels of these trace gases over the AS are found comparatively higher over the southern region than over the northern region leading to slightly negative north-south gradients. The short lived species having oceanic sources like ethene and propene show large variability with higher mixing ratios over southern parts of both the marine regions. The present study shows that the two marine regions are completely different from the perspective of surface level distributions of these trace species.

The distributions of ozone and CO are compared with the results from the 3D-MOZART model run at PRL. The model results broadly captured the main features over the northern BoB. However, ozone is found to be overestimated and CO is found to be slightly underestimated over the southern BoB and AS.

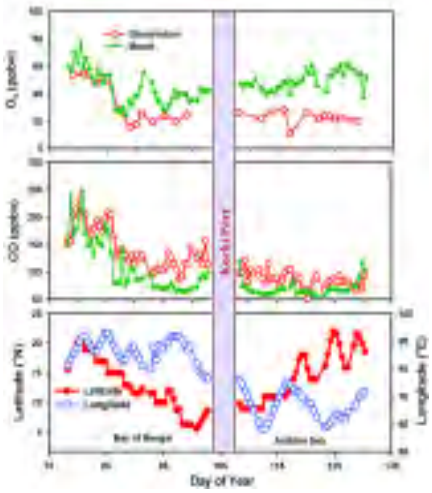

Figure 55: A comparison of observed and MOZART model estimated surface distributions of O_3 and CO over the Bay of Bengal and Arabian Sea during ICARB 2006.

(S. Srivastava, S. Venkataramani, V. Sheel and S. Lal)

Trace gases over the Bay of Bengal during an inter-monsoon period

Trace gases were measured along with meteorological parameters over the Bay of Bengal onboard the multi disciplinary Sagar Kanya cruise (SK-277) from the inter-monsoon season. Continuous measurements of ozone (O_3), carbon monoxide (CO) and nitrogen oxides (NO_x) were conducted with in-situ gas analyzers from 28 October to 17 November, 2010. Air samples were collected at every 4 hour interval during day and night hours. These samples were analyzed for non-methane hydrocarbons (C_2-C_4),

methane (CH_4), carbon monoxide (CO) and carbon dioxide (CO_2). While no significant day-night variation was observed for O_3, which is a typical characteristic of remote marine regions, values of O_3 and CO were lower in the southern part of the track and higher in the northern part. Both these gases were highest during the early hours of 6 November, touching around 60 ppbv and 290 ppbv respectively. CO_2 values were highest during 3-4 November nearing 390 ppmv. NO and NO_2 values were below 0.2 ppbv and 1.5 ppbv, respectively during most part of the cruise. In general, trace gases exhibited higher values in the eastern part of the transit between 2 and 13 November. Further analysis is being done to ascertain the influence of air masses from different source regions on the observed variations of these trace gases. Influence of cyclone 'Jal' on trace gases during 4-7 November also seems to be an interesting prospect.

(C. Mallik, S. Venkataramani and S. Lal)

Seasonal variation of carbon monoxide using satellite observation and a chemical transport model

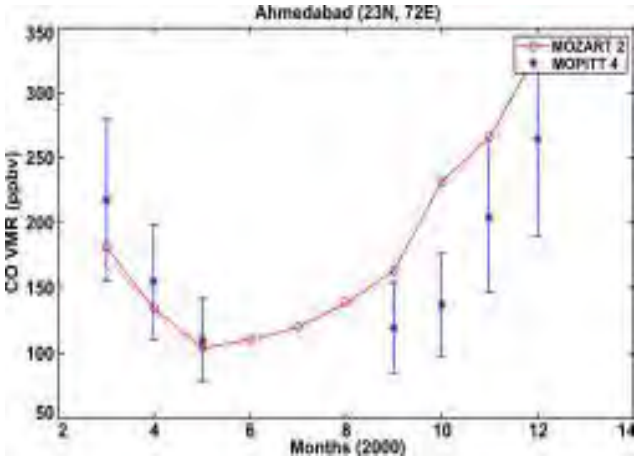

Figure 56: Seasonal variation of the mixing ratio of CO (in parts per billion) over Ahmedabad for the year 2000.

The seasonal variation of one of the major tropospheric pollutants, carbon monoxide (CO), over India and south-east Asia, including China was studied. The ten year data (2000-2010) for analysis have been taken from the Measurement of Pollution in the Troposphere (MOPITT) instrument, onboard the NASA's Terra satellite (version-4) and compared with simulation by the chemical transport model MOZART (Model of Ozone and Related Chemical Tracers). Although the amplitude of the seasonal variation differs over various polluted locations studied over land, they all show a similar pattern. As an example we show in Figure 56 the case for Ahmedabad for the year 2000, when MOPITT provides a high sensitivity CO data. There is a dip during the monsoon period as hydroxyl radicals, which are the main sink of CO, get enhanced due to high water vapor content of the atmosphere. The maximum concentration of CO is observed during winter (December-January) due to lower amount of OH radicals and also due to the fact that polluted air is transported from the middle Asia and the southern European regions which increases the level of pollution over India. Except for the summer months, the model overestimates CO concentrations compared to satellite observed values. The difference can arise from the poor representation of anthropogenic sources of CO in the emission inventory used in the model. Over the Indo-Gangetic plain, both the satellite observations and model values show high levels of CO during winter, due to increased anthropogenic activities and trapping of these emissions.

(Varun Sheel and Kabitri Nag)

Fluctuations in Sodium airglow intensity observed over Indian stations and a few case studies based on thermal and wind structures

Systematic measurements using sodium (Na) airglow photometers were carried out from Mt. Abu (24.6°N, 72.7° E) and Gadanki (13.5°N, 79.2°E) during cloudless and moonless nights of winter and spring equinoctial months during 2006-2009. The fluctuations of 5 minutes to 3 hours are analyzed to determine the impact of mesospheric gravity waves on Na airglow intensity. The power spectra derived from Na airglow intensity variation over both Mt. Abu and Gadanki indicate the occurrence of 15-30 min periods. Further, a few case studies were performed using mesospheric temperature and horizontal wind obtained from Sounding of Atmosphere using Broadband Emission Radiometry (SABER) and TIMED Doppler Interferometer (TIDI) onboard Thermosphere Ionosphere Mesosphere Energetics and Dynamics (TIMED) satellite nearly over both the places. This investigation revealed that whenever the convective and dynamical instabilities occur within Na airglow layer, the wave periodicities are found to be shorter. Larger periodicities are observed when the instabilities occurred above the Na airglow layer or not occurred within the emission layer. It is suggested that the gravity wave breaking mechanism probably altered the periodicities of the waves.

(S. Sarkhel, R. Sekar, D. Chakrabarty, and A. Guharay)

Seasonal characteristics of gravity waves in the middle atmosphere over Gadanki

Seasonal characteristics of gravity wave within the periodicity range of 0.5-4 hours are investigated in the middle atmosphere (35-72 km) over Gadanki in terms of potential energy, wave dissipation rate, vertical component

of horizontal momentum flux using long term (1998-2008) Rayleigh lidar temperature data. Considerable energy and momentum flux (Figure 57) are found to be carried over by the gravity waves. Dissipation rate (rate of change of dissipation with altitude) decreases sharply with altitude. Obtained energy and momentum flux exhibit dominant annual oscillation in both upper stratosphere and mesosphere. Slope of the vertical wave number spectra in the upper stratosphere is found to be steeper and closer to the theoretically estimated slope than the mesospheric one. This indicates that the mesosphere may be more suitable to support nonlinear wave interactions.

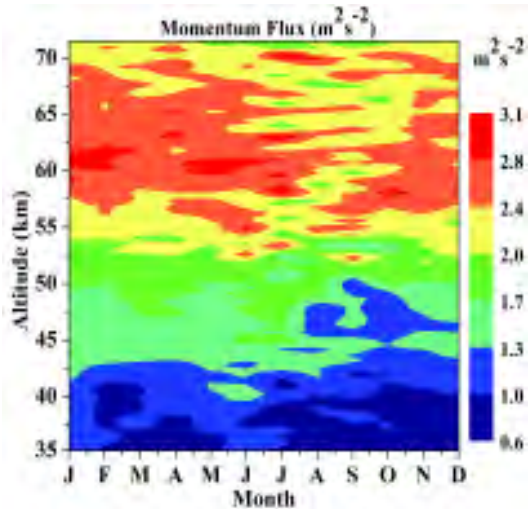

Figure 57: Estimated momentum flux for all the months of a year (folded during 1998-2008) in the middle atmosphere. Maximum standard error is found to be 0.4 m^2s^{-2} during July.

(A. Guharay and R. Sekar)

Signature of latitudinal coupling during a major sudden stratospheric warming in the tropics

Signature of a major Sudden Stratospheric Warming (SSW) is observed during late February of 2007 over Gadanki, a tropical station. Although SSW is a polar region phenomenon, our study has revealed that significant latitudinal coupling occurs in terms of wave dynamical features preceding and following this dramatic event. Significant air mass travels from low to high latitude before and during the warming episode. This indicates that there is a transport of heat for the sustenance of the event. Enhancement of the planetary wave amplitude starts well ahead at high latitude and reaches low latitude at the time of warming. The Planetary wave progresses towards high latitude after the event. Increase in the amplitude of gravity waves is found at the final stage of the warming period at high latitude.

(A.Guharay and R. Sekar)

Study of Sudden Stratospheric Warming and their impact on ozone over Mt. Abu

Sudden Stratospheric Warming (SSW) events are mostly observed in high- and mid-latitudes. A few strong SSW events do influence tropical and sub-tropical middle atmosphere also, depending upon their strength and background atmospheric conditions. Two major SSW events during December 1998 and March 1999, associated with vortex displacement and vortex splitting respectively, have been studied using Rayleigh Lidar observations over Mt. Abu and MPIC-PRL 2-D atmospheric model. Maximum increase in stratopause temperature was found to be 19 ± 2.5 K, and stratopause height (at ~52 km) was elevated, on 18 December 1998. Another event on 9 March 1999 showed an increase in stratopause temperature by 15 ± 2 K at a height of ~44 km. MPIC-PRL 2D atmospheric model was run using Lidar observed temperatures, with and without SSW, and found that the ozone concentrations, in the altitude region of 36-45 km, were higher during SSW over Mt. Abu.

(Som Sharma, Varun Sheel, S. Lal, Y. B. Acharya and H. Chandra)

Detection of solar cycle variations in oxygen green line emission rate using the Hilbert-Huang transform

Ground based photometric observations of mesospheric OI 557.7 nm green line nightglow emission rate, made over Kiso (35.79°N, 137.63°E), Japan for a period of sixteen years were spectrally analyzed using the Hilbert-Huang Transform (HHT). The spectrograms showed the presence of semi-annual, annual and quasi-biennial oscillations, which were seen earlier in the wavelet analysis of the same data series. In addition, due to the use of the HHT, which is capable of dealing with non-stationary as well as non-linear data series, it was possible to detect the very low frequency solar cycle variation in the emission rate. Results show that there is a significant solar cycle effect on the oxygen green line emission rate. The mean amplitude of variation is nearly 20% and it is maximum around midnight. A correlation analysis between the means of the emission rate and the solar radio flux at 10.7 cm also showed that the effect of solar activity on the oxygen green line emission rate peaks at midnight.

This work was done in collaboration with U. Das and C. J. Pan of Institute of Space Science, National Central University, Jhongli, Taiwan.

(H. S. S. Sinha)

Simultaneous observations of low latitude mesospheric turbulence by rocket and radar

A coordinated experimental campaign, using Langmuir Probe (LP) on-board a RH 300 Mk-II rocket launched from Sriharikota (13.6°N, 80.2°E) and the MST radar from Gadanki (13.5°N, 79.2°E), was conducted on 8 April 2005 to investigate mesospheric turbulence in the Indian low latitude region. Such simultaneous observations of the same turbulent region have not been reported earlier. Electron density irregularities in 1m to 1 km scale size range were detected by LP in 69.6-72.0 km, 74.5-75.5 km and 77.5-78.5 km height regions. Wavelet analysis of the electron density fluctuations showed the presence of thin layers of turbulence with thickness ranging from 100 m to 300 m. The wavelet spectrum of electron density irregularities matched with the Heisenberg model ensuring that the fluctuations were due to turbulence. The MST radar observations showed two distinct scattering layers, one at ~ 65 km and another at ~75 km. Spectral parameters of the radar echoes clearly showed that the electron density fluctuations responsible for the radar echoes were of turbulence origin with a signature of small amount of anisotropy. Energy dissipation rates estimated from rocket-borne measurements were found to be in the range of 1-100 $mWkg^{-1}$ and those derived from radar spectral width measurements were in the range of 28.4-47.0 $mWkg^{-1}$. The rms velocity fluctuations were estimated to be 0.2-3.0 m s^{-1} from the rocket observations and 0.15-3.0 ms^{-1} from the radar observations. For the common altitude region of 74.5-75.5 km, the vertical rms velocity fluctuations derived from rocket observations were 0.5-0.7 ms^{-1} and those from the radar were ~0.7 ms^{-1}. A detailed comparison of parameters of common region suggests that rocket and radar based estimations of turbulence parameters are consistent with each other. Present results compare well with those obtained in an earlier campaign as well as with those reported by others from other low latitude locations.

This work was done in collaboration with A.K. Patra and D. Selvaraj of National Atmospheric Research Laboratory, Gadanki, India, U. Das of Institute of Space Science, National Central University, Jhongli, Taiwan and J. Datta of ISRO Headquarters, Bangalore, India.

(H. Chandra, H. S. S. Sinha and R. N. Misra)

Effect of compositional variations on the seasonal variability in daytime optical emissions

Analysis of systematic observations of daytime optical OI 630.0 nm emissions from a mid-latitude station for over a year showed a decrease in the emission intensities during summer months although, on an average, the solar zenith angle is smaller in summers and the solar flux was high during that period. This is in contrast to the predictions of the optical emission models, as both these factors, namely smaller solar zenith angles and larger solar fluxes, contribute to larger emission intensities. This apparently controversial observation has been explained to be due to the compositional variability brought in by the heating of the upper atmosphere during the summer season wherein there is a transport of neutral oxygen atoms to the winter hemisphere from the summer hemisphere. This reduction in the oxygen densities contributes to reduced emission intensity in the summer months. The variation in the O to N_2 ratio over a year (smaller ratio in the summer when compared to the winter months) measured by the GUVI (Global Ultra-Violet Imager) on board the TIMED (Thermosphere Ionosphere Mesosphere Energetics and Dynamics) satellite confirms our explanation.

(D. Pallamraju and F. I. Laskar)

Dayside effects of magnetospheric substorms on the low latitude ionosphere-thermosphere system

Magnetospheric substorm is primarily a night-side phenomenon. However, based on a case study, it was shown that the eastward electric field associated with the onset of the expansion phase of a magnetospheric substorm caused positive bay disturbances in the deviations of the northward component of magnetic field (ΔH) over Indian low latitude stations in the noon sector and also at the stations in the 210° magnetic meridian (MM) magnetometer network in the afternoon sector. The onset of the susbtorm caused characteristic signatures in the global storm/substorm indices as well as in the energetic particle fluxes measured by the Los Alamos National Laboratory 1991–080 satellite at geosynchronous altitude. The OI 630.0 nm dayglow intensities over two low latitude stations also registered enhancements during this period (1124–1205 Indian Standard Time (IST); IST = UT + 5.5 h). The investigation adduced the response of 630.0 nm dayglow intensities over low latitudes corresponding to the onset of the expansion phase of a magnetospheric substorm and also confirmed the presence of positive bays in the deviations of the northward component of magnetic field (ΔH) over both Indian and 210 MM sectors. Modeling work is now underway to understand the causative mechanism for the enhancement in the 630.0 nm dayglow intensity under the influence of eastward electric field perturbation. Further, the mechanism through which the susbtorm phenomenon affects the dayside low latitude ionosphere is also being investigated.

(D. Chakrabarty and R. Sekar)

F-region variability over the anomaly crest region

Day to day variability in the critical frequency of F-layer (f_0F_2) over Ahmedabad is examined from hourly data for the months of January, March and July for the high sunspot year 1969 and low sunspot year 1996. Daily variations on different days of the month, normalized deviations from mean and the standard deviations at each hour are studied. The normalized standard deviations are up to ± 30% during night hours and up to ± 15% during day hours. While the variability during day hours is mainly because of the variability in the electric field (electrojet strength) that gives rise to vertical drift and subsequent ionization anomaly, the variability during night hours is also contributed by the variability in thermospheric neutral winds and temperature.

(H Chandra and Som Sharma)

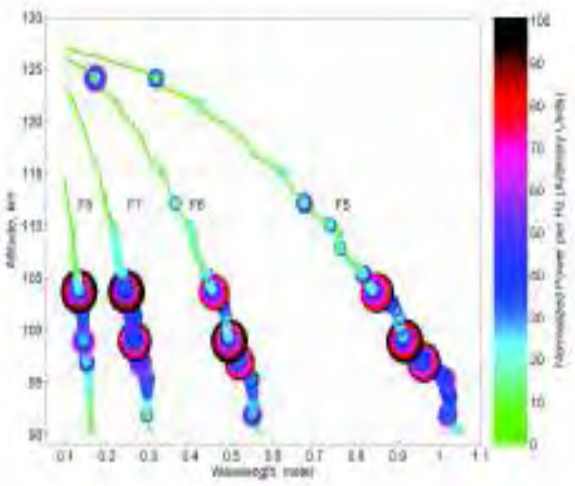

Figure 58: Detection of small scale irregularities (up to $\lambda \approx$ 13 cm) in the nighttime over an equatorial station Trivandrum (8.5°N, 76.9°E). Presence of irregularities with various scale sizes and their relative power at different altitudes as seen by narrow band filters F5 to F8, having center frequencies of 785 Hz, 1456 Hz, 2689 Hz and 5000Hz, respectively. The diameter as well as the color of rings represents the relative strength of different scale sizes.

Detection of small scale plasma irregularities in the nighttime equatorial E-region

Nature of plasma density irregularities present in the nighttime E-region over an equatorial station Trivandrum (8.5°N, 76.9°E) was studied using a rocket-borne Langmuir probe. It was found that irregularities were present over a large scale size range (few km to 1 m) in regions of both positive and negative electron density gradients. The amplitude of these irregularities was in the range of 0.01% to 15% of the ambient density. Spectral indices of irregularities in large (few km $>\lambda>$ 50 m), medium (50 m $>\lambda>$ 10 m) and small (10 m $>\lambda>$ 1 m) scale size ranges were -1.7 ± 0.1, -2.2 ± 0.4 and -2.7 ± 0.5, respectively. With the use of a set of eight onboard narrow band filters, it was possible to detect irregularities with scale sizes as small as 13 cm, in 97–104 km altitude region (Figure 58). It was suggested that in presence of an appropriate gravity wave wind, vertical shears in the zonal neutral winds could produce regions of upward and downward electric field where gradient drift instability (GDI) could operate depending upon the nature of the vertical electron density gradients as proposed by others. There are observations in equatorial regions where vertical shears in zonal neutral winds were detected. Thus a wind driven GDI was invoked as the mechanism for irregularities observed in positive gradient regions. The power spectrum of irregularities showed an unusual behavior in 102 ± 1.4 km altitude region, where an almost flat spectrum was observed in the scale size range of 15 m–120 m.

This work was done in collaboration with R. Pandey of Mohanlal Sukhadia University, Udaipur

(H. S. S. Sinha and R. N. Misra)

Martian Ionosphere at Olympus Mons and Syrtis Major

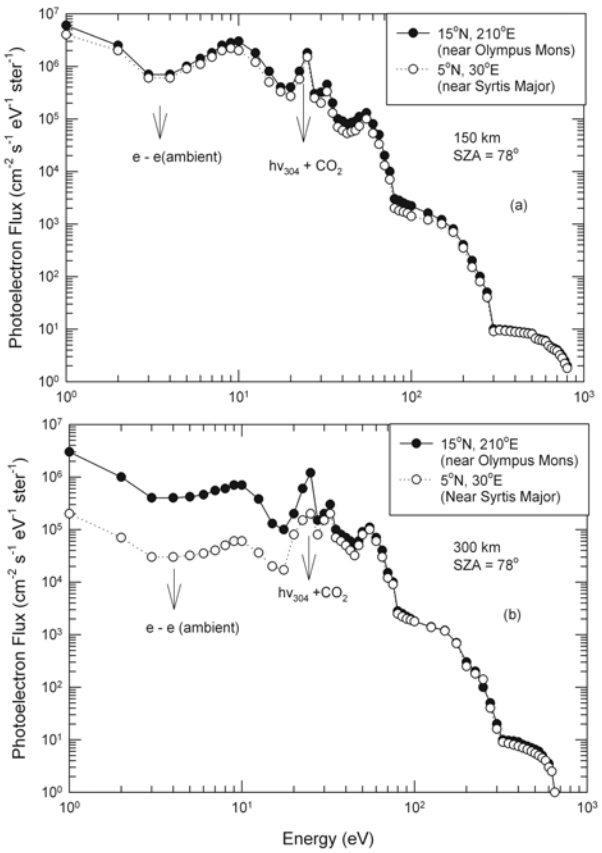

Figure 59: The photoelectron flux energy spectra at (a) 150 Km and (b) 300 Km in the Martian ionosphere over Olympus Mons and Syrtis Major.

The photoelectron flux, ion production rates and electron densities were calculated in the Martian ionosphere close to Martian regions namely Syrtis Major (5°N, 30°E) and Olympus Mons (15°N, 210°E) where the magnetic fields are horizontal and vertical respectively. These calculations are made at solar zenith angle of 78° during moderate solar activity using models of photoelectrons based on yield spectrum method. The vertical transport of photoelectrons is inhibited by horizontal magnetic fields at Olympus Mons. In this case local loss calculation is used. Photoelectron transport is allowed in the vertical magnetic fields at Syrtis Major. For this case a photoelectron transport model is developed and applied. The estimated ion production rates were then used in a one-dimensional continuity and vertical diffusion model to calculate ion and electron density. It is found that photoelectron transport reduces the flux by an order of magnitude between energy range 1 to 20 eV at higher altitudes (>250 km). The photoelectron energy spectra at (a) 150 km and (b) 300 km are shown in the Martian ionosphere over Olympus Mons and Syrtis Major (Figure 59).

This work is carried out in collaboration with S.P. Seth, Bhavans R.A. College, Ahmedabad.

(S.A. Haider)

Meteor impact perturbation in the lower ionosphere of Mars

Analysis of 1500 electron density profiles obtained from radio occultation experiment onboard Mars Global Surveyor was carried out to study the physical characteristics of meteoric plasma layers over Mars during the months of January to June, 2005. It is found that 157 electron density profiles were strongly perturbed with peak densities $\sim$1-3 x10^{10} m^{-3} at an altitude between 80 km and 100 km due to ablation of meteoroids and subsequent ionization of meteoric atoms. These profiles are used to estimate Total Electron Content (TEC) in the lower atmosphere of Mars. Our analysis suggests that meteoroids ablation caused enhancements in TEC by a factor of $\sim$ 1.5 to 3.0 which changes with season, latitude, longitude and solar zenith angle. Maxima in TEC were observed on 21 January, 15 March and 22 May, 2005, when comets 2007 P42, 88P Howell and 4015 Wilson-Harrington intersected the orbit of Mars from a close distance of 1.5 AU, 3.16 AU and 1.18 AU respectively. TEC were found to be increased by a factor of $\sim$ 5 to 7 on these days. This is a significant increase in TEC, which might be associated with the meteor showers that were produced when Mars crossed the dust stream that was left along the orbit of these comets.

This work is carried out in collaboration with Mr. Bhavin Pandya, C.U. Shah college, Ahmedabad.

(S.A. Haider)

Model results of production and loss rates, ion and electron densities in the lower ionosphere of Mars

The production and loss rates, ion and electron densities are calculated using energy loss method and continuity equation under the steady state chemical equilibrium condition. The primary ionization source in the model is taken as galactic cosmic rays. The chemical model couples ion-neutral, electron-neutral and photodissociation of positive and negative ions, electron photo-detachment, ion-ion, ion-electron recombination processes through over 100 chemical reactions. The electron density is calculated using charge neutrality condition. Of the 35 ions considered in the model the production rates and loss rates of 16 major ions ($CO_2^+CO_2$, $H_3O^+H_2O$, $H_3O^+(H_2O)_2$, $H_3O^+(H_2O)_3$, $H_3O^+(H_2O)_4$, $O_2^+(CO_2)_2$, H_3O^+, CO_4^-, CO_3^-, $CO_3^-H_2O$, $CO_3^-(H_2O)_2$, NO_2^-, $NO_2^-H_2O$, $NO_2^-(H_2O)_2$, $NO_3^-H_2O$ and $NO_3^-(H_2O)$) are dominant. The model calculation suggests that maximum electron density occurs at $\sim$ 30 to 40 km due to high efficiency of electron attachment to O_x molecules, which entails that the concentrations of negative ions is higher than that of electron below around 30 km. The electron density is mainly controlled by water cluster ions of $NO_2^-(H_2O)_n$, $CO_3^-(H_2O)_n$ and $H_3O^+(H_2O)_n$ for n = 1 to 4.

(Varun Sheel and S.A.Haider)

Development of electron energy analyzer for collision experiments

A tandem cylindrical mirror analyzer (CMA) was designed and fabricated for electron energy analysis in collision experiments. This will be used for analysing the Auger electrons originating from the core vacancies in molecules. The analyzer will be deployed in conjunction with the ion-momentum spectrometer at Indus-1 synchrotron and IUAC ion accelerator.

(Koushik Saha, B. Bapat)

Laser ablation Cluster Mass Spectrometry

Laser ablated materials are good candidates for the production of clusters with very large mass range. Clustering of ablated atoms is known to be enhanced by

collisions with rapidly expanding gas-puffs. A laser ablation cluster source puffed by a pulsed supersonic gas jet has been developed. Mass spectrometry of these clusters is done in a time of flight mass spectrometer which has been augmented to the ablation source. To enhance the efficiency of the mass spectrometer, a pulsed ionization scheme and multi-particle recording capability are being implemented. Eventually, it is intended to create mixed species clusters and study their photochemical reactions.

(A.K. Saxena, S.B. Banerjee, I. A. Prajapati, K. P. Subramanian and B. Bapat)

Auger electron spectrometer for elemental analysis of surfaces

The project aims to develop a compact electron spectrometer for measuring the Auger electron spectrum of a solid target bombarded by photons or charged particles. A cylindrical retarding potential analyzer was designed and fabricated. It was used to observe the emitted electrons in various configurations and conditions, such as UV photoionisation of gaseous targets, and electron impact ionization of solid and gaseous targets, with and without the application of an electric field to extract the electrons. By scanning the retarding voltage a pass curve (electron counts vs. retarding voltage) was generated. Differentiation of the pass curve is expected to yield a normal spectrum. Difficulties, stemming mainly from random electrons and specular scattering of the incident beam, made it difficult to derive a spectrum in most cases, except the case of UV photoionisation of gases. An algorithm was developed to smooth the pass curve while searching for deviation from a smooth pattern, based on a segmented least squares fitting. This approach has been applied to identification of Auger lines from a solid (ZnS and aluminium) as well as gaseous targets Ar, N_2 and CO_2, under electron impact. Work is on to make the algorithm robust and to make it capable of determining the line strengths and line widths.

(B. Bapat, S. B. Banerjee, Koushik Saha)

Modeling the dissociation patterns of small molecular dications

Collaboration has been initiated to concurrently compute and experimentally measure the kinetic energy spectra of fragments resulting from dissociative ionization of molecules. Comparison of theory and kinematically complete experiments will give information about excited molecular ion states that can not be obtained by conventional spectroscopy techniques.

This work is being done in collaboration with K. R. Shamsunder of IISER Mohali.

(Amrendra Pandey and B. Bapat)

SCIENCE

Geosciences Division

The research activities of Geosciences Division focus on understanding of the origin and evolution of the planet Earth and its various components, with special emphasis on timescales and processes. The major areas of research of the division are: Solid Earth Geochemistry, Geomorphology and Tectonics, Paleoclimate & Paleoenvironmental Studies, Hydrology, Aqueous Geochemistry, Oceanography and Paleoceanography, and Atmostheric Chemistry. The methodologies followed center on the measurements of abundances of elements, radioactive isotopes, ratios of radiogenic isotopes and light stable isotopes, and thermal/optical luminescence properties of materials using modern analytical tools.

Quantifying the nitrogen budget of the Indian Ocean

Primary productivity is mostly limited by the unavailability of reactive nitrogen in the sunlit surface layer of tropical oceans. The supply of such new nitrogen to the surface ocean is through upwelling, N_2 fixation by diazotrophs (e.g. *Trichodesmium*, Figure 60), riverine flux and atmospheric deposition. The relative and absolute importance of these processes in the Indian Ocean is has been evaluated. N_2 fixation is estimated directly for the first time using the $^{15}N_2$ tracer technique in the Arabian Sea during the spring inter-monsoon 2009. Estimates are double the values reported earlier and can account for a substantial fraction of the nitrogen gained by the Arabian Sea. Carbon uptake rates are also estimated using the ^{13}C tracer technique. Further, contribution of atmospheric deposition and riverine fluxes to new productivity in the two biogeochemically different basins of the northern Indian Ocean, the Arabian Sea and the Bay of Bengal, is quantified. An upper bound of the contribution of atmospheric deposition to new productivity in the northern Indian Ocean is ~2.5%. On an average 1.73 Tg Ny^{-1} is deposited into the northern Indian Ocean through dry and wet deposition of aerosols. On the other hand, most of the dissolved

Figure 60. An example of *Trichodesmium* blooms observed during the sampling period (May 2009)

inorganic nitrogen (DIN) (~81% in the case of the Arabian Sea and 96% in the case of the Bay of Bengal) through riverine flux is not transported to the ocean and is consumed on the course of the rivers or in the estuaries. Coastal Bay of Bengal and Arabian Sea receive ~0.38 Tg Ny^{-1} and ~0.06 Tg Ny^{-1}, respectively, through rivers. A large variation in the contribution of DIN through river fluxes to new productivity is found in both these basins. Our estimate of nitrogen fluxes through N_2 fixation, aerosols and rivers is a step towards significantly reducing the uncertainty in the global nitrogen budget.

(N. Gandhi, R. Ramesh and A. Singh)

A new model for Rayleigh isotopic fractionation in open systems

Application of stable isotopes is extended further by simulating nitrogen loss process in the Arabian Sea. An equation describing isotopic fractionation in open systems, wherefrom material is not only removed with isotopic fractionation, but fresh material of a different isotopic composition is added from an external source, is derived. This model is further applied to understand other oceanographic processes as well. With the help of a new data set, spatiotemporal variation in the oxygen isotopic composition and salinity (δ^{18}O-S) relation of the northern Indian Ocean is studied. While the results are consistent with positive P-E (excess of precipitation over evaporation) over the Bay of Bengal and negative P-E over the eastern Arabian Sea, a significant spatiotemporal variability in the slope (also intercept) of the relation is observed in the Bay; the temporal variability is difficult to discern in the Arabian Sea. Both the slope and intercept appear to be sensitive to rainfall; the slope (intercept) is higher (lower) during years of stronger monsoon. The observed variability in the δ^{18}O-S relation implies that caution needs to be exercised in paleosalinity estimations, especially from the Bay of Bengal, based on δ^{18}O of marine organisms.

(R. Ramesh and A. Singh)

Quantifying new production in the Indian Ocean

Although phytoplankton only account for approximately 1% of photosynthetic biomass, they account for approximately >50% of the net primary productivity of the biosphere and play a key role in biogeochemical cycling and climate processes. To quantify the ocean's role as a reservoir of anthropogenic carbon dioxide, a detailed knowledge of the carbon fixation during photosynthesis by phytoplankton is required. For this, ^{13}C and ^{15}N tracers were used in the different parts of the Indian Ocean and Southern Ocean to measure primary and new production, precursor of export production that is relevant to the sequestration of carbon from the atmosphere to the deep ocean. The major findings are as follows:

In the Arabian Sea (AS), nitrogen isotopic data of surface suspended particles suggest that recently fixed nitrogen by *Trichodesmium* (N_2- fixer) contributes as high as ~79% of the nitrogen in surface suspended particles during spring. Fickian diffusive fluxes of nitrate into the surface layer can account for 67% and 78% of the observed nitrogen uptake in the coastal and open ocean regions, respectively. During winter, our study provides the first evidence of photo-inhibition in the surface waters of the region. When light intensity exceeds 1200 μmol $m^{-2}s^{-1}$, surface productivity decreases due to photo-inhibition. Further, the highest specific uptake rate is found in the morning, followed by the evening and the noon during winter.

In the Bay of Bengal (BOB), the highest surface productivity is found to be at the center of the eddy while the lowest, outside. The intermediate surface productivity values are associated with the locations proximal to the eddy. Euphotic-depth-integrated primary and new productivity values are found to be twice higher at the center of the eddy than that outside. Higher new productivity and *f*-ratios observed within eddy suggest that eddies aid in exporting most of the total production to the deep.

In the tropical Indian Ocean (TIO), shoaling of thermocline in the thermocline ridge located in the TIO also influences the new productivity. It is found that surface light intensity along with nutrient availability dictates the productivity in the TIO. Higher surface light intensity reduces the surface productivity but on the other hand, it enhances the overall depth-integrated productivity in the TIO(Figure 61). A comparison of earlier findings with the present study rules out any significant change in productivity in the TIO over the past 3-decades.

In the Southern Ocean (SO), the productivity varies from 185 to >900 mg C $m^{-2}d^{-1}$ in different zones of the SO (Figure 62). The zonal variations in productivity accompany variations in SST, salinity and nutrients. The SO shows a large latitudinal variability in chl *a*, productivity, new productivity and *f*-ratios. The maximum possible *f*-ratio and minimum regenerated production in the SO are found to be 0.78 ± 0.12 and 1.5 mmol N $m^{-2}d^{-1}$, respectively. The higher *f*-ratio indicates its capability of exporting most of the total production to the deep under favorable conditions.

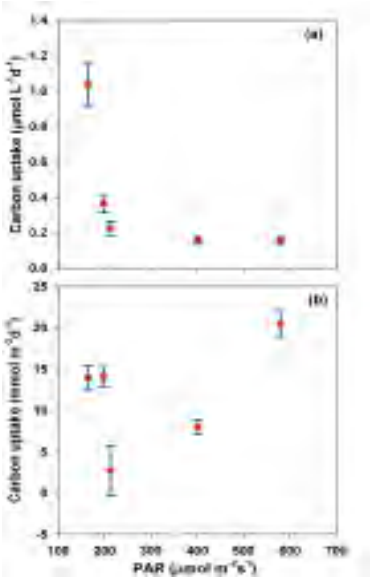

Figure 61: Variation of (a) surface carbon uptake rate and (b) euphotic-depth-integrated carbon uptake rates with photosynthetically-active-radiation (PAR) at different sampling locations in the TIO. Errors associated with the values are 1 - sigma standard deviation.

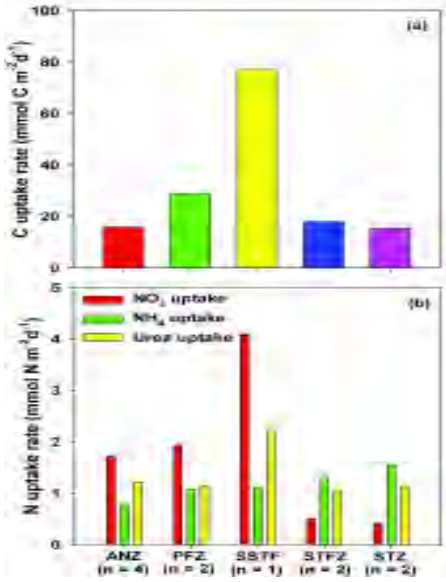

Figure 62: Average (a) carbon and (b) nitrogen (NO_3, NH_4 and Urea) uptake rates in different zones (ANZ, PFZ, SAZ, and STZ) of the SO. Number of sampling locations (*n*) for the respective zones are shown on the x-axis. Errors associated with the values are 1-sigma standard deviation.

(N. Gandhi, R. Ramesh and A. Singh)

Depositional history of alluvial sediments in the Lower Narmada Basin

Quaternary sediments occupying large areas of Gujarat, referred to as Gujarat alluvial plains, are of marine, fluvial and aeolian origin. Various types of soils have developed on tectonically active landforms. Radiocarbon dating of sediments/soils of several exposed sections, to investigate depositional processes, indicate that the top ~200 cm of Lower Narmada Basin was deposited during mid to late Holocene (0-4500 yr), due to large historic and paleofloods and later uplifted tectonically. A paleosol layer, observed at a depth of 10-15 m in the cliff section at Kanjeta was found to have deposited during late Pleistocene (~15-10 ka BP) in a more humid climate (Figure 63). Stable carbon and oxygen isotopes of both soil carbonates and soil organic matter indicate significant increase in the monsoon rains, in an otherwise semi-arid Gujarat region, around 1.6 ka and 12.5 ka BP.

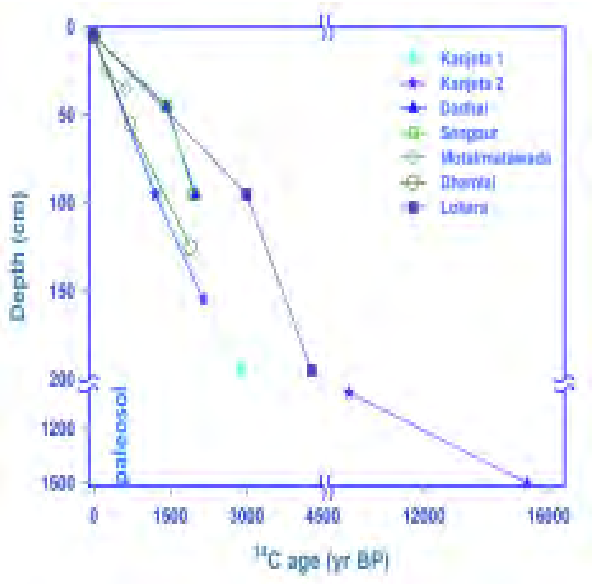

Figure 63: Radiocarbon age profiles of sediment/soil sections from Lower Narmada Basin.

(A. H. Laskar, R. Ramesh, M. G. Yadava)

A record of Summer Monsoon in the Andaman Islands during last ~3 ka

Speleothems which are carbonate rocks of various shapes, generally column like, often seen in natural caves, are considered to be a very good proxy of the terrestrial climate. Two stalagmites, collected from Andaman Islands, dated by radiocarbon and U-Th methods and analysed for changes in the oxygen and carbon stable isotopes ratios, are found to have recorded the past monsoon history of the Islands during last 3 ka (Figure 64). It is observed that for the period 2.1 to 1.8 ka BP rainfall was ~33 % lower than the present. This duration coincides with the warm period in mid-latitudes (called Roman Warm Period). However, between 1.3 to 0.9 ka BP when another warm period was experienced at mid-latitudes (known as Medieval Warm Period) strong monsoon rainfall (~6 % more than the

present) is observed. Moreover, small reduction in rainfall (~3 % less than the present) is observed during the Little Ice Age. Results indicate the variable coupling between Indian monsoon and the mid-latitude climate events. In the recent ~400 yr, monsoon at the Islands has more or less remained unchanged.

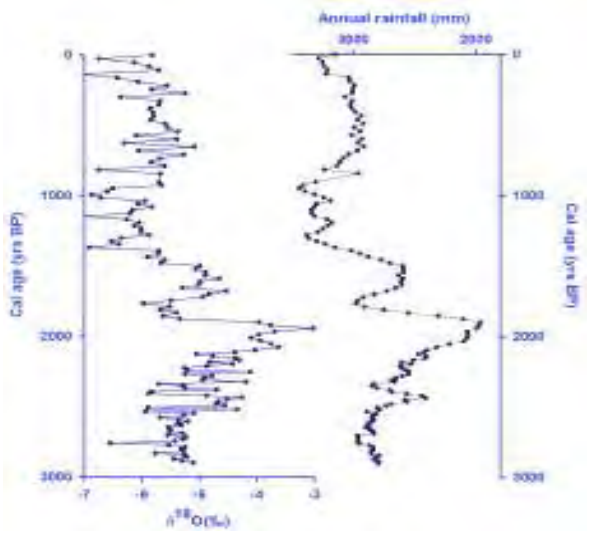

Figure 64. Reconstruction of past monsoon changes over last 3 ka using oxygen isotope composition ($\delta^{18}O$) of the Andaman stalagmites.

(A. H. Laskar, R. Ramesh, M. G. Yadava)

Holocene glaciations in Dronagiri valley Central Himalaya

It has been suggested that a majority of glaciers (Central and Eastern Himalaya) are summer accumulation and ablation type, implying that Indian Summer Monsoon (ISM) is the major source of moisture for the growth and sustenance of the glaciers in this region. In order to understand the role of ISM in glacier dynamics, relict moraines, in the monsoon dominated Dronagiri valley (Dhauli Ganga basin) in the Central Himalaya, were investigated (Figure 65a). Three distinct phases in glaciations of decreasing magnitude could be identified based on detailed geomorphologic mapping and are named as Dronagiri Stage-1 (DGS-1), DGS-2 and DGS-3 respectively (Figure 65b). Chronology based on both optical and radiocarbon dating suggests that DGS-1 (maximum valley glaciations) reaching up to 3384 m occurred between 8.3 ka and 6.5 ka, DGS-2 glaciation which reached up to 3600 m is dated between 4.4 ka to 4.0 ka whereas the youngest DGS-3 glaciation is bracketed between 4.0 ka and 1.6 ka and was terminated around 3800 m respectively (modern glacier snout is at 4200 m, Figure 65(a)). In addition to this, two short lived glacier advances have been dated to 1572 cal yr BP–685 cal yr BP and post 685 cal yr BP respectively. The later is attributed to the Little Ice Age (LIA) cooling event.

The study suggests that in the monsoon dominated region like Dronagiri valley, precipitation has less influence on the changes in ice volume instead; it is the decrease in air temperature which influences the snow accumulation. It is important to note that none of the advances mentioned above are associated with the periods of strengthened ISM during the Holocene. Instead, the oldest glaciations (DGS-1) seem to correlate with the globally identified 8.2 ka cooling event, DGS-2 corresponds to the Mid-Holocene aridity and the DGS-3 occurred during fluctuating ISM. Study pertaining to the regional and global implications of the above results is in progress.

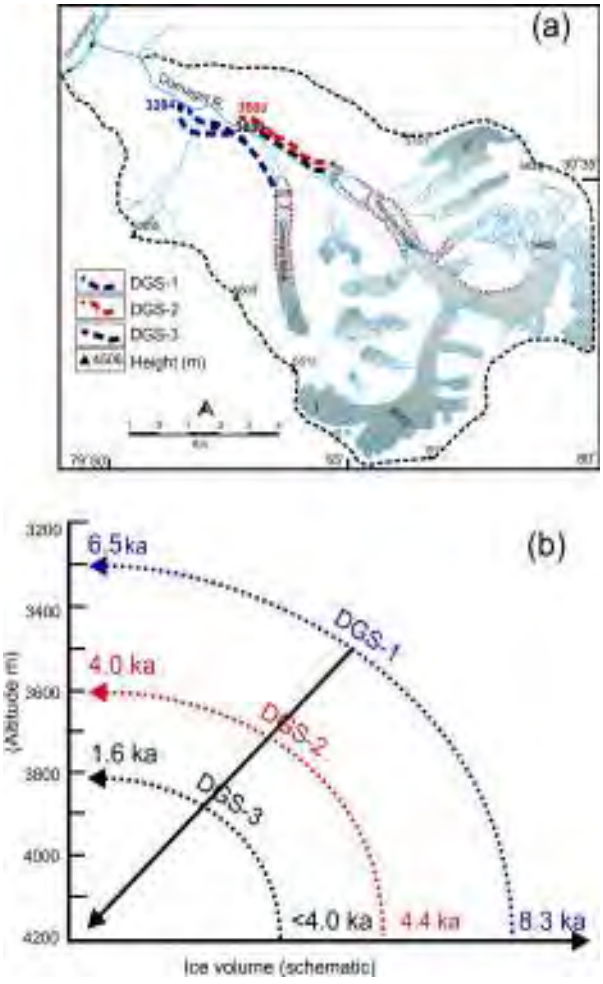

Figure 65 (a) Map of Durnagiri valley showing three glacial advances with decreasing lateral extent. These are marked as DGS-1, DGS-2 and DGS-3. (b) Schematic representation of ice volume associated with DGS-1 (8.3 ka to 8.5 ka), DGS-2 (4.4 ka to 4 ka) and DGS-3 (<4 ka to 1.6 ka).

This work was done in collaboration with S.P. Sati and Y.P. Sundriyal, of the HNB Garhwal University, Srinagar

(N. Juyal, R. Bhushan, A. D. Shukla and A.K. Singhvi)

Mid- Holocene sedimentation in Great Rann, western India

Quaternary tectonic, sea level and climate change are the major contributing factors responsible for landscape evolution in areas proximal to the continental margins. The Great Rann of Kachchh in western India is one such terrain that provides an opportunity to study temporal changes in land-sea configuration and its impact on the Late Quaternary sedimentation. Preliminary investigation based on major elements, clay mineralogy, TOC and C/N ratio provided insights to the temporal changes in the sedimentation pattern (paleoenvironment) and sediment provenance during the last 6000 years. Low concentration of major elements (viz. Al, Ti, Fe and Mg), TOC, and high C/N ratio between 6000 years to 4000 years has been interpreted as increased continental input to the Great Rann sedimentation whereas higher concentration of major elements, TOC and low C/N ratio after 4000 years which continued till around 2000 years is interpreted as marine contribution. It was observed that for last 6000 years clay mineralogy was dominated by Illite ($\sim$60%) with subordinate Smectite and Kaolinite ($<$20%), implying that both continental and marine sediments in Great Rann owe their genesis to Himalayan source rocks. However, the above inferences would remain speculative unless the study is supported by the trace element and isotopic analyses which is in progress.

This work was carried out in collaboration with A.K. Tyagi, Institute for Plasma Research, Gandhinagar.

(A. D. Shukla, R. Bhushan and N. Juyal)

Methodological studies on luminescence dating of Volcanic Ash beds

Dating of young volcanic ashes has been problematic on account of the absence of secured chronometric methods with sufficient sensitivity. Earlier attempts to date volcanic ashes using volcanic glass and feldspar met with limited success, being limited by athermal fading of dating signal due to quantum tunneling of trapped charges from lattice defects. A systematical examination of the protocols used in the luminescence dating on volcanic ash samples from various horizons in India was carried out. Geochemically, all these ashes horizons on this study have been designated as the youngest Toba ash (securely dated to $\sim$74 ka). Polyminerallic fine (4-11 μm) grains extracted from the ash layers were analyzed using four different protocols, viz., i) TL multiple aliquot additive dose (MAAD) method using the blue emission, ii) isothermal (ITL) MAAD in red emission, iii) Infrared stimulated luminescence- single aliquot regeneration protocol (IRSL- SAR) with stimulation at 50°C, and 4) post infrared (PIR) IRSL SAR with stimulation at 300°C in blue emission and a preheat of 320°C. PIR-IRSL gave highest D_e along with lowest athermal fading rate (g-value) of 0-1.6 %/decade. Fading corrected ages, using the PIR-IRSL D_e values of ashes in central and western India were 75 ± 18, 80 ± 12 and 71 ± 6 ka. Some of the Ash horizons gave younger ages of 29 ± 3 and 42 ± 4 ka respectively and given their geochemical similarity with the Toba ash, the only way to reconcile with these ages is that these are in a secondary, reworked horizon. The study offered for the first time the prospects of dating of volcanic ash bed up to few hundred thousand years in a secured manner.

This study was carried out in collaboration with MAJ Williams, Univ. of Adelaide, Australia; Rachna Raj and L.S.Chamyal, M.S. University Baroda and Sheila Mishra, Deccan College, India.

(R.H. Biswas, Navin Juyal and A.K. Singhvi)

Optical dating of Tsunami deposits

Studies at PRL during the past years has shown the efficacy of luminescence in the dating of tsunami sands and the possible use of dispersion (or its absence thereof) in the luminescence signal in estimating the potentially transportable sediment fluxes. As a part of a National Program on the Geological Records of Tsunamis, we provided chronologies of some of the key sections in India. A suite of samples from Andaman Islands identified as being of tsumigenic origin provided ages in the range 200-3000 years. These are being collated with other evidences to understand the recurrence intervals. Further, samples from Guhagarhin in coastal Karnataka were dated 65 year and suggest that these were deposited during the 1945 Makaran Tsunami event. Importantly, the samples were rich in quartz, were well bleached as indicated by the fact that the minimum age and the central ages models gave nearly identical De values. Further analyses on other coastal sites in Tamilnadu are in progress.

This work was carried out in collaboration with J. Malik of IIT Kanpur, S. Srinivasulu and Hema Achyuthan of Anna University; P. Udayganesan, S. Chaturvedi of Shasthra University and A. Gurjar of NIO, Goa.

(P. Chitrabhanu and A.K. Singhvi)

Luminescence dating of Alkali Sulphates: Gypsum and Barite

Following the success of electron spin resonance dating of Gypsum, we attempted luminescence dating of Gypsum (CaSO4.2H2O) and Barite (BaSO4). In the case of Gypsum it was seen that the loss of water with storage for a week at 50°C changes the luminescence glow curve shape but does not alter the dose information. The OSL shows a similar behavior and this provides a way to date gypsum using standard TL/OSL dating protocols. Given that gypsum is also used in several places in daily life, its use in accident dosimetry now becomes possible, given that the minimum detectable dose is ~ 0.2 Gy.

In nature, $BaSO_4$ occurs in hot springs, sedimentary rocks, underground ore deposits, marine sediments, limestones and in meteorites. As of now there are no secured methods to date barites. We therefore explored the possibility of dating barites using luminescence techniques. Barite samples (museum specimen with a typical XRD pattern) exhibited thermoluminescence with glow peaks at 100°C and 240°C. Optically-stimulated luminescence under blue light stimulation gave a multi component decay, with a typical minimum detectable doses of ~200 μGy. The samples were insensitive to infra-red stimulation and did not provide any signal in the blue emission window. The alpha efficiency for TL was 0.15 ± 0.03. The dose response of high temperature peak at 240°C up to 500 Gy was linear. The fading of TL/OSL signal was nonlinear and progressively decreased from the initial value of 10-30%year. The fading rate was higher for sample with Mn that could be detected using electron spin resonance. The samples were amenable to standard analysis protocols and further studies are underway to optimize the dating protocols and the fading aspects.

This work was carried out with the help of M.S. Pandian and P.S.R. Rao of Pondicherry University

(S.K.Sharma and A.K.Singhvi)

Radiation dosimetry of sediments at single grain level

Ideally, the equivalent dose (De) for all single grains from a sediment stratum should be single valued. However appreciable scatter in De's are routinely observed and normally heterogeneous predepositional daylight bleaching of the luminescence of quartz at grain level is implicated. Morthekai, 2007 demonstrated that a major fraction of this scatter arises due to heterogeneous distribution of radiation emitters. This is due to the fact that in a sediment matrix, most of the beta dose is contributed by randomly distributed ^{40}K and the net dose received by individual grains depends on the distance from a ^{40}K hotspot. As this distance fluctuates randomly, for different feldspar grains the dose received by quartz grains also fluctuate. Using these fluctuation, Morthekai, 2007, demonstrated that the distribution for quartz matrix with random hotspots distribution, give a skewed dose distribution function. This work was further refined using an improved range energy formulation and by incorporating porosity and water content for computation. Further, this work also implied that single aliquots formed from several single grains with varied dose values should also show distribution in the dose values. This dispersion in single aliquot palaeodoses was computed using Monte Carlo simulations and was used to deduce the limits of the precision of age analysis (Figure 66). The simulations also enable quantification of several other parameters useful for age determination. These included: 1) estimation of minimum number of aliquots required for a robust estimate of palaeodose, 2) maximum scatter in mean paleodose distribution for multigrain single aliquots, 3) the ratio of maximum to minimum palaeodose, a factor that enables distinction between dose heterogeneity and bleaching heterogeneity.

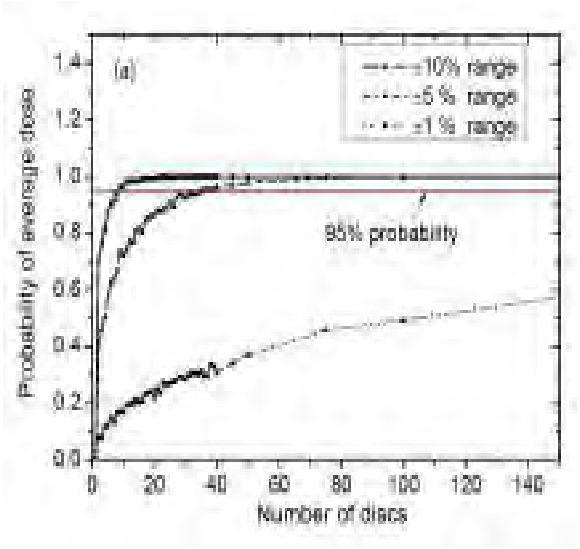

Fig 66: Variation maximum average single aliquot dose value for different number of aliquots

This work was carried out in association with Y. S. Mayya and P. Selvam of BARC, Mumbai.

(N. Chauhan and A.K. Singhvi)

Time resolved Luminescence Spectroscopy and Feldspar Luminescence

Infrared Stimulated Luminescence dating is applicable to feldspars and has a dynamic datable range from few years to few million years because of its high saturation dose in

respect of luminescence production. However, its applicability is beset with athermal fading of luminescence signal at a rate faster than that predicted by the kinetic considerations. This limits its use to samples of ages < 40 ka. Some correction procedures have been suggested that can be used for correcting the underestimated ages. As an alternative, we attempted to find a optically stable signal by examining various measurement techniques to avoid correction procedures as these invariably involve extrapolation and imply greater systematic errors. Towards this, we recently set up a time-resolved luminescence measurement system. In this instrument, the sample is stimulated with a train of IR pulses of milli sec duration and the IR stimulated photons in blue band are detected during and after each pulse (a schematic diagram is given in Figure 67.) Time correlated optical decay curve is then obtained and analyzed using a software developed in house.

Using this instrument, measurement of charge transport in band-tail states over few tens of nanoseconds coupled to a new analysis procedure provided new insights. Analysis of temperature evolution of IRSL curves showed that the underlying kinetics is of non-Arrhenius type and that the IR excited trapped charges are transported in the band-tail states by variable range hopping with phonons assisting the hopping rate. The data from different feldspars (both alkali and plagioclase feldspars) are expected to provide stable signal. Further refinements of the model and experiments are in progress.

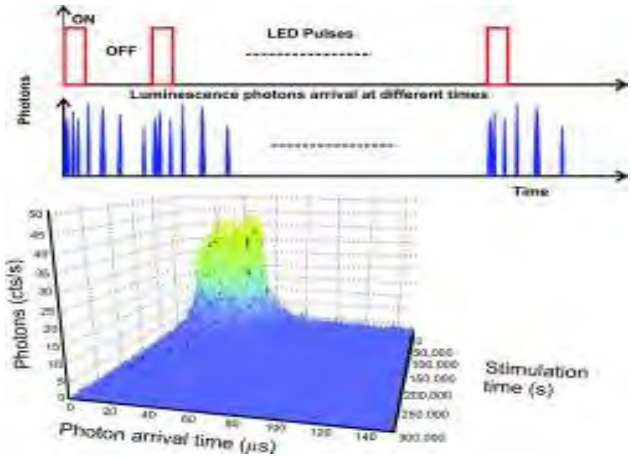

Figure 67: Schematic diagram of time-resolved infra-red stimulated luminescence (TR-IRSL). A TR-IRSL data of K-feldspar is also shown.

(P. Morthekai and A. K. Singhvi)

Variation in the luminescence Sensitivity of Quartz

Naturally occurring ubiquitous quartz has been an important material for geochronology. Despite a large body experimental data, an intriguing question of unpredictable and widely varying TL and OSL sensitivity (spanning ten orders of magnitude) has remained unexplained. As OSL/TL phenomenon are driven by the point defects, their fluorescence sensitization/quenching can be meaningfully addressed if their nature and identity in quartz samples with contrasting sensitivities are established. Fluid inclusions in quartz, metamorphism and the presence of aqueous fluids all can affect luminescence behavior. We systematically explored these factors, using photoluminescence (PL), Fourier transform infra-red (FTIR) and Laser Ablation breakdown spectroscopy (LIBS). Sediments were processed using standard protocols and the OSL sensitivity of individual grains (150-210μm) was measured following a fixed test dose of 10Gy in a single grain TL/OSL reader. The dull (<150photons/s as initial BLSL intensity) and bright quartz grains (>150 photons/s) were hand-picked using a vacuum suction system with a capillary and these were used for other spectroscopic studies.

Photoluminescence (PL) excitation under 242 nm wavelength gave emission bands at 395 nm associated with $(H_3O_4)^o$ recombination-centers respectively. The PL and OSL sensitivity correlated. The PL decay of 395 nm emission exhibited a single exponential decay with mean life of 110 μs. FTIR spectra in diffuse reflectance mode in 400-4000 cm^{-1} range, gave a clear indication of fluid inclusions and free water co-existing within structure. A broad band between 3000 and 3800 cm^{-1} was due to fluid inclusion s and a peak around 3420 cm^{-1} indicated molecular H_2O in quartz. Absence of 3600 cm^{-1} band suggested the absence of Si-OH groups. A systematic increase of H_2O signal in quartz lattice contrasted with a decrease of OSL sensitivity. This suggested that the emission centers were in close proximity of H_2O molecules and influenced the non-radiative relaxation processes. Laser induced Breakdown Spectroscopy of samples with contrasting OSL sensitivity indicated that they have identical composition (major and minor elements), except for the presence of Ba in high sensitivity samples. Initial analysis further suggested that Ba most likely resides at interstitial sites and helps in the stabilization of defects that act as recombination center i.e. Ba probably complexed with H_2O, forms $Ba(OH)_2$ and thereby helps increase the OSL sensitivity. This work is being persued and we expect to use this in a variety of novel non geochronological applications of quartz.

This work was done in collaboration with M.D. Sastry and his group at the Gemological institute of India, Santa Chawla of NPL, Delhi, M. S. Pandian, and P.S.R. Rao of Pondicherry University.

(S.K. Sharma and A.K. Singhvi)

Enhanced chlorophyll-a levels in the Bay of Bengal during early North-East Monsoon: Role of eddies

Several vertical profiles within the euphotic zone of the northern Indian Ocean were occupied during a cruise (SS-259) onboard FORV Sagar Sampada to assess the distribution of chlorophyll-a (representative of plankton biomass) and nutrients during the early north-east monsoon season (November 2008). The column integrated chlorophyll-a concentration over the Arabian Sea and the North Bay of Bengal exhibit high concentrations (Figure 68). However, the southernmost station in the Bay of Bengal shows enhanced chlorophyll-a concentration compared to other stations in the south Bay. This is attributed to eddy pumping of nutrients from subsurface to surface waters of the Bay during the study period due to cyclonic conditions. The observed salinity in the Bay of Bengal shows a strong north-south gradient with higher salinity in the southern part of the Bay. Therefore, the supply of nutrients through fluvial input (dominantly from the northern region) is insignificant. Thus, the enhanced chlorophyll-a concentration over the southern-most station can be either due to eddy mediated biological production or lateral advective transport of nutrients.

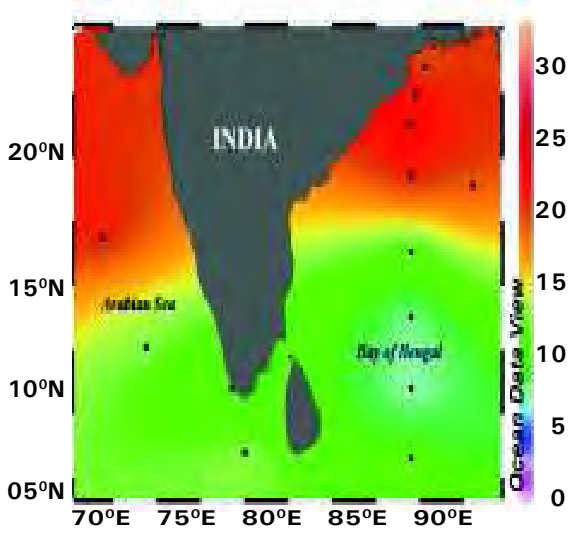

Figure 68: Column integrated chlorophyll-a (mg/m^2) levels in the northern Indian Ocean during November, 2008.

(B. Srinivas, Jayati Chaterjee, Ravi Bhushan)

Evidence for recent abrupt rise in dissolved $^{87}Sr/^{86}Sr$ ratios of the Ganga

The present day Ganga river water is characterized by high $^{87}Sr/^{86}Sr$ and moderately high Sr concentration which has led to the suggestion that the Ganga and the Brahmaputra rivers play a key role in the Sr isotope evolution of seawater during the Cenozoic. Better understanding of their contribution to marine Sr isotope evolution, however, require knowledge of temporal variations in their $^{87}Sr/^{86}Sr$. In this study an effort has been made to reconstruct the $^{87}Sr/^{86}Sr$ of the evolution of the Ganga water by analyzing carbonate nodules collected from different depths of two sediment cores raised from the Kanpur (50 m long) and Jagdishpur (25 m long) in the Ganga plain which represent the depositional history of ~100 ka and ~35 ka respectively. The $^{87}Sr/^{86}Sr$ ratios of the carbonate nodules range from 0.7142 - 0.7189 in the Kanpur and 0.7142 - 0.7367 in the Jagdishpur cores (Figure 69). The nodules in general, display significantly lower $^{87}Sr/^{86}Sr$ ratio compared to contemporary Ganga river water at Kanpur. The higher values of $^{87}Sr/^{86}Sr$ ratio observed in Jagdishpur core near its top is consistent with that of the present day Ganga water at Kanpur. This increase in $^{87}Sr/^{86}Sr$ indicates recent abrupt increase in $^{87}Sr/^{86}Sr$ ratio of the Ganga. This sudden rise in $^{87}Sr/^{86}Sr$ ratio of the Ganga is probably due to increase in the relative proportion of Sr from the Lesser Himalaya containing silicates and carbonates with more radiogenic $^{87}Sr/^{86}Sr$. The cause of enhanced contribution from the Lesser Himalaya is not clear; this could be due to enhanced agricultural activities and deforestation and or climatic variability during recent times resulting in more erosion in the Lesser Himalaya.

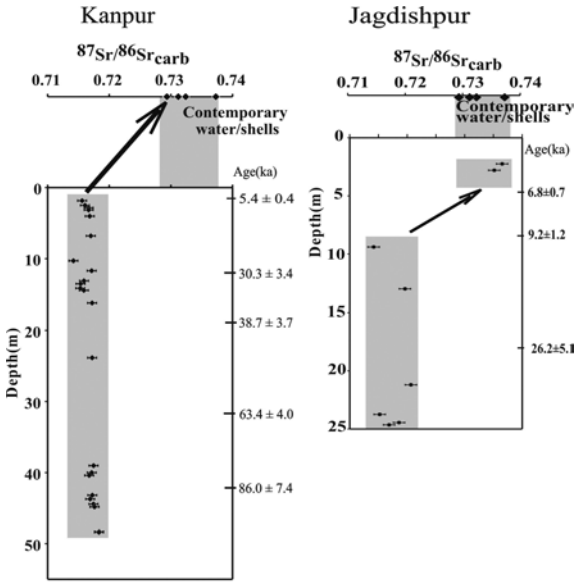

Figure 69: Variations in $^{87}Sr/^{86}Sr$ ratios of the carbonate nodules with depth from the Kanpur and the Jagdishpur sediment cores.

This work was done in collaboration with R. Sinha, IIT, Kanpur and S.K. Tandon, Delhi University.

(Waliur Rahaman and Sunil K Singh)

Nd isotopes in Ganga and Bay of Bengal coastal water

Our work on dissolved Nd concentration and $^{143}Nd/^{144}Nd$ in the Ganga river system and the Bay of Bengal were continued. Towards this last year preliminary measurements of Nd isotopic composition were carried out in the Ganga river system in the plain. This year work was focused on Nd isotopic composition in (1) the headwaters of the Ganga and in (2) the estuary and coastal water of Bay of Bengal. The ε_{Nd} values of the Bhagirathi and Alaknanda rivers at Devprayag are in the range -13.5 to -19.0 and -12.9 to -18.7 respectively. These values compare with ε_{Nd} of -14.2 measured at Manihari during 2008 monsoon. These results seem to show discernible seasonal trend. This is likely a result of differences in mineral weathering rates and their mixing proportions. Further work is in progress to elucidate the features regulating the seasonal trend. In the coastal region of the Bay of Bengal, the ε_{Nd} values cluster around -15.3 in the upper 100 m of the water column.

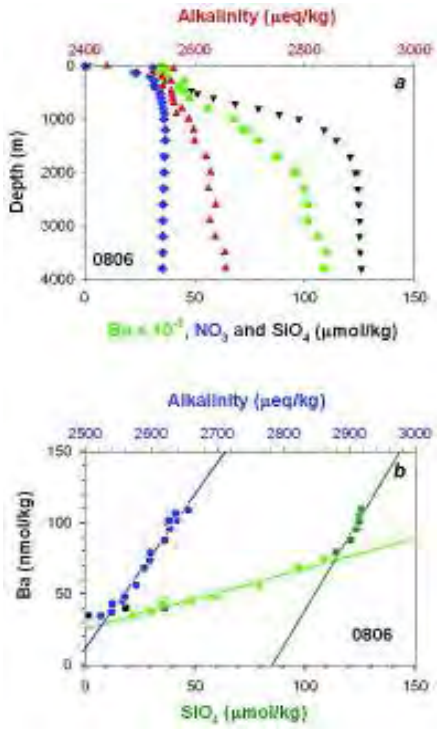

Figure 70: a. Depth profiles of dissolved silicate (inverted black triangle), nitrate (blue diamond), barium (green square) and alkalinity (red triangle) showing depletion in surface followed by sub-surface enrichment in the water column of the Bay of Bengal. b. The concentration of dissolved barium is linearly correlated with alkalinity in the entire water column (blue circles) but the dissolved silicate only up to a depth of 1200 m (light green squares) and correlation becomes poor below 1200 m (dark green squares), whereas it shows hardly any correlation with nitrate (not shown in the figure). The black symbols represent data for depth < 100 m and are excluded from the correlations.

(Jayati Chatterjee and Sunil K Singh)

Distribution of the dissolved barium, alkalinity and major nutrients in the water column of the Bay of Bengal

The concentration of the dissolved barium at the mouth of the Ganga-Brahmaputra (G-B) Rivers is high due to desorption from particulate phase in this turbulent water mixing zone. The dissolved barium is dispersed in the surface and sub-surface waters of the Bay of Bengal (BoB) through water circulation. The concentrations of dissolved barium, alkalinity and major nutrients in the water column of the BoB have been analyzed to determine their interrelation and from it the biogeochemical processes regulating dissolved Ba distribution in this oceanic region. Typical depth profiles of dissolved barium, alkalinity and major nutrients are shown in Figure 70a. Preliminary results seem to indicate the preferential association of barium with alkalinity throughout the water column compared to dissolved silicate (Figure 70b).

(Ravi Bhushan, Satinder Pal Singh and Sunil K Singh)

Temporal variation in $^{87}Sr/^{86}Sr$ and ε_{Nd} in sediments of southeastern Arabian Sea: Impact of monsoon and surface water circulation

The Sr and Nd isotopic compositions in the silicate fractions of sediments were measured in two well dated gravity cores from the Arabian Sea archiving a depositional history of ~40 ka. The $^{87}Sr/^{86}Sr$ and ε_{Nd} in the northern core (SS-3104G; 12.8°N, 71.7°E) show limited variations compared to the southeastern core (SS-3101G; 6.0°N, 74.0°E). The limited variability in the isotope composition of sediments of the northern core indicates their stable supply from different sources including aeolian dust, over the period of the core deposition ~ 40 ka (Figure 71 a). In contrast, the variations in the isotopic composition of SS-3101G core reflect temporal variations in the mixing proportions of sediments from the Himalaya, Deccan plateau and peninsular granite/gneisses. The isotopic profiles of Sr and Nd in this core exhibit two major excursions, at. ~9 ka and ~20 ka, coinciding with periods of Holocene Intensified Southwest Monsoon and the Last Glacial Maximum (LGM) respectively (Figure 71 b). These excursions can be explained in terms of changes in the erosion patterns in the source region and surface circulation in the Northern Indian Ocean caused by variation in the intensity of SW and NE monsoon. The intensification of NE monsoon and associated strengthening of the East Indian Coastal Current during the LGM transported sediments with higher $^{87}Sr/^{86}Sr$ and lower ε_{Nd} from the western Bay of Bengal to the Arabian Sea. In contrast, enhanced SW monsoon at ~9 ka caused the transport of sediments from the Arabian Sea, particularly Indus derived,

to the southeastern Arabian Sea. This study highlights the impact of monsoon variability and ocean surface currents in determining the isotopic composition of sediments deposited in the southeastern Arabian Sea during ~40 ka.

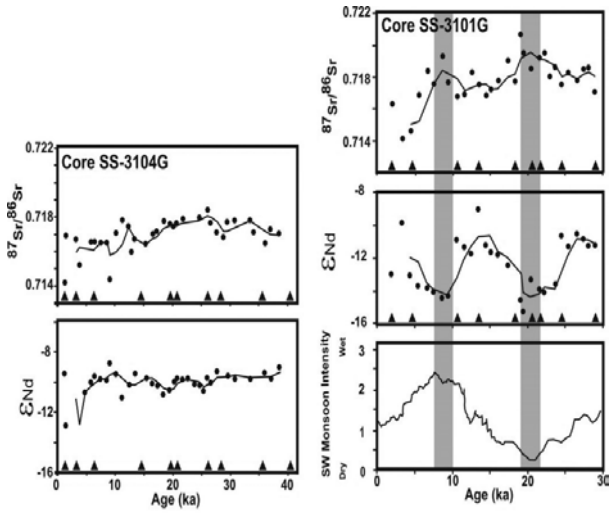

(a) (b)

Figure 71: The temporal variation in the Sr and Nd isotopic compositions in the silicate fraction of the sediments of the cores (a) SS-3104G and (b) SS-3101G. The temporal variation in the intensity of the SW monsoon is also shown.

(Ravi Bhushan, Vineet Goswami and Sunil K Singh)

Re-Os isotopes in black shales from the Himalaya and Aravalli: Implications to their age and Post-depositional processes

Re-Os isotopes in black shales from the Lower Tal formation (just above the Pc-C boundary), Lesser Himalaya and Jhamarkotra formation, Lower Aravalli have been investigated to assess their potential to determine their depositional ages. The measured $^{187}Os/^{188}Os$ ratios of the Himalayan shales vary widely (1.363 to 2.116), but linearly with $^{187}Re/^{188}Os$ (51 to 137). Following the bivariate approach used by Singh et al. [1999], the $^{187}Os/^{188}Os$-$^{187}Re/^{188}Os$ systematics of these shales provided a depositional age of 541 ± 8 (2σ) Ma (Figure 72) with an initial $^{187}Os/^{188}Os$ ratio of 0.90 ± 0.02 (2σ). The Re-Os age of black shales obtained in this study is consistent with the reported radiometric ages for Pc-C boundary at other locations of the world. In contrast to the Himalayan shales, the Aravalli shales showed "open system" behavior with respect to Re and Os indicating their post-depositional alteration (weathering). These shales have ^{188}Os concentration similar to that of shales of similar depositional ages, however, with significantly lower Re/Os ratios (average: 2.5) relative to average black shales (160). This suggest much higher mobility of Re compared to Os during weathering of shales. Given that the Jhamarkotra shales deposited at ~2000 Ma ago, it can be estimated that most of Re (~95%) from them is mobilized since their depositions. These results underscore the importance of weathering of trace lithologies, such as black shales in regulating the global riverine Re budget.

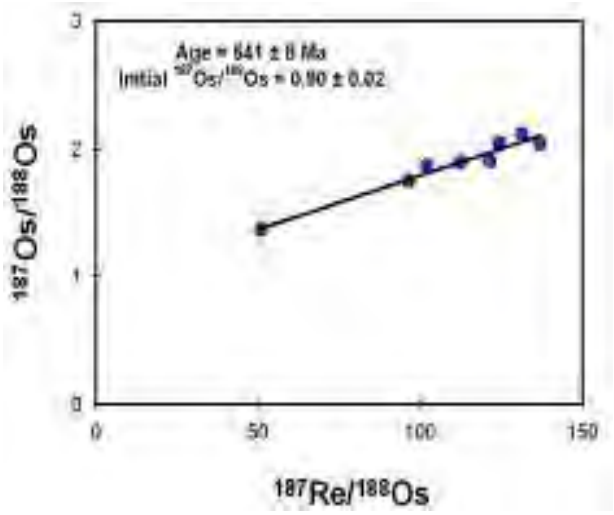

Figure 72: Re-Os isochron of black shales from the Lower Tal Formation.

This work was done in collaboration with H. Bhu from MLS University, Udaipur.

(Sunil K Singh and Gyana Ranjan Tripathy)

Volcanology of Barren Island (Andaman Sea)

We have been carrying out volcanological and geochemical studies on the Barren Island Volcano, located in the Andaman Sea. During our last field trip to the island we discovered a variety of lava flow, which is transnational between pahoehoe and aa lava flows, known as toothpaste lava. This flow of subalkalic basalt shows abundant squeeze-ups of viscous toothpasate lava near its entry into the sea. The squeeze-ups are sheets and slabs, up to several meters across and tens of centimetres thick, extruded from boccas. They are often prominently curved, have striated upper surfaces with close-spaced, en echelon linear ridges and grooves, broad wave-like undulations perpendicular to the striations, and sometimes, clefts. Textural, geochemical, and Sr–Nd isotopic data on the squeeze-ups and the exposed aa flow core indicate very crystal-rich, viscous, and isotopically very homogeneous lava. We envisage that a greatly reduced speed of this viscous flow at the coastline, possibly aided by a shallowing of the basal slope, led to lateral spreading of the flow, which caused tension in its upper parts. This, with continued lava supply at the back, led to widespread tearing of the flow surface and extrusion of the squeeze-ups. The larger

slabs, while extruding in a plastic condition, curved under their own weight, whereas their surfaces experienced brittle deformation, forming the en echelon grooves. The extruded, detached, and rotated sheets and slabs were carried forward for some distance atop the very slowly advancing aa core, before the flow solidified.

This work was done in collaboration with H.C. Sheth of IIT Bombay.

(A. Kumar, J.S. Ray and N. Awasthi)

Geochemistry of Mud Breccia from Mud Volcanoes of Andamans

Mud volcanoes are subaerial and submarine geological structures, whose surface morphology vaguely resembles that of a real volcano on a much smaller scale, form as a result of emission of depressurized multiphase fluids and argillaceous material from deep seated sources. Mud volcanoes located on convergent margin forearcs such as the Andaman & Nicobar Islands provide a window to the subducting slab by acting as conduits for fluids, sediments and clasts of altered and/or metamorphosed ophiolites from deep down the subduction zone. In order to chemically characterize the subducting sediments in the Andaman Subduction Zone we have studied mud breccias from several mud volcanoes from the middle and north Andaman Islands. X-ray differaction studied reveal that these mud breccias dominantly made up of clay minerals such as kaolinite, smectite and chlorite. Their trace element contents fall in-between those of altered oceanic crust and sediments of Bay of Bengal. ε_{Nd} of mud breccias vary from -3.4 to -2.0, whereas $^{87}Sr/^{86}Sr$ ratios cluster around 0.709. Mixing calculations suggest that these values can be explained by a two component mixing of ~75 % altered Indian oceanic crust basalt and ~25% of Bay of Bengal sediments. Thus, the mud breccias, which represent the contributions from the slab to the mantle wedge, clearly have been derived from the subducting Indian plate and chemically are mixtures of altered oceanic crust and sediments.

(A. Kumar, J.S. Ray and N. Awasthi)

Evidence for the supply of soluble phosphorous over the Bay of Bengal: Role of anthropogenic sources viz-a-viz mineral dust

Atmospheric deposition of phosphorous to seawater can play a significant role in surface primary production. In order to characterize the sources, size distribution, temporal variability in the abundances and to assess their impact on surface waters of the bay, water soluble inorganic phosphorous ($P_{Inorg} = PO_4^{3-}$) concentration has been measured in atmospheric aerosols, collected from the marine atmospheric boundary layer (MABL) of Bay of Bengal during the late NE- monsoon (January-April) season. Our study provides the field based evidence for the role of chemical processing of dust in supplying bioavailable phosphorus to the surface waters of the Bay. The prevalent strong correlation of total aerosol Ca with water soluble Ca^{2+} ($R^2 = 0.98$; n = 23; p-value < 0.0001) and non sea salt sulphate ($R^2 = 0.85$; n = 23; p-value < 0.0001) over the Bay (Figure 73), indicate the uptake of acidic species by alkaline dust. This hypothesis is further supported by the low equivalent ratio of $NH^{4+}/nss\text{-}SO_4^{2-}$ (Av: 0.40 ± 0.20), suggesting excess acid over NH_4, a major neutralizing species in the atmosphere. In addition, the significant linear relation between phosphate and nss-Ca^{2+} indicate their source from apatite dissolution during long-range transport. Significant linear relationship with soluble NH_4^+ during January 2009 and March-April 2006 highlights the importance of anthropogenic common source, ammonium phosphate (a fertilizer).The anthropogenic fraction of water soluble inorganic phosphorous accounts for ~70-80 % of P_{Inorg} over Bay of Bengal. These results have implications to surface biogeochemistry via the supply of bio-available P.

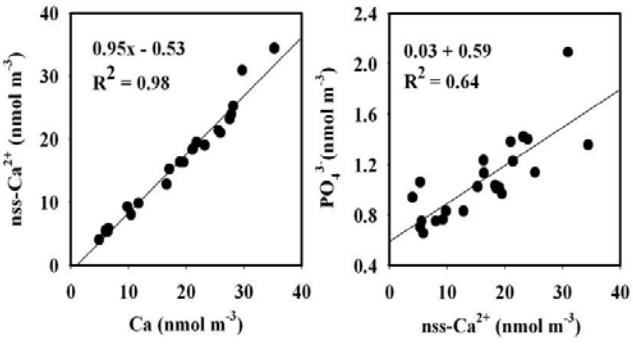

Figure 73: The significant linear relation of water soluble Ca^{2+} with total aerosol Ca and soluble inorganic phosphate suggest the role of chemical processing in the supply of this nutrient to the Bay.

(Bikkina Srinivas and M.M.Sarin)

Carbonaceous aerosols from an urban location (Kanpur) in the Indo-Gangetic Plain

A comprehensive study on carbonaceous aerosols for 1-year (Jan 2007- Feb 2008) from an urban location (Kanpur) in the Indo-Gangetic Plain (IGP) suggest that boundary layer dynamics, varying strength of emission sources and secondary aerosol formation all contribute significantly to the seasonal trend in the mass concentrations of elemental

carbon (EC), organic carbon (OC) and water-soluble OC (WSOC). Carbonaceous aerosols contribute nearly one-third of the PM_{10} mass during wintertime whereas their contribution is only ~10% during summer (Figure 74). A three to four fold increase in EC, OC and K^+ concentrations during wintertime and significant correlation between OC and K^+ suggest dominance of biomass burning (biofuels and agriculture waste). The fractional mass of EC varies from 0.4% (during summer) to 7.7% (during winter). However, large scatter between EC and K^+ is attributed to the contribution of EC from multiple sources (biomass and fossil-fuel). The relatively high OC/EC ratio (average: 7.4 ± 3.5) also supports that emissions from biomass burning is overwhelming for particulate OC (Figure 74). The WSOC/OC ratios vary from 0.21 to 0.70 over the seasonal cycle; with relatively high ratios in summer, suggesting significance of secondary organic aerosols (SOA). The long-range transport of mineral aerosols from Iran, Afghanistan and the Thar Desert (western India) is more pronounced during summer months. The temporal variability in the concentrations of selected inorganic constituents and neutralization of acidic species (SO_4^{2-} and NO_3^-) by NH_4^+ and Ca_2^+ reflects conspicuous changes in the source strength of anthropogenic emissions. The neutralization by NH_4^+ is dominant during wintertime and Ca^{2+} in summer. This study has provided the first data set on the scattering OC (~30% of the PM_{10} mass) over the IGP highlighting its importance in the estimation of total scattering coefficient and single scattering albedo on a regional scale.

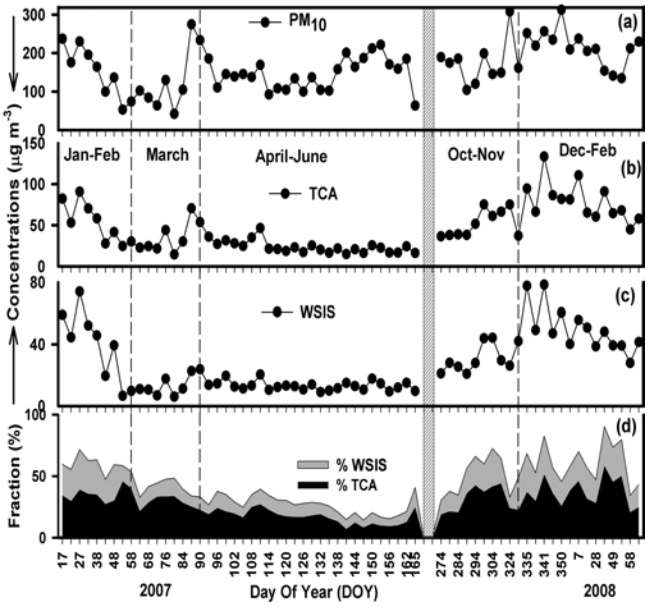

Figure 74: Temporal variability of mass concentrations of (a) PM10; (b) total carbonaceous aerosols (TCA = 1.6 × OC + EC); (c) WSIS (sum of cations and anions) and (d) fractional contribution of TCA and WSIS to PM_{10} during the sampling period. The time-period between June and September, shown by a vertical bar, represents the monsoon period and no samples were collected.

This work is done in collaboration with S. N. Tripathi of IIT, Kanpur

(Kirpa Ram and M.M.Sarin)

Biomass burning emissions and impact on atmospheric Poly Aromatic Hydrocarbons (PAHs) over north-eastern Himalyan region.

Atmospheric $PM_{2.5}$ aerosols (particulate matter of diameter ≤ 2.5 μm) are studied from a high precipitation-low dust site at Barapani (Shillong, 25.7°N; 91.9°E; 1064 m a.s.l.) from Northeastern Himalayan region during the drier months (Jan 2010 and March 2009 & 2010), to assess the airborne concentrations of elemental carbon and organic carbon (EC and OC), polycyclic aromatic hydrocarbons (PAHs) and their isomer ratios. The pronounced mass fraction of total carbonaceous aerosols (TCA: 75 ± 15 %), OC/EC ratios (6.8 ± 3.2) in conjunction with PAHs/EC (2.8 ± 1.1 mg g^{-1}), suggest the impact of agricultural-waste burning emissions via long-range transport to the Northeastern Indian region. The meteorological wind pattern coupled with the fire hot spots derived from the Along Track Scanning Radiometer (ATSR) satellite indicate that the fire activity in the fields in Southeast Asia is a dominant source of aerosols over the sampling region. Assessing the atmospheric chemistry of PAHs isomers in these aged aerosols, reveal that their reactivity is higher during the spring March as compared to those in wintertime Jun. However, 4- and 6-ring PAHs isomers appear to retain their source-signatures even in the aged air-parcels, unlike 3- and 5- ring compounds.

Logistic help for sample collection was provided by NE-SAC, Shillong

(Prashant Rajput and M.M.Sarin)

Temporal variability of carbonaceous, inorganic species and heavy metals in atmospheric fine mode aerosols from high-altitude site in western India

Atmospheric fine-mode particulate matter ($PM_{2.5}$), collected for full one-year (Jan to Dec-2007) from a high-altitude site (Mt. Abu, 24.6°N, 72.7°E, 1680 m asl) in western India, have been studied to assess the temporal variability and long-range transport of carbonaceous, inorganic species and selected heavy metals. During the winter (Jan-Feb; Oct-Dec), mass concentrations (in $\mu g\ m^{-3}$) of elemental carbon (EC), organic carbon (OC) and water-soluble organic carbon (WSOC) varied as 0.2 – 2.8 (Av = 0.8 ± 0.6), 0.5-9.8 (Av = 3.5 ± 2.2) and 0.4-8.7 (Av = 2.6 ± 1.9) respectively. However, concentrations are

significantly lower during rest of the year (Mar – Sep), representing the background levels at this high-altitude site. The high concentrations during the wintertime are attributed to the advective transport of pollutants from the Indo-Gangetic Plain (IGP). The OC/EC ratio is quite uniform (~ 5.5) throughout the year reflecting the dominance of biomass burning emissions; an inference also supported by the significant linear relationship of nss-K^+ with OC and EC (r^2 = 0.71 and r^2 = 0.80 respectively). The WSOC/OC ratio exhibit large variability (range: 0.38 – 0.92) during the winter season. The higher WSOC fraction in wintertime is associated with the aged aerosols due to photo-oxidation. The diagnostic ratios of chemical constituents viz. nss-K^+/EC, nss-K^+/OC, nss-SO_4^{2-}/EC, nss-SO_4^{2-}/OC, Pb/EC and Cd/EC, have been used to assess the impact of anthropogenic sources on ambient aerosols at this high-altitude site.

(Ashwini Kumar, Kirpa Ram and M.M. Sarin)

Evaluation of aerosol acidity in an urban environment using aerosol inorganic equilibrium model

Most of the heterogeneous and aqueous phase chemical processes in ambient atmosphere depend on aerosol pH. However, there is no direct measurement technique available to determine this key property (aerosol acidity, expressed as aerosol H^+ ion concentration, [H^+]). Uncertainty in determining it may seriously constrain the assessment of chemical pathways influencing earth-atmosphere system including climate. Aerosol acidity can be inferred indirectly from measurement of related atmospheric constituents. Towards this, data on chemical constituents viz. water soluble Cl^-, NO_3^-, SO_4^{2-}, NH_4^+, Na^+, K^+, Mg^{2+} and Ca^{2+} from $PM_{2.5}$ samples (particles with aerodynamic diameter $< 2.5\ \mu m$) collected at Ahmedabad (23°02'N, 72°32'E) during December 2006 - January 2007 were used to derive H^+ ion concentration in ambient aerosol using a thermodynamic equilibrium model, ISORROPIA-II. The model assumes gas phase NH_3, HCl and HNO_3 are in dynamic equilibrium with the deliquescent particles at a given temperature and relative humidity. The H^+ ion concentration varied from 3.5 - 60 nmol m^{-3}, which represents typical fine mode aerosol acidity in an urban environment. In order to experimentally evaluate the temporal variability in the calculated [H^+], pH of the water extract of samples was measured and calculated corresponding to atmospheric concentrations (Figure 75). Both modelled and measured [H^+] are found in good agreement in their temporal variability. These preliminary results suggest that the [H^+] calculated from the thermodynamic equilibrium considerations can be reliably used for the studies involved in variability of aerosol acidity and its influence on heterogeneous chemical processes in ambient atmosphere in this region. We have successfully applied the model results for assessing enhanced secondary organic aerosol formation at high aerosol acidity conditions.

(R. Rengarajan, A. K. Sudheer)

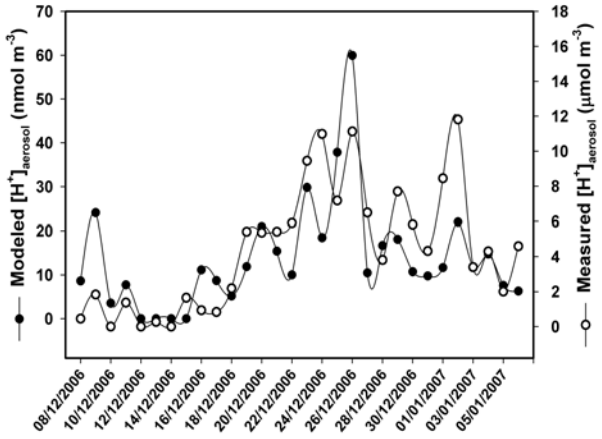

Figure 75: H^+ ion concentration determined from the measured pH of aerosol water extract shows significant correlation with that calculated by equilibrium model.

Radium isotopes in Godavari Estuary

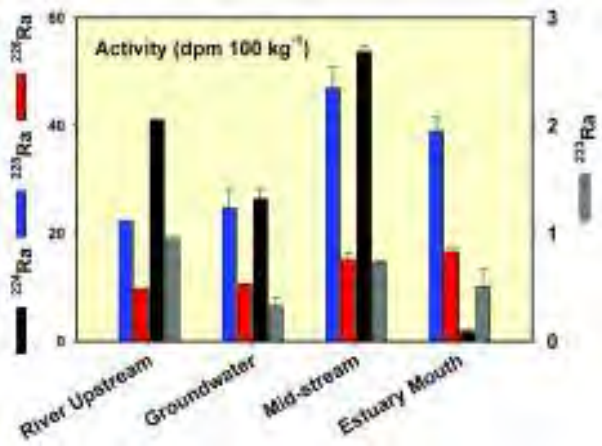

Figure 76: Activities of ^{223}Ra, ^{224}Ra, ^{228}Ra and ^{226}Ra in the Godavari *estuary.*

In order to quantify marine mixing processes and submarine groundwater discharge (SGD) and SGD-driven nutrient fluxes, concentration of nutrients, ^{223}Ra (half-life = 11.4 d), ^{224}Ra (3.7 d), ^{228}Ra (5.7 y) and ^{226}Ra (1622 y) in seawater, river water and coastal groundwater were measured in two field trips to the Godavari estuary. Short-lived isotopes of Ra (^{223}Ra and ^{224}Ra) were measured on-site using Radium delayed coincidence counter (RaDeCC) system and ^{228}Ra, ^{226}Ra were measured in the laboratory using HPGe gamma spectrometer. Spatial variability in radium activities along the estuary is shown in Figure 76. Apparent age of estuarine water is determined using Ra isotopes due to their relative decay periods. Using ^{224}Ra/^{228}Ra activity ratio of river,

groundwater and estuary, the apparent age of water in the Godavari bay is estimated to be 3-5 days. Work on mass balance model based on ^{226}Ra to calculate the SGD fluxes is in progress.

This work was done in collaboration with V.V.S.S. Sarma of Regional Centre, NIO, Vishakapatnam

(R. Rengarajan)

IWIN National Programme

Retreat of several Himalayan glaciers and snow packs is a cause of concern for huge population in southern Asia dependent on the glacial-fed rivers emanating from Himalayas. There is considerable uncertainty about how cryospheric recession in the Himalayan region will respond to climate change, and how the water resource availability will be affected. As a first step towards quantifying the contribution of glacier melt-water, hydrograph separation of River Ganga at Rishikesh into its constituent components, namely (i) surface runoff; (ii) glacial ice-melt; and (iii) groundwater discharge was performed. A three component mixing model was employed using the values of $\delta^{18}O$ and electrical conductivity (EC) of the river water, and its constituents, to estimate the time varying relative fraction of each component. It was found that the relative fraction (Figure 77) of the surface runoff peaks (70-90%) during winter, due to near zero contribution of glacial ice-melt, and essentially represents the melting of surface snow from the catchment. The contribution of glacial ice-melt to the stream discharge peaks during summer and monsoon, reaching a maximum value of ~ 40% with an average of 32%. The fraction of groundwater discharge varies within a narrow range (15 ± 5%) throughout the year. Based on the variation in the *d*-excess values of river water, it is also suggested that the snow-melt and ice-melt component has significant fraction derived from winter precipitation with moisture source from mid-latitude westerlies, also known as western disturbances.

In order to study the nature of kinetic isotope fractionation involved during condensation under supersaturated condition, laboratory experiments were undertaken to investigate isotopic composition of liquid and solid condensates sampled from the ambient vapour. It was observed (Figure 78) that liquid and solid condensates are progressively more depleted in heavier isotopes with increasing extent of super-saturation ($S_{i\text{-}max}$ = actual vapour pressure at ambient temperature and Rh / saturation vapour pressure at condensation temperature). It was also observed that liquid condensate samples collected at periodic interval are progressively enriched in heavier isotopes. It is inferred that kinetic fractionation is governed by the degree of supersaturation at the time of condensation and leads to depletion of heavier isotopes in condensed phase.

For inter-laboratory calibration (ILC) exercise under IWIN National Programme, four secondary laboratory standards were prepared. Two of the secondary laboratory standards were synthesized at PRL, to have relatively depleted and enriched isotopic composition. This was achieved respectively by distillation and evaporation. The other two of the standards were natural water samples. A set of these four secondary laboratory standards were provided to all the IWIN Partners having their own IRMS laboratory. The certified values of isotopic composition of these standard samples were obtained from isotope hydrology laboratory of IAEA, Vienna. Among all the laboratories, the values obtained from IWIN-IRMS laboratory of PRL were in excellent agreement with the IAEA certified values (within ±0.06‰ for $\delta^{18}O$ and ±0.52 ‰ for δD).

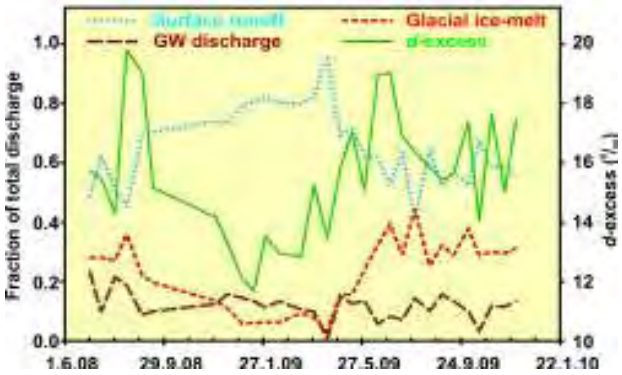

Figure 77: Estimated fractions of 'surface runoff', 'groundwater discharge' and 'glacial ice-melt' contribution to the total discharge of the Ganga River at Rishikesh corresponding to each observation of river water $\delta^{18}O$ and EC. Also shown is the temporal variation of river water *d*-excess.

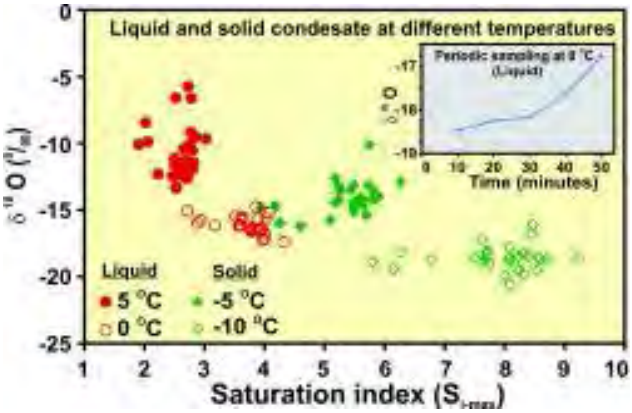

Figure 78: The $\delta^{18}O$ of solid condensate (collected at -5 and -10 °C) and liquid condensates (collected at 0 and 5 °C) plotted against Si-max. The inset plot shows variation in $\delta^{18}O$ of liquid condensate collected at an interval of 10 minutes for 50 minutes.

(R.D. Deshpande, A.S. Maurya, Miral Shah, S.K. Gupta)

SCIENCE

Theoretical Physics

The Theoretical Physics Division has been active in the fields of particle physics, astroparticle physics and cosmology, atomic physics, nuclear physics, quantum mechanics, complex systems, statistical mechanics and optics. Concerted effort has gone into understanding the nature of dark matter and dark energy, mechanisms of baryogenesis, the nature of the chiral transition in matter at high density, effect of viscosity in quark-gluon plasma, the structure of masses and mixing of fermions, especially neutrinos, and how future experiments can shed more light on it, and recent results in top physics and their impact on ongoing LHC experiments. Progress has also been made on the topics of random matrix ensembles, foundations of statistical mechanics, applications of coupled-cluster methods in atomic physics calculations, density profiles of quantum degenerate matter and in the study of properties of optical vortices.

Spectral properties of two-body random matrix ensembles for boson systems with spin

For *m* number of bosons, carrying spin (s = ½) degree of freedom, in Ω number of single particle orbitals, each doubly degenerate, we introduce and analyze embedded Gaussian orthogonal ensemble of random matrices generated by random two-body interactions that are spin (S) scalar [BEGOE(2)-s]. Embedding algebra for the BEGOE(2)-s ensemble and also for BEGOE(1 + 2)-s that includes the mean-field one-body part is U(2&Ω)⊃ U(&Ω) ⊗ SU(2) with SU(2) generating spin. A method for constructing the ensembles in fixed-(*m*,S) spaces has been developed. Numerical calculations show that for BEGOE(2)-s, the fixed-(m,S) density of states is close to Gaussian and level fluctuations follow GOE in the dense limit. For BEGOE(1 + 2)-s, generically there is Poisson to GOE transition in level fluctuations as the interaction strength (measured in the units of the average spacing of the single particle levels defining the mean-field) is increased. The interaction strength needed for the onset of the transition is found to decrease with increasing S. Propagation formulas for the fixed-*(m,S)* space energy centroids and spectral variances are derived for a general one plus two-body Hamiltonian preserving spin. Derived also is the formula for the variance propagator for the fixed-(m,S) ensemble averaged spectral variances. Using these, covariances in energy centroids and spectral variances are analyzed. Variance propagator clearly shows that the BEGOE(2)-s ensemble generates ground states with spin $S = S_{max}$. This is further corroborated by analyzing the structure of the ground states in the presence of the exchange interaction in BEGOE(1 + 2)-s. Natural spin ordering (S_{max}, S_{max} -1, S_{max} -2, ...) is also observed with random interactions. Going beyond these, we have also introduced pairing symmetry in the space defined by BEGOE(2)-s. Expectation values of the pairing Hamiltonian show that random interactions exhibit pairing correlations in the ground state region.

This work was done in collaboration with N.D. Chavda and V.Potbhare of M.S. University of Baroda, Vadodara.

(V.K.B. Kota, Manan Vyas)

One plus two-body random matrix ensembles with parity: Density of states and parity ratios

One plus two-body embedded Gaussian orthogonal ensemble of random matrices with parity [EGOE(1 + 2)-II] generated by a random two-body interaction (modeled by GOE in two particle spaces) in the presence of a mean-field, for spin less identical fermion systems, is defined in terms of two mixing parameters and a gap between the positive and negative parity single particle (sp) states. Numerical calculations are used to demonstrate, using realistic values of the mixing parameters appropriate for some nuclei, that the EGOE(1 + 2)- II ensemble generates Gaussian form (with corrections) for fixed parity eigenvalue densities (i.e. state densities). The random matrix model also generates many features in parity ratios of state densities that are similar to those predicted by a method based on the Fermi-gas model for nuclei. We have also obtained a simple formula for the spectral variances defined over fixed-(m_1, m_2) spaces, where m_1 is the number of fermions in the + ve parity sp states and m_2 is the number of fermions in the -ve parity sp states. Similarly, using the binary correlation approximation, in the dilute limit, we have derived expressions for the lowest two shape parameters. The smoothed densities generated by the sum of fixed-(m_1, m_2) Gaussians with lowest two shape corrections describe the numerical results in many situations. The model also generates preponderance of + ve parity ground states for small values of the mixing parameters and this is a feature seen in nuclear shell model results.

(V.K.B. Kota, Manan Vyas and P.C. Srivastava)

Binary correlation results for neutrinoless double beta decay nuclear transition matrix elements

PRL Scientists have proposed 3 years back a statistical theory for calculating nuclear transition matrix elements for neutrinoless double beta decay and it is based on the bivariate Gaussian form for the corresponding transition strength densities. The transition matrix elements are generated by an effective two-body operator. Two major gaps in the statistical theory are: (i) establishing the bivariate Gaussian form by deriving expressions for the fourth order bivariate cumulants; (ii) generating good estimates for the bivariate correlation coefficient. Extending the binary correlation approximation theory known before to two orbits (proton and neutron orbits) and for two operators, formulas are derived for both (i) and (ii). Numerical calculations for several candidate nuclei showed that the fourth order cumulants are small in general giving bivariate Gaussian form for the transition strength density. The bivariate correlation coefficients are found to be in the range 0.6-0.8.

(V.K.B. Kota and Manan Vyas)

Deformed Shell Model Results for Two Neutrino Double Beta Decay of ^{82}Se

Half-lives $T_{1/2}^{2\nu}$ for two neutrino double beta decay has been calculated for ^{82}Se, a nucleus for which experimental data is available, using deformed shell model (DSM) based on Hartree-Fock states employing a modified Kuo interaction in ($^2\pi_{3/2}$, $^1\phi_{5/2}$, $^2\pi_{1/2}$, $^1\gamma_{9/2}$) space. We have tested that DSM gives good spectroscopic results for the parent nucleus ^{82}Se and the daughter nucleus ^{82}Kr. For the half life calculations, we have taken, for projection and band mixing in DSM, for ^{82}Se, 7 intrinsic states with $K=0^+$ up to 5 MeV excitation, for the intermediate nucleus ^{82}Bρ, 36 intrinsic states with $K=1^+$ up to 6 MeV excitation and for the final nucleus ^{82}Kr, 26 intrinsic states with $K=0^+$ up to 6 MeV excitation. The calculated half-life using DSM is ~ 3.56 x 10^{20} yr. This is within a factor of 4 of the best adopted experimental value (0.92 ± 0.07) x 10^{20} yr. On the other hand, with the well known QRPA model and its relatives (RQRPA and SRQRPA), with a set of 22 calculations by groups in Europe, the calculated half life is in the range 7.66 x 10^{18} yr - 8.14 x 10^{21} yr.

This work was done in collaboration with R. Sahu of Berhampur University, Berhampur.

(V.K.B. Kota and P.C. Srivastava)

Shell-model description of odd $^{71\text{-}81}$Ga isotopes

Large scale shell model calculations have been carried out for both positive and negative parity states of odd-mass $^{71"81}$Ga isotopes in ($^1\phi_{5/2}, 2\pi, ^1\gamma_{9/}$ model space with two recent effective shell model interactions, JUN45 and jj44b. All the calculations of present work have been performed at the HPC facility of PRL using the shell model code ANTOINE and the computing time is several days for each isotope as the matrix dimensions involved are quite large. For instance, for ^{71}Ga isotope in $\phi_{5/2}\pi\gamma_{9/}$ space the dimension is 30582379 in the m-scheme adopted in ANTOINE. One of the aims is to explain high-spin states for ^{71,73,75,77}Ga which have been experimentally identified recently [I. Stefanescu et al., Phys. Rev. C 79, 064302 (2009)]. The calculations are used to predict high-spin states for ^{79,81}Ga and very little is known experimentally. The calculated positive parity states in ^{71,73,75}Ga are higher in energy in comparison to experimental findings, while for ^{77,79}Ga, the positive parity states are in better agreement. Thus, as one approaches towards N = 50 the results for positive parity states are quite good.

Both the interactions predict the leading configurations for protons to be of $\Pi(\phi^3_{5/2})$ and $\Pi(\pi_{3/2}\phi^2_{5/2})$ for ^{79}Ga and ^{81}Ga. These results show that more fine tuning of the effective interactions is required and also, more experimental data for positive parity states is needed to ascertain the importance of $\nu\gamma_{9/2}$ orbital.

(P.C. Srivastava)

Investigating anchor and probe lines for studies of temporal variation of fine structure constant in Na and Mg^+

It is a challenging problem to find out the role of the correlation effects in the isotope shift (IS) studies in many-electron atomic systems. The difficult part in this study lies in evaluating the specific mass shift (SMS) which involves two-body interactions between the electron momenta. Knowledge of ISs are useful in a number of applications ranging from nuclear physics to astrophysics. Mainly they are used to extract the relative root mean square (rms) nuclear charge radii and to probe the isotopic abundances of different elements in the astronomical objects. However, their effects are of same order of magnitudes with the effect that can be caused due to the temporal variation of the fine structure constant over a large period of time. So ISs can be treated as a possible systematic error in the astronomical studies of possible temporal variation of the fine structure constant. To find out the same, it is important to determine ISs and fine structure constant sensitivity parameters in different atomic systems. We have studied them using the relativistic coupled cluster method in Na and Mg^+.

(B. K. Sahoo)

Possibility of unambiguous detection of nuclear anapole moment using singly ionized barium and radium

The dominant contribution to parity nonconservation (PNC) in atomic systems comes from nuclear spin independent (NSI) component of the neutral weak current interaction due to exchange of Z_0 boson between nucleons and electrons. A significant size of contribution to atomic PNC can also arise due to nuclear anapole moment (NAM), if at all it exists, which will depend on the nuclear spin explicitly. Its existence has been reported from Cs PNC experiment. However the reported result does not agree well with the results obtained result using nuclear models. The disadvantage of inferring NAM from the Cs PNC measurement is that the PNC effect is dominated by the NSI interaction in this atom. There are also recent proposals to measure PNC in various atomic systems; especially in the singly charged ions. However, contributions to PNC will be dominated again by the NSI interaction in the considered transitions in those proposed experiments. If the low-lying $S\rightarrow D_{5/2}$ transitions in Ba^+ and Ra^+ are considered for the PNC light-shift measurements, it can infer the existence of NAM in an unambiguous way. In a recent work, we have given a proof-of-principle to measure quadrupole and PNC induced light-shifts in the $S\rightarrow D_{3/2}$ and $S\rightarrow D_{5/2}$ transitions in Ba^+ and Ra^+ by estimating magnitudes of the corresponding observables that can lead to probe the existence of NAM.

This work has been carried out in collaboration with P. Mandal and M. Mukherjee of Raman Centre for Atomic Molecular, and optical sciences, India Association for the cultivation of science, Kolkata.

(B. K. Sahoo)

General order relativistic coupled-cluster theory and application to precise estimate of black-body radiation shift of Al^+ clock frequency measurement

Due to advances in cooling and trapping techniques of atomic systems, high precision calculations in heavy atomic systems are essential to explain the very accurately measured results. Development of relativistic many-body methods that can be used to obtain different properties in large atomic systems very precisely is known to be a long time standing research problem for many years now. Relativistic coupled-cluster (RCC) theory is able to provide remarkable results in tandem with the measurements in the laboratories due to its potential of considering perturbations to all orders. However, this method has been employed successfully by various groups in the world at different level of approximations. Recently, we have developed a general order RCC method which opens-up the possibility to carry out high-accuracy calculations throughout the periodic table. This can be employed for studies in several important areas of fundamental physics such as probes of symmetry violations, search for the variation in the fundamental constants and atomic clocks. As a demonstration, we have employed the method for the calculation of polarizabilities and estimated uncertainty in the black body radiation shift of the Al^+ ion atomic clock, which is currently one of the most promising atomic clocks with the potential to be many times more accurate than today's time measuring devices. The accuracy of our result is about five times better than what can be achieved in the corresponding experiments. Consequently, the precision of the Al^+ clock can be considerably improved.

This work has been done in collaboration with Mihály Kállay and H. S. Nataraj (Department of Physical Chemistry and Materials Science, Budapest University of Technology and Economics, Budapest, Hungary) B. P. Das (Indian Institure of Astrophysics, Bangalore) Lucas Visscher (Amsterdam Centre for Multiscade Modeling, V U University Amsterdam, The Netherlands)

(B. K. Sahoo)

Mass determination at LHC in presence of invisible particles

We are involved at the analysis for *determination of mass scale at the hadron collider in the presence of invisible particles* (say, dark matter particles). This is quite a challenging task at any hadron collider (like LHC), especially, when we expect most of the signatures originating from the new physics beyond the Standard Model (BSM) contain two or more invisible particles. Several indirect methods were proposed with their own limitations for determination of new physics masses indirectly or at least to have some form of correlation between masses in the decay chain. Hence becoming heavily model dependent and they might work in certain scenarios. We are developing some interesting new variables and exploring different features of them.

This work is done in collaboration with K. C. Kong (University of Kansas, USA), K. Matchev and M. Park (University of Florida, USA).

(Partha Konar)

Signature based collider search strategy at LHC

In an another newly developing project we demonstrated some very exciting alternative 'signature based search strategy' for new physics (present publication). We apply a model-independent, agnostic approach to the collider phenomenology of supersymmetry, in which all mass parameters are taken as free inputs at the weak scale. Our exhaustive search reveals several quite dramatic yet unexplored multilepton signatures with up to 8 isolated leptons (plus possibly up to 2 massive gauge or Higgs bosons) in the final state. Such events are spectacular, background-free for all practical purposes, and may lead to a discovery in the very early stage of LHC operations at 7 TeV. Presently, we are trying to explore this farther.

This work is done in collaboration with K. Matchev, M. Park, G. Sarangi (University of Florida, USA).

(Partha Konar)

An SO(10) model with adjoint fermions for double seesaw neutrino masses

An SO(10) model where the Higgs scalar in the 10 and 120 representations are used for generating fermion masses is quite predictive, though the absence of 126 representation cannot give rise to neutrino masses through the usual type-I or type-II seesaw mechanisms. We propose an extension of such an SO(10) model by adding fermions in the adjoint representation 45 and a symmetry breaking scalar belonging to the 16 dimensional representation. This couples the adjoint fermions to the standard fermions belonging to the 16 dimesnional and induces neutrino masses through the 'double seesaw' mechanism. In order to enhance the predictivity of the model we impose mu-tau flavour symmetry on the Yukawa matrices in the 10 and 16 whereas for the 120 it is antisymmetric. We discuss the conditions that the mass matrices must obey so that the model can reproduce the tri-bimaximal mixing pattern.

This work was done in collaboration with Joydeep Chakrabortty and Amitava Raychaudhuri of Harish Chandra Research Institute.

(Srubabati Goswami)

2540 km: Bimagic baseline for neutrino oscillation parameters

We show that a source-to-detector distance of 2540 km offers multiple advantages for a low energy neutrino factory with a detector that can identify muon charge. At this baseline, for any neutrino hierarchy, the wrong-sign muon signal is almost independent of CP violation and the third mixing angle in certain energy ranges. This reduces the uncertainties due to these parameters and allows the identification of the hierarchy in a clean way. In addition, part of the muon spectrum is also sensitive to the CP violating phase and the third mixing angle, so that the same setup can be used to probe these parameters as well.

This work was done in collaboration with Amol Dighe from Tata Insitute of Fundamental Research and Shamayita Ray from Cornell University.

(Srubabati Goswami)

Texture 4 zero Dirac and Majorana Mass Matrices and neutrino phenomenology

We study the implications of Dirac and Majorana mass matrices with texture zeros within the type I seesaw mechanism. For the Dirac mass matrices we consider the 4 zero textures. For the Majorana mass matrices we consider a non-diagonal form which also contains 4 zeros and are more minimal than usually considered diagonal matrices. The later can motivated by flavour symmetries. We enumerate all such possible matrices and obtain the ones that are consistent with low energy phenomenology.

(Srubabati Goswami and H. Zeen Devi)

Domain growth in chiral phase transition

We investigate the kinetics of chiral phase transitions in quark matter. We discuss the phase diagram of this system in both a microscopic framework (using the Nambu-Jona-Lasinio model) and a phenomenological framework (using

a Landau free energy). Then, we study the far-from-equilibrium coarsening dynamics subsequent to a quench from the chirally-symmetric phase to the massive quark phase. Depending on the nature of the quench, the system evolves via either *spinodal decomposition or nucleation and growth.* The morphology of the ordering system is characterized using the order-parameter correlation function, structure factor, domain growth laws, etc.

This work has been done in collaboration with A. Singh and S. Puri from the School of Physics, Jawaharlal Nehru University, New Delhi.

(H. Mishra)

Cavitation and thermal dilepton production in QGP

We study the non-ideal effects arising due to viscosity (both bulk and shear), equation of state and cavitation on thermal dilepton production from QGP at RHIC energies. We calculate the first order corrections to the dilepton production rates due to shear and bulk viscosities. Ignoring the cavitations can lead to a wrong estimation of dilepton spectra. We show that the shear viscosity can enhance the thermal dilepton spectra whereas the bulk viscosity can suppress it. We present the combined effect of bulk and shear viscosities on the dilepton spectra.

(Jitesh R. Bhatt, Hiranmaya Mishra, V. Sreekanth)

Shear viscosity, cavitation and hydrodynamics at LHC

We study evolution of quark-gluon matter in the ultrarelativistic heavy-ion collisions within the frame work of relativistic second-order viscous hydrodynamics. In particular, by using the various prescriptions of a temperature-dependent shear viscosity to the entropy ratio, we show that the hydrodynamic description of the relativistic fluid become invalid due to the phenomenon of cavitation. For most of the initial conditions relevant for LHC, the cavitation sets in very early during the evolution of the hydrodynamics in time less than about 2 fm/c. The cavitation in this case is entirely driven by the large values of shear viscosity. Moreover we also demonstrate that the conformal term used in equations of the relativistic dissipative hydrodynamic can influence the cavitation time.

(Jitesh R. Bhatt, Hiranmaya Mishra, V. Sreekanth)

Dark energy from Neutrinos and Standard Model Higgs potential

If neutrino mass is a function of the Higgs potential then minimum of the total thermodynamic potential (which is the Higgs potential minus the neutrino pressure) can shift from the standard electro-weak vaccum expectation value v = 246.2 GeV by a small amount which depends on the neutrino pressure. If the neutrino mass is a very steep function of the Higgs field then the equilibrium thermodynamic potential can act like the dark energy with $\omega \sim -1$. Choosing the neutrino mass as logarithmic function of the Higgs field and a heavy mass scale, we find that the correct magnitude of the cosmological density of the present universe $\rho_\lambda \sim (0.002\ \text{eV})^4$ is obtained by choosing the heavy mass at the GUT scale.

This work has been done in collaboration with Gaetano Lambiase from the University of Salerno, Italy.

(Hiranmaya Mishra, Subhendra Mohanty)

Vacuum structure and chiral symmetry breaking in strong magnetic fields for hot and dense quark matter

We investigate chiral symmetry breaking in strong magnetic fields at finite temperature and densities in a 3 flavour Nambu Jona Lasinio model including the Kobayashi Maskawa't Hooft determinant term, using an explicit structure for the ground state in terms of quark antiquark condensates. The mass gap equations are solved self consistently and are used to compute the thermodynamic potential. We also derive the equation of state for strange quark matter in the presence of strong magnetic fields which could be relevant for proto-neutron stars.

This work has been done in collaboration with Amruta Mishra from IIT Delhi.

(Bhaswar Chatterjee, Hiranmaya Mishra)

Axigluon models and constraints from B-physics

The recent results on top quark pair production and forward-backward asymmetry seem to indicate a new source, beyond the standard model of particle physics, being operative. A viable class of models that can explain the experimental results is the so called axigluon models, where unlike the usual quantum chromodynamics, there is an additional heavy gluon with specific texture of axial vector coupling to quarks. It has been pointed out that constraints from B-meson mixing strongly disfavors a significant portion of the parameter space preferred in order to explain the forward-backward asymmetry in the top pair production. However, the model typically considered assumes a heavy additional generation which plays essentially no role in the low energy phenomenology. On the other hand it has been known for a while that extending the standard model by including an additional generation of fermions can resolve many of the

anomalies seen in the low energy sector. The additional generation should lie close to the electroweak scale to have any impact on the phenomenology. The present work is an attempt to suitably merge the two in a way to be able to explain both the low energy anomalies as well as top pair forward-backward asymmetry data. As an aside and an independent study, the assumptions and charge assignments within the considered axigluon model can be altered to explore the consequences for B-physics.

(Namit Mahajan)

New physics in tau decays and implications

The large hadron collider is expected to make use of the polarization of the tau leptons, produced in the decays of heavier particles, in order to gain important information about the decaying parent particle. It is expected that there is physics beyond the standard model well within the reach of the large hadron collider. If so, it is plausible that the same new physics affects the decays of less massive particles like tau leton and B-hadrons. With BES-III expected to deliver high precision data on tau decays, it is important to study the impact of specific new physics scenarios on tau decays in conjunction with the results from collider experiments and B-factories. A realistic assessment of the effect of new physics on tau decays, in particular decays of polarized tau leptons, is essential to correctly extract the desired information about the new heavier particles expected to show up in the collider experiments. This work proposes to systematically explore the impact of new physics on tau lepton in order to estimate the expected induced deviation in the polarized tau measurements at the large hadron collider.

(Namit Mahajan)

Cosmological implications of non standard supersymmetry breaking

Supersymmetric extension of the standard model is one of the most theoretically sound and phenomenologically rich extension, capable of simultaneously addressing various outstanding issues in particle physics. The most common and standard way to break supersymmetry is to specify what are called the soft supersymmetry breaking terms. However, in reality there could be non standard terms that can accomplish this task, over and above the usually specified soft terms. Such non standard terms may have direct relevance for cosmology and early universe. This work explores cosmological consequences of specific type of non standard supersymmetry breaking terms, consistent with the formal field theory requirements and obvious phenomenological constraints. It is expected that there will be distinctive signatures which can point to the presence of non standard terms.

(Namit Mahajan)

Crafting the core asymmetry to lift the degeneracy of optical vortices

The stability and the propagation dynamics of a vortex core could be a great concern in the context of optical communication through such beams and also from the fundamental point of view. We introduce an asymmetry in the core of a higher charge optical vortex by using appropriate computer generated hologram. The splitting of a higher charge optical vortex core into the unit charge vortices has been found to depend on the extent of asymmetry. For a second order vortex, the trajectories of split unit charged vortices and their separation have been recorded with the change in asymmetry of the core. There is a good agreement between experimentally obtained and theoretically calculated results.

(Ashok Kumar, Pravin Vaity, R. P. Singh)

Intensity correlation properties of high-order optical vortices passing through a rotating ground-glass plate

The first-order coherence or the field correlation of optical vortices has already been investigated to a considerable extent. However, we present for the first time a study of the intensity correlation properties of optical vortices passing through a rotating ground-glass (RGG) plate and compare them with those of the TEM_{00} mode of a He–Ne laser beam passed through the same RGG. We have observed that the intensity correlation curves for optical vortices decrease much faster than the corresponding curve for a TEM_{00} mode of the He–Ne laser. The rate of decay of the correlation increases with the increase of order of the vortices. Our experimentally observed results are supported by exact analytical results.

(Ashok Kumar, J. Banerji, R. P. Singh)

Wigner distribution of elliptical quantum optical vortex

Phase space, which is a fundamental concept in classical mechanics, remains useful when passing to quantum mechanics. On the line of probability density distribution functions in classical systems, quasiprobability distributions have been introduced in quantum mechanics. Among them, the Wigner function stands out because it is real, non-singular, yields correct quantum-mechanical operator averages in terms of phase space integrals, and possesses positive definite marginal distributions. Once

the Wigner distribution is known, the other properties of the system can be calculated from it.

We propose experimental methods to prepare a generalized quantum elliptic vortex by coupling two squeezed states using beam splitter or dual channel directional coupler and calculate the Wigner quasiprobability distribution function of this generalized quantum vortex. The quantum interference due to the coupling between two modes promises the generation of controlled entanglement for quantum computation and quantum tomography.

(Abir Bandyopadhyay and R. P. Singh)

Airy beams propagation through photorefractive materials

In 1979, Berry and Balazs observed non spreading Airy wave packet as the solution of the Schrödinger equation. This Airy packet has remarkable features: its non-dispersive nature and ability to accelerate in absence of any external potential. Due to analogy between the quantum mechanical Schrödinger equation and the paraxial diffraction equation, optics provides an experimental way to realize such wave packets called Airy beams.

We generate two dimensional Airy beams using a cubic phase mask and study its propagation through photorefractive material experimentally. The experimental results show the diffraction free nature as well as the acceleration of Airy beams. Using beam propagation method, we confirm the experimental results. We also study the effect of an applied electric field on the propagation of Airy beams through photorefractive materials numerically. It is observed that the applied field leads to interaction between the lobes of Airy beams.

(Pravin Vaity, Ashok Kumar, Shashi Prabhakar, R. P. Singh)

Information content of optical vortex fields

We study, experimentally as well as theoretically, the spatial coherence function and the Wigner distribution function for one-dimensional projections of optical vortices of different orders. The information entropy derived from the spatial coherence functions has been used to quantify the information content of the vortices and compared with those obtained for the Gaussian beam. The experimental results verify the theoretical findings of Agarwal and Banerji [Opt. Lett. 27, 800 (2002)].

We have tested a fundamental property of vortices. In contrast to Gaussian fields, vortices are very unique in their 1D projection. This uniqueness is evident in the two point correlation function of the 1D projections of a Gaussian and the optical vortex fields. It is of a Gaussian shape for a Gaussian field; however, for vortices, it has characteristic shapes that depend on the order of the vortex.

(Ashok Kumar, Shashi Prabhakar, Pravin Vaity, R. P. Singh)

Revealing the order of a vortex through its intensity record

We show that the intensity distribution of an optical vortex contains information of its order. Specifically, the number of dark rings in the Fourier transform of the intensity is found to be equal to the order of the vortex. Based on this property and the orthogonality of Laguerre polynomials, we demonstrate the feasibility of an experimental technique for determining the order of optical vortices.

(Shashi Prabhakar, Ashok Kumar, J. Banerji, R.P. Singh)

Making copies of optical vortices

We demonstrate a technique for making copies of optical vortices. It has been shown that by using suitable diffractive optical elements, several copies of optical vortices could be created with the same topological charge. We have devised such diffractive optical elements using a spatial light modulator which could be used to make copies of the vortices without inverting the charge. The nature of the topological charge was investigated with the interferometric technique. We have also presented theoretical results that are in excellent agreement with our experimental findings. We anticipate that these results may find applications ranging from optical manipulation to quantum information.

(Ashok Kumar, Pravin Vaity, J. Banerji, R. P. Singh)

On the foundations of statistical mechanics

We know from the most used prescription of Gibbs we calculate the phase space averages of dynamical quantities and we find that these phase averages agree very well with experiments. Clearly actual experiments are not done on a hypothetical ensemble they are done on the actual system in the laboratory and these experiments take a finite amount of time. Thus it is usually argued that actual measurements are time averages and they are equal to phase averages due to ergodicity. Aim of this work is to show that ergodicity is not relevant for equilibrium statistical mechanics (with Tolman and Landau). The solution of the problem is seen in the very peculiar nature of the macroscopic observables and with the very large number of the degrees of freedom involved in macroscopic systems

as first pointed out by Khinchin. These ideas are critically analyzed and in some cases a critique is also presented. The role of chaos (classical and quantum) where it is important and where it is not important is also investigated in detail. We criticise the ideas of E. T. Jaynes who says that the ergodic problem is conceptual one and is related to the very concept of ensemble itself which is a by-product of frequency theory of probability, and the ergodic problem becomes irrelevant when the probabilities of various micro-states are interpreted with Laplace-Bernoulli theory of probability (Bayesian viewpoint).

(Navinder Singh)

Dissipative quantum dynamics of Excitation Energy Transfer in Photosynthesis: Non-Markovian Quantum Master Equations and the Markovian Limit

Dissipative quantum dynamics of Excitation Energy Transfer (EET) in Photosynthesis is studied using non-Markovian Quantum Master Equations and the validity regime of Markovian limit is investigated. A numerical algorithm for solving the non-Markovian master equation in the second Born approximation based on an auxiliary function method is introduced and used to propagate the traditional dimer system that models excitation energy transfer in photosynthesis. Specifically, the coupled integro-differential equations for the reduced density matrix are solved by an efficient auxiliary function method in both the energy and site representations. In addition to giving exact results to this order, the approach allows us to access the range of the reorganization energy and decay rates of the phonon auto-correlation function for which the Markovian Redfield theory and the second order approximation is useful. For example, the use of Redfield theory for $\lambda > 10$ cm^{-1} in Fenna- Mathews-Olson (FMO) type systems is shown to be fundamentally flawed. Further, results for the evolution of states in the dimer system, with and without initial coherence, are compared. In some special cases we also give analytical results for the validity of the Markovian approximation.

This work is done in collaboration with Paul Brumer of the University of Toronto.

(Navinder Singh)

Plausible mechanisms of long coherence effects observed in excitation energy transfer in photosynthetic systems

Plausible mechanisms for observed long coherence effects in photosynthetic excitation energy transfer (EET) observed by 2D photon echo experiments has been proposed. We construct two models, (1) based upon the division of phonon degrees of freedom into strongly coupled component (through Polaron transformation) and the weakly coupled component (through dynamical disorder), and (2) based on the elegant Kenkre-Knox theory of exciton transport. The presence of zero phonon mode is the central cause of long coherence. The cause of decay (or origin of irreversibility) is also being investigated.

This work is going on in collaboration with Mukesh Tuwari (DAICT, Gandhinagar) , and V. M. Kenkre (University of New Mexico, USA)

(R. Amritkar and Navinder Singh)

Position swapping and pinching in Bose-Fermi mixtures with two-color optical Feshbach resonances

The density profiles of the quantum degenerate Bose-Fermi mixture of ^{174}Yb-^{173}Yb, experimentally observed recently, is examined in the mean field regime. In this mixture there is a possibility of tuning the Bose-Bose and Bose-Fermi interactions simultaneously using two well separated optical Feshbach resonances, and it is a good candidate to explore phase separation in Bose-Fermi mixtures. Depending on the Bose-Bose scattering length aBB, as the Bose-Fermi interaction is tuned the density of the fermions is pinched or swapping with bosons occurs.

This work is done in collaboration with P. Muruganandam, Bharathidasan University, Thiruchirapalli.

(S. Gautam and D. Angom)

Phase separation of binary condensates in harmonic and lattice potentials

A modified Gaussian ansatz to study binary condensates, trapped in harmonic and optical lattice potentials, both in miscible and immiscible domains is proposed. The ansatz is an apt one as it leads to the smooth transition from miscible to immiscible domains without any a priori assumptions. In optical lattice potentials, we analyze the squeezing of the density profiles due to the increase in the depth of the optical lattice potential. For this we develop a model with three potential wells, and define the relationship between the lattice depth and profile of the condensate.

(S. Gautam and D. Angom)

Fock-space relativistic coupled-cluster calculations of two-valence atoms

An all particle Fock-space relativistic coupled-cluster method for two-valence atomic systems is developed.

Based on which a scheme is formulated to employ the coupled-cluster wav3e functions in atomic properties calculations. The excitation energies, magnetic hyperfine structure constants and electric dipole matrix elements of Sr, Ba and Yb is then calculated using the method. Further more, the electric quadrupole HFS constants and the electric dipole matrix elements of Sr^+, Ba^+ and Yb^+ are calculated. For these the one-valence coupled-cluster wave functions obtained as an intermediate in the two-valence calculations is used.

(B.K. Mani and D. Angom)

Rayleigh-Taylor instability in binary condensates

A scheme to initiate and examine Rayleigh-Taylor instability in the two species Bose-Einstein condensates is proposed. The ^{85}Rb-^{87}Rb mixture as an excellent candidate to observe it experimentally. The instability is initiated by tuning the ^{85}Rb-^{85}Rb interaction through magnetic Feshbach resonance. We show that the observable signature of the instability is the damping of the radial oscillations. This would perhaps be one of the best controlled experiments on Rayleigh-Taylor instability. We also propose a semi analytic scheme to determinate stationary state of binary condensates with the Thomas-Fermi approximation for the axis symmetric traps. The time evolution of the density profiles of the two condensates are shown in Figure 79.

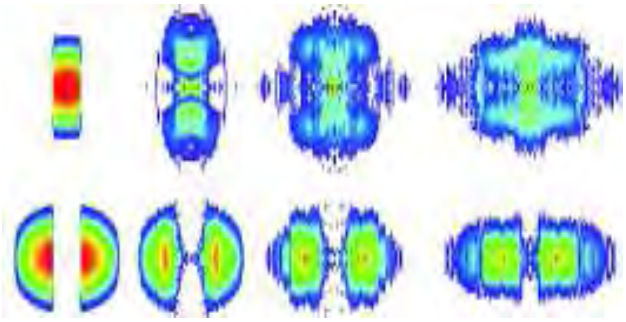

Figure 79: Evolution of the TBEC with RTI. The first and second row are density profiles of ^{85}Rb and ^{87}Rb BECs respectively after increasing a11 to 408 a_o. Starting from left, the density profiles are at 0, 24.5, 49.0 and 73.5 milliseconds after the increase of a11.

(S.Gautam and D. Angom)

Properties calculated by relativistic coupled-cluster theory without truncation: Hyperfine constants of Mg^+, Ca^+, Sr^+, and Ba^+

An iterative scheme for coupled-cluster properties calculations without truncating the dressed properties operator is developed and demonstrated. For validation, magnetic dipole hyperfine constants of alkaline Earth ions are calculated with relativistic coupled-cluster and role of electron correlation examined. Then, a detailed analysis of the higher order terms is carried out. Based on the results, an optimal form of the dressed operator is defined. Which is recommended for properties calculations with relativistic coupled-cluser calculations.

(B. K. Mani and D. Angom)

Ground state geometry of binary condensates in axisymmetric traps

The ground state interface geometry of binary condensates in the phase separated regime undergoes a smooth transition from planar to ellipsoidal to cylindrical geometry. This occurs for the condensates with repulsive interactions as the trapping potential is changed from prolate to oblate. The correct ground state geometry emerges when the interface energy is included in the energy minimization, whereas energy minimization based on Thomas-Fermi approximation gives incorrect geometry. The planar and cylindrical interface geometries have less interface area and minimize the interface energy. These are the prefered ground states in the cigar and pan-cake shaped trap configurations. To illustrate, the density profile of ^{85}Rb-^{87}Rb in the cylindrical geometry is shown in Figure 80.

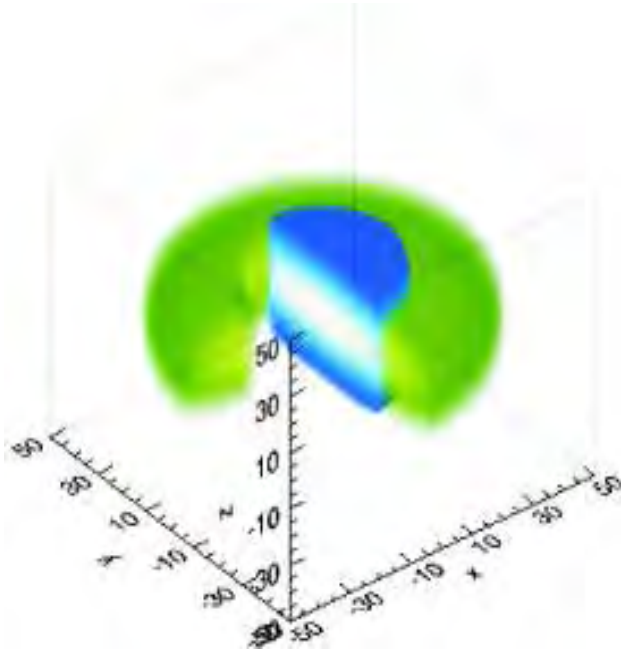

Figure 80: The false colour coded cutaway view of of the density profiles for the cylindrical interface of the ^{85}Rb-^{87}Rb condensate mixture.

(S. Gautam and D. Angom)

Experimental signatures of cosmological neutrino condensation

Super fluid condensation of neutrinos of cosmological origin at a low enough temperature can provide simple and elegant solution to the problems of neutrino oscillations and the accelerated expansion of the universe. It would give rise to a late time cosmological constant of small magnitude and also generate tiny Majorana masses for the neutrinos as observed from their flavor oscillations. We show that carefully prepared beta decay experiments in the laboratory would carry signatures of such a condensation, and thus, it would be possible to either establish or rule out neutrino condensation of cosmological scale in laboratory experimentσ.

This work was done in collaboration with Azam, BARC, Mumbai.

(Jitesh Bhatt and Utpal Sarkar)

Top polarization, forward-backward asymmetry and new physics

A study is made of how the measurement of top polarization at the Tevatron can be used to characterize and discriminate among different new physics models that have been suggested to explain the anomalous top forward-backward asymmetry reported at the Tevatron. Top polarization is found to have the advantage of catching the essence of the parity-violating effect characteristic of the different new physics models that have been suggested. Other observables constructed from these asymmetries are shown to be useful in discriminating between the models, even after taking into account statistical errors. Some signals at the 7 TeV LHC were also investigated.

This work was done in collaboration with D. Choudhury and P. Saha of University of Delhi and R.M. Godbole of CHEP, Indian Institute of Science, Bangalore.

(S. D. Rindani)

Isolating CP-violating γZZ coupling in $e^+e^- \to \gamma Z$ with transverse beam polarizations

The process $e^+e^- \to \gamma Z$ at the ILC with transverse beam polarization in the presence of anomalous CP-violating γZZ coupling λ_1 and $\gamma\gamma Z$ coupling λ_2 was studied with a view to experimental determination of the anomalous couplings. It was found that if the final state spins are resolved, then it becomes possible to fingerprint the anomalous coupling $Re\lambda_1$, otherwise not accessible separately. Experimental limits on $Re\lambda_1$ achievable at a future linear collider (ILC) with centre-of-mass energy of 500 GeV or 800 GeV with realistic initial beam polarization and integrated luminosity were found to be of the order of few times of 10^{-2} when the helicity of the Z is used and 10^{-3} when the helicity of γ is used. Possible methods by which one can isolate events with a definite helicity for one of the final-state particles were also discussed.

This work was done in collaboration with B. Ananthanarayan, S.K. Garg and M. Patra of CHEP, Indian Institute of Science, Bangalore.

(S. D. Rindani)

CP properties of the Higgs boson in associated production with a top quark pair

The spin and CP properties of a Higgs boson are analysed in a model-independent way in its associated production with a top-ant top pair in high-energy e^+e^- collisions. The prospects of establishing the CP quantum numbers of the Higgs boson in the CP-conserving case as well as those of determining the CP-mixing if CP is violated are studied. The combined use of the total cross section and its energy dependence, the polarisation asymmetry of the top quark and the up-down asymmetry of the ant top with respect to the top-electron plane is explored. It is found that combining all three observables remarkably reduces the error on the determination of the CP properties of the Higgs Yukawa coupling. Furthermore, the top polarisation asymmetry and the ratio of cross sections at different collider energies are shown to be sensitive to the spin of the particle produced in association with the top quark pair.

This work was done in collaboration with R.M. Godbole of CHEP, Indian Institute of Science, Bangalore, and C. Hangst and M. Mühlleitner of Karlsruhe Insitute of Technology, Karlsruhe, Germany.

(S. D. Rindani and P.Sharma)

Viability of exact tri-bimaximal mixing in an SO(10) grand unified model

General structures of the charged lepton and the neutrino mixing matrices leading to tri-bimaximal leptonic mixing are determined. These are then integrated into an SO(10) model within which detailed fits to fermion masses and mixing angles are given. It is shown that one can obtain excellent fits to all the fermion masses and quark mixing angles keeping tri-bimaximal leptonic mixing intact. Various perturbations to tri-bimaximal mixing which can arise in the model are considered and their impact on the predictions of the reactor mixing angle q is numerically discussed.

(A. S. Joshipura and Ketan M. Patel)

Fermion masses and SO(10) models

Detailed analysis of many SO(10) models for their viability or otherwise in explaining all the fermion masses and mixing angles was carried out. This study is made for both supersymmetric and non-supersymmetric models and with minimal $(10+126)$ and non-minimal $(10+126+120)$ Higgs content. Extensive numerical fits to fermion masses and mixing are carried out in each case assuming dominance of type-II or type-I seesaw mechanism. Required scale of the B-L breaking is identified in each case. In supersymmetric case, several sets of data at the GUT scale with or without inclusion of finite supersymmetric corrections are used. All models studied provide quite good fits if the type-I seesaw mechanism dominates while many fail if the type-II seesaw dominates. This can be traced to the absence of the b-t unification at the GUT scale in these models. The minimal non-supersymmetric model with type-I seesaw dominance gives excellent fits. In the presence of a 45_H and an intermediate scale, the model can also account for the gauge coupling unification making it potentially interesting model for the complete unification. Structure of the Yukawa coupling matrices obtained numerically in this specific case is shown to follow from a very simple U(1) symmetry and a Froggatt-Nielsen singlet.

(Anjan S. Joshipura and Ketan M. Patel)

Forward-backward asymmetry in top quark production from light colored scalars in SO(10) model

The forward-backward asymmetry in top pair production at Tevatron has been reconfirmed by the CDF collaboration with 5.3 fb^{-1} of accumulated data. These measurements also report that the asymmetry is the largest in regions of high invariant mass M_{tt} and rapidity difference ΔY. We consider light colored sextet scalars appearing in a particular non-supersymmetric SO(10) grand unification model within the 126 scalar representation. These scalar states have masses in the range of 300 GeV"2 TeV consistent with the requirements of gauge coupling unification and bounds on the proton lifetime. The cross section and the total asymmetry can be simultaneously explained with the contributions of these scalars within 1sigma. We find that the simultaneous fitting of the cross section, the total asymmetry and the asymmetries in different rapidity and M_{tt} bins gives only a marginal improvement over the SM contribution. We also study various production mechanisms of these colored sextet scalars at the LHC.

(Ketan M. Patel, Pankaj Sharma)

Parity Breaking in Supersymmetric Left-Right Symmetric Models

One of the problems with the supersymmetric left-right symmetric models is the parity violation. We provided the simplest and fully consistent solution to this problem by introducing a bi-triplet scalar field, and spontaneous D-parity violation. We have now studied the different scenarios of spontaneous breaking of D-parity in both non-supersymmetric and supersymmetric version of the left-right symmetric models (LRSM). In case of the models with only doublet Higgs scalars we do not require the bi-triplet scalars, and our proposal can be implemented in the simplest version of the model. We then extended our analysis to explore the possibility of a TeV scale $SU(2)_R$ breaking scale M_R and hence TeV scale right handed neutrinos. We studied these models from both minimization of the scalar potential as well as the coupling constant unification point of view. We show that although minimization of the scalar potential allows the possibility of a TeV scale M_R and tiny neutrino masses in LRSM with spontaneous D-parity breaking, the gauge coupling unification at a high scale $\sim 10^{16}$ GeV does not favour a TeV scale symmetry breaking except in the supersymmetric left-right (SUSYLR) model with Higgs doublet and bidoublet. The phenomenology of neutrino mass is also discussed.

One of these works was done in collaboration with D. Borah of the Indian Institute of Technology, Bombay, India.

(Sudhanwa Patra, Anjishnu Sarkar and Utpal Sarkar)

Asymmetric Dark Matter and Baryogenesis

In the present universe, there is 5% visible matter and 25% dark matter, while the rest is dark energy. To explain why the amount of visible matter is comparable to the dark matter, we proposed the asymmetric dark matter model, where the same mechanism generates more matter compared to antimatter and also an asymmetric dark matter. We extend this result to provide an elegant explanation and for predicting the correct amount of dark matter, originating from a dark matter asymmetry, in terms of the observed baryon asymmetry of the universe. We realize this scenario in baryon (lepton) number conserving models where two or more neutral singlet scalars decay into two or three baryonic (leptonic) dark matter scalars, and also decay into quarks (leptons) through other on-shell and/or off-shell exotic scalar bilinears. The produced baryon (lepton) asymmetries in the dark matter scalar and in the standard model quarks (leptons) are thus equal and opposite. The dark matter mass is predicted to be in a range of a few GeV to a few TeV depending on the baryon

(lepton) numbers of the decaying scalars and the dark matter scalar. The dark matter scalar can interact with the visible matter through the exchange of the standard model Higgs boson, opening a window for the dark matter direct detection experiments. These models also provide testable predictions in the searches for the exotic scalar bilinears at LHC.

This work has been completed in collaboration with P. Gu and M. Lindner of the Max-Planck Institute at Heidelberg, Germany and X. Zhang of Institute of High Energy Physics, Chinese Academy of Sciences, Beijing, China.

(Utpal Sarkar)

Reconciling Dark Matter observations with relic density calculations via Sommerfeld effect.

We show that a 4 TeV wino dark matter can explain the positron and antiproton fluxes observed by PAMELA and at the same time give a thermal relic abundance of dark matter consistent with WMAP observations if a non-perturbative phenomenon called Sommerfeld effect is incorporated in the calculation of the relic density and the dark matter annihilation in the galaxies.

This work was done in collaboration with D.P. Roy of HBCSE-TIFR, Mumbai.

(Subhendra Mohanty and Soumya Rao)

Publications in Journals

Astronomy and Astrophysics

1. Munari, U., Joshi V.H., Banerjee, D.P.K., Ashok, N.M., Valisa, P., Milani, A., Siviero, A., Dallaporta, S. and Castellani, F., 2011, "*The 2010 nova outburst of the symbiotic mira V407 Cyg*" Mon. Not. R. Astron. Soc. Letters, v. 410, p. L52-L56.

2. Banerjee, D.P.K., Das, R.K., Ashok, N.M., Rushton, M.T., Eyres, S.P.S., Maxwell, M.P., Worters, H.L., Evans, A. and Schaefer, B.E., 2010, "*Near-infrared studies of the 2010 outburst of the recurrent nova U Scorpii*" , Mon. Not. R. Astron. Soc. Letters, v. 408, p. L71-L75.

3. Chandrasekhar, T. and Tapas, Baug, 2010, "*Lunar occultations of sources in the near-infrared towards the Galactic Centre*", Mon. Not. R. Astron. Soc, v.408, p.1006-1010.

4. Thone, C.C. Et al with Baliyan, K.S. Ganesh, S., 2010, "*Photometry and spectroscopy of GRB 060526: a detailed study of the afterglow and host galaxy of a z = 3.2 gamma-ray burst*", A&A v. 523, p. 70- 90.

5. Joshi, U. C., Ganesh, S., Baliyan, K.S., 2010, "*Near opposition photometry of comet C/2007 N3 (Lulin)*", Mon. Not. R. Astron. Soc. Letters, v. 412, p. L58-L62

6. Rani, B, Gupta, A, Joshi, U. C., Ganesh, S. Wiita, P. J., 2010, "*Quasi-periodic Oscillations of ~15 Minutes in the Optical Light Curve of the BL Lac S5 0716+714*", ApJ Letters, v. 719, p. L153-L157.

7. Chandra, Satish, Vats, H. O. and Iyer K. N., 2010, *"Differential rotation measurement of soft X-ray corona"*, Mon. Not. R. Astron. Soc., v. 407, p. 1108–1115.

8. Vats, H. O. and Chandra, Satish, 2011, *"North–south asymmetry in the solar coronal rotation",* Mon. Not. R. Astron. Soc. Letters, v. 413, p. L29–L32.

9. Chandra, Satish and Vats, H. O., 2011, *"Periodicities in the rotation period of solar corona and sunspot numbers"*, Mon. Not. R. astro. Soc., (in press).

10. Naik, Sachindra, Das, M. Jain, C., and Paul, B., 2010, *"An X-ray Bright Nucleus in Low Surface Brightness Galaxy UGC 6614"*, MNRAS, v. 404, p 2056-2060.

11. Rao, A. R., et al. (including Sachindra Naik), 2011, *"Detection of GRB 090618 with the RT-2*

Experiment on Board the Coronas-Photon Satellite", The Astrophysical Journal, v. 728, p.42-49.

12. Naik, Sachindra, Paul, B., Kachhara, C. and Vadawale, S. V., 2011, *"Suzaku observation of the transient X-ray pulsar GRO J1008-57"*, MNRAS, v. 413, p. 241-248.

13. Rastogi, R.G., Janardhan, P., Ahmed, K., Das, A.C., and Bisoi, S.K., 2010, *"Unique observations of a geomagnetic SI^{+} – SI^{s} pair: Solar sources and associated solar wind fluctuations"*, J. Geophys. Res., v. 115, p. A12110.

14. Janardhan, P., Bisoi, S.K., and Gosain, S., 2010, *"Solar Polar Fields during Cycles 21 – 23: Correlation with Meridional Flows",* Sol. Phy., v. 267, p. 267 – 277.

15. Dewangan, L. K.,and Anandarao, B. G., 2010, *"A study of the massive star forming region M8 using Spitzer-IRAC images"*, MNRAS, v. 407, p.1170.

16. Kumar, M. S. N., Velusamy, T. , Davis, C. J., Varricatt, W. P. and Dewangan, L. K., 2010, *"Ring-like features around young B stars"*, A &A, v. 519, p. 99.

17. Jain, Rajmal, 2010, *"Exploring the Dynamic Solar Corona – Research Highlights"*, Space Research Today, v. 177, p. 4-15.

18. Jain, Rajmal, Aggarwal, Malini, Sharma, Raghunandan, 2010, *"Evidence of decay of flux ratio of Fe to Fe-Ni line features with electron temperature in solar flares"*, Journal of Astrophysics and Astronomy, v. 31, Issue 3, p.155-163.

19. Jain, Rajmal, Awasthi, Arun Kumar, Rajpurohit, Arvind, Singh, Aschwanden, Markus J., 2011, *"Energy-Dependent Timing of Thermal Emission in Solar Flares"*, Solar Phys., v. 270, p. 137–149.

Solar Physics

20. Bhattacharyya, R., Low, B. C., and Smolarkiewicz, P. K., 2010, "*On Spontaneous Formation of Current Sheets: Untwisted Magnetic Fields"*, Physics of Plasmas, 17, p. 112901-1 to 112901-17.

21. Gosain, S., Tiwari, S. K., and Venkatakrishnan, P., 2010, "*On the Estimate of Magnetic Non-potentiality of Sunspots Derived Using Hinode SOT/SP Observations: Effect of Polarimetric Noise"*, the Astrophysical Journal, v. 720, p. 1281-1289.

22. Gosain, S, and Venkatakrishnan, P., 2010, "*The Evolution of the Twist Shear and Dip Shear during X-class Flare of 2006 December 13: Hinode Observations",* The Astrophysical Journal Letters, v.720, p. L137-L143.

23. Joshi, Anand D., Mathew, Shibu, K. Srivastava, Nandita, Martin, Sara, F., and Gupta, Sudhir, K., 2010, *"A Dual Beam H-Alpha Doppler System To Acquire, Analyse And Anticipate Solar Eruptive Events Directed Towards Earth",* Indian J. Radio Space Phys., v.39, p. 315-318.

24. Joshi, Anand D. and Srivastava, Nandita, 2011, *"Kinematics of Two Eruptive Prominences Observed by EUVI/STEREO"*, Astrophysical Journal, v.730, p.104-114.

25. Louis, Rohan Eugene, Luis R. Bellot Rubio, Mathew, S.K., and Venkatakrishnan P., 2011*,"Supersonic Downflows at the Umbra–Penumbra Boundary of Sunspots"*, ApJ, v.727, p.49 – 59.

26. Maurya R.A. and Ambastha A., 2010, *"Sub-surface Meridional Flow, Vorticity, and the Lifetime of Solar Active Regions",* Astrophysical Journal Letters, v. 714, p. L196- L201.

27. Singh, J., Raghavendra, Prasad, B., P. Venkatakrishnan, K., Sankarasubramanian, Banerjee, D., Bayanna, A. R., Mathew, S. K., Murthy, J., Subramanian, P., Ramesh, R.,. Kathiravan, K., Nagabhushana, K., Mahesh, P. K., Manoharan, P. K., Uddin, W., Sriram, S., Kumar, A., Srivastava, N., Rao, K., Nagendra, C. L., Chakraborthy, P., Sriram, K. V., Venkateswaran, R., Krishnamurthy, T., Sreekumar, P., Sarma, K. S., Murthy, R., Navalgund, K. H., Samudraiah, D. R. M., Narayan Babu, P., and Patra, A.. 2011, *"Proposed Visible Emission Line Space Solar Coronagraph"*, Current Science, v.100, No.2, p. 167-174.

28. Tiwari, S.K., Venkatakrishnan, P. and Gosain, S., 2010, "*Magnetic Non-potentiality of Solar Active Regions*2010, "*Magnetic Non-potentiality of Solar Active Regions and Peak X-ray Flux of the Associated Flares"*, the Astrophysical Journal, v. 721, p. 622-629.

29. Venkatakrishnan, P., and Tiwari, S.K., 2010, *"Magnetic Tension of Sunspot Fine Structures",* Astronomy and Astrophysics, v. 516, p.L5-L9.

Planetary Sciences and PLANEX Program

30. Mishra, R.K., Goswami, J.N., Tachibana, S., Huss, G.R., and Rudraswami, N.G., 2010, *"^{60}Fe and ^{26}Al in chondrules from unequilibrated chondrites : Implications for early solar system processes", ApJ (Letters)* v.714, p. L217-221.

31. Goswami. J. N.,2010, Chandrayaan-1 Mission: An overview and significant science results In *"New advances in Lunar Exploration"* (Ed. Z. Ouyang, W. H.Ip, Z. Teng), p. 14-20 (Macau Univ. of Science Technology).

32. Narendranath, S., Ahiray, P.S. , Sreekumar, P., Kellett, B.J., Alha, L., Howe, C.J., Joy, K.H., Grande, M., Huovelin, J., Crawford, I., Unnikrishnan, U., Lalita, S., Subramaniam, S., Weider, S.Z., Nittler, L., Gasnault , Rothery, O. D., Fernandes, V.A., Bhandari, N., Goswami. J. N., Wieczorek, M.A., the CIXS teamIcarus, 2011, *"Lunar X-ray fluorescence observations by the Chandrayaan-1 X-ray Spectrometer (C1XS): Results from a lunar highland region"*, v.214, p.53-66.

33. Banerjee, D. and Vadawale, S., 2010, *"Theoretical modelling of X-ray fluorescence signals for different lunar compositions and dependence on solar activity"*, Advances in Space Research, v.46, p.651-656.

34. Banerjee, D., Toyoda, S., Takada, M. and Shimada, A., 2011, *"Component resolved optically stimulated luminescence investigations and age determination for a quartz sample from marine terrace sediments in Fukui region, Central Japan",* Advances in ESR Applications, v.27, p.7-10.

35. Durga, Prasad, K. and Murty, S.V.S., 2011, *"Wireless Sensor Networks – A potential tool to probe for water on moon",* Adv. Space Res. v. 48, p. 601-612.

36. Mishra, R.K., Goswami, J.N., Tachibana, S., Huss, G.R., and Rudraswami, N.G., 2010*, "^{60}Fe and ^{26}Al in Chondrules from Unequilibrated Chondrites: Implications for Early Solar System Processes",* Ap. J. Lett., v.714, p. L217-L221.

37. Murty, S.V.S., Mahajan, R.R., Jenniskens, P., Shaddad, M.H. and Eldien, B., 2010, *"Noble gases and nitrogen in the Almahata Sitta ureilite",* Meteorit. Planet. Sci., v.45, p.1751-1764.

38. Pabari, J. P., Acharya, Y. B., Desai, U. B., Merchant, S. N. and Krishna, B. G., 2010, *"Radio Frequency Modelling for Future Wireless Sensor Network on Surface of the Moon",* International Journal of Communications, Network and System Sciences, v. 3, No. 4, p. 395-401.

39. Pabari, J.P., Yadav, S. and Singh, R., 2010, *"Microwave Detection of Soil Moisture using C-band Rectangular Waveguide",* Sensors & Transducers Journal, v. 120, Issue 9, p.134-141.

40. Peter Hoppe, Jan Leitner, Elmar Gröner, Marhas, K.K., Bradley S. Meyer, and Sachiko Amari, 2010, *"Nano SIMS studies of small presolar SiC grains: new insights into supernova nucleosynthesis, chemistry, and dust formation",* Astrophysical Journal, v.719, p.1370-1384.

41. Pieters, C.M., Besse, S., Boardman, J., Buratti, B., Cheek, L., Clark, R.N., Combe, J.P., Dhingra, D., Goswami, J.N., Green, R.O., Head, J.W., Isaacson, P., Klima, R., Kramer, G., Lundeen, S., Malaret, E., McCord, T., Mustard, J., Nettles, J., Petro, N., Runyon, C., Staid, M., Sunshine, J., Taylor, L.A., Thaisen, K., Tompkins, S., and Whitten, J., 2011, *"Mg-spinel lithology: A new rock type on the lunar farside"* J. Geophys. Res.v.E116, p. E00GO8(1-14).

42. Price, M.C., Kearsley, A. ., Burchell, M. ., Hörz, F., Borg, J., Bridges, J.C., Cole, M.J., Floss, C., Graham, G., Green, S.F., Hoppe, P., Leroux, H., Marhas, K.K., Park, N., Stroud, R., Stadermann, F. J. and Wozniakiewicz, P. J., 2010, *"Comet 81P/ WILD 2: The size distribution of finer (sub 10 micrometer) dust collected by the stardust spacecraft"* Meteoritics & Planetary Science, v. 45, p.1409-1428.

43. Toyoda, S., Sato, F., Banerjee, D. and Ishibashi, J., 2011, *"Characteristics of the radiation induced ESR signals in Barite",* Advances in ESR Applications, v.27, p.4-6.

Space and Atmospheric Sciences

44. Banola, S., Maurya R. N. and Chandra, H., 2010, *"Solar and geomagnetic activity control on equatorial VHF Scintillations in the Indian region"* J. Ind. Geophys. Union, v. 14, p.195-209.

45. Chakrabarty, D., Sekar, R., Sastri, J.H., Pathan, B. M., Reeves, G.D., Yumoto, K., and Kikuchi, T.,

2010. *"Evidence for OI 630.0nm dayglow variations over low latitudes during onset of a substorm",* J. Geophys. Res., v. 115, p.A10316 (1-10).

46. Chandra, H., Som, Sharm and Soe, Win, Aung, 2010, *"F-region variability over the anomaly crest region"* Ind. J Radio & Space Phys., v.39, p.302-307.

47. Chandra, H., and Vyas, G.D., 2010, *"Abnormally low F-layer ionization over Ahmedabad during the night of 26-27 November 1984"* Ind. J Radio & Space Phys., v.39, p.346-352.

48. Chandra, H. and Rastogi, R.G., 2011, *"Space weather event of 25 September 1998: ionospheric Response",* J. Ind. Geophys. Union, v.15, p. 45-59.

49. Das, U., Pallamraju, D. and Chakrabarti, S., 2010, *"Effect of an X-Class solar flare on the OI 630 nm dayglow emissions"*, J. Geophys. Res., v.115, p. A08302 (1-6).

50. Das, U. and. Sinha, H.S.S., 2010, *"Winter Equatorial Mesospheric Neutral Turbulence"*, Current Science, v. 99, 1, p. 80-85.

51. Guharay, A., Venkat Ratnam, M., Nath, D. and Dumka, U.C., 2010, *"Investigation of saturated gravity waves in the tropical lower atmosphere using radiosonde observations",* Radio Science, v.45, p. RS6008 (1-14).

52. Haider, S.A., Seth, S.P., Brain, D.A., Mitchell, D.L., Majeed, T., and Bougher, S.W., 2010, *" Modeling photoelectron transport in the Martian ionosphere at Olympus Mons and Syrtis Major: MGS observations",* Journal of Geophysical Research, v.115, p.A08310 (1-15).

53. Haider, S.A., Sheel, V., Smith, M.D., Maguire, W.C., and Molina-Cuberos, G.J, 2010, *"Effects of dust storms on the D region of the Martian ionosphere: Atmospheric Electricity",* Journal of Geophysical Research, v. 115, p. A12336 (1-10).

54. Kedia, S., Ramachandran, S., Kumar, A., and Sarin, M.M., 2010, *"Spatiotemporal gradients in aerosol radiative forcing and heating rate over Bay of Bengal and Arabian Sea derived on the basis of optical, physical and chemical properties",* Journal of Geophysical Research, v. 115, p. D07205 (1-17).

55. Kondo, Y., Sahu, L., Moteki, N., Khan, F., Takegawa, N., Liu, X., Koike, M., and Miyakawa, T., 2011, *"Consistency and traceability of black carbon measurements made by laser-induced incandescence, thermal-optical transmittance, and filter-based photo-absorption techniques",* Aerosol Science and Technology, v. 45, p. 295–312.

56. Kushawaha, R.K. Sunil Kumar, S., Jan, M.R., Prajapati , I.A., Safvan, C.P., and Bapat B., 2010 *"Triple F^+ ejection from SF_6 bombarded by swift ions"* J. Phys. B: At. Mol. Opt. Phys. v. 43, p. 205204 (1-5).

57. Matsui, H., Kondo, Y., Moteki, N., Takegawa, N., Sahu, L.K., Zhao, Y., Fuelberg, H. E., Sessions, W. R., Diskin, G., Blake, D. R,; Wisthaler, A., and Koike, M., 2011, *"Seasonal variation of the transport of black carbon aerosol from the Asian continent to the Arctic during the ARCTAS aircraft campaign",* Journal of Geophysical Research, v. 116, p. D05202 (1-19).

58. Pallamraju, D., U. Das, and S. Chakrabarti, 2010, *"Short and long timescale thermospheric variability as observed from OI 630.0 nm dayglow emissions from low latitudes"*, J. Geophys. Res., v.115, p. A06312 (1-9).

59. Rai R.K., Mittal Mithilesh and Chandra H.,2010, *"Lonospheric drifts over Udaipur during counter electrojet event"*, J. Ind. Geophys. Union, v. 14, P.177-182.

60. Rajesh, P.K. Liu, J.Y., Sinha H.S.S., and Banerjee, S.B., 2010, *"Appearance and extension of airglow depletions",* J. Geophys. Res., v. 115, p. A08318 (1-8).

61. Ramachandran, S., and Kedia, S., 2010, *"Black carbon aerosols over an urban region: Radiative Forcing and climate impact",* Journal of Geophysical Research, v. 115, p. D10202 (1-11).

62. Rastogi R G, Chandra H and Yumoto K, 2010, *"Equatorial electrojet in East Brazil",* J. Earth System Sci., v.119, P.497-505.

63. Sahu, L.K., Lal, S., and Venkataramani, S., 2011, *"Impact of monsoon circulations on oceanic emissions of light alkenes over Bay of Bengal"*, Global Biogeochem. Cycles, v. 24, p. GB4028 (1-10).

64. Sarkhel, S., Sekar, R., Chakrabarty, D., and Sridharan, S., 2010. *"A case study on the possible altitude-dependent effects of collisions on sodium airglow emission",* J. Geophys. Res., v. 115, p. A10306 (1-7).

65. Shinozuka, Y., Redemann, Livingston, J.M., Russell, P.B., Clarke, A.D., Howell, S.G., Freitag, S., O'Neill, N.T., Reid, E.A., Johnson, R., Ramachandran, S., McNaughton, C.S., Kapustin, V.N., Brekhovskikh, V., Holben, B.N., and McArthur, L.J.B., 2010, *"Airborne observation of aerosol optical depth during ARCTAS: vertical profiles, inter-comparison, fine-mode fraction and horizontal variability",* Atmospheric Chemistry and Physics Discussions, v. 10, p. 18315-18363.

66. Sheel Varun, Lal S., Richter, A., Burrows, J.P. 2010, *"Comparison of satellite observed tropospheric NO2 over India with model simulations",* Atmos. Env., v.44, p. 3314-3321.

67. Sinha, H.S.S., Pandey, R.,and Misra, R.N., 2010, *"In situ measurement of nighttime plasma density irregularities over an equatorial station Trivandrum",* J. Geophys. Res., v. 115, p. A11308 (1-8).

68. Sharma, Som, Chandra, H., Vats, H.O., Pandya N. Y., and Rajmal Jain, 2010, *"Ionospheric Modulations due to Solar Flares over Ahmedabad",* Ind. J. Rad. Space Phy. v. 39, p. 296-301.

69. Sunder, Raman, R., and Ramachandran, S., 2011, *"Source apportionment of the ionic components in precipitation over an urban region in western India",* Environmental Science and Pollution Research, v. 18, p. 212-225.

70. Sunder Raman R., Ramachandran, S., and Rastogi, N., 2010, *"Source identification of ambient aerosols over an urban region in western India",* Journal of Environmental Monitoring, v. 12, p. 1330-1340.

Geo-Sciences

71. Kumar, A., Sarin, M.M., and Srinivas, B., 2010, *"Aerosol iron solubility over Bay of Bengal: Role of anthropogenic sources and chemical processing",* Marine Chemistry, v. 121, p.167-175.

72. Ram, Kirpa., Sarin, M.M., and Tripathi, S.N., 2010, *"Inter-comparison of thermal and optical methods for determination of atmospheric black carbon and attenuation coefficient from an urban location in northern India"*, Atmospheric Research, v. 97, p. 335-342.

73. Cherian, R., Venkataraman, C., Kumar, A., Sarin, M. M., Sudheer, A.K., and Ramachandran, S., 2010 *"Source identification of aerosols influencing atmospheric extinction: Integrating PMF and PSCF with emission inventories and satellite observations",* Jour. Geophy. Res-Atmospheres, v. 115, p. D22212.

74. Ram, Kirpa, Sarin, M.M., and Tripathi, S.N., 2010, *"A 1 year record of carbonaceous aerosols from an urban site in the Indo-Gangetic Plain (IGP): Characterization, sources and temporal variability",* Jour. Geophy. Res.–Atmospheres, v.115, p. D24313.

75. Ram, Kirpa, Sarin, M.M., and Hegde, P., 2010, *"Long-term record of aerosol optical properties and chemical composition from a high-altitude site (Manora Peak) in Central Himalaya. Atmos"*. Chemical Physics, v. 10, p. 11791-11803.

76. Ram, Kirpa, and Sarin, M.M., 2011, *"Day-night variability of EC, OC, WSOC and inorganic ions in urban environment of Indo-Gangetic Plain: Implications to secondary aerosol formation",* Atmospheric Environment, v. 45, p. 460-468.

77. Rengarajan, R., Sudheer, A.K., and Sarin, M.M., 2011, *"Aerosol acidity and secondary organic aerosol formation during wintertime over urban environment in western India",* Atmospheric Environment, v. 45, p. 1940-1945.

78. Singh, A., Jani, R.A., and Ramesh, R., 2010, *"Spatiotemporal variations of the $\delta^{18}O$-salinity relation in the northern Indian Ocean",* Deep-Sea Res., Part I, v.57, p.1422-1431.

79. Gandhi, N., Singh, A., Ramesh, R., and Sheshshayee, M.S., 2010, *"Nitrogen sources for new production in the NE Indian Ocean",* Advances in Geosciences, v.24, p.55-67.

80. Gandhi, N., Ramesh, R., Srivastava, R., Sheshshayee, M.S., Dwivedi R.M.,and Raman, M., 2010, *"Nitrogen uptake rates during spring in the north-eastern Arabian Sea"*, International Journal of Oceanography, v.2010, p.1-10.

81. Gandhi, N., 2010, *"Improving the estimation of new production using the ^{15}N tracer technique: a case*

study from the northern Indian Ocean", National Academy Science Letters, v.33, p. 335-339.

82. Gandhi, N., Ramesh, R., Prakash, S., and Kumar, S., 2011, *"Nitrogen sources for new production in the NE Arabian Sea",* Journal of Sea Research, v.65, p. 265-274.

83. Gandhi, N., Kumar, S., Ramesh, R., and Sheshshayee, M.S., 2011, *"Measurement of marine productivity using ^{15}N and ^{13}C tracers: some methodological aspects",* Journal of Earth System Science, v.120 , p.99-111.

84. Managave, S.R., Sheshshayee, M.S., Borgaonkar, H.P., and Ramesh, R., 2010, *"Intra-annual oxygen isotope variations in central Indian teak cellulose: possibility of improved resolution for past monsoon reconstruction",* Current Science, v.98, p. 930-937.

85. Managave, S.R., Sheshshayee, M.S., Ramesh, R., Borgaonkar, H.P., Shah S.K., and Bhattacharyya, A., 2011, *"Response of cellulose oxygen isotope values of teak trees in differing monsoon environments to monsoon rain fall",* Dendrochronologia, v. 29, p. 89-97.

86. Kumar, S., Ramesh, R., Dwivedi, R. M., Raman, M., Sheshshayee, M. S., and D'Souza, W., 2010, *"Nitrogen uptake in the northeastern Arabian Sea during winter cooling",* International Journal of Oceanography, Article ID 819029, p.1-10.

87. Laskar, A.H., Sharman, N., Ramesh, R., Jani, R.A., and Yadava, M. G., 2010, *"Paleoclimate and paleovegetation of Lower Narmada Basin, Gujarat, Western India, inferred from stable carbon and oxygen isotopes",* Quaternary International, v. 227, p. 183-189.

88. Prakash, S., Ramesh, R., Sheshshayee, M.S., Mohan, R., and Sudhakar, M., 2010, *"Effect of high level iron enrichment on potential nitrogen uptake by marine plankton in the Southern Ocean",* Current Science, v. 98, p.1400-1404.

89. Srivastava, R., Ramesh, R., Jani, R.A., Anilkumar, N., and Sudhakar, M. 2010, *"Stable oxygen, hydrogen isotope ratios and salinity variations of the surface Southern Indian Ocean waters",* Current Science, v. 98, p.1395-1399.

90. Managave, S.R., Sheshshayee, M.S., Bhattacharya, A., and Ramesh, R., 2011, "Intra-annual variations of teak cellulose $\delta^{18}O$ in Kerala, India: implications to the reconstruction of past summer and winter monsoon rains", Climate Dynamics, v.37, p. 555-567.

91. Ramesh, R., Tiwari, M., Chakraborty, S., Managave, S.R., Yadava M. G., and Sinha, D. K., 2010, *"Retrieval of south Asian monsoon variation during the Holocene from natural climate archives",* Current Science, v. 99, p.1770-1786.

92. Awasthi, N., Ray, J.S., Laskar, A.H., Kumar, A., Sudhakar, M., Bhutani, R., Sheth, H.C., and Yadava, M.G., 2010, *"Major ash eruptions of Barren Island Volcano (Andaman Sea) during the past 72 kyr: clues from a sediment core record",* Bulletin of Volcanology, v. 72, p.1131-1136.

93. Sheth, H.C., Ray, J.S., Kumar, A., Bhutani, R., and Awasthi, N., 2011, *"Toothpaste lava from the Barren Island volcano (Andaman Sea)",* Journal of Volcanology and Geothermal Research, v. 202, p.73-82.

94. Nagar, Y.C., Sastry, M. D., Bhushan, B., Kumar, A., Mishra, K. P., Shastri, A., Deo, M.N., Kocurek, G., Magee, J.W., Wadhawan, S.K., Julay, M., Pandian, M.S., Shukla, A.D., and Singhvi, A.K., 2010, *"Chronometry and formation pathways of gypsum using Electron Spin Resonance and Fourier Transform-Infrared Spectroscopy Quaternary Geochronology"*, v.5, p. 691-704.

95. Singhvi, A.K., Williams, M.A.J.,Rajaguru, S.N., Misra, V.N., Chawla, S., Stokes, S., Chauhan, N. Francis, T., Ganjoo R.K, and Humphreys, G.S., 2010, *"A ~200 ka record of climatic change and dune activity in the Thar Desert, India",* Quaternary Science Review, v. 29, p. 3095-3105.

96. Thakur, V.C.Pandey, A.K., Nautiyal, N.M., Sundriyal, Y.P., Khanduri, B.M. Shinde, D.P., Suresh, N., and Singhvi, A.K., 2010, *"Geo-archeology at Khajnawar in Western Uttar Pradesh plain: Suggestion for a historical earthquake and climate change",* Current Science, v.98, p. 1112-1117.

97. Kundu, H.K., Thakkar, M.G., Biswas, R.H. Singhvi, A.K., 2010*,"Optical dating of sediments in Kari river basin and slip rate along Katrol hill fault (KHF) Kachchh, India",* Geochronometria. v.37, p.21-28.

98. Biswas, R.H., Morthekai, P., Gartia, R.K., Chawla, S., and Singhvi, A.K., 2011, *"Thermoluminescence of Meteorite Interior: a possible tool for the stimation of cosmic ray exposure ages",* Earth and Planet. Sci. Lett. v.304, p.36-44.

99. Deshpande, R.D., Maurya, A.S., Kumar, B., Sarkar, A., and Gupta, S.K. 2010. *"Rain-Vapor Interaction and Vapor Source Identification using Stable Isotopes from Semi-Arid Western India".* Journal of Geophysical Research, v.115, p. D23311.

100. Maurya, A.S., Shah, Miral, Deshpande, R.D., Bhardwaj, R.M., Prasad, A. and Gupta, S.K., 2011, *"Hydrograph separation and precipitation source identification using stable water isotopes and conductivity: River Ganga at Himalayan foothills".* Hydrological Processes, V,25, p.1521-1530.

101. Juyal, N., Thakkar P.S., and Sundriyal Y.P., 2011, *"Geomorphic evidence of glaciations around Mount Kailash (Inner Kora): implication to past climate",* Current Science. v.100, p.535-541.

102. Juyal, N., Sundriyal, Y.P., Rana, N., Chaudhary, Shipra, and Singhvi A.K., 2010*, "Late Quaternary aggradation and incision in the monsoon-dominated Alaknanda valley, Central Himalaya, Uttrakhand, India",* Journal of Quaternary Science.v.25, p.1293-1304.

103. Das, S.K., Dobhal D.P., and Juyal N., 2010, *"Variability of aerosol optical depth and recent recessional trend in Dokriani Glacier, Bhagirathi Valley, Garhwal Himalaya",* Current Science, v.99, p.1816-1821.

104. Basavaiah, N., Apple, N.E., Lakshmi, B.V., Deenadayalan, K., Satayanarayana, K.V.V., Mishra, S., Juyal N., and Malik, M.A., 2011, Journal of Geophysical Research, v.115, p.1-17,

105. Juyal N., 2010, *"Cloud burst-triggered debris flows around Leh".* Current Science,v. 99, p.1166-1167.

106. Rahaman, W., and Singh, S. K. and Raghav, S., 2010, *"Dissolved Mo and U in rivers and estuaries of India: Implication to geochemistry of redox sensitive elements and their marine budgets",* Chemical Geology, v.278, p.160–172,

107. Rahaman, W., Singh, S.K., Sinha, R., Tandon, S.K., 2011*,"Sr, C and O isotopes in carbonate nodules from the Ganga Plain: Evidence for recent abrupt rise in dissolved $^{87}Sr/^{86}Sr$ ratios of the Ganga",* Chem. Geol., v.285. p.184-193.

108. Singh, S.P., Singh, S.K., Bhushan, R., 2011, *"Behaviour of dissolved redox sensitive elements (U,Mo and Re) in the water column of the Bay of Benga"I*, Marine Chemistry, v.126. p.76-88.

109. Tripathy, G. R., Singh, S. K., Bhushan, R. and Ramaswamy, V., 2011, *"Sr-Nd isotope composition of the Bay of Bengal Sediments: Impact of Climate on Erosion in the Himalaya",* Geochemical Journal v. 45, p.175-186.

Theoretical Physics

110. Sahoo, B.K., 2010, "*Accurate estimate of α variation and isotope shift parameters in Na and Mg^+ ",* J. Phys. B v. 43, p. 231001 (1-7) (Fast Track Communication).

111. Budker, D., Sahoo, B.K., Angom, D., and Das, B.P., 2010, *"An Overview of Some Experimental and Theoretical Aspects of Fundamental Symmetry Violations in Atoms",* Pramana v. 57, p. 1041-1056.

112. Sahoo, B.K., Mandal, P., and Mukherjee, M., 2011, *"Parity Nonconservation Studies in Odd-isotopes Single Trapped Atomic Ions",* Phys. Rev. A v. 83, p. 030502(R) (1-4).

113. Ka'llay, M., Nataraj, H.S., Sahoo, B.K., Das, B.P., and Visscher, L., 2011, *"Relativistic general- order coupled- cluster method for high-precision calculations: Application to the Al^+ atomic clock",* Phys. Rev. A v. 83, p. 030503 (R) (1-4).

114. Kumar, A., Vaity, P., and Singh, R.P., 2010, *"Diffraction characteristics of an optical vortex passing through an aperture-Iris Diaphragm",* Opt. Commun., v. 283, p. 41-45.

115. Kumar, A., Banerji, J., and Singh, R. P., 2010, *"Intensity correlation properties of high-order optical vortices passing through a rotating round-glass plate"*, Opt. Lett., v. 35, p. 3841-3843.

116. Jaiswal, V.K., Singh, R. P., and Simon, R., 2010, *"Producing optical vortices through forked holographic grating: study of polarization",* J. Mod. Opt., v. 57, p. 2031-2038.

117. Kumar, A., and Singh, R. P., 2011, *"Experimental and theoretical investigation of loss of coherence on scattering of a beam with helical wavefront",* Opt. Commun., v. 284, p. 1510-1516.

118. Kumar, A., Vaity, P., and Singh, R. P., 2011, *"Crafting the core asymmetry to lift the degeneracy of optical vortices",* Opt. Express, v. 19, p. 6182-6190.

119. Bandyopadhyay, A., and Singh, R. P., 2011, *"Wigner distribution of elliptical quantum optical vortex",* Opt. Commun., v. 284, p. 256- 261.

120. Patra, S., Sarkar, A., and Sarkar, U., 2010, *"Spontaneous Left-Right Symmetry Breaking in Supersymmetric Models with only Higgs Doublets",* Phys. Rev. D, v. 82 p. 015010 (1-9).

121. Gu, P., Ma, E., and Sarkar, U., 2010, *"Pseudo-Majoron as Dark Matter"*, Phys. Lett. B v. 690, p.145-148.

122. Gu. P., and Sarkar, U., 2010, *"Leptogenesis with Linear, Inverse or Double Seesaw"*, Phys. Lett. B, v. 694, p.226-232.

123. Gu, P., and Sarkar, U., 2011, *"Leptogenesis Bound on Spontaneous Symmetry Breaking of Global Lepton Number",* Eur. Phys. Jour. C v. 71, p. 1560 (1-4).

124. Borah, D., Patra, S., and Sarkar, U., 2011, *"TeV scale Left Right Symmetry with spontaneous D-parity breaking",* Phys. Rev. D 83 (2011) 035007 [13 pages]

125. Gu, P., Lindner, M., Sarkar, U., and Zhang, X., 2011, *"Weakly Interacting Dark Matter and Baryogenesis"*, Phys. Rev. D v. 83 p. 055008 (1-6).

126. Vyas, M. and Kota, V.K.B., 2010, *"Random matrix structure of nuclear shell model Hamiltonian matrices and comparison with an atomic example",* Eur. Phys. J. A- Hadrons and Nuclei, v. 45, p. 111-120.

127. Vyas, M., and Kota, V.K.B., 2010, *"Spectral Properties of Embedded Gaussia Unitary Ensemble of Random Matrices with Wigner's SU(4) Symmetry",* Ann. Phys. (N.Y.), v. 325, p.2451-2485.

128. Castilho Alcarás, J.A., and Kota, V.K.B., 2010, *"On the calculation of inner products of Schur functions"* Brazilian J. of Phys., v.40, p.172-179.

129. Srivastava, P.C., and Mehrotra, I., 2010, *"Large scale shell model calculations for odd-odd $^{58-62}$Mn isotopes",* Eur. Phys. J. A- Hadrons and Nuclei, v. 45, p.185-192.

130. Jha, T.K., Mishra, H., and Sreekanth, V., 2010, *"Bulk viscosity in hyperonic star and r-mode instability"* Phys. Rev. C v. 82, p. 025803 (1-9).

131. Bhatt, J., Mishra, H., and Sreekanth, V., 2011, *"Thermal photons in QGP and non-ideal effects",* JHEP v. 1011, p.106 (1-22).

132. Mahajan, N. and Rangarajan, R., 2011, *"Remarks on non-gaussian fluctuations of the inflaton and constancy of zeta outside the horizon",* Phys. Rev. D, v. 83, p. 043510 (1-8).

133. Singh, N., 2010, *"Quantum transport in mesoscopic systems: Coulomb Blockade and Kondo effect",* Resonance - J. Sci. Edu., v. 15, p. 988.

134. Godbole, R.M., Rao, K., Rindani, S.D., and Singh, R.K., 2010, *"On measurement of top polarization as a probe of top-antitop production mechanisms at the LHC"*, JHEP v. 11, 144, p. 1-27.

135. Rindani, S.D., and Sharma, P, 2010, *"Decay-lepton correlations as probes of anomalous ZZH and $_{\gamma}$ZH interactions in $e^+e^- \rightarrow ZH$ with polarized beams",* Phys. Lett. B v. 693, p. 134-139.

136. Ananthanarayan, B., Patra, M., and Rindani, S.D. 2011, *"Top-spin analysis of new scalar and tensor interactions in e^+e^- collisions with beam polarization''*, Phys. Rev. D v. 83, p. 016010 (1-13).

137. Gautam, S., Muruganandam, P., and Angom, A., 2011, *"Position swapping and pinching in Bose-Fermi mixtures with two-color optical Feshbach resonances",* Phys. Rev. A, v. 83, p. 023605 (1-7).

138. Gautam, S., and Angom, D., 2011, *"Phase separation of binary condensates in harmonic and lattice potentials",* J. Phys. B, v. 44, p. 025302 (1-11).

139. Mani, B. K., and Angom, D., 2011, *"Fock-space relativistic coupled-cluster calculations of two-valence atoms",* Phys. Rev. A, v. 83, p. 012501 (1-21).

140. Gautam, S., and Angom, D., 2010, *"Rayleigh-Taylor instability in binary condensates",* Phys. Rev. A, v. 81, p. 053616 (1-5).

141. Mani, B. K., and Angom, D., 2010, *"Atomic properties calculated by relativistic coupled-cluster Mg^+, Ca^+, Sr^+, and Ba^+",* Phys. Rev. A, v. 81, p. 042514 (1-11).

142. Gautam, S., and Angom, D., 2010, *"Ground state geometry of binary condensates in axisymmetric traps",* J. Phys. B., v. 43, p. 095302 (1-7).

143. Azam, M., Bhatt, J., and Sarkar, U., 2011, *"Experimental signatures of cosmological neutrino condensation",* Phys. Lett. B v. 697 p. 7-10.

144. Konar, P. K., Matchev, K., Park M., and Sarangi, G., 2010, *"How to look for super symmetry under the LHC lamppost",* Phys. Rev. Lett. v. 105. p. 221801 (1-4).

145. Chakraborty, S., Choubey, S., Goswami, S., and Kar, K., 2010, *"Collective Flavor Oscillations Of Supernova Neutrinos and r-Process Nucleosynthesis",* J. Astroparticle Phys. and Cosmology, v. 1006, p.1-24.

146. Dighe, A., Goswami, S., and Ray, S., 2010, *"2540 km: Bimagic baseline for neutrino oscillation parameters",* Phys. Rev. Lett. v. 105, p. 261802 (1-4).

147. Das, S., and Mohanty, S., 2011, *"Very special relativity is incompatible with Thomas precession",* Mod. Phys. Lett. A v. 26, p. 139-150.

148. Esteves, J.N., Joachim, F.R., Joshipura, A.S., Romao, J.C., Tortola, M.A., and Valle, J.W.F., 2010, *"A_4-based neutrino masses with Majoron decaying dark matter",* Phys. Rev. D v. 82, p. 073008 (1-8).

149. Joshipura, A.S., and Patel, K.M., 2010, *"Quasi-degenerate neutrinos and SO (10)",* Phys. Rev. D v. 82, p. 31701 (1-5).

150. Joshipura, A.S., and Kodrani, B.P., 2010, *"Fermion number conservation and two Higgs doublet models without tree level flavour changing neutral currents",* Phys. Rev. D., v. 82, p. 115013 (1-7).

151. Joshipura, A.S., Patel, K.M., and Vempati, S.K., 2010, *"Type I seesaw mechanism for quasi degenerate neutrinos",* Phys. Lett. B v. 690, p. 289-295.

152. Samanta, G.K., Kumar, S.C., Devi, K., and Ebrahim-Zadeh M., 2010, *"Multicrystal, continuous-wave, single-pass second-harmonic generation with 56% efficiency",* Opt. Lett., v. 35, p. 3513-3515.

153. Kumar, S.C., Das, R., Samanta, G.K., and Ebrahim-Zadeh M., 2011, *"Optimally-output-coupled, 17.5 W, fiber-laser-pumped continuous-wave optical parametric oscillator",* Appl. Phys. B, v. 102, p. 31-35.

154. Kumar, S.C., Devi, K., Samanta, G.K., and Ebrahim-Zadeh M., 2011, *"Fiber laser based green pumped continuous-wave, singly resonant optical parametric oscillator",* Laser Phys., v. 21, p. 782–789.

155. Patel, K. M., 2011, "An SO(10)XS4XZn model of Quark-Lepton Complementarity, Phys. Lett., v. B695, p. 225-230.

156. Resmi, V., Ambika, G., and Amritkar, R.E., 2010, *"Synchronized states in chaotic systems coupled indirectly through a dynamic environment"* Physical Review E, v. 81, p. 046216 (1-7).

157. Harikrishnan, K.P., Misra, R., Ambika, G., and Amritkar R. E., 2010,*"Parametric characterization of a chaotic attractor using the two scale Cantor measure"* Physica D, v. 239, p. 420-42.

Library & Information Services

158. Alam, M.N. and Pandey, P., 2010, *"SpaceCat: an online union catalogue for space science serials in India",* Interlending & Document Supply, v. 38, p. 200–209.

159. Alam, M.N. and Pandey, P., 2010*,"Design and Development of Prototype Astronomical Digital Image Library using Greenstone Digital Library Software"*, DESIDOC Journal of Library & Information Technology, v. 30, p. 25-30.

Publications in Proceedings of Symposia

Astronomy and Astrophysics

1. Ashish Raj, Ashok, N.M., Banerjee, D.P.K., and Munari, U., "*Detection of first overtone emission bands of CO in Nova V496 Sct* ", 29th Astronomical Society of India Meeting, Raipur University, Raipur, February 21-23, 2011.

2. Joshi, U. C., Fan, J. H., Ganesh, S., Baliyan, K. S., 2010, "*Study of polarization in Oj287*", IAUS 267, p. 111.

3. Terada, Y., Harayama, A., et al. (including Sachindra Naik), 2010, "*Systematic surveys of the non thermal emission from white dwarfs with Suzaku and INTEGRAL*", AIP Conference Proceedings, v.1248, p. 215-216.

4. Paul, B., Devasia, J., Maitra, C., James, M., Naik, Sachindra, Indulekha, K. 2010, "*Intensity and energy dependent profiles of transient HMXB pulsars GRO J1008-57, 1A 1118-61 and GX 304-1",* The First Year of MAXI Conference Proceedings, id. 17.

5. Kumar, M. S. N., Grave, J. M. C., and Dewangan, L. K., 2010, "*Massive star-formation studies with GLIMPSE*", A Multi-wavelength Perspective ASI Conference Series, v. 1, p. 147-153.

6. Bisoi, Susanta, K., "*Deep GMRT 150 MHz observations of the DEEP2 fields: Searching for high red-shift radio galaxies revisited*", 29th ASI Scientific meeting, Raipur, February 23-25, 2011.

7. Bisoi, Susanta, K., 2011, "*Solar Polar Fields During Cycles 21-23: Correlation with Meridional Flows*", 1st Asia-Pacific Solar Physics Meeting, March 21-24, Indian Institute of Astrophysics, Bangalore.

8. Bisoi, Susanta, K., 2011, *"Deep GMRT 150 MHz observations of the DEEP2 fields: Searching for high red-shift radio galaxies revisited"*, Poster presentation at Diffuse Relativistic Plasma Workshop, RRI, Bangalore.

9. Vats, H.O.*"Solar Rotation"*, 25th Annual IAPT convention and symposium of Atronomy, Astrophysics and Space Science, October 21-23, 2010, Saurastra University, Rajkot.

10. Vats, H.O., "*Overview of collaborative solar research programs"*, Recent trends in astronomy and space

science, October 29, 2010, Saurastra University, Rajkot.

11. Vats, H.O., 2011, *"Measurements of solar rotation from the near Earth observations of the interplanetary magnetic field (IMF)"*, National Conference on Recent Trends in Theoretical and Experimental Physics (NCRTTEP-2011) February 18-19, VP & RTP science college Vallabh Vidyanagar .

12. Jain, R., 2010, "*Energy-dependent timing of thermal emission in solar flares"*, Scientific Assembly of COSPAR, July 18-25, Breman, Germany.

13. Jain, R., 2010 "*X-ray Diagnostics of Fe and Fe/Ni line Features seen during Solar Flares",* International Workshop on '*Solar Plasma Spectroscopy: Achievements and Future Challenges'*, 13-15 September , DAMTP, University of Cambridge, UK.

14. Awasthi, Arun, 2010, *"X-Ray Plasma diagnostics of precursor phase in Solar flares"*, National Level Seminar on '*Solar Activity & Cosmic Ray Modulation'*, 09-10 October, Satna, Madhya Pradesh.

15. Awasthi, Arun, 2011, "*Multi-wavelength study of precursor phase emission in Solar flares".* 1st Asia Pacific Solar Physics Meeting, 21-24 March, IIA, Bangalore.

16. Jain, R., 2011, "*Plasma and Current Experiment*", Brainstorming session on "*Mars Science and Exploration",* 24-25 March, PRL, Ahmedabad.

Solar Physics

17. Denis, S., Coucke, P., Gabriel, E., Delrez, C., and Venkatakrishnan, P., 2010, *"Multi-Application Solar Telescope: Assembly, Integration, And Testing"* in Ground-based and Airborne Telescopes III. Edited by Stepp, Larry M. Gilmozzi, Roberto, and Hall, Helen J. Proceedings of the SPIE, v. 7733, p. 773335-1.

18. Kumar, B., Mathur, S., Garcia, R.A., and Venkatakrishnan, P., 2010, *"Can major flares excitehigh-frequency global waves in the Sun?"*, in the Proceedings of Fourth HELAS International Conference on Seismological challenges for stellar structure, Eds. S. Jimenez Reyes, P. Palle, and T. Roca Cortes, Astronomical Notes, v. 331, No. 9-10, p. P03

19. Kumar, B., Venkatakrishnan, P., Mathur, S., Tiwari, S.K., and Garcia, R.A., 2011, *"Analysis of peculiar penumbral flows observed in the active region NOAA 10930 during a major solar flare"*, in the Proceedings of GONG2010/SOHO24 International Conference on A new era of seismology of the Sun and solar-like stars, Eds. T. Appourchaux, A. Baglin, W. Chaplin, J. C-Dalsgaard, L. Gizon, M. Thompson, T. Sekii, and J. Leibacher, Journal of Physics: Conference Series, v. 271, Issue 1, p. 012020.

20. Maurya, R. A., Ambastha, A, and Reddy, V., 2010, *"Kinetic and Magnetic Helicities in Solar Active Regions",* in the Proceedings of GONG2010/SOHO24 International Conference on A new era of seismology of the Sun and solar-like stars, Eds. T. Appourchaux, A. Baglin, W. Chaplin, J. C-Dalsgaard, L. Gizon, M. Thompson, T. Sekii, and J. Leibacher, Journal of Physics: Conference Series, v. 271, p. 1- 6.

Planetary Sciences and PLANEX Program

21. Acharya, Y.B., 2010, "*X-ray Sensors for Earth Observation, Signatures"*, Newsletter of the Indian Society of Remote Sensing –Ahmedabad Chapter, V. 22, No.3, P 44-48, Aug-Oct.

22. Arivazhagan, S., Anbazhagan, S., 2011, "*Comparison of Lunar analog rock spectra with Clementine data"*, 42nd Lunar and Planetary Science Conference, Houston, Texas, USA, #1009.

23. Chauhan, P., Kaur, P., Srivastava, N., Bhattacharya, S., Lal D., Ajai and Kiran, A.S., 2011, "*Studies of lunar dark halo craters in north western mare Nectaris using high resolution Chandrayaan-1 data"*, 42nd Lunar and Planetary Science Conference, Houston, Texas, USA, #1338.

24. Chauhan, P., Srivastava, N., Kaur, P., Bhattacharya, S., Ajai, Kiran Kumar, A.S., Goswami, J.N. and Navalgund, R.R., 2011,"*Evidences of multiphase modification over the central peak of Tycho crater on Moon from high resolution remote sensing data",* 42nd Lunar and Planetary Science Conference, Texas, USA, #1341.

25. Goswami, J. N. and Annadurai, M.2011, "*Chandrayaan-2 mission*" 42nd Lunar and Planetary Science Conference, Texas,USA, #2042.

26. Shanmugam M., Acharya, Y.B., Goyal, S.K. and Murty, S.V.S., 2011, "*Alpha particle X-ray spectometer (APXS) on-board chandrayaan-2 rover*", 42nd Lunar and Planetary Science Conference, Houston, Texas, USA #1232.

Space and Atmospheric Sciences

27. Gupta, S.P., 2010, *"Balloon and rocket borne sensors to measure electrical parameters in atmosphere/ ionosphere",* Proceedings of SERC School on electrodynamical coupling of atmospheric region, IIG, Nav Mumbai,p .406-426.

28. Sekar, R., Acharya, Y.B., Chakrabarty, D., Pallamraju, D. Gupta, S. P., and Pathan, B. M., 2011, "*Investigations on the effects of annular solar eclipse in the equatorial ionosphere",* Proceedings of the National Workshop: Results on Solar Eclipse (NaWRoSE), SPL, VSSC, January 27-28, p59.

Geo-Sciences

29. Juyal, N.,2011, Quaternary glaciation in Indian Himalaya. In "*Report of the Study group on Himalayan glacier"* Chapter-2, pp 1-23, Prepared by the Study Group on Himalayan Glaciers for the Office of the Principle Scientific Advisor to the Government of India (PSA/2011/2), March.

30. Ramesh, R., Singh, A., and Gandhi, N., 2010, *"Applications of stable isotopes in oceanography",* International Conference organized by National Association for Applications of Radioisotopes and Radiation in Industry (NAARRI), Mumbai on '*Isotope Technologies and Applications - New Horizons'* during December 13-15.

31. Ramesh, R., Srivastava, R., and Sudhakar, M., 2011, "*Stable isotopes and salinity variation in the southern Indian Ocean*", Proceedings of the Conference on Science and Geopolitics of Arctic & Antarctic, New Delhi, during January 14-15.

32. Goswami, Vineet, Singh, Sunil, K. and Bhushan, Ravi, 2010, *"Impact of OMZ on the distribution of redox sensitive trace elements in the Arabian Sea",* AOGS.

33. Singh, Satinder, Pal, Singh, Sunil, K. and Bhushan, Ravi, 2010, "Distribution of Redox Sensitive Elements (U, Mo, Re) in Bay of Bengal", AOGS.

34. Bhushan, Ravi, and Dutta, Koushik, 2010 "Radiocarbon in the Northern Indian Ocean", AOGS.

35. Bhushan, Ravi,2010, GEOTRACES–"*Indian Ocean Perspective"*, Invited talk given at Workshop on Advances in Science of Climate Change and Indian Monsoon held at Indian Institute of Tropical Meteorology, Pune,31 August – 01 September.

36. Rengarajan, R., Sudheer, A. K., and Singh, S. K.,2010, "Strontium isotope composition of mineral dust over a semi-arid location in western India", Implication to the provenance, AOGS 2010 Conference, Hyderabad, 5-9 July.

37. Rengarajan, R., Soares Melena and Michiel Rutgers Van der Loeff, 2010, *"Ocean Iron Fertilisation: ^{234}Th as tracer of export production of POC",* AOGS 2010 Conference, Hyderabad, 5-9 July.

38. Bikkina, Srinivas, Sarin,M.M., Kumar, A., and Rengarajan, R., 2010, *"Atmospheric dry deposition of N, P and Fe to the Bay of Bengal",* AOGS 2010 Conference, Hyderabad, 5-9 July.

39. Kumar, A., Sarin, M.M., Sudheer, A.K., and Rengarajan, R., 2010, *"Spatio-temporal variability of atmospheric NH_4^+, NO_3^- and SO_4^{2-} concentrations over Indian region",* 11th International Global Atmospheric Chemistry Conference,Halifax, Canada, 11-16 July.

40. Martin, P.M. Rutgers van der Loeff, P. Vandromme, N. Cassar, F. Ebersbach, M. Iversen, R. Rengarajan, M. Soares, H. González, Richard Lampitt, Richard Sanders, V. Smetacek, W. Naqvi, 2010, *"Particle export during the Lohafex iron fertilization experiment",* In: Biennial Challenger 2010 Conference, Southampton, U.K., 6-9 September.

41. Martin, P., M. Rutgers van der Loeff, P. Vandromme, N. Cassar, F. Ebersbach, M. Iversen, R. Rengarajan, M. Soares, H. González, Richard Lampitt, Richard Sanders, V. Smetacek, W. Naqvi, 2010, *"Combining water column data with sediment trap and satellite observations for improved marine carbon export estimates. In: COCOS (Coordination action Carbon Observing System)",* Bergen, Norway, 23-26 June .

42. Gustafsson, O., Martin, Kruså, Rebecca, Sheesley, P.S., Praveen, P.S.P., Rao, P.D., Safai, K. Budhavant, R. Rengarajan, A.K., Sudheer, and M.M. Sarin, 2010, *"Radiocarbon source apportionment of carbonaceous aerosol components of South Asian Atmospheric Brown Clouds"*, EGU General Assembly, Vienna, Austria, 2 – 7 May.

43. Bluszcz, A., Li, S.H., and Singhvi, A.K., (Eds).2010, Proceedings of the Second Asia Pacific Luminescence and Electron Spin Resonance Conference, Ahmedabad, India - Part - I, Versita press, Warsaw, Poland, p. 71

44. Deshpande, R.D., and Gupta, S.K.,2010. *"Groundwater dating using ^{14}C, ^{4}He and $^{4}He/^{222}Rn$ methods –A case study of the North Gujarat Cambay Region, India".* Proceedings of Workshop on Radon Contamination in groundwater and application of isotopes in groundwater studies, Central Ground Water Board, Bengaluru, India, p. 103-110.

45. Rahaman, W., and Singh, S. K., 2010, *"Mo in estuaries: Impact on global oceanic budget of Mo AOGS2010",* Hyderabad, July 5-9, 2010.

46. Chatterjee, J. and Singh, S.K., 2010, *"Chemical and Isotope Composition of Saline/alkaline Soils in the Ganga Plain and Impact of Their Dissolution on River Chemistry AOGS2010",* Hyderabad, July 5-9, 2010.

47. Goswami, V., Singh, S. K. and Bhushan, R., 2010, *"Isotopic Composition of Dissolved Nd in the Arabian Sea: Tracing the water masses, Symposium on Indian Ocean Marine Living Resources",* Cochin, December 2-3.

Theoretical Physics

48. Budker, D., Sahoo, B. K., Angom, D., and Das, B. P., 2010, "*An overview of some experimental and theoretical aspects of fundamental symmetry violations in atoms"* in Proceedings of IXth National Laser Symposium, Part II: Laser Applications, Eds : L. M. Gantayet, et al., Pramana, v. 75, p. 1041-56.

49. Kumar, A., Vaity, P., and Singh, R. P., 2010, "*Decay of high order elliptical optical vortices",* National Laser Symposium-19, Dec 1-4, RRCAT Indore, India, p. 3153 (1-4).

50. Kumar, A., Vaity, P., Prabhakar, S., and Singh, R. P., 2010, *"Decoherence of optical vortices in scattering"*, Photonics-2010, Dec 12-15, IIT Guwahati, India, p. 555.

51. Jaiswal, V. K., Vaity, P., Diktiya, A., Singh, R. P., and Kandpal, H. C., 2010, "*Spatial distribution of polarization in phase singular optical beams"*, Photonics-2010, Dec 12-15, Guwahati, India, p. 554.

52. Kumar, A., Prabhakar, S., Vaity, P., and Singh, R. P.2010, "*Two point correlation function for optical vortices"*, Photonics-2010, Dec 12-15, Guwahati, India, p. 556 (1-3).

53. Vaity, P., Kumar, A., Prabhakar, S., and Singh, R. P., 2010, "*2-D Airy beam propagation through photorefractive materials",* Photonics-2010, Dec 12-15, Guwahati, India, p. 523 (1-2).

54. Kumar, A., Vaity, P., and Singh, R. P., 2011, "*Degeneracy of optical vortices and the core asymmetry",* XXXV Optical Society of India Symposium- International Conference on Contemporary Trends in Optics and Optoelectronics, Jan 17-19, IIST Thiruvananthapuram, India, p. 342-343.

55. Singh, R. P., Kumar, A., Vaity, P., and Prabhakar, S., 2011,"*Dynamic light scattering of optical vortices",* XXXV OSI Symposium- International Conference on Contemporary Trends in Optics and Optoelectronics, Jan 17-19, IIST Thiruvananthapuram, India, p. 37-38.

56. Vaity, P., Kumar, A., Prabhakar, S., and Singh, R. P., 2011, "*Airy beams interaction through photo-refractive material in presence of an applied electric field*", XXXV Optical Society of India Symposium-International Conference on Contemporary Trends in Optics and Optoelectronics, Jan 17-19, IIST Thiruvananthapuram, India, p. 315-316.

57. Rangarajan, R., 2010, *"Gravitino Production during Reheating and Implications for Leptogenesis",* Proceedings of the XVIII DAE-BRNS High Energy Physics Symposium at Banaras Hindu University, Varanasi.Symposium-19, Dec 1-4, RRCAT Indore, India, p. 3153 (1-4).

58. Mishra, H., Puri, S., and Singh, A., 2010, *"Kinetics of chiral phase transitions in quark matter",* in *"Gribov-80 Memorial Volume, Quantum Chromodynamics and beyond"*, World Scientic, World Scientific , Singapore, proceedings of Gribov -80 meeting, ICTP 26-28 May , Trieste, Italy, p-527-540.

59. Chatterjee, B., Mishra, H., Mishra, A. 2010, "Chiral symmety breaking in 3-flavor Nambu-Jona Lasinio model in magnetic background", Proceedings of International conference on Physics and Astrophysics of Quark Gluon Plasma, Goa, India, Dec. 6-10.

Library & Information Services

60. Nishtha, A., 2010, "*Scientometric study of doctoral theses of Physical Research Laboratory"* Proceeding of International conference Library & Information Services in Astronomy VI (LISA VI): 21st Century Astronomy Librarianship organized by IUCAA, Pune ASP Conference Series, v. 433, p 102-108.

Books Edited/Review Articles

Books Edited

1. Desai J.N., Ashok N.M., Kamble V.B. and Pandya P.S., 2010, "*Evolution of Our Understanding of Planetary Motions*", Vigyan Prasar, Department of Science and Technology, Government of India.

2. Kota, V.K.B. and Pratap, A. (eds.) 2010, "*New Frontiers in Nuclear, Hadron and Mesoscopic Physics*", Allied Publishers Pvt. Limited, New Delhi.

3. Kota, V.K.B., and Haq, R.U. (eds.) 2010, "*Spectral Distributions in Nuclei and Statistical Spectroscopy*", World Scientific, Singapore.

Review Articles

1. R. Sekar, and D. Chakrabarty, 2011, "*Aeronomy of the Earth's Atmosphere and Ionosphere*", IAGA Special Sopron Book Series, Edited by M. A. Abdu, Dora Pancheva and Archana Bhattacharyya, 2011, v. 2, Part 3, 251-268.

2. Sheel Varun, S.A. Haider, V.Singh, W.C.Maguire and G.J.Molina-Cuberos, 2010, "*Zonal Variability of Neutral Density, Temperature and Ion Production Rates in the Martian troposphere",* in Advances in Geosciences, Eds. Anil Bhardwaj et al., v. 19, p. 225-235, World Scientific, Singapore.

3. Ramesh, R., Tiwari, M., Chakraborty, S., Managave, S.R., Yadava, M.G. and Sinha, D.K., 2010, "*Retrieval of south Asian monsoon variation during the Holocene from natural climate archives*", Current Science, v. 99 (12), p.1770-1786.

4. Gandhi, N., Prakash, S., Ramesh, R., and Kumar, S., 2010, "*Nitrogen uptake rates and new production in the Indian Ocean*", Ind. J. Mar. Sci., v. 39(3), p.362-368.

5. Sudhakar, M., Ramesh, R., and R. Ravindra, 2010, "*Indian Multidisciplinary Expeditions to the Southern Ocean*" Special Section in Current Science, v. 99 (10), p.1378-1424.

6. Rengarajan, R., Srinivas Bikkina and Sarin, M.M., 2010, *"Atmospheric deposition of Reactive Nitrogen over continental sites and oceanic regions of India"* A review in ING Bulletins on Regional Assessment of Reactive Nitrogen, Bulletin No. 4 Ed. Himanshu Pathak, SCON-ING, New Delhi, ppi-vi & 1-12.

7. Gómez, J.M.G., Kar, K., Kota, V.K.B., Molina, R.A., Relaño, A., and Retamosa, J., 2011, "*Many-Body Quantum Chaos: Recent Developments and Applications to Nuclei*", Physics Reports v. 499, p.103-226.

Other Publications

PRL Technical Reports

1. Rajesh T. A.*"Microcontroller based 1-Wire temperature sensor network"*, PRL-TN-2011-100, Physical Research Laboratory, Ahmedabad, December, 2010.

2. Shah P. and Pallamraju, D., *Real-Time automated software for operation of multiple CCD cameras and interfacing with the balloon telemetry"*, PRL Technical Note, March, 2011.

Publications for Education

1. Srivastava , N. and Venkatakrishnan, P.,"*Multi-Application Solar Telescope (MAST) for the Udaipur Solar Observatory"*, PRL news, July, 2010.

2. Vats, H.O., Translation of space science and astronomy comic books in Hindi: Following books were translated in Hindi:

    1. What are cosmic rays?
    2. What is the solar wind?
    3. What is the ozone hole?
    4. What are the Polar Regions?
    5. What is the Aurora?
    6. What is the upper atmosphere?
    7. What is the geomagnetic field?
    8. What is the Global warming?

    These are printed by Space Science Office, DOS, Bangalore and are distributed to libraries of schools, colleges, universities and institutes.

Other Publications

1. Prasad Durga K. and Srivastava, N. "*The thirst for Water on Moon"*, PLANEX NEWS LETTER, v.1, Issue 1, p. 6-8, January, 2011.

2. Kadlag Y. U. "*Origin and evolution of solar system"*, PLANEX NEWS LETTER, v.1, Issue 1,p.4-5, January, 2011.

3. Sarkar U., "*Flavors of Research In Physics"* , INSA-Ahmedabad local Chapter (for Gujarat and Rajasthan), 2010.

4. Shyam Lal, "*Physics of Climate Change*", in: Flavours of Research in Physics (ed. U. Sarkar), Indian National Science academy, New Delhi, p.101-112, 2010.

5. Ramesh, R. "*Dating of dinosaurs to meteorites*", in: Flavours of Research in Physics (ed. U. Sarkar), Indian National Science academy, New Delhi, p.137-144, 2010.

6. Sheth, H. C., Ray, J. S., Senthil Kumar, P., Duraiswami, R. A., Chatterjee, R. N., and Gurav, T., *"Recycling of flow-top breccia crusts into molten interiors of flood basalt lava flows: Field and geochemical evidence from the Deccan Traps, in Topics in Igneous Petrology (Eds: J. Ray et al.)"*, Springer- Berlin, Chapter 8, p. 161-180, 2011.

Facilities and Services

Activities on the promotion of National Language

As a part of implementation and progressive use of Hindi in PRL, the Hindi Pakhwada was celebrated at PRL from September 14 - 28, 2010. The highlights of the celebrations included word quiz, essay, elocution, Hamara Karya, self written poetry competitions.

A Technical Seminar in Hindi on Global perspective of Scientific/Technical programme in PRL was held at PRL on 18 March, 2011.Thirty members presented their papers in this Seminar.

Vishwa Hindi Divas was organised in PRL on 10.1.2011 and an essay competition was held on Importance of yoga in our lives.

Shri R.S. Gupta, Hindi Officer-II & OSD delivered lectures in Hindi at workshops held by various Departments like Space Applications Centre, Airport Authority, Food Corporation of India, Income Tax, Doordarshan on different topics including Various applications of computers in Hindi.

Computer Centre

To cater to the High Performance Computing needs of our scientists, Computer Centre is equipped with High Performance Compute Cluster having 20 compute nodes, 1 master node with 64GB RAM on each node, 10TB storage capacity having 3.2 TF peak computing performance and 2.2 TF sustained computing performance. The HPC cluster has a Backup node, I/O node, Management node, Storage node, and a Visualization node. The HPC facility is homed in a special chamber that is maintained at controlled temperature and humidity and has a dual UPS system for round the clock operation. The primary network of HPC is with Infiniband and secondary network is Gigabit. Computer Center has Dell server having 16 AMD processors, 64GB RAM with 4TB disk capacity. Centre also has four HP servers, each having four AMD processors, 4 GB RAM, 1.5 TB disk spaces providing computing power with large disk storage. Computer centre has also IBM Power5 4 CPU based server providing additional computing power. The Internet connectivity is 10Mbps through BSNL Optical Fiber Cable. Local Area network at main campus is upgraded providing 10Gbps backbone between Computer Centre and Multi storied building and replacing all active components to provide 1Gbps bandwidth at desktop level. All the computing machines are connected to our high-speed local area network (LAN) to provide easy, fast and reliable access to more than 300 PC's and a few workstations distributed throughout all the campuses of our laboratory. PRL dispensary in the colony campus opposite IIM is now connected to the Main Campus over a 1Gbps Optical Fiber link. Through this link, the PRL Medical Officers access the Dispensary database housed in the CoWAA cell in computer center. Through the same Optical Fiber link, the

students and PDFs have a round the clock access to PRL LAN/Internet from their rooms via a few Wi-Fi devices installed in the buildings. Students from Thaltej Hostel also can access Computing services and Internet through Wi-Fi devices. The connectivity between Udaipur Solar Observatory (USO) and PRL Main Campus is 2 Mbps through BSNL – MLLN (Managed Leased Line Network). Mt.Abu is also connected to PRL main campus over 2 Mbps MLLN link provided by BSNL. Our Thaltej Campus is connected over a Optical Fiber providing 34 Mbps bandwidth through BSNL link. Thus, round the clock connectivity has been provided to users from Thaltej, USO, and Mt. Abu. Our main campus is also connected to Thaltej via BSNL's 2 Mbps MLLN for voice communication providing intercom telephone facility between the campuses. The Centre provides centralized virus free E-mails by automatically scanning all incoming E-mails. Anti-Spam filter has been centrally installed to fight the Spam mails. The center also provides web enabled email service. Internet authorizations, monitoring and reporting functions have been added to have optimal usage of Internet bandwidth.

To cater to the High end computing needs, PRL has become resource partner of C-DAC's Grid Garuda Project. The Grid Garuda network is integrated to PRL LAN providing seamless access of Garuda resources to PRL scientists.

PRL SPACENET connectivity for Data, Intranet, and video conferencing has been established at Main Campus, USO and IR Observatory over IP to interact with ISRO centers.

Mathematical, numerical and visualization application software like IMSL, IDL, Mathematica, SigmaPlot, MATLAB, Lahey FORTARN 95, and Data Explorer etc. have also been installed to cater the needs of the scientific community.

Library & Information Services

Library always strives to act as a facilitator in the research carried out in the laboratory by making available latest resources in different subject areas. As a part of fulfilling this objective, PRL Library subscribes to full-text databases like Science Direct, IOP Archive, PROLA, GSA Archive, SPIE Digital Library. This year Science Archive (access from 1880) and Nature archive (access from 1987) have been added to the digital collection of the library. As no library can be completely self-sufficient, it also provides document delivery service through ILL. The Library also assists the students in procuring the book-grant books. A book exhibition was organized by the Library in the month of July 2010.

In all, 376 books (scientific and general), 89 hindi books and 103 CDs/DVDs were added in the Main, Thaltej and USO libraries during 2010-11. During this period, number of visitors, visiting the library was 2432 and number of documents issued was 5349. The number of ILL requests for articles from other institutes fulfilled by PRL Library was 260 and that of requests of PRL staff fulfilled by other libraries was 215. Number of photocopies made, in house were 50191 and by outside agency were 78172.

The library homepage acts like a window through which it is possible to access the digital content subscribed by PRL as well as open access content. It gives link to 150 online journals out of the 158 journals subscribed by the library. It also provides access to the institutional repository consisting of journal articles published by the PRL authors from 1995 to present using the Greenstone Digital Library Software (GSDL software). This year photographs have also been added to the institutional repository so as to preserve and retrieve them quickly.

Workshop

PRL Workshop provides support to scientists and engineers, in designing, developing and manufacturing precise mechanical components and systems for different scientific experiments. Workshop has most of the manufacturing and measuring equipments to carry out precision work carried out by the user. It has wide range of machines such as metal cutting machines, welding machines and CNC Lathe Machine in machine shop. The workshop also carries out sheet and structural metal fabrication jobs. The high vacuum welding joints are also carried out by using TIG welding machine. Various high precision jobs including optical component adapters and mounts are being fabricated at the workshop.

Some of the major works carried out during the year are listed below

(1) A LED holder for Luminescence measurement

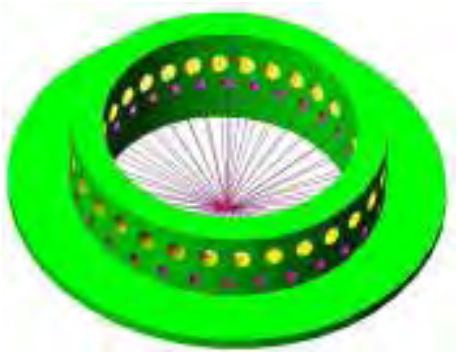

The multiple LED holder made of aluminum for concentrating light on quartz & feldspar samples to obtain luminescence was fabricated. Thirty red LEDs and another thirty blue LEDs are placed in the holder in an inclined manner on a circular array, so as to concentrate light at the centre of the ring.

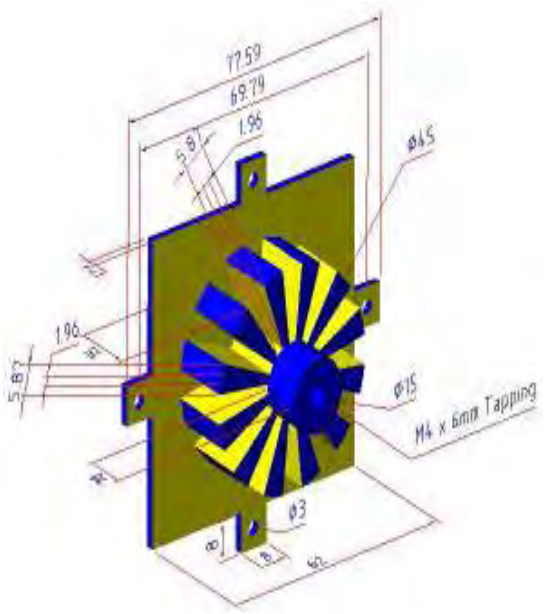

(2) Heat Sink for maintaining Silicon Drift Detector (SDD) temperature

Various heat sink designs were made and accordingly fabricated in the workshop for dissipating the heat produced in a SDD and the built-in thermo-electric cooler. One heat sink was manufactured in SAC which used the EDM process. The material of the heat sink was copper.

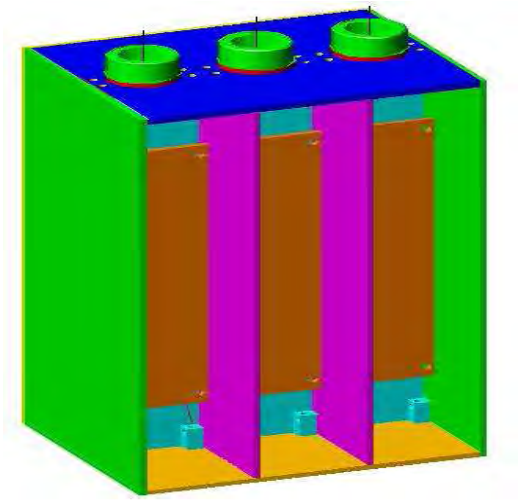

(3) Three channel large area Silicon Drift Detectors (SDD) package

A compact package has been designed to house three large area Silicon drift Detectors. Copper is used on the front side to efficiently drain out heat generated within detectors hybrid packages. Charge Sensitive preamplifier (CSPA) and shaping amplifier (SA) of each detector is mounted in respective Aluminum compartment so that electronics is immune from EMI noise. Back panel is used to interface electronics with backend instrumentation and bias supplies.

(4) Reflectron rings assembly

An assembly of mutually insulated aluminium rings for creating a retarding field in a reflectron time-of-flight mass spectromter was fabricated. It consists of 11 aluminum rings of dia.120 mm with inside hole of 60mm. The rings were manufactured on CNC lathe machine.

(5) Actuator System for correcting telescope flexure

After initial testing of the PARAS Cassegrain unit in early 2010, it was found that the 50 μm core optical fiber is required to be moved with a precision of 1 to 3 μm at the telescope focal plane to correct for telescope flexures and maintain the optics axis alignment. Hence two precision PI motors (X-axis and Y-axis) with two precision linear stages (Newport make) in tandem were assembled in our workshop. The 50 μm core optical fibre along with a CCD separated by about 30 mm was mounted on the top of the linear stage. The whole assembly now works in such a way that the telescope axis is determined by taking star exposure using CCD initially and then the fiber is brought in at the same place with a precision of 3 μm by moving the linear stages using the PI motor.

(6) Lead shield for gamma source

Cast lead rings were manufactured for shielding a gamma scintillation counter. A RCC mould was designed and manufactured for the casting. After casting, each lead brick was machined to the required dimensions. An aluminum holder for the radioactive source to be mounted inside the shield was also manufactured.

(7) The workshop has also made some critical precise components for following system/experiments

- Drift tube and lens assembly (for mass spectrometer)
- Retarding potential analyzer (for electron analysis)

- Parts for cylindrical mirror electron energy analyzer (for molecular fragmentation experiments at RRCAT, Indore and IUAC, Delhi
- 3-way target block (for laser ablation supersonic jet source)
- Complete TOF spectrometer with mesh holders, drift tube etc (for cluster studies)
- M.S. Structure/ Trolley for Cluster Chamber
- An Automated door closure system for LIDAR system at PRL
- Aerosol sampling manifold system
- Sliding system for heaters and compact ducting system

Honorary Fellows

Professor J. E. Blamont

Professor A. M. J. Tom Gehrels *

Professor D. Lal, FRS

Professor M. G. K. Menon, FRS

Professor U. R. Rao

Professor P. Crutzen

Professor K. Kasturirangan

Professor A. Hewish

* Deceased July, 2011

Honorary Faculty

R. K. Varma
FNA, FASc, FNASc, NASI Senior Scientist

S. Krishnaswami
FNA, FASc, FNASc, FTWAS, INSA Senior Scientist

R. G. Rastogi
FNA, FASc, FNASc

S. K. Bhattacharya
FASc, FNASc

S. K. Gupta
FNASc

A. C. Das

N. Bhandari
FNA, FASc, FNASc, INSA Honorary Scientist

D. P. Dewangan
FNASc

S. P. Gupta

Harish Chandra

H. S. S. Sinha

U. C. Joshi

R. Sridharan
FASc, FNASc, CSIR Emiritus Scientist

Honorary Technical Faculty

R. N. Misra

Academic Faculty

Name	Designation	Specialisation	Academic Qualification
Goswami J. N. *FNA, FASc, FNASc, FTWAS*	Director	Solar System Studies (Pre - Solar Processes)	Ph D, PRL, Guj. Univ. (1978)
Ambastha A. K.	Professor	Solar Plasma Physics, Coronal Structure and Polarization	Ph D, PRL, Gujarat Univ. (1981)
Amritkar R. E. *FASc*	Senior Professor	Nonlinear Dynamics &Chaos	Ph D, IISc, Bangalore (1978)
Ashok N. M.	Professor	Close Binary Stars, NovaeIR spectroscopy	Ph D, PRL, Gujarat Univ. (1983)
Baliyan K. S.	Associate Professor	AGNs, Comets, Atomic Physics, Milky Way	Ph D, Roorkee Univ. (1986)
Banerjee D.	Associate Professor	Thermoluminscence & Planetary Physics	Ph D, PRL, Gujarat Univ. (1996)
Banerjee D. P. K.	Professor	Novae, Be Stars,Planetary Nebulae, IR and Optical Studies	Ph D, PRL, Gujarat Univ. (1991)
Banerji J.	Professor	Classical Optics, Quantum Physics	Ph D, City Univ. (New York) (1982)
Bapat B.	Associate Professor	Atomic & Molecular Processes	Ph D, TIFR, Mumbai Univ. (1997)

Name	Designation	Specialisation	Academic Qualification
Bhatt J. R.	Associate Professor	Astrophysics	Ph D, IPR, MS Univ. (1992)
Bhattacharyya R.	Reader	Plasma Physics	Ph D Jadavpur Univ, Kolkata, (2006)
Bhushan Ravi	Scientist-SE	Oceanography and Paleoclimatology	Ph D, MS Univ.(2009)
Chakrabarty A.	Reader	Extra- solar planets, Star Formation & Instrumentation	Ph D, PRL, Gujarat Univ. 1999)
Chakrabarty D.	Scientist-SE	Upper Atmoshere and Geomagnetic Storm	Ph.D, PRL, MLS Univ. (2008)
Chandrasekhar T.	Professor	High Angular Resolution Studies, Late type stars Solar Coronal, Studies Comets	Ph D, PRL, Gujarat Univ. (1982)
Deshpande R. D.	Scientist-SF	Application of Environmental Tracers in Hydrology	Ph D, PRL, MS Univ. (2007)
Gosain S.	Scientist-SD	Solar Physics and Instrumentation	Ph D, MLS Univ. (2007)
Goswami S.	Associate Professor	High Energy Physics	Ph D, Calcutta Univ. (1998)
Haider S. A. *FASc*	Professor	Planetary and Cometary Atmospheres	Ph D, Banaras Univ. (1984)
Jain R.	Professor	Solar Physics	Ph D, PRL, Gujarat Univ. (1983)
Janardhan P.	Professor	Solar Radio Astronomy & Space Weather	Ph D, PRL, Gujarat Univ. (1992)
Joshi B.	Scientist- SD	Solar Physics, Astronomy	Ph D, ARIES, Kumaun Univ. (2007)
Joshipura A. S. *FNA, FASc, FNASc*	Outstanding Scientist	Particle Physics	Ph D, Bombay Univ. (1979)
Juyal N.	Scientist-SE	Quaternary Geology & Paleoclimate	Ph D, M.S.Univ.(2004)
Kota V. K. B.	Senior Professor - H	Nuclear Physics	Ph D, Andhra Univ. (1977)
Kumar B.	Scientist-SD	Solar Physics	Ph D, PRL, MLS Univ. (2007)
Konar, Partha	Reader	Particle Physics	Ph D, Allahabad Univ.(2005)

Name	Designation	Specialisation	Academic Qualification
Lal S. *FNA, FASc, FNASc*	Senior Professor	Atmospheric Chemistry and Trace Gases	Ph D, PRL, Gujarat Univ. (1982)
Mahajan N.	Reader	Particle Physics	Ph D, Delhi Univ. (2003)
Marhas K. K.	Reader	Solar System studies	Ph D, PRL, DAVV Indore (2001)
Mathew S. K.	Associate Professor	Solar Magnetic & Velocity Fields	Ph D PRL, Gujarat Univ. (1999)
Mishra H.	Associate Professor	Strong Interaction Physics & Nuclear Astrophysics	Ph D, IOP, Utkal Univ. (1994)
Mohanty S.	Professor	Astroparticle Physics	Ph D, Wisconsin Univ. (1989)
Murty S. V. S. *FASc*	Senior Professor	Isotope Cosmochemistry	Ph D, IIT, Kanpur (1981)
Naik S.	Reader	High Energy Astro- physics, X-ray Binaries	Ph D,TIFR,Mumbai Univ. (2003)
Navinder Singh	Reader	Theoretical condensed matter and Statistical physics	PhD. RRI,Bangalore (2006)
Pallam Raju D.	Associate Professor	Space and Atmospheric Sciences	Ph D, PRL, DAVV Indore(1996)
Rai V.	Reader	Stable Isotope Cosmochemistry	Ph D, PRL, MS Univ. (2001)
Ramachandran S.	Associate Professor	Atmospheric AerosolsRadiative & Climate Impacts	Ph D, PRL, MS Univ. (1996)
Ramesh R. *FNA, FASc, FNASc, FTWAS*	Senior Professor	Paleoclimatology, Oceanography & Modelling	Ph D, PRL, Gujarat Univ. (1984)
Rangarajan R.	Associate Professor	Particle Physics & Cosmology	Ph D, Univ. of California, Santa, Barbara (1994)
Rao B. G. A.	Senior Professor	Star formation, Planetary Nebulae, AGB Stars and Imaging Fabry Perot Spectroscopy	Ph D, PRL, Gujarat Univ. (1978)
Ray J. S.	Associate Professor	Isotope Geochemistry	Ph D, PRL, MS Univ. (1998)
Rengarajan R.	Scientist-SE	Atmospheric aerosols & aqueous geochemistry	Ph D, PRL, MLS Univ.(2004)
Rindani S. D. *FASc, FNA, FNASc*	Senior Professor-H	Particle Physics	Ph D, IIT, Bombay (1976)
Sahoo B.K.	Reader	Atomic Physics	Ph D, Bangalore Univ.(2006)

Name	Designation	Specialisation	Academic Qualification
Sahu L.K.	Reader	Atmospheric Science, Trace gases	Ph D, PRL, MLSU, (2005)
Samanta G.K.	Scientist-SD	Laser and nonlinear optics	Ph D, Universitat Politecnica de Catalunya University, Barcelona, (2009)
Sarin M. M. *FASc, FNA, FNASc*	Senior Professor	Geochemistry and Oceanography	Ph D, PRL, Gujarat Univ. (1985)
Sarkar U. *FNA, FASc, FNASc*	Senior Professor	Particle Physics	Ph D, Calcutta Univ. (1984)
Sekar R.	Professor	Upper Atmospheric & Ionospheric Physics	Ph D, PRL, Gujarat Univ. (1991)
Sharma Som K.	Scientist-SE	Middle Atmosphere & Long Term Atmospheric Changes	Ph D, PRL, Gujarat Univ. (2010)
Ganesh S.	Scientist-SE	Milky Way, Comets, AGN, Astronomical polarimetry	Ph.D, Guj. Univ. (2011)
Sheel V.	Reader	Modelling of Lower Atmosphere	Ph D, PRL, Gujarat Univ. (1996)
Singal A. K.	Associate Professor	Radio Astronomy & Astrophysics	Ph D, TIFR, Bombay Univ. (1986)
Singh A. D.	Associate Professor	Atomic Physics	Ph D, Bangalore Univ. (1998)
Singh R. P.	Scientist – SF	Laser Physics	Ph D, JNU, New Delhi (1994)
Singh S. K.	Associate Professor	Isotope Geochemistry	Ph D, PRL, MS Univ. (1999)
Singhvi A. K. *FNA, FASc, FNASc, FTWAS*	Outstanding Scientist	Palaeoclimatology and Geochronology	Ph D, IIT, Kanpur (1975)
Srivastava N.	Associate Professor	Solar Physics	Ph D, PRL, Ravi Shankar Shukla Univ. (1994)
Subramanian K. P.	Associate Professor	Experimental Atomic and Molecular Physics	Ph D, PRL, Gujarat Univ. (1987)
Vadawale S. V.	Reader	High Energy Astrophysics and X - ray Spectroscopy	Ph D, TIFR, Mumbai Univ. (2003)
Vats H. O.	Associate Professor	Space Weather & Radio Astronomy	Ph D, PRL, Gujarat Univ. (1979)
Venkatakrishnan P.	Senior Professor-H	Solar Physics	Ph D, Bangalore Univ. (1984)
Yadava M. G	Scientist-SE	Palaeoclimate, Radiocarbon dating and Stable isotopes	Ph D, PRL, DAVV Indore (2003)

Technical Faculty

Name	Designation
Acharya Y. B.	Engineer-G
Adhyaru P. R.	Engineer-SE
Dadhania M. B.	Engineer-SF
Dholakia G. G.	Scientist-SG
Jokhakar D. H.	Engineer-SE
Narayanan R.	Scientist-SF
Prajapati I. A.	Scientist-SE
Rao D. K.	Scientist-SE
Shah A. B.	Engineer-SF
Shah K. J.	Scientist-SE
Shah R. R.	Engineer-SF
Shukla A. D.	Scientist-SE
Singh Mahendra	Engineer-SF
Ubale G. P.	Engineer-SE
Venkataramani S.	Scientist-SE


पी.आर.एल. में गतिविधियां
Events at PRL

पी.आर.एल. में गतिविधियां
Events at PRL

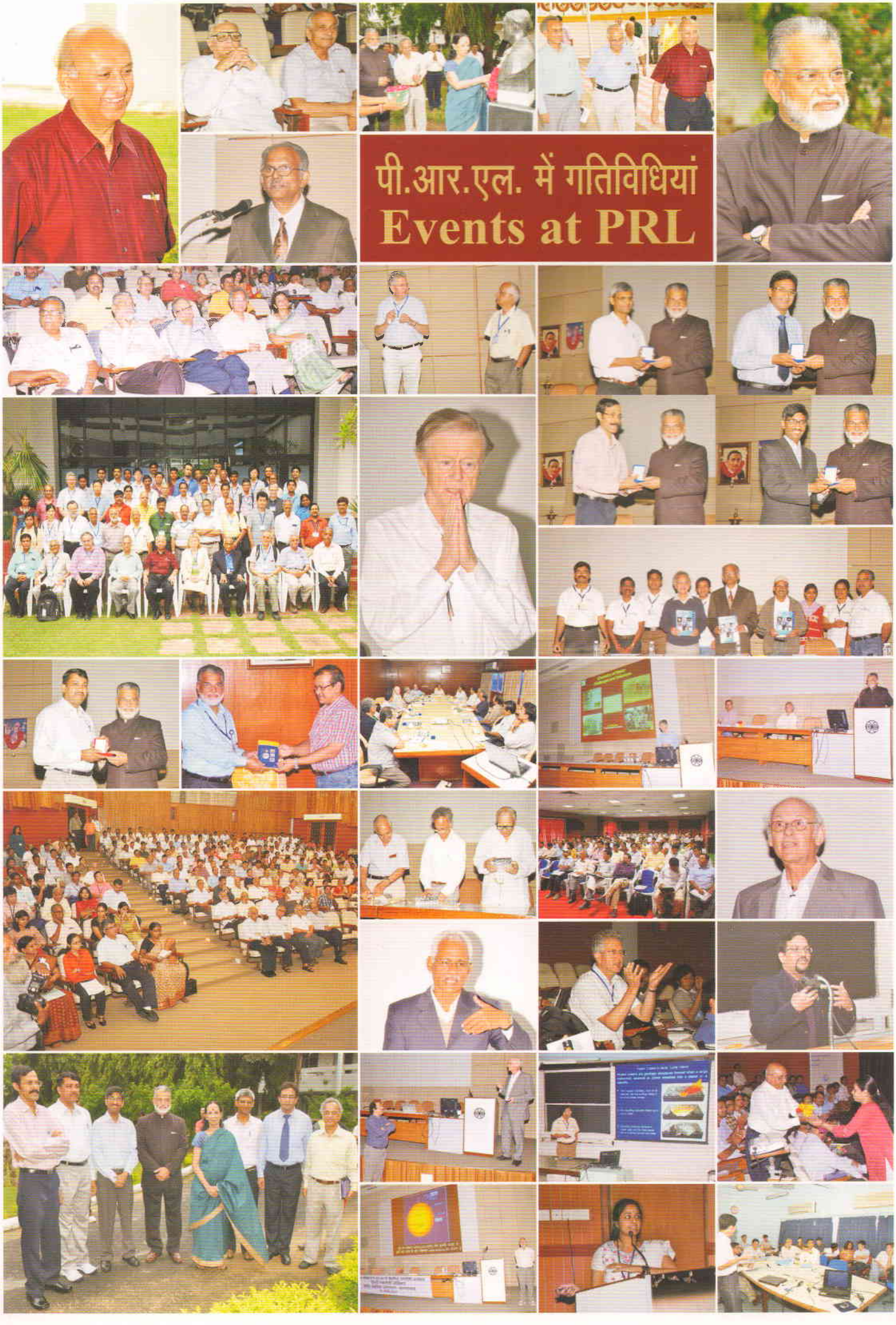
पी.आर.एल. में गतिविधियां
Events at PRL